

INVESTIGATION OF SURFACE PROPERTIES OF QUINCE SEED EXTRACT
AND ASSESSMENT OF ITS PERFORMANCE AS A NOVEL POLYMERIC
SURFACTANT

A THESIS SUBMITTED TO
THE GRADUATE SCHOOL OF NATURAL AND APPLIED SCIENCES
OF
MIDDLE EAST TECHNICAL UNIVERSITY

BY

EMRAH KIRTIL

IN PARTIAL FULFILLMENT OF THE REQUIREMENTS
FOR
THE DEGREE OF DOCTOR OF PHILOSOPHY
IN
FOOD ENGINEERING

DECEMBER 2020

Approval of the thesis:

**INVESTIGATION OF SURFACE PROPERTIES OF QUINCE SEED
EXTRACT AND ASSESSMENT OF ITS PERFORMANCE AS A NOVEL
POLYMERIC SURFACTANT**

submitted by **EMRAH KIRTIL** in partial fulfillment of the requirements for the degree of **Doctor of Philosophy in Food Engineering, Middle East Technical University** by,

Prof. Dr. Halil Kalıpçılar
Dean, Graduate School of **Natural and Applied Sciences**

Prof. Dr. Serpil Şahin
Head of the Department, **Food Engineering**

Assist. Prof. Dr. H. Mecit Öztop
Supervisor, **Food Engineering, METU**

Prof. Dr. Serpil Şahin
Co-Supervisor, **Food Engineering, METU**

Examining Committee Members:

Prof. Dr. Meryem Esra Yener
Food Engineering, METU

Assoc. Prof. Dr. H. Mecit Öztop
Food Engineering, METU

Prof. Dr. Gülüm Şumnu
Food Engineering, METU

Prof. Dr. Nihal Aydoğan
Chemical Engineering, Hacettepe University

Assist. Prof. Dr. Elif Yolaçaner
Food Engineering, Hacettepe University

Date: 30.12.2020

I hereby declare that all information in this document has been obtained and presented in accordance with academic rules and ethical conduct. I also declare that, as required by these rules and conduct, I have fully cited and referenced all material and results that are not original to this work.

Name, Last name : EMRAH KIRTIL

Signature :

ABSTRACT

INVESTIGATION OF SURFACE PROPERTIES OF QUINCE SEED EXTRACT AND ASSESSMENT OF ITS PERFORMANCE AS A NOVEL POLYMERIC SURFACTANT

Kırtıl, Emrah
Doctor of Philosophy, Food Engineering
Supervisor: Assoc. Prof. Dr. Mecit Halil Öztop
Co-Supervisor: Prof. Dr. Serpil Şahin

December 2020, 247 pages

The use of sustainable ingredients from natural sources has shown an increase in recent years. For stabilization of dispersions, proteins and polysaccharides are increasingly being used in combination for their synergistic properties. Various studies have focused on developing biopolymers that merge the functions of proteins and polysaccharides in a single molecule. Quince seed extract (QSE) is a natural biopolymer that display this exceptional attribute in its native state. However, the literature is still lacking in demonstrating its potential as a natural stabilizer through analysis of the extract's interfacial properties.

This dissertation has two main objectives; to assess the performance of QSE as an emulsion stabilizer and to examine its air-water and oil-water interfacial properties. Quince seed extract provided a similar stability to emulsions compared to same concentrations of Xanthan gum but at smaller apperant viscosities. Overall, QSE concentrations >0.3 w/v yielded physically stable emulsions even after 5 months. QSE was effective in lowering surface tension at an air-water interface even at concentrations as low as 0.025 % w/v (reduction of eq. ST from 72 mN/m to 58.9

mN/m). By QSE addition alone equilibrium surface tension could be lowered to ~36 mN/m, which is lower than the lowest ST that can be achieved with many other surface active biopolymers. Critical aggregation concentration (CAC) was identified as 0.165 % w/v,. In addition to these findings, the study; provides the possibility of obtaining more information on the processes happening during adsorption and describing their mechanism with established theories.

Keywords: Quince Seed Extract, Polymeric Surfactant, Dispersion Stability, Colloidal Dynamics, Interfacial Phenomena

ÖZ

AYVA ÇEKİRDEĞİ EKSTRESİNİN YÜZEY ÖZELLİKLERİNİN İNCELENMESİ VE YENİ BİR POLİMERİK YÜZEY AKTİF MADDESİ OLARAK PERFORMANSININ DEĞERLENDİRİLMESİ

Kırtıl, Emrah
Doktora, Gıda Mühendisliği
Tez Yöneticisi: Doç. Dr. Mecit Halil Öztop
Ortak Tez Yöneticisi: Prof. Dr. Serpil Şahin

Aralık 2020, 247 sayfa

Doğal kaynaklardan elde edilen sürdürülebilir malzemelerin endüstride kullanımı son yıllarda artış göstermiştir. Dispersiyonların stabilizasyonu için, özellikle, proteinler ve polisakkaritler, sinerjistik özellikleri nedeniyle kombinasyon halinde kullanılmaktadır. Proteinlerin ve polisakkaritlerin işlevlerini tek bir molekülde birleştiren biyopolimerler geliştirmeye odaklanan çeşitli çalışmalar vardır. Bazı biyopolimerler bu istisnai niteliği doğal hallerinde sergiler. Ayva çekirdeği ekstresi (QSE) bu eşsiz biyopolimerlerden biridir. Ancak literatür, ekstraktın ara yüzey özelliklerinin analizi yoluyla doğal bir stabilizatör olarak potansiyelini göstermekte yeterli bir seviyeye ulaşmamıştır.

Bu tezin iki temel amacı vardır; QSE'nin emülsiyon stabilizatörü olarak performansını değerlendirmek ve ayva çekirdeği ekstraktının hava-su ve yağ-su arayüzey özelliklerini incelemek. Ayva çekirdeği ekstresi, aynı konsantrasyonlardaki ksantan sakızı ile karşılaştırıldığında emülsiyonlara benzer bir stabilite sağlamıştır, ve bunu daha düşük kesme viskozitelerinde gerçekleştirmiştir.

Genel olarak, 0.3 (w/v)'ten yüksek ayva çekirdeđi ekstratı ile, 5 ay sonra bile fiziksel olarak stabilitesini koruyan emülsiyonlar oluşturmuştur. QSE, %0.025 w/v kadar düşük konsantrasyonlarda bile (eq. ST'nin 72 mN/m'den 58.9 mN/m'ye düşürülmesi) hava-su arayüzünde yüzey gerilimini düşürmede etkili olduđu görüldü. Tek başına QSE ilavesi ile denge yüzey gerilimi ~36 mN / m'ye düşürülebilir; bu, diđer birçok yüzey aktif biyopolimer ile elde edilebilen en düşük ST'den daha düşüktür. Kritik agregasyon konsantrasyonu (CAC), benzer hidrokolloidlere kıyasla daha düşük olan %0.165 w/v olarak tanımlandı. Bunların yanısıra, bu çalışma; adsorpsiyon sırasında meydana gelen süreçler hakkında daha fazla bilgi edinme ve bunların mekanizmalarını yerleşik teorilerle açıklama imkanı sağlayacak; ve ayrıca okuyuculara bu ekstraktın uygulaması ve emülsiyonlarda stabilite artırıcı olarak kullanımı hakkında doğrudan bilgi sağlayacaktır.

Anahtar Kelimeler: Ayva Çekirdeđi Ekstresi, Polimerik Yüzey Aktif Madde, Dispersiyon Kararlılığı, Kolloidal Dinamikler, Arayüzey Olayları

To my beloved Mother

ACKNOWLEDGMENTS

I would like to start my thanks with Assoc. Prof. Dr. H. Mecit Oztop. He is the best advisor a PhD student could have. He is the reason I currently am graduating with so many studies outside of my dissertation. He believed in me more than I believed in myself and kept encouraging me to do my best. His support and guidance helped me overcome any obstacle I encountered on the way. For that, I cannot thank him enough. I also would like to thank Prof. Dr. Serpil Şahin for her suggestions and guidance throughout my dissertation studies.

The other major thanks goes to Prof. Clayton Radke from University of California Berkeley. He accepted me to his laboratory before I even got a scholarship. That's why, I was grateful to him even before starting to work in his laboratory. However, once there, starting from our first meeting, he has changed my idea of how a researcher should approach his research. He has taught me a lot about work ethics and fascinated me with his energetic, positive, kind and humble personality. He has introduced me to a whole new research area that fascinated me so much that I plan to pursue it in my post-doctoral studies. He has taught the correct way to guide a student through his studies and how valuable the opinion of someone who is an expert on the subject could be in solving problems. There are countless positive things I could say about him, he is one of the most influential people in my life and also one that made this dissertation possible and shaped my future studies.

I would also like to thank my friends who have aided me throughout this process. First of all, I would like to thank my closest friends, Ayça Aydoğdu, Sevil Çıkrıcı and Bade Tonyalı, who are now like a family to me. I owe everything I am and I have to them. They have taught me how to be a good, honorable person and how to actually care for people. I have discovered the meaning of happiness with them, they have made me feel whole for the first time in my life. They still and will be the first ones that I will share my sorrow and joy. Thanks for being there for me anytime I

needed. They are the most important achievements in my life and the most important things ODTU and my PhD education has given me.

I also would like to thank Enis Kurtkaya for his friendship, support, patience and help. He listened to every minor problem that I had in USA with inhuman patience and tried his best to help me solve them. He was even so kind to help me with my experiments. He is one of the best, kindest and most selfless people one can meet. No words are enough to express my gratitude for everything he has done for me. I have the best wishes for him. I would also like to thank my dearest friend, Gökhan Açıkgöz, who is the sweetest, most naïve person one can know. He has opened his house to me countless times and spoiled me with delicious food.

Life is a bumpy road, so are friendships. There can be highs and lows. Selen Guner and I have gone through a lot, during our time in METU. What really matters is, despite everything, we managed to stay friends. In the last 2 years that I was roommates with her, our bond even deepened. She is the nicest, most energetic, positive, thoughtful, helpful, funny and intelligent person I have known. I am so glad to have known her and feel so lucky that she considers me a friend.

I am so lucky to have the best family one could hope for. I feel so blessed to grow up feeling loved, supported and appreciated for every minor thing I have done. I am 36 now but my mother Gülsen Kırtıl, father Mustafa Kırtıl and brother Savaş Doğanay Kurtul still support me as if I am a child. They are still the first people I call when I have the tiniest problem. I hope one day I will be able to pay it back to them, even just a little bit.

I also would like to thank all my colleagues; namely Esmanur İlhan, Kübra Ertan, Özge Güven, Seren Oğuz, Derya Uçbaş, Alperen Köker, İlhami Okur, Yağmur Balabanlı, Hilmi Eriklioğlu, Ozan Taş, Hilal Samut, Ülkü Ertuğrul and Begüm Köysüren, that made our work environment a friendly and compassionate place. Every research assistant in our department is like hand-picked for their beautiful personality. I was so lucky to be working in a department where everyone was

helpful, kind and positive towards each other. I would also like to thank all Öztop Lab members for their help with my experiments. I am sure all of them will have very successful careers.

Some of my colleagues were also my close friends so they deserve a special thanks. Eda Yıldız, was the first person I have greeted every morning, the last that I said goodbye every evening. She also was the person that I visited when I was bored of working on my dissertation, where she always cheered me up. I cannot thank her enough. Gökcem Tonyalı, is one of the funniest and sincerest people I have known. She made me feel energized and young whenever I went up for a chat. I would also like to thank Cansu Diler, for her positive attitude and always smiling face, that lifted me up whenever I am down. Serap Namlı and Şahin Namlı hold a special place in my heart for kindly and tirelessly listening to my problems and sharing my deepest secrets. Their advices and positive encouragement helped me through my darkest times.

I would also like to acknowledge and thank Fulbright Doctoral Dissertation Research Program for providing me the funding and support to pursue a significant portion of my PhD studies in UC Berkeley.

TABLE OF CONTENTS

ABSTRACT.....	v
ÖZ	vi
ACKNOWLEDGMENTS	viii
TABLE OF CONTENTS.....	xiii
LIST OF TABLES	xviii
LIST OF FIGURES	xix
CHAPTERS	
1 INTRODUCTION	1
1.1 Use of Hydrocolloids for Stabilization of Dispersions	1
1.1.1 Whey Protein.....	3
1.1.2 Xanthan Gum	3
1.1.3 Quince Fruits and the Extract of its Seeds	4
1.1.3.1 Physicochemical Properties of Quince Seed Extract	5
1.1.3.1.1 Molecular Weight	6
1.1.3.1.2 Monosaccharide Composition	7
1.1.3.1.3 Chemical Structure	9
1.1.3.1.3 Amino Acid Composition	11
1.1.3.1.3 Other Physicochemical Properties	13
1.2 Nuclear Magnetic Resonance Relaxometry	15
1.2.1 Theory	16
1.2.2 Droplet Size Measurement and Emulsion Characterization	23

1.3	Surface Chemistry and Interfacial Science	24
1.3.1	Definition of Interface and Interfacial Forces	26
1.3.2	Adsorption of Polymeric Surfactants onto a Fluid Interface	28
1.3.3	Properties of an Effective Polymeric Surfactant	32
1.3.3.1	Absolute Interfacial Coverage	33
1.3.3.2	Strong Solvation	37
1.3.3.3	Strong Affinity Toward the Interface	43
1.3.3.4	Steric Stabilization	50
1.3.3.5	Rate of Adsorption	53
1.4	Objective of the Study	58
2	MATERIALS & METHODS	61
2.1	Materials	61
2.1.1	Characterization Emulsion Stabilization Properties of Quince Seed Extract as a New Source of Hydrocolloid	61
2.1.2	Investigation of Surface Properties of Quince Seed Extract	61
2.1.3	Examination of Interfacial Properties of Quince Seed Extract on a Sunflower Oil – Water Interface	62
2.2	Methods	62
2.2.1	Characterization Emulsion Stabilization Properties of Quince Seed Extract as a New Source of Hydrocolloid	62
2.2.1.1	Extraction of Quince Seeds	62
2.2.1.2	Emulsion Preparation	62
2.2.1.3	Confocal Microscopy	64
2.2.1.4	Rheological Characterization	64
2.2.1.5	Visual Assessment of Creaming	65

2.2.1.6	Particle Size Measurements	66
2.2.1.7	Nuclear Magnetic Resonance (NMR) T ₂ Relaxometry Experiments	66
2.2.2	Investigation of Surface Properties of Quince Seed Extract	67
2.2.2.1	Experimental Design	67
2.2.2.2	Quince Seed Extract Preparation	69
2.2.2.3	Sample Preparation	69
2.2.2.4	Dynamic Surface Tension Measurements	69
2.2.2.5	Surface Rheology	72
2.2.2.5.1	Theoretical Background	72
2.2.2.5.2	Dilatational Rheology Measurements	73
2.2.2.6	z-Average Particle Size	74
2.2.2.7	Estimation of Diffusion Coefficient from Tensiometer Measurements....	75
2.2.2.8	Estimation of Diffusion Coefficient using NMR Relaxometry Measurements	77
2.2.3	Examination of Interfacial Properties of Quince Seed Extract on a Sunflower Oil – Water Interface	77
2.2.3.1	Experimental Design	77
2.2.3.2	Quince Seed Extract Preparations	79
2.2.3.3	Sample Preparation	79
2.2.3.4	Dynamic Interfacial Tension Measurements	79
2.2.3.5	Dilatational Interfacial Rheology Measurements	81
2.2.3	Statistical Analysis	83
3	RESULTS & DISCUSSION	85
3.1	Characterization Emulsion Stabilization Properties of Quince Seed Extract as a New Source of Hydrocolloid	85

3.1.1	Rheological Characterization	85
3.1.1.1	Linear-Viscoelastic Behaviour	85
3.1.1.2	Flow Characteristics	88
3.1.2	Particle Size Distribution	91
3.1.3	NMR T ₂ Relaxation Measurements	94
3.1.4	Emulsion Stability	97
3.1.5	Emulsion Microstructure	102
3.2	Investigation of Surface Properties of Quince Seed Extract	103
3.2.1	Equilibrium Surface Tension	103
3.2.2	Dynamic Surface Tension Curves	111
3.2.3	Dilatational Surface Rheology	122
3.3	Examination of Interfacial Properties of Quince Seed Extract on a Sunflower Oil – Water Interface	140
3.3.1	Equilibrium Interfacial Tension	140
3.3.2	Dynamic Interfacial Tension Curves	148
3.3.3	Dilatational Interfacial Rheology	156
4	CONCLUSION & RECOMMENDATIONS	169
	REFERENCES	173
	APPENDICES	
A.	Statistical Analysis	213
	CURRICULUM VITAE	245

LIST OF TABLES

TABLES

Table 1.1. Summary of some recent publications using biopolymers as emulsion stabilizers either as modified polysaccharides or protein-polysaccharide Maillard conjugates	29
Table 2.1. Composition of the O/W emulsions	63
Table 2.2. Experimental design for investigation of surface properties of QSE ...	67
Table 2.3. Experimental design for investigation of interfacial properties of QSE	77
Table 3.1. Effect of XG and QSE concentration on consistency (K), flow index (n) and correlation coefficient of power law model (R^2) and length of linear viscoelastic range in 2% (w/v) WPI stabilized emulsions containing 20% v/v O/W	86
Table 3.2. Effect of XG and QSE concentration on elastic (G') and loss modulus (G'') in 2wt% WPI stabilized emulsions containing 20% v/v O/W	87
Table 3.3. z-average diameters of QSE aggregates	107
Table 3.4. Average E' , E'' and $\tan\Delta$ values for QSE at an air-water surface	120
Table 3.5. Diffusion coefficients estimated from tensiometer measurements and NMR Relaxometry data	136
Table 3.6. Average E' , E'' and $\tan\Delta$ values for QSE at an oil-water interface	156

LIST OF FIGURES

FIGURES

Figure 1.1. Proposed structure of QSG-2 (\rightarrow : Covalent bonds, - - - : <i>H</i> -bonds) (R1: 1, 2, 3, 5-Araf or 1, 4-Glcp, R2: -NH ₂ group of proteins)	10
Figure 1.2. Schematic of magnetization occurred by placing a sample into an external magnetic field in <i>z</i> direction (B_0)	17
Figure 1.3. Schematic showing the direction that protons are facing in samples. (a) Without the presence of an external magnetic field, (b) under the influence of an external magnetic field of B_0	18
Figure 1.4. Schematic depicting the precessional motion of protons	19
Figure 1.5. Precessional motion of protons. (a) Without an RF pulse application, (b) phasing of protons right after an RF pulse application	20
Figure 1.6. Relaxation of transverse (M_{xy}) and longitudinal (M_z) magnetization after application of a 90° RF pulse	20
Figure 1.7. A representative exponential relaxation curve of longitudinal magnetization for a sample with a T_1 of 10 ms	21
Figure 1.8. A representative exponential relaxation curve of transversal magnetization for a sample with a T_2 of 10 ms	22
Figure 1.9. Schematic displaying the attractive forces between molecules inside the liquid interior and at the interface	27
Figure 1.10. A schematic and representative experimental curve demonstrating the change in equilibrium surface tension with surfactant concentration	34
Figure 1.11. Flocculation of droplets in a colloidal system	41
Figure 1.12. Effect of δ/R of Gibbs free energy of a dispersion	42
Figure 1.13. Representation of trains-tails-loops configuration of a polymer at an interface	44
Figure 1.14. Representational adsorption models depending on copolymer type (a) <i>A</i> – <i>B</i> copolymer (b) <i>A</i> – <i>B</i> – <i>A</i> copolymer (c) Graft copolymer (d) Random copolymer	49

Figure 1.15. Schematic representation of the interaction between particles with adsorbed polymer layers	52
Figure 1.16. A representative curve displaying typical dynamic interfacial tension response of polymeric surfactants in dilute solutions	55
Figure 2.1. Schematic representation of the pendant drop measurement setup for measurement at an air-water interface	70
Figure 2.2. Schematic representation of the pendant drop measurement setup for measurement at an oil-water interface	80
Figure 3.1. Effect of XG and QSE concentration on flow behavior of 2 %w/v WPI stabilized emulsions containing 20% v/v sunflower oil	91
Figure 3.2. Change in volume–moment mean diameter (d_{43}) of 2 %w/v WPI stabilized emulsions containing 20%v/v sunflower oil with respect to storage time and quince seed extract/xanthan gum concentration	92
Figure 3.3. Effect of gum type and concentration on Day 0 volume–moment mean diameter (d_{43}) measurements	93
Figure 3.4. Mean NMR T_2 relaxation times of 2 %w/v WPI stabilized emulsions containing 20% v/v sunflower oil with respect to storage time and quince seed extract/xanthan gum concentration	95
Figure 3.5. T_2 relaxation times acquired through bi-exponential fitting of NMR relaxation data of 2 %w/v WPI stabilized emulsions containing 20% v/v sunflower oil with respect to storage time and quince seed extract/xanthan gum concentration	96
Figure 3.6. Images of (a) emulsions on Day 0 prepared with xanthan gum in decreasing gum concentration from left to right (0.75X, 0.5X, 0.3X, 0.2X, 0.1X, NOX) (b) emulsions on Day 0 prepared with quince seed extract in decreasing gum concentration from left to right (0.75Q, 0.5Q, 0.3Q, 0.2Q, 0.1Q, NOX) (c) emulsions prepared with xanthan gum on Day 2 (d) emulsions prepared with quince seed extract on Day 2 (e) emulsions prepared with xanthan gum on Day 10 (f) emulsions prepared with quince seed gum on Day 10 (g) 0.2X on Day 30 (h) 0.2Q on Day 30	

(i) emulsions prepared with xanthan gum on Day 150 (j) emulsions prepared with quince seed gum on Day 150.....	99
Figure 3.7. Effect of gum type and concentration on creaming index (%CI) of 2wt% WPI stabilized emulsions containing 20%v/v sunflower oil	100
Figure 3.8. Confocal microscopy images of samples 0.1X, 0.1Q, 0.5X, 0.5Q on day 0 (left) and day 30 (right)	102
Figure 3.9. (a) Equilibrium Surface Tension Isotherm (b) Equilibrium Surface Tension Isotherms (x-axis drawn at a logarithmic scale)	106
Figure 3.10. (a) Equilibrium surface tension of QSE solutions at different pHs (b) Equilibrium surface tension of QSE solutions at different NaCl concentrations .	111
Figure 3.11. Effect of concentration on the surface tension profile of QSE solutions	112
Figure 3.12. (a) Effect of pH on the surface tension profile of QSE solutions (b) Effect of NaCl concentration on the surface tension profile of QSE solutions.....	117
Figure 3.13. Idealized illustration of the effect of pH on the adsorbed QSE layer (a) pH close to 4.2 (b) when $\text{pH} \ll$ or $\gg 4.2$	118
Figure 3.14. (a) Frequency dependence of E' and E'' of QSE solutions with varying concentrations (b) Frequency dependence of E' and E'' of QSE solutions with varying pHs and NaCl concentrations	125
Figure 3.15. Concentration dependence of (a) E' (storage modulus) (b) E'' (loss modulus), pH dependence of (c) E' (storage modulus) (d) E'' (loss modulus), NaCl concentration dependence of (e) E' (storage modulus) (f) E'' (loss modulus) for frequencies 0.01-0.1 Hz	129
Figure 3.16. (a) Equilibrium Interfacial Tension Isotherm (b) Equilibrium Interfacial Tension Isotherm (x-axis drawn at a logarithmic scale)	133
Figure 3.17. (a) Equilibrium interfacial tension of QSE solutions at different pHs (b) Equilibrium interfacial tension of QSE solutions at different NaCl concentrations	145

Figure 3.18. (a) Effect of concentration on the surface tension profile of QSE solutions (b) Effect of pH on the surface tension profile of QSE solutions (c) Effect of NaCl concentration on the surface tension profile of QSE solutions 148

Figure 3.19. (a) Frequency dependence of E' and E'' of QSE at an oil-water interface with varying concentrations (b) Frequency dependence of E' and E'' of QSE at an oil-water interface with varying pHs and NaCl concentrations 160

CHAPTER 1

INTRODUCTION

1.1 Use of Hydrocolloids for Stabilization of Dispersions

Preparation of a wide range of food products involves the dispersion of oil into water. However, in lyophobic colloidal dispersions such as food emulsions, the continuous water phase does not have the desire to wet the dispersed oil phase (Adams et al., 1998). The dispersion of oil in water increases the contact area, hence the interfacial tension between the two phases and carries the system to a higher overall free energy state. In agreement with the thermodynamic dictum that all systems wish to be in their minimum energy state, the two phases have a tendency to separate and minimize interfacial area (Damodaran, 2005; McClements, 2004). These thermodynamically unstable systems can be kinetically stabilized by minimizing the rate of separation. Some favored methods of accomplishing this are, addition of amphiphilic molecules that adsorb on the interface and decrease interfacial tension, or addition of non-adsorbing thickening polysaccharides that reduce particle movements and collisions in emulsions by increasing the viscosity of the continuous phase (Bouyer et al., 2012).

There is a growing trend in recent years from both the academia and the industry towards the use of "clean-labeled" ingredients obtained from renewable resources. Biopolymers are being used for their stabilizing, emulsifying, viscosity-enhancing, micro-encapsulating, and gelling properties, among others (Farahmandfar et al., 2017). Proteins and polysaccharides, in particular, are becoming increasingly popular as alternatives to already well-established synthetic surfactants (Bouyer et al., 2012; Covis et al., 2014; Dalgleish, 2006; Dickinson, 2003). In addition to their

environmental impact, synthetic surfactants may cause acute toxic symptoms in animals and humans (Cserhádi et al., 2002; Effendy and Maibach, 1995; Liwarska-Bizukojc et al., 2005). Thus, replacing them with much safer alternatives would be of significant benefit.

Proteins are adsorbing biopolymers; that is, they adsorb to the interface, decreasing surface tension, and easing the emulsification process. Even though proteins, compared to low molecular weight surfactants, adsorb more slowly to the interface; during emulsification process, where turbulent hydrodynamic conditions are present, they can adsorb quite rapidly (Seta et al., 2014; W. Wang et al., 2014). Once adsorbed, these polymers with their high molecular weight and complex structure form a highly viscoelastic gel layer on the interface which provides an additional layer of protection to droplet coalescence during subsequent processing and storage (Benjamins et al., 1996; Bos and Van Vliet, 2001; Dickinson, 2001, 1999, 1998). Non-adsorbing polysaccharides, on the other hand, contribute to dispersion stability by forming an extended network in the continuous phase that enhances its viscosity, even create a gel thus hindering droplet movements and encounters (Bouyer et al., 2013). Merging the advantages of proteins (interfacial adsorption, reduction in interfacial tension) and polysaccharides (steric repulsion, viscosity enhancement) in the same system, and coming up with the most appropriate conditions (concentration, pH, ionic strength, temperature) to increase their stabilizing properties, poses a great potential in improving dispersion stability (Dickinson, 2008a, 2008b; Evans et al., 2013; Guzey and McClements, 2006).

Various strategies have been developed for this purpose. One common approach involves the chemical modification of biopolymers' native structure. By dry heating of protein and polysaccharides, amino group in proteins become covalently attached to the carbonyl group of a reducing end on the polysaccharide backbone through *Maillard* reaction (Anal et al., 2019; Kontogiorgos, 2019). In systems stabilized by such biopolymers, the protein can first adsorb at the interface, and polysaccharides linked to the proteins extend from the interface to the bulk phase, and provide a steric

stabilization. Systems stabilized by this approach have shown enhanced kinetic stability compared to systems stabilized by proteins and polysaccharides alone or in combinations (Anal et al., 2019; Bouyer et al., 2013; C. Gao et al., 2017; W. Y. Liu et al., 2018; Vernon-Carter et al., 2008). There are several natural gums that possess this exceptional attribute in their native state. Out of these, gum Arabic is the most widely used adsorbing biopolymer and considered a benchmark emulsifying, encapsulating, and film-forming agent (Vernon-Carter et al., 2008). Gum Arabic is an extensively branched complex hetero-polyelectrolyte composed of L-arabinose and D-galactose, and minor proportions of 4-*O*-methyl-D-glucuronate, and L-rhamnose. The gum's surface-activity comes from its protein content (1-2% w/w) (Goycoolea et al., 1997; Orozco-Villafuerte et al., 2003; Ray et al., 1995). However, the use of this gum is restricted by its high cost (Dickinson, 2018).

During this dissertation three different hydrocolloids were used, whey protein, xanthan gum and quince seed extract. Now we will briefly talk about these biopolymers.

1.1.1 Whey Protein

Whey protein isolate (WPI) is a mixture α -lactalbumin and β -lactoglobulin and several other minor proteins (Sun et al., 2007) and is widely used as a natural emulsifier in food products (Sun and Gunasekaran, 2009). When dissolved in emulsions, WPI tends to be rapidly adsorbed on the surface of oil droplets in the form of a stabilizing monolayer that prevent droplet agglomeration through a combination of electrostatic and steric interactions (Djordjevic et al., 2004; Gwartney et al., 2004).

1.1.2 Xanthan Gum

In addition to surfactants, polysaccharides are often added in order to thicken emulsions, thereby decreasing the rate of common destabilization mechanisms such

as flocculation, creaming, sedimentation or Ostwald ripening (Bouyer et al., 2012). Xanthan gum (XG) is one of the most preferred polysaccharides in this regard. XG is an anionic polysaccharide produced by the bacterium, *Xanthomonas campestris*. The structure consists of a β -(1-4)-D-glucose main chain and side chains of α -D-mannose, β -D-glucuronic acid and β -D-mannose as terminal residues (Bouyer et al., 2012). The polymer, when dissolved in water, exists as multiple forms of helices that is in interaction with one another, forming a complex yet loosely bound network (Jansson et al., 1975; Melton et al., 1976). This particular arrangement gives the gum its unique thickening and shear thinning properties (Benmouffok-Benbelkacem et al., 2010). The high low-shear viscosity and powerful shear-thinning characteristic, gives xanthan gum solutions high stability against collapse of colloidal suspensions, yet makes it easy to mix and swallow.

1.1.3 Quince Fruit and the Extract of Its Seeds

Quince is a fruit of west Asian region, which is commonly cultivated in Caucasus regions, Syria, Afghanistan, Iran, Dagestan and Antalya (Trigueros et al., 2011). Quince belongs to the genus *Cydonia* and the scientific name of ordinary quince is *Cydonia oblonga* (Abbastabar et al., 2015). In the region, fruit flesh has been traditionally used in treatment of inflammatory bowel disease whereas the seeds are used to treat diarrhea and stomach ulcers (Rahimi et al., 2010). Pulp and peel extracts of the fruit have illustrated radical scavenging properties and antioxidant activity (Rahimi et al., 2010). A mature fruit contains roughly 10 seeds (Abbastabar et al., 2015). Seeds are reported to contain various amino acids as well as phenolic compounds and antioxidants such as citric, ascorbic, malic acid (Silva et al., 2005). Seeds also embody a mucinous material, which could be extracted upon mixing with water. Though the seeds have been used for years in Turkish culinary for gelling, they have recently attracted researchers' attention, which caused a recent increase on the amount of research on the subject. A number of researchers have demonstrated applications for this new source of hydrocolloid (Abbastabar et al., 2015; Hakala et

al., 2014; Jouki et al., 2014; Ritzoulis et al., 2014; Trigueros et al., 2011). Studies revealed that, basic constituents of quince seed mucilage were cellulose, water soluble polysaccharides (with the major component being partially O-acetylated (4-*O*-methyl-*D*-glucurono)-*D*-xylan and high proportion of glucuronic acid residues) and the amino acids Ara, Xyl, Gal and Glc in proportions 8:54:4:34 (Ritzoulis et al., 2014; Vignon and Gey, 1998). In a recent study by Abbastabar et al. (2015), the mucilage was shown to possess great gelling capacity and introduced enhanced viscosity and shear thinning behavior to solutions (Abbastabar et al., 2015). Though the protein content of the seed extract had been known for years, recently the emulsifying properties of quince seed extract have been extensively studied and confirmed for a pH range of 6-8 (Ritzoulis et al., 2014).

Quince seed extract (QSE) has shown similar characteristics to Gum Arabic and, thus, have raised some interest among researchers. The seed extract has shown very high emulsification and foaming properties (Deng et al., 2019). This is related to its high hydrophobic amino acid content, which gives the hydrocolloid its exceptional surface activity (Deng et al., 2019). However, research up until now, has mostly concentrated on the chemical and physical analysis of quince seed mucilage's water-soluble carbohydrates. There still is a considerable amount of research needed to examine the gum's potential in stabilizing dispersions, such as investigation of its surface properties and use of the gum in a real dispersed system.

1.1.3.1 Physicochemical Properties of Quince Seed Extract

The identification of the molecular structure is critical in a surface study like this one because the composition of the interfacial layer is defined by the relative intensities of the many kinds of interactions. These interactions, in turn, are influenced by the specific affinity for the interface and various physicochemical parameters, such as differences in the sizes and shapes, surface activity, overall electrical charges, and hydrophobicity of the molecules (Bos and Van Vliet, 2001; Dickinson, 2001, 1999).

To best our knowledge, a thorough chemical analysis of the extract is not yet carried out. Thus, we still do not have exact information on the polymer's chemical structure. We have tried to gather pieces of information from different studies and come up with a complete hypothetical molecular model. However, this approach may be prone to some errors. As stated in Phillips (2008), "natural polymers are never uniform or simple; their functionality depends on more than one structural feature" (Phillips, 2008). The extract is known to be a complex combination of high molecular weight polysaccharides and proteins. Even after a complete analysis of carbohydrate structure, the term "protein" when it is covalently bonded to a polysaccharide, is rather generic and poorly biochemically defined. The information in the literature of the protein fractions concerning their amino acid composition, folding patterns, or physicochemical characteristics currently is insufficient for a complete structural identification (Kontogiorgos, 2019).

Additionally, the hydrocolloids extracted from fruit seeds are responsible for keeping the seeds moist and enable them to survive in varying climactic conditions (Alizadeh Behbahani et al., 2017; Huang et al., 2008; Koocheki et al., 2009b). Thus, the seed composition is subject to changes depending on the growing conditions, subspecies, age, and other botanical characteristics of the tree as well as harvest season and maturity of the raw material (Buffo et al., 2001). As a result, control of the functionality and reproducibility of the results may be poor. Additionally, the presence of so many unknowns and uncontrollable parameters, introduce an inconsistency that acts as a challenge in interpretation of the results.

1.1.3.1.1 Molecular Weight

The weight-average molecular weight of QSE was reported as 9.61×10^6 Da while the number average molecular was reported as 4.153×10^6 Da (Rezagholi et al., 2019), which is greater than wt. av. molecular weight of most common hydrocolloids used in commercial applications; such as Xanthan Gum (2.0×10^6 Da)(Jindal and Singh Khattar, 2018), gum Arabic (7.2×10^5 Da) (Duvallet et al., 1989), Guar Gum

(1.45×10^6 Da) (Khouryieh et al., 2007), Locust bean gum (1.6×10^6 Da) (Doublier and Launay, 1981), Gellan gum (1.64×10^6 g Da)(Sworn and Kasapis, 1998). High molecular weight biopolymers, though slow to adsorb on the interface, can enhance protein foam stability due to their thickening and gelling properties (Rezaghali et al., 2019).

In another study by Wang et al. (2018), the extract was subjected to a two-step purification process in order to remove proteins and any insoluble matter. The researchers have identified three different homogenous fractions of polysaccharides with a Sepharose fast flow column. These carbohydrate fractions, QSG-1, QSG-2, and QSG-3, had average molecular weights of 1250 Da, 1.4×10^6 Da, and 1529 Da, respectively. The major fraction was identified as the one with the highest molecular weight (QSG-2), and further efforts were carried out to map out the molecular structure of this complex polysaccharide (Wang et al., 2018).

1.1.3.1.2 Monosaccharide Composition

An analysis of the mucilage itself reveals the presence of the monosaccharides, Xyl, Glc, Ara, Man, Gala, with their relative amounts in this order. Different studies identified different monosaccharide proportions but in almost all Xyl and Glc were the principal monosaccharides (Abbastabar et al., 2015; Hakala et al., 2014; Rezaghali et al., 2019; Vignon and Gey, 1998; Wang et al., 2018). Vignon & Gey (1998) revealed that the mucilage contained Ara, Xyl, Gal and Glc in the proportions 8:54:4:34. Uronic acid content was determined to be 20%. Carboxyl reduction followed by total hydrolysis and GC-MS analysis allowed the identification of the uronic acid as 4-*O*-methylglucuronic acid. This finding was supported by Lindberg et al. (1990)'s study that showed that the major water-soluble polysaccharide in the mucilage of quince tree seeds is a partially *O*-acetylated (4-*O*-methyl-*D*-glucurono)-*D*-xylan with an exceptionally high proportion of glucuronic acid residues (Lindberg et al., 1990). Rezaghali et al. (2019) also identified Xyl as the most dominant monosaccharide in quince seed mucilage, followed by Man, Glc and Glca. Thus,

the researchers suggested that the gum consisted of a xylan and/or mannon backbone with glucose, galactose, arabinose and glucuronic acid at the branches (Rezaghali et al., 2019; Vignon and Gey, 1998).

Wang et al. (2018) carried out a more detailed analysis and came up with a different model. The three fractions previously mentioned (QSG-1, QSG-2 and QSG-3) exhibited vastly different monosaccharide compositions. QSG-1 and QSG-3 were both rich in glucose and xylose. QSG-3 was especially high in glucose (4.3:0.9 glucose/xylose ratio). So they hypothesized that glucose and xylose were in the backbones of each of these fractions. QSG-2, on the other hand, contained Ara, Glu, Xyl, Gala and Glca in the molar proportion of 4.0:0.3:15.2: 4.2:3.8. Xylose was the most dominant monosaccharide in this large molecule and presumably was present at the backbone.

Even the first study in quince seed mucilage dating back to 1932, reports the presence of celluloses that were not easily separable from the water-soluble gum by dilute acid or alkali treatments at room temperature (Renfrew and Cretcher, 1932). Despite multiple purification steps in other studies, the cellulosic fractions still remained attached to the water-soluble polysaccharides. It was concluded that the strong interactions between cellulose microfibrils and the acidic glucuronoxylan resulted in their coexistence in the mucilage (Ha et al., 1998; Hakala et al., 2014; Vignon and Gey, 1998) Without any purification, Hakala et al. (2014) reported the crude gum extract to be composed of roughly 46% of celluloses and hemicelluloses. This amount was based on the amount of glucose, and considering the fact that water-soluble fractions also contain glucose at the branches (Wang et al., 2018), cellulose content should be less than that under the light of the more recent findings. Cellulosic portions come from the cellulose nanofibrils stored on the epidermal layer of the seeds and have a tendency to self-assemble into a helicoidal organization when dispersed in water (Ha et al., 1998; Hakala et al., 2014; Renfrew and Cretcher, 1932). This attribute assigns the extract a shear-thinning behavior, slippery texture and possible lubrication function, which was also observed in our samples. The smaller MW fractions (QSG-1 and QSG-3) were likely the cellulose and hemicelluloses.

1.1.3.1.3 Chemical Structure

Most studies when examining the structure as a whole, have found out that the gum was a glucuronoxylan with a very high proportion of glucuronic acid residues (Abbastabar et al., 2015; Lindberg et al., 1990; Ritzoulis et al., 2014; Vignon and Gey, 1998). However, as previously mentioned, the extract is composed of at least three identifiable different homogenous polysaccharide fractions. A detailed chemical structure analysis for separate fractions was only recently carried out by Wang et al. (2018). Thus, here we will try to merge the results of previous studies and reanalyze them under this recent information.

Lindberg et al. (1990) proposed that the extract was composed of a glucan, a galactomanno-glucan and an acidic arabinoxylan fraction. They claimed that the major water-soluble polysaccharide of quince seed mucilage was partially O-acetylated (4-*O*-methyl-D-glucurono)-D-xylan having an exceptionally high proportion of glucuronic acid residues. Vignon & Gey (1998) found the molar proportions of D-Xyl and 4-*O*-methyl-D-GlcA to be 2:1, and also associated the cellulose microfibrils with a glucuronoxylan possessing high proportions of glucuronic acid residues. All these seem to fit with the findings of Wang et al. (2018).

As previously mentioned, QSG-1 and QSG-3 fractions mainly contained glucose and xylose (with QSG-3 being especially high in glucose). This seems to support the earlier findings that claim cellulose microfibrils were glucuronoxylans (Ritzoulis et al., 2014; Vignon & Gey, 1998). The glucose residues, were present as (1→2)-linked glucopyranosyl uronic acid and (1→4)-linked glucopyranosyl at a molar ratio of 2.2:0.3 (Wang et al., 2018). Thus, QSG-1 and QSG-3 can be identified as cellulose and hemicelluloses composed of glucose, xylose, and glucuronic acid residues at different ratios.

The major and bulky proportion (QSG-2) had a more complicated structure. The fraction was very high in xylose (Ara, Glu, Xyl, Gala and GlcA in the molar proportions of 4.0:0.3:15.2:4.2:3.8). The xylose residues were composed of (1/4) and

(1→2, 4)-linked xylopyranosyls at a molar ratio of 5.9:4.5. These (1→4) and (1→2, 4)-linked xylopyranosyls residues produced the backbone with branching points at the 2nd position of xylose sugar ring. Quince seed extract had a degree of branching (DB) value of 0.42, which indicates that it is a highly branched molecule (Whistler, 1954). This branched structure provides easier hydration related to a higher hydrogen bonding capability. The branches contained 1,2- α -D-GlcpA residues and 1, 2, 3, 5-L-Araf, and were terminated with T-GalpA and T-Arap residues. Considering all these, the molecular structure of QSG2 (major polysaccharide fraction in quince seed extract) was proposed as shown in Fig. 1.1;

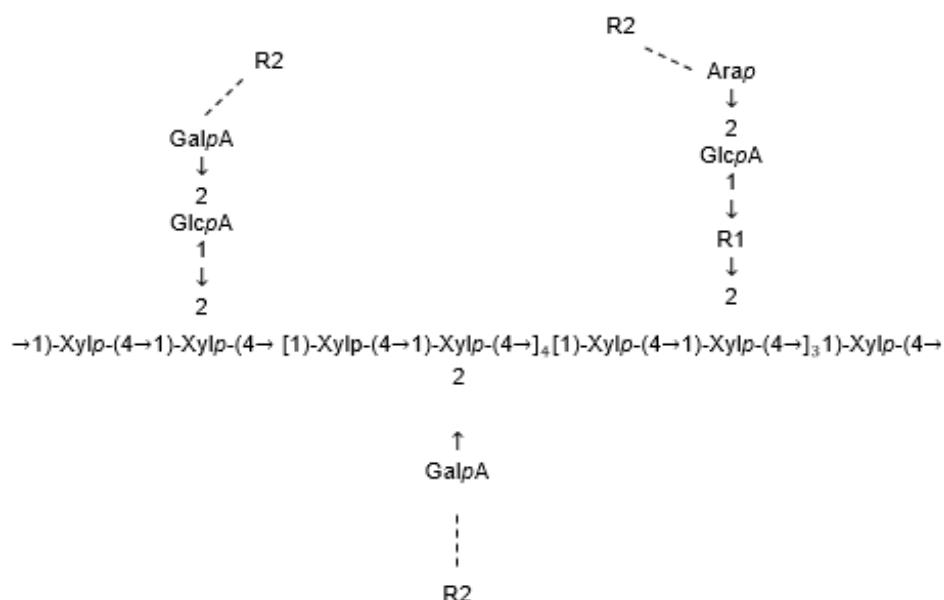


Figure 1.1. Proposed structure of QSG-2 (\rightarrow : Covalent bonds, - - - : *H*-bonds) (R1: 1, 2, 3, 5-Araf or 1, 4-Glcp, R2: -NH₂ group of proteins)

Therefore, overall, QSG-2 is a highly branched heteroxylan composed of a (α →4)- β -D-Xylp-(1→2, 4)- β -D-Xylp backbone with 1, 2- α -D-GlcpA, 1, 2, 3, 5-L-Araf or 1, 4- β -D-Glcp attached to O-2 position forming the side chains. To find the exact positions of uronic acid linkages in the polysaccharide sequence, further attempts are required.

Crude extract contains approximately 20% proteins as determined by our previous study (Emrah Kirtil and Oztop, 2016). Proteins are integrated into the gum structure as apparent in its high emulsification and foaming capabilities (Deng et al., 2019; Emrah Kirtil and Oztop, 2016). Molecular weight of proteins in QSE ranged between 15-60 kDa (Deng et al., 2019). Proteins were, presumably covalently bonded to the extract through the reducing end of the monosaccharides at the ends of the branches (Arap and GalpA) and the amino groups of proteins. Additionally, non-covalent interactions (H-bonding, steric exclusion, electrostatic and hydrophobic) could occur to bind the proteins to the polysaccharide chain. H-bonding, being the strongest among these, can form within polymers containing amide and carbonyl groups in adjacent chains. The partially positively charged hydrogen atoms in N-H groups of one chain can attach to the partially negatively charged oxygen atoms in C=O groups on another (Anal et al., 2019; Reid, 2018). In similar hydrocolloids with surface active properties such as gum Arabic and mesquite gum, proteins are known to be attached to the polysaccharide chain either covalently or non-covalently (Bouyer et al., 2013; Kontogiorgos, 2019; Vernon-Carter et al., 2008). This indicates that the surface-active fractions of the extract are mostly positioned at the branches. This type of graft co-polymer structure was shown to be highly favorable in emulsion stabilization, which will be discussed further in the upcoming sections (Tadros, 2009).

1.1.3.1.4 Amino Acid Composition

Deng et al. (2019) identified the amino acid profile of QSE proteins. CPI contained almost all of the essential amino acids in amounts exceeding that of required by adults as determined by WHO/FAO (“WHO | Protein and amino acid requirements in human nutrition,” 2018). The only exception to this was a slight lack of methionine. Glu (26.81%) and Asp (11.45%) were the most abundant amino acids. These amino acids are known to have excellent antioxidant capacities due to the abundance of excess electrons willing to interact with free radicals. Acidic amino

acids constitute 38.26% of the whole profile. This coupled with the fact that the seeds also contain organic acids (0.5 to 0.8 g/kg) such as citric, ascorbic, malic, quinic, shikimic and fumaric acid explains the extract's negative surface charge at neutral pHs (Silva et al., 2005).

What is even more essential and directly related to our study is the exceptionally high amount of hydrophobic amino acids. Hydrophobic amino acids composed 33.27% of the whole amino acid profile, which was higher than that of some other seed proteins such as cumin seed proteins (32.95%) and peony seed proteins (20.87%) (Z. Gao et al., 2017; Siow and Gan, 2014). A higher amount of hydrophobic amino acids provides more sites on the chain that could attach to the interface and is directly related to the polymer's surface activity (Kontogiorgos, 2019). Basically, for strong adsorption, the molecule needs to be "insoluble" in the dominant medium and has a substantial affinity ("anchoring") to the interface. However, for long term stabilization, the molecule needs to be soluble and be in strong interactions with solvent molecules (Tadros, 2009). So molecules that are composed of sites with both of these two attributes prove to be the most suitable for emulsion and foam stabilization. Considering how soluble the rest of the molecule is, the high hydrophobicity of the proteins is favorable for strong surface adsorption.

Surface hydrophobicity which is associated with the hydrophobic regions exposed at the protein surface is just as essential to surface activity as hydrophobic amino acid composition. It gives the extent of availability of those hydrophobic regions to the interface (Beverung et al., 1999; Sosa-Herrera et al., 2016). Surface hydrophobicity value of QSE proteins was 932.8 (Deng et al., 2019) which was considerably greater than that of *Akebia trifoliata* var. *australis* seed protein isolate (319.4) and *grandis* seed protein isolate (649) (Du et al., 2012; Yu et al., 2017). This high surface hydrophobicity suggests the presence of unaggregated proteins in the QSE protein dispersion that is responsible for the rapid adsorption on the air/water interface.

Disulfide bonds (SS) and Sulfhydryl groups (SH) are essential functional groups in protein conformation, as they grant structural stability to protein macromolecules and is one of the most dominant protein-protein interaction that influences the proteins' native conformation (Hu et al., 2010). Free SH groups and SS bonds of QSE proteins were found as 9.73 $\mu\text{M/g}$ and 19.79 $\mu\text{M/g}$, respectively (Deng et al., 2019). This suggests that most of the cysteine exists as disulfide bonds rather than free SH groups. Disulfide bonds are strong covalent bonds that can interconnect the peptide chains in proteins; thus, proteins with more disulfide bonds tend to have a higher resistance against structural disintegration. Presence of disulfide bonds is also associated with a reduced conformational entropy, a tighter and more stable folded structure, and improved thermal stability (Du et al., 2012). A highly stable structure may not be desirable when used for its surfactant properties, since proteins go through a type of denaturation at the interface, unfolding from its native state to expose the hydrophobic regions to the interface (Dickinson, 2018; Karbaschi et al., 2014; Young and Torres, 1989). A higher stability obstructs and extends this procedure.

1.1.3.1.5 Other physiochemical properties

QSE has a high charge density compared to some other similar polyelectrolyte biopolymers (such as ghatti and Arabic gums) (Rezagholi et al., 2019). This is associated with the high uronic acid content (20% by wt.) in the form of glucuronic and galacturonic acids (Vignon and Gey, 1998). A thorough analysis by Deng et al., 2019, on the change of extract's zeta potential with pH, indicated that the gum had a maximum positive charge of 26.7 mV at pH 2.0 and a minimum negative charge of -38.1 mV at pH 10. The gum had 0 net charge at pH 4.2, which was accordingly identified as the isoelectric point (Deng et al., 2019). The protein solubility, emulsifying properties and foaming capacity of the gum was found to be directly correlated with the zeta charge of the extract, as observed by the overlapping trend curves of these properties with the zeta potential curve. Protein solubility and

emulsifying/foaming capacity of the gum was lowest at its isoelectric point (pH 4.2) and increased at either ends of the pH spectrum. However, basic conditions fortified these properties more than acidic ones, presumably due to the extract's higher content of groups with an affinity towards releasing H⁺ to the solution, resulting in a higher net negative charge.

QSE yielded relatively good thermal stability, with the thermal degradation starting at 95.1 °C (in the form of protein denaturation). The peak denaturation temperature was reported as 103.4 °C, which is higher than that of many plant proteins (Deng et al., 2019). The strong resistance against denaturation was associated with the high content of disulfide bonds and strong hydrophobic interactions in the protein's native state, as supported by the high hydrophobic amino acid content ($\cong 33\%$ by wt).

In our previous research, emulsions obtained with QSE and sunflower oil (20% v/v) yielded a typical shear thinning flow behavior with negligible yield stresses (maximum $\tau_0 \leq 1 Pa$). The power law index (n) decreased and consistency index (k) increased with increasing concentrations (from 0.05 to 1% w/v), which points out to formation of solutions with higher apparent viscosity and stronger pseudoplastic behavior as concentrations increase (Emrah Kirtil and Oztop, 2016). Apparent viscosities also changed with respect to pH, where it was at a maximum around the isoelectric point of pH 4.2 and decreased as you get farther from that to either ends of the pH spectrum (Deng et al., 2019).

Time Domain Nuclear Magnetic Resonance Relaxometry (TD-NMR) is a method whose application in food samples is still new. This dissertation contains applications of NMR in assessment of emulsion stability and measurement of self-diffusion coefficient. Thus, we find it necessary to explain the methods theory and some of its application related to our study.

1.2 Nuclear Magnetic Resonance Relaxometry

Many different methods have been employed for analysis of real or model food systems, yet the destructive nature of most methods poses challenges in time-dependent monitoring of system dynamics. NMR and its imaging based counterpart Magnetic Resonance Imaging (MRI) are relatively new and non-invasive procedures for investigation of colloidal food systems. In literature, the method has been used in particle size measurement, investigation of shear induced particle diffusion, determination of dispersed phase ratio and emulsion stability analysis. This dissertation aims to design various colloidal systems (such as gels and emulsions) by using quince seed extract and to examine microstructural changes in these systems using custom designed NMR sequences.

Magnetic resonance imaging (MRI) is a technique that has been traditionally used in medical applications to investigate the structure of soft tissue as a tool for clinical diagnosis and has emerged from the utilization of radio frequency range pulses as a means of attaining information on the internal structures of human tissues. Nevertheless, MRI has proven to be a strong analytical tool for engineering research as well, due to its accuracy and versatility. Currently MRI can be used in characterization of many biological and non-biological systems (D'Avila et al., 2005). Magnetic Resonance Imaging (MRI), is performed with an NMR instrument equipped with magnetic gradient coils that can spatially gather the data thus creating two dimensional and three dimensional images that display areas having different physicochemical properties (e.g. water content) with different contrasts (D'Avila et al., 2005; Hashemi et al., 2010). In other words, MRI provides spatial distribution of the signal due to presence of gradient in three axes.

NMR Relaxometry on the other hand does not require gradients (except for diffusion measurements). It features the use of a radio frequency (RF) pulse in order to create a temporary disturbance on a sample placed into another static magnetic field. The relaxation of excited signal is then monitored and various information on the object can be attained (Hashemi et al., 2010). In contrast to MRI, for an NMR Relaxometry

experiment the signal attained comes from the whole sample and spatial information is not obtained. However, it is possible to differentiate signal coming from compartments with varying proton environments (e.g. cellular organelles, water compartments with different mobilities in hydrogels).

The non-invasive, non-destructive nature of both methods and the fact that both qualitative and quantitative data on physical and chemical properties of a wide range of samples can be gathered, have made NMR Relaxometry and MRI popular in food related applications (Cornillon and Salim, 2000).

1.2.1 Theory

The basic principle behind the techniques is nuclear magnetism. Nuclear magnetism emerges from the spins of nucleons (protons or neutrons). In order to obtain a net nuclear magnetization moment, the nucleus should contain an odd number of nucleons. For the experiments any element with an odd number of nucleons can be used; though mostly hydrogen is preferred. This owes to hydrogen's abundance in organic samples (presence in water and oil), and high MR sensitivity (H^+ gives the highest signal) (Konez, 2011).

To acquire a signal from a sample; it is initially placed into a large static magnetic field (B_0) (Fig. 1.2). For this purpose, a variety of magnets (i.e. permanent, superconductive) with a wide range of field strengths (0.2 T to 7.0 T); can be employed (Hashemi et al., 2010). When placed into the magnetic field, the protons within the sample align themselves with this external magnetic field (in z direction) (Fig. 1.3).

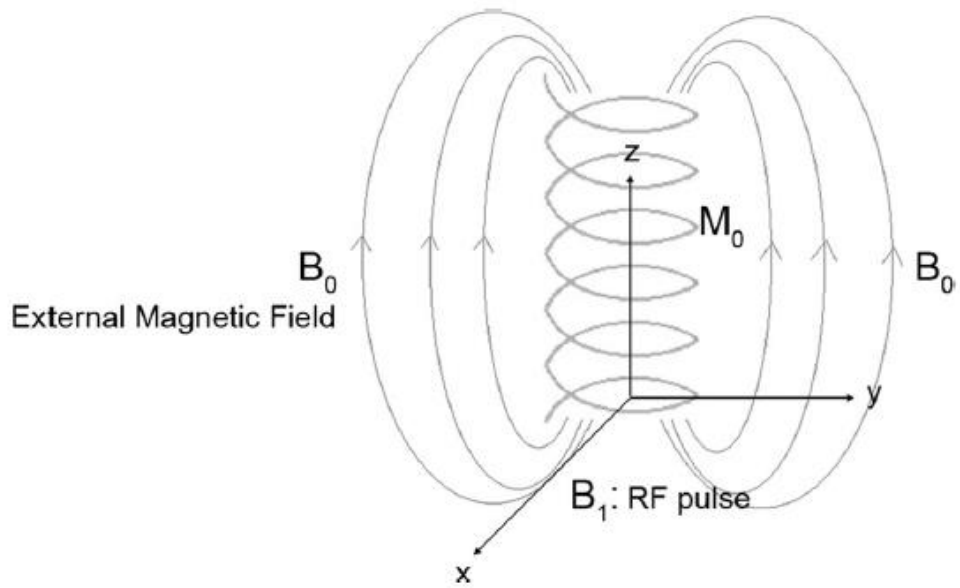


Figure 1.2. Schematic of magnetization occurred by placing a sample into an external magnetic field in z direction (B_0)

Every proton possesses a magnetic moment. As seen in Fig. 1.3, the magnetic moments of protons are aligned either in the same direction or in the opposite direction with the external magnetic field. The former ones possess a lower free energy than the latter. The number of protons that are aligned in the same direction with B_0 are slightly higher than the ones that face the opposite direction. However, this slight difference is enough to create a net magnetic field in the sample in +z direction. This magnetic field is referred to as longitudinal magnetization.

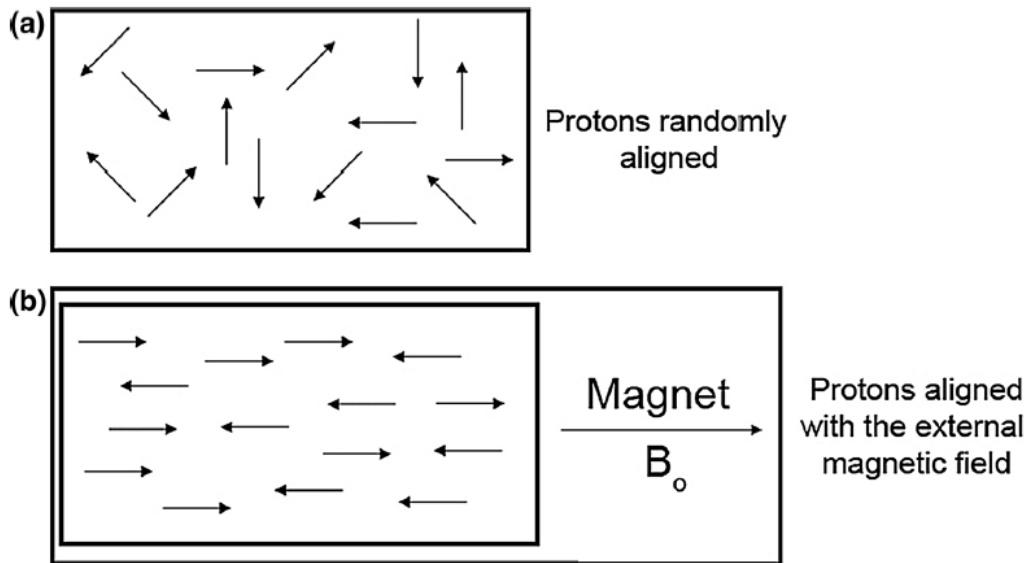


Figure 1.3. Schematic showing the direction that protons are facing in samples. (a) Without the presence of an external magnetic field, (b) under the influence of an external magnetic field of B_0

The protons do not directly face the external magnetic field all the time. Instead, they make a spin top like movement called precession, shown in Fig. 1.4. The frequency of this circular motion is identified with the following relation;

$$\omega = \gamma B_0 \quad (1.1)$$

where ω = angular precessional frequency of proton, γ = gyromagnetic ratio and B_0 = strength of the external magnetic field (Hashemi et al., 2010).

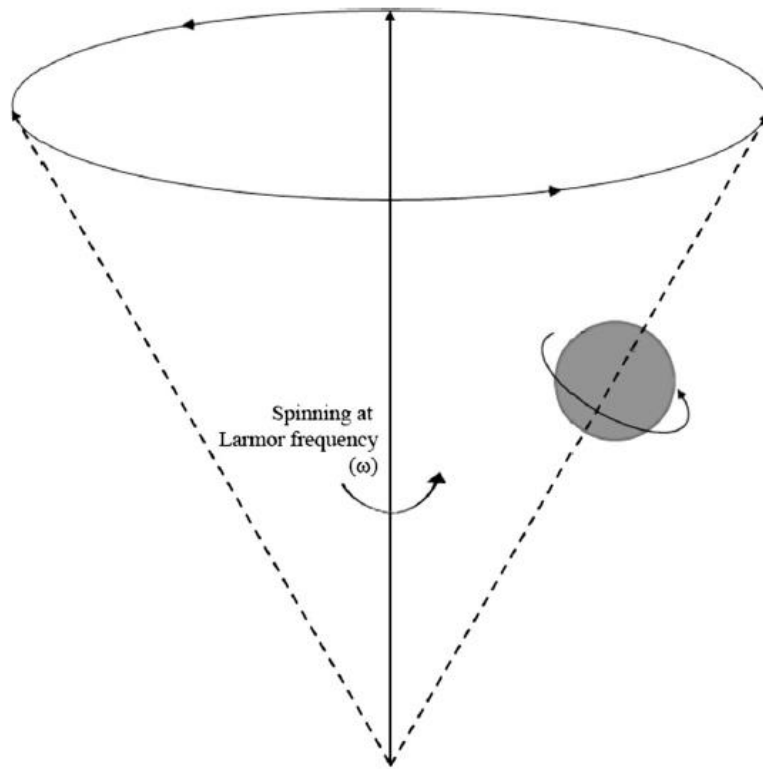


Figure 1.4. Schematic depicting the precessional motion of protons

All the protons have the same frequency owing to the relation above. The magnetization on the xy plane due to this precession is called transverse magnetization. However, the precessing protons are not in-phase. What this means is; though the protons precess at the same frequency they are not at the same position at the same time. An illustration is given in Fig. 1.5. Therefore, the randomly precessing protons cancel each other out and the net magnetization along the xy plane (transverse magnetization) becomes zero (Bernstein et al., 2005).

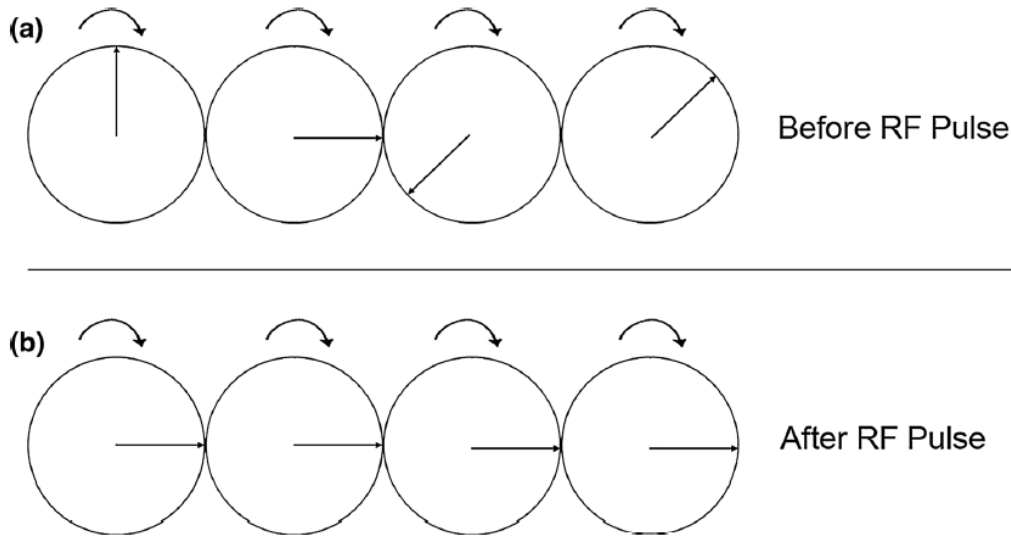


Figure 1.5. Precessional motion of protons. (a) Without an RF pulse application, (b) phasing of protons right after an RF pulse application

To tip away the net magnetization from the z-axis to the xy plane, an RF pulse is applied. Owing to this RF pulse, some of the protons align themselves opposite to B_0 which causes a decline in longitudinal magnetization, also precessional movement of protons get in-phase with each other giving rise to a transverse magnetization. When RF pulse is removed, the protons turn back to their previous states. This process is called relaxation. The relaxation of longitudinal and transverse magnetization is measured to attain information on the sample. Fig. 1.6 displays the stages of disturbance and relaxation through changes of net magnetization (Bernstein et al., 2005; Konez, 2011).

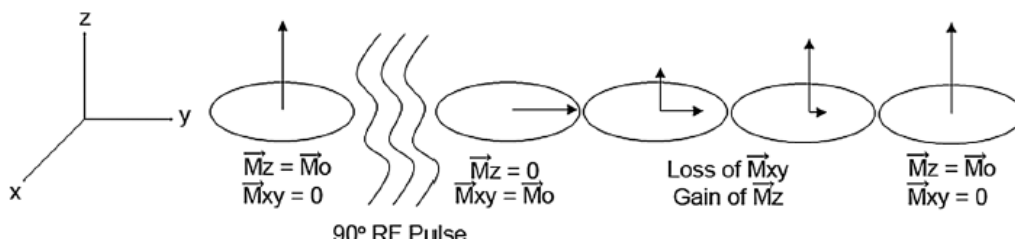


Figure 1.6. Relaxation of transverse (M_{xy}) and longitudinal (M_z) magnetization after application of a 90° RF pulse

Longitudinal relaxation time, T_1 , (also referred to as spin-lattice relaxation time) refers to the time it takes for the spins to realign themselves along the axis of the external magnetic field, and is computed from the recovery curve (displayed in Fig. 1.7) of M_z component of the magnetization vector with the relation;

$$M_z(t) = M_0(1 - e^{-\frac{t}{T_1}}) \quad (1.2)$$

where T_1 is the time constant of magnetization recovery curve, $M_z(t)$ is the component of magnetization along the z-axis, and M_0 is the initial magnetization.

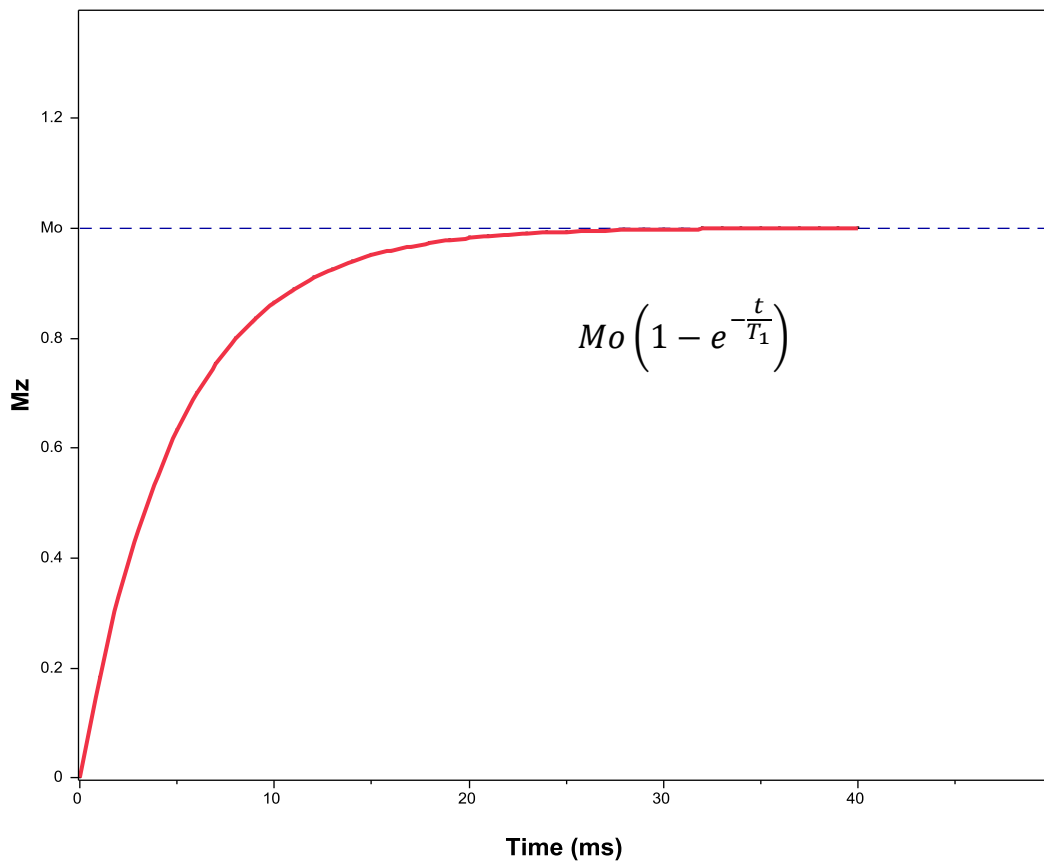


Figure 1.7. A representative exponential relaxation curve of longitudinal magnetization for a sample with a T_1 of 10 ms.

Transverse relaxation time, T_2 , (also referred to as spin-spin relaxation time) refers to the time it takes for the transverse magnetization, to decay to the

equilibrium value of zero. M_{xy} component of the magnetization is shown with the relation;

$$M_{xy}(t) = M_0(e^{-\frac{t}{T_2}}) \quad (1.3)$$

where T_2 is the time constant of magnetization decay curve in Fig. 1.8, $M_{xy}(t)$ is the component of magnetization on the xy plane and M_0 is the initial magnetization (Hashemi et al., 2010).

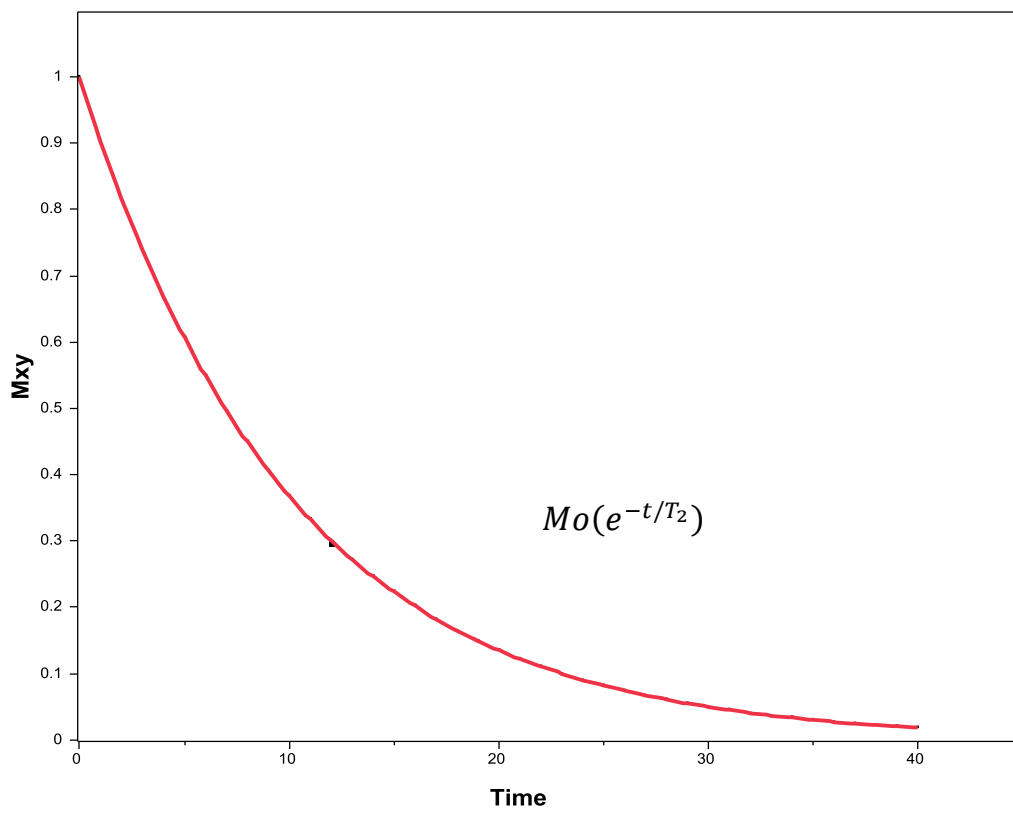


Figure 1.8. A representative exponential relaxation curve of transversal magnetization for a sample with a T_2 of 10 ms.

Molecular tumbling rate (the rotation correlation time) is important in relaxation. The changes of the state of oil and water, as well as their interaction with the surrounding macromolecules can significantly influence T_1 times. T_2 relaxation time (also known as spin-spin relaxation time) is a measure of the effectiveness of energy transfer between neighboring spins, and is expected to be shorter for closer proximity

between molecules. Thus, T_2 is shortest in solids (molecules packed closely resulting in a higher energy transfer efficiency between spins), followed by oil and water. T_2 relaxometry measurements, coupled with T_2 relaxation spectra, are known to yield information on water content, physical properties of water and interaction of water with the surrounding macromolecules (Bernstein et al., 2005; Hashemi et al., 2010; Kirtil et al., 2014; Zhang and McCarthy, 2013, 2012).

1.2.2 Droplet Size Measurement & Emulsion Characterization

Pulsed field gradient spin echo (PFGSE) sequence is one of the most commonly employed sequences in TD NMR studies (Colnago et al., 2015). The method's introduction dates back to late 1960s. Since then, it has been used to measure the water self-diffusion coefficient, viscosity, and droplet size in numerous studies (Colnago et al., 2015; Ling et al., 2016; Mitchell et al., 2014). The characterization is done by exploiting the restricted diffusion of molecules through observation of the geometrical restriction of their mean free path (Guthausen, 2016). However, PFGSE requires an additional hardware accessory that is not present in all TD-NMR spectrometer by default. PFGSE provides rapid characterization of emulsion mean drop sizes and can readily be employed on opaque, concentrated and complex emulsions where other common methods droplet size measurement methods (such as dynamic light scattering, microscopic observations, and ultrasound spectrometry) would not function (Cullen et al., 2001; Guthausen, 2016; Ling et al., 2016). Recent studies on the subject focus on using PFG NMR's strengths to characterize emulsions that would prove challenging to measure with conventional droplet size measurement methods. More recently Ling *et al.* (Ling et al., 2016) have demonstrated that bench-top PFG NMR devices could distinguish between restricted diffusion inside emulsion particles and the transverse shear-induced particle diffusion that takes place as the particles collide during flow along a capillary. The study was the first to use NMR in quantitative measurement of shear induced

diffusion of particles in a concentrated emulsion (Ling et al., 2016). In another recent study by Kock and Colgano (Kock and Colnago, 2016), TD NMR relaxometry was shown to be a rapid monitoring method for to detect chitosan coagulation with pH.

1.3 Surface Chemistry and Interfacial Science

In analysis of a surface-active material, a comprehensive understanding of the adsorption mechanism is crucial in the determination of its functionality. These involve, but not limited to, foaming and emulsification applications that are widely employed in the production of pharmaceuticals, cosmetics, and foods, as well as mining and oil industry (Karbaschi et al., 2014). In addition to industrial applications, examination of the dynamics of interfacial layers is also critical from a fundamental point of view as it generates the possibility of understanding the interaction of molecules, change in their conformations, and the process of molecular aggregation formation (Karbaschi et al., 2014). In literature, for years there have been many studies on surfactant equilibrium adsorption properties (i.e., adsorption isotherms), and with the increasing availability of modern technologies, advanced investigations dedicated to adsorption kinetics, interfacial viscoelastic behavior and changes of the interfacial electric charge are becoming possible (Möbius et al., 2001).

As surface active molecules adsorb to an oil-water interface, changes occurring in interfacial properties are an indication of the individual sub-processes at play (Beverung et al., 1999). These examinations are conducted by a variety of complicated scientific instruments (Arabadzhieva et al., 2011). Out of these, interfacial tension remains to be the easiest and most accessible dynamic quantity of a fluid interface. This method features the formation of a fresh interface and the subsequent determination of interfacial tension as a function of time (Karbaschi et al., 2014). Surface-active molecules, as they adsorb to the interface, decrease the interfacial tension, which facilitates the dispersion of two phases within one another. This is explained by a reduction in Gibbs' free energy of the system (W. Wang et al., 2014). This process though simple in principle provides data related to both the state

and denseness of the interfacial layers and the surfactant exchange between the interface and solution bulk as well as the stability of the dispersion (Arabadzhieva et al., 2011; Benjamins et al., 1996; Liggieri et al., 2002; Ravera et al., 2005; Senkel et al., 1998).

However, the reduced interfacial tension is not the only parameter that governs stability. Kinetically stabilized emulsions by large molecule surfactants were demonstrated to remain stable for years, despite having an interfacial tension of around 30-40 mN/m; whereas emulsions formed by certain lower paraffin hydrocarbons do not remain stable even when the interfacial tension is extremely low (W. Wang et al., 2014). Emulsion and foam stability have been associated with interfacial skin formation, which refers to the generation of a gel-like network and is more dominantly observed in interfacial adsorption of macromolecular species (Freer et al., 2004a). This means, equal surface forces do not essentially mean equal foam or emulsion stabilities. Thus, it would be wrong to explain stability of dispersions solely by the magnitude of repulsive interactions acting normal to the film surface. There happens to be another factor that plays a role in dampening external disturbances, hence preventing film rupture. The barriers against coalescence are thin liquid films, attributes of which are governed by interfacial rheological properties of the respective surfactant layer (Santini et al., 2007).

Dilatational surface rheology method is based on the application of periodic expansion and contraction to the interface with subsequent measurement of the change in interfacial tension as a response to these perturbations (Miller et al., 1996). This methodology gives information on the interface's resistance to deformation. When the dispersion consists of two (or more) fluid phases in particular, deformation of one material implies a deformation of all the constitutive phases. As such, dilatational rheology measurements give us an insight on the stability of dispersed system against disturbances it could infer during formation, processing (such as spraying and atomization), and storage (Rodríguez Patino and Rodríguez Niño, 1999). Additionally, unlike surface tension which operate normal to the surface, interfacial dilatational elasticity is associated with forces that act tangential to the

surface (Santini et al., 2007b). There are a multitude of studies in literature that have demonstrated a correlation between surface dilatational properties and stability of dispersed systems (Cao et al., 2013; Davis and Foegeding, 2006; Langevin, 2000; Stubenrauch and Miller, 2004; Tadros, 2009; Vernon-Carter et al., 2008; Zhang et al., 2011).

1.3.1 Definition of Interface and Interfacial Forces

Interface is defined as the thin boundary region that separates macroscopic chunks of matter from their surroundings and from one another (Berg, 2010). The term “interface” is the more general for any phase boundary, whereas the more commonly used “surface” term only refers to the boundary between a condensed phase and a gas (Berg, 2010; Shaw, 1992). In this review, for consistency, we will use the term “interphase” for any disperse system boundary.

Interfaces are separated from material bulk in their physical and chemical attributes that govern them some unique set of properties. The existence of short range forces of attraction between molecules that define the macroscopic phase (solid, liquid, gas) that the material will exist in, is a well-known phenomenon. Surface and interfacial tension can be readily explained by these forces. All molecules inside the bulk of a liquid is under the influence of equal forces of attraction from all directions on average. However, molecules located at the interface experience unbalanced attractive forces that causes a net inward pull. This phenomenon is depicted for a liquid-air interface in Fig. 1.14.

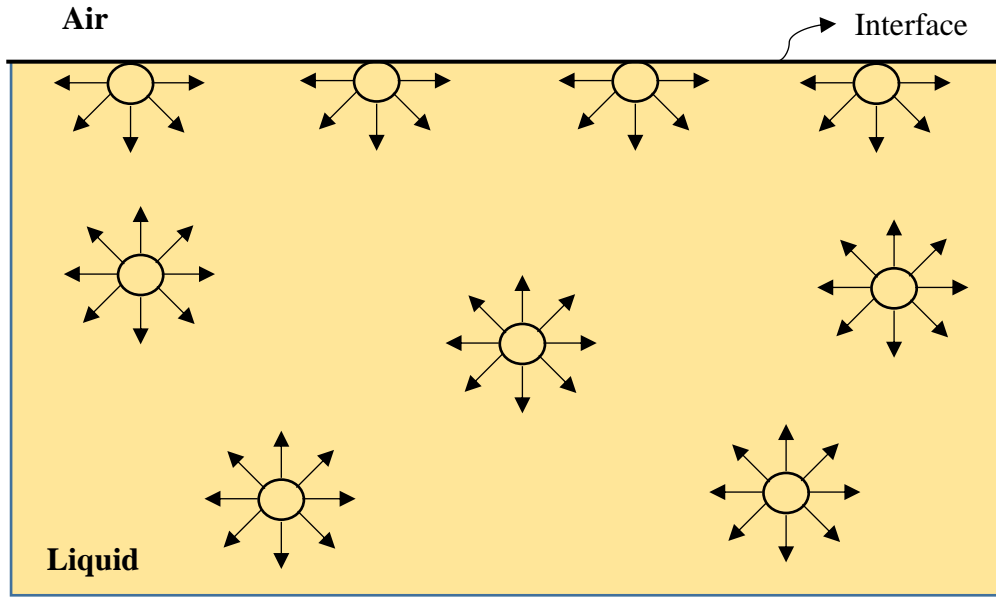


Figure 1.9. Schematic displaying the attractive forces between molecules inside the liquid interior and at the interface

Interfacial tension is born out of this force that is only observed at interfaces. It can be defined in several ways. One common approach is to identify it as the energy necessary to create new surfaces. Accordingly, we can write;

$$dW = \gamma dA \quad (1.4)$$

Where dW is the change in the energy input (J), γ is the interfacial tension (mN/m) and dA is the change in interfacial contact area (m^2). As evident from Eqn. 1, γ (mJ/m^2) is the energy that is required to increase the interfacial area by one unit. Another approach is to identify it as force per unit length exerted on the adjacent phase boundary (N/m) (Berg, 2010; Shaw, 1992). Homogenization methods (in the form of mixing for instance) applied to two immiscible fluids increase the interfacial contact area. The excess energy owing to the increase in area, results in a thermodynamically unstable state for the dispersed system. Emulsifiers, which are amphiphilic molecules, when adsorbed on the interface, decrease interfacial tension, hence increasing the system's thermodynamic stability. For the case of polymers, the

hydrophobic regions attach firmly to the interface or become dissolved inside the oil phase, while hydrophilic regions are dissolved by the water molecules (Dickinson, 2009; Guzmán et al., 2016; McClements, 2009).

1.3.2 Adsorption of Polymeric Surfactants onto a Fluid Interface

The use of polymeric surfactants is commonplace in preparation of many disperse systems, such as in dyestuff, agrochemicals, inks, pharmaceuticals, ceramics, cosmetics, and food products (Arabadzheva et al., 2011; Farahmandfar et al., 2017; Tadros, 2009). Compared to low molecular weight surfactants, they provide prolonged stability and help modify the system's rheological properties (Kontogiorgos, 2019; Seta et al., 2014). In recent years, the public's growing interest has led pharmaceutical, cosmetic, and food industries to spend resources on developing natural alternatives to synthetic polymers (Bouyer et al., 2013; Covis et al., 2014; Dickinson, 1993; Vernon-Carter et al., 2008). For a polymer to exhibit surface activity, it should possess sites with the ability to adsorb on the interface. These sites act as an anchor for the rest of the polymer. In polymers of biological origin, two main categories of anchoring sites have been identified;

- (i) Hydrophobic groups connected to glycosidic residues along the carbohydrate chain (i.e. methyl, octenyl, acetyl, phenolic, etc.)
- (ii) Regions of covalently bound protein or polypeptide (Dickinson, 2018).

Homopolymers, that consist of repeating units of a single type of monomer, are not the most suitable types of polymers for stabilization of dispersions (Tadros, 2009). However, they can be modified by the addition of the aforementioned groups into block and graft type copolymers, which confers them interfacial activity. Typical examples are cellulose derivatives and modified starches where, to a hydrophilic chain, hydrophobic groups are covalently bound (methyl, hydroxypropyl, etc.) in an alternating pattern (BeMiller and Whistler, 2009; Lee et al., 2005; Whistler and

BeMiller, 1973; Xiao and Grinstaff, 2017). Another such modification is the introduction of short peptide blocks into a polysaccharide chain. This is made possible by heating of a dry protein and polysaccharide mixture in controlled temperature and relative humidity conditions which causes the amide groups of proteins to be covalently bound to polysaccharides through Maillard reaction (Akhtar et al., 2002; Jasniewski et al., 2016). This approach, also known as conjugation, proves more advantageous compared to the use of proteins alone or in combination with carbohydrates, since the stabilization function of these conjugates are less affected by changes in pH, temperature and salt content (Anal et al., 2019; Zha et al., 2019). In recent years, many studies have been published on the conjugation of various proteins and carbohydrates to come up with a designed biopolymer with superior properties to already available ones (Bi et al., 2017; Hamdani et al., 2018; Koshani et al., 2015; Zha et al., 2019). Table 1.1 lists some of the recent publications regarding the use of chemically or enzymatically modified carbohydrates and protein-polysaccharide *Maillard* conjugates for emulsion stabilization.

Table 1.1. Summary of some recent publications using biopolymers as emulsion stabilizers either as modified polysaccharides or protein-polysaccharide Maillard conjugates

Polysaccharide	Modification Method	References
Sugar Beet Pectin	Enzymatic Modification	(Siew and Williams, 2008) (Funami et al., 2007) (Chen et al., 2016) (H. Chen et al., 2018) (Zhang et al., 2016)

Table 1.1. (continued)

Inulin	*OSA, DDSA & β -lactoglobulin	(López-Castejón et al., 2019) (Kokubun et al., 2018)
Kudzu Starch	*OSA	(Zhao et al., 2017)
Alginate	*DDSA	(J. S. Yang et al., 2012)
Corn Starch Dextrin	*OSA	(Pan et al., 2019)
Dextran	Glycidyl phenyl ether	(Desbrières et al., 2017)
Waxy Maize Starch	*OSA	(W. Liu et al., 2018) (Ye et al., 2017)
Quinoa Starch	*OSA	(Li et al., 2020)
Cotton Cellulose Nanocrystals	H ₂ SO ₄ Hydrolysis	(Capron and Cathala, 2013)
Corn Fibre Gum	*OSA	(Wei et al., 2020)
Gum Arabic	*AGp	(Han et al., 2019) (Hu et al., 2019)
Brea Gum	--	(Castel et al., 2017)
Asafoetida Gum	--	(Saeidy et al., 2018)

Table 1.1. (continued)

Polysaccharide-Protein Complex	Preparation Conditions	References
Dextran + Wheat protein	Dry heating (1:1) @ 60 °C & 75% RH for 5 days	(Wong et al., 2011)
Corn fibre gum + β -Lactoglobulin, whey protein isolate	Dry heating (1:3) @ 75 °C & 79% RH for 2 days	(Yadav et al., 2012)
Maltodextrin + whey protein isolate	Heating in an aqueous solution @ pH 8.2 (1:1) @ 90 °C for 3,5,8 & 24 h	(Mulcahy et al., 2016)
Galactose + β -Lactoglobulin	Dry heating (1:1) @ 40 °C for 24 h & 50 °C for 48 h, 44% RH	(Corzo-Martínez et al., 2012b)
Dextran + β -Conglycin	Dry heating (10:10) @ 60 °C & 75% RH for 6 days	(Zhang et al., 2012)
Glucose, lactose, maltodextrin & dextran + Rice protein hydrolysate	Heating in an aqueous solution @ pH 11 (1:1), 100 °C for 0, 5, 10, 20, 30 & 40 min	(Li et al., 2013)
Corn Starch + Sodium Caseinate	Heated in an aqueous solution of pH7.5 (1:2.5) @ 75 °C for 3,6,9,12 and 24 h	(Consoli et al., 2018)

Table 1.1. (continued)

Galactose + Bovine sodium caseinate	Dry heating (1:0.2) @ 60 °C for 4 h & 50 °C for 72 h, 67% RH	(Corzo-Martínez et al., 2012a)
Fenugreek gum + Soy whey protein	Dry heating (1:1, 1:3, 1:5) @ 60 °C & 75% RH for 3 days	(Kasran et al., 2013a) (Kasran et al., 2013b)
Pectin + Egg white protein	Dry heating (1:1) @ 60 °C & 79% RH for 6–48 h	(Al-Hakkak and Al-Hakkak, 2010)
Low Methoxy Pectin + β -Lactoglobulin	Dry heating (4:1, 2:1, 1:1) @ 60 °C & 74% RH for 16 days	(Setiowati et al., 2017)
Gum Arabic + Canola protein isolate	Heated in an aqueous solution of pH7 (1:2) @ 90 °C for 15 min	(Jasniewski et al., 2016)
Fructose & inulin + Egg white protein	Dry heating (2:1) @ 60 °C & 79% RH for 3 days	(Jing et al., 2011)

*Abbreviations: OSA: octenyl succinic anhydride, DDSA: dodecenyl succinic anhydride, AGp, arabinogalactan-peptide complex

1.3.3 Properties of an Effective Polymeric Surfactant

The path to better predict the behavior of surfactant polymers before attempting an application would be through a fundamental understanding of the mechanism of adsorption throughout their appropriate operational conditions and even by development of "conformational maps" that clearly defines the conformation that the

material takes at the surface. This approach would provide us the necessary information to design a biopolymer that can take the most compact structure at the shortest amount of time while occupying a thick and elastic interface with extending chains solvated through the bulk phase. There are numerous intrinsic properties that confer a polymer superior interfacial properties, such as chemical identity, electrical charge, distribution of hydrophobic groups along the carbohydrate chain, and how these groups and the rest of the polymer are organized (Dickinson, 2018, 1998). These intrinsic attributes help shape the properties that a functional surfactant polymer should have. A good polymer surfactant that provides effective stabilization against phase separation in dispersions should satisfy the following criteria:

1. Absolute coverage of the particles or droplets by the surfactant. Any uncovered spots may cause flocculation as a consequence of van der Waals attraction or bridging.
2. Strong solvation (hydration) of the main polymer chain
3. Strong affinity (hence, adsorption) of the surfactant molecule to the surface of particle or droplet.
4. A reasonably thick and elastic adsorbed layer to provide adequate steric stabilization
5. A rate of adsorption that is adequate for complete monolayer coverage to occur over a timescale appropriate for the process of emulsion preparation (Dickinson, 2018, 2003; Fler, 2010; Guzmán et al., 2016; Semenov and Shvets, 2015; Tadros, 2009, 2006).

Not the mechanism of polymer adsorption in a fluid-fluid interface will be discussed by going over each of the crucial properties listed above.

1.3.3.1 Absolute Interfacial Coverage

The amount of surfactant is vital in determining the equilibrium interfacial tension. The change in interfacial tension with surfactant concentration follows the trend shown in Fig. 1.15. As the number of molecules adsorbed on the interface (at equilibrium) increases, surface tension decreases. At some point, the interface is saturated with the surfactant. After this point, there is little to no effect of further surfactant addition on interfacial tension. The saturation concentration for the surfactant is called *critical micellization concentration* (CMC) for small molecule surfactants. For polymers, this concentration is referred as *critical aggregation concentration* (CAC). Further polymer addition after CAC, causes the polymers to form aggregates in the dispersed phase (Arabadzchieva et al., 2011; Berg, 2010; Krstonošić et al., 2019). These aggregates are reversible, and in the case of any possible interfacial dilution, they can be redistributed on the interface. If the polymer is soluble in the dispersed phase, the layers they form at the interface are called *Gibbs* monolayers. On the contrary, if the polymers are insoluble in the bulk phase and only spreads at the interface, the layers they form are called *Langmuir* films (Bos and Van Vliet, 2001; Freer et al., 2004a; Radke, 2014; Wüstneck et al., 1996). The reason for this differentiation comes from the difference in the behavior of these two interfaces to any type of interfacial perturbations in the form of expansion or contraction, which is the subject of surface rheology.

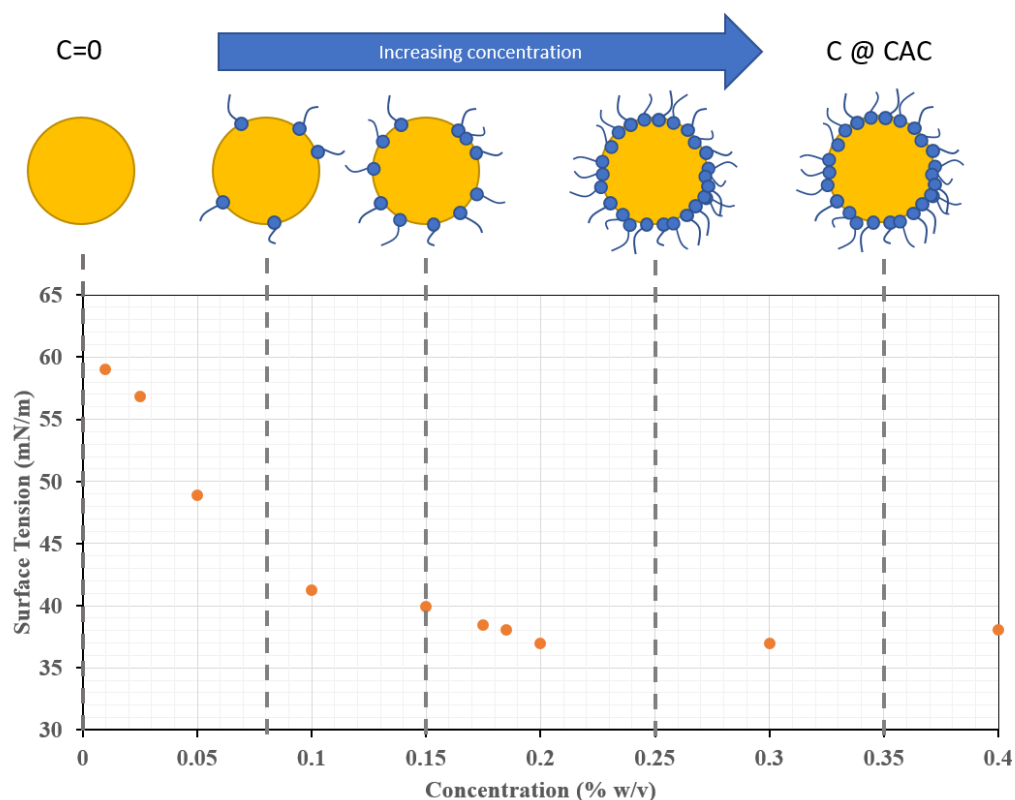


Figure 1.10. A schematic and representative experimental curve demonstrating the change in equilibrium surface tension with surfactant concentration

Thus, by surfactant addition, it is only possible to decrease the equilibrium surface tension up to a certain value. This value changes with the surfactant type and the two phases being dispersed. Surfactant concentration, though, is not the sole parameter in determining the equilibrium interfacial tension. Electrostatic potential of the polyelectrolyte and the conformation of the molecule are also crucial parameters (Young and Torres, 1989). However, at a constant pH and salt concentration, each surfactant displays an intrinsic CMC (or CAC) for the given two phases. At this point it causes the system to acquire the minimum equilibrium interfacial tension for that specific surfactant. However, for some surfactants, even after CMC (or CAC) interfacial tension still decreases. This decrease is much smaller in scope compared to the dependency of interfacial tension on concentration before CMC. Change in interfacial tension beyond that of the critical concentration is usually interpreted to changes on the aggregation

in the bulk phase, which could affect the interface. Another reason could be multilayer adsorption. Some surfactants can form more than a single layer on the interface. Thus, even after saturation, continued molecular rearrangements and multilayer formation can result in a reduction in equilibrium interfacial tension (Beverung et al., 1999; Gashua et al., 2016; Krstonošić et al., 2019; Semenov and Shvets, 2015; W. Wang et al., 2014; Wüstneck et al., 1996).

Complete coverage of the interface by the surfactant dramatically reduces the energy necessary for emulsion formation while also helping the system to preserve its final dispersed state. Bare patches on the surfactant that are devoid of surfactant can act as points of initiation for dispersion destabilization mechanisms such as flocculation and coalescence (Bouyer et al., 2013; Dickinson, 2017; T. Tadros et al., 2004). Therefore, it is clear that surfactant addition will help in stabilizing any type of dispersions, particularly up until its saturation concentration. In the special case of polymeric surfactants, not all of the molecule adsorbs onto the interface. Only the hydrophobic sections that are readily accessible can permanently be attached to the interface. That is why the saturation point (CAC) of these molecules is usually higher. Despite requiring a higher amount of emulsifying ingredient for their formation, once formed, these hydrocolloid-stabilized dispersions tend to be more resilient to destabilization (Anal et al., 2019; Dickinson, 2018; Fler, 2010). Among many others, one of the critical reasons for the prolonged stability with polymer surfactants is their ability to be irreversibly adsorbed (Freer et al., 2004b; Karbaschi et al., 2014), which will be discussed in detail in the upcoming sections.

1.3.3.2 Strong Solvation

The primary requirement for steric stabilization is for the polymer to be soluble in the continuous phase. The role of polysaccharides at interfaces is primarily controlled by their bulk solution characteristics, which are defined thermodynamically by the variations in the free energy of mixing (G_{mix}) of the polymer-solvent system. Description of solution properties dictates the fate of the biopolymer at the interface as it interacts with the solvent. As an example, if the polymer's arrangement at a hydrophobic liquid interface is less favorable than the interactions between polysaccharide chains and solvent, it will avoid positioning itself on the interface. On the contrary, if the solvent cannot properly dissolve the polymer, it may lead to self-association or interfacial anchoring (Fleer, 2010; Netz and Andelman, 2003).

The driving force for mixing is usually entropy, not interaction energy. In other words, despite the common conception of “like dissolves like”, miscible materials do not form a solution solely because the interaction between the molecules of the two materials is more favorable than the interactions between each material's own molecules (Gooch, 2012; Shaw, 1992). We also have to consider the increased entropy associated with the increased volume available to each element. The increase in entropy is proportional to the number of moles being mixed. Polymers have much larger molecular sizes and specific volumes than small molecules, which makes the number of molecules involved in mixing much fewer for the same amount ingredient. On the other hand, the energetics of mixing stay the same on a per-volume basis for small molecule and polymeric mixtures. Therefore, the free energy of mixing for polymers is considerably higher, which makes their solvation less favorable, despite a favorable interaction between solute and solvent. Consequently, for polymers, entropic considerations are more dominant in determining their solvation characteristics. For this reason, we rarely come across with concentrated solutions of polymers.

The total free energy of interaction (G_{total}) for a colloidal system stabilized by polymeric surfactants, is given by;

$$G_{total} = G_{mix} + G_{elastic} + G_{vdW} + G_{electr} \quad (1.5)$$

where each G refers to different components of free energy in the mixed system. G_{mix} is the mixing interaction between the polymer molecules and the solvent, $G_{elastic}$ is related to the loss of conformational entropy of the molecular chains, G_{vdW} is due to van der Waals interactions and G_{electr} is due to electrostatic interactions. Out of these, $G_{elastic}$ and G_{electr} are always positive which indicates repulsion. G_{vdW} , on the other hand, is always negative indicating attraction (Kontogiorgos, 2019; Tadros, 2011, 2009). G_{electr} only exists for hydrocolloids that carry a net electrostatic charge, otherwise it is zero. For polyelectrolytes, the process of solvation is even more complicated as additional factors such as charge density, ionic strength and pH come into effect, and act alongside the steric effects (Fleer, 2010). The unpredictability of electrostatic interactions necessitates a per-case based approach and make it harder to make general assumptions that are valid for any surfactant-solute combination, pHs and ionic strengths. Some carbohydrates have been shown to show interfacial activity only at certain pH ranges such as okra and sugar beet pectin that stabilize emulsions through a combination of electrostatic and steric stabilization effects only at the acidic range of the pH scale (Alba et al., 2016; Leroux et al., 2003).

During mixing, as chains from different materials interact, there occurs some overlapping due to volume reduction. As chains have less space available to move freely, their conformational entropy ($G_{elastic}$) decreases. The sum of G_{mix} and $G_{elastic}$ gives the free energy of steric stabilization ($G_{steric} = G_{mix} + G_{elastic}$). The sign of G_{mix} depends on the *Flory-Huggings* parameter. The Flory-Huggins theory is based on the second law of thermodynamics and assigns two contributions to G_{mix} ; the enthalpy (ΔH_{mix}) and entropy of mixing (ΔS_{mix}) (Flory, 1953).

$$\Delta G_{mix} = \Delta H_{mix} - T\Delta S_{mix} \quad (1.6)$$

$$\Delta S_{mix} = -k[\eta_1 \ln \varphi_1 + \eta_2 \ln \varphi_2] \quad (1.7)$$

$$\Delta H_{mix} = \eta_1 \varphi_2 \chi kT \quad (1.8)$$

where k is the Boltzmann constant, χ is the dimensionless *Flory-Huggins* interaction parameter, φ_1, φ_2 are the volume fractions and η_1, η_2 are the number of molecules of the solvent and polysaccharide molecules, respectively. Upon some rearrangement, ΔG_{mix} becomes;

$$\Delta G_{mix} = kT[\eta_1 \ln \varphi_1 + \eta_2 \ln \varphi_2 + \chi \eta_1 \varphi_2] \quad (1.9)$$

Flory-Huggins interaction parameter (χ) that describes polymer-solvent interactions plays a decisive role here. This parameter is a powerful tool to determine the suitability of a certain solvent to the particular polymer used. If $\chi > 0.5$, $G_{mix} < 0$ such that mixing causes attraction between polymer chains, thus, the material is poorly soluble in the solvent. For $\chi < 0.5$, $G_{mix} > 0$ and mixing causes repulsion between molecules. For this case, the solvent can be termed good since this means the molecules will repel each other and will be dissolved inside the solvent (Kontogiorgos, 2019; Parkinson et al., 2005; Tadros, 2009). There is the rare case where $\chi = 0.5$ ($G_{mix} = 0$). In this case, the polymer chains an ideal conformation when dissolved in the solvent and no excluded effects are observed. In other words, the chains neither attract nor repel each other. The solvent that provides this special case is called the θ -solvent whereas the temperature that this occurs is called the θ -temperature (Alba et al., 2018; Kpodo et al., 2017). There is also the other rare case where despite a negative G_{mix} (attractive mixing interactions), a stable dispersion can be obtained. This is caused by a $G_{elastic}$ high enough to compensate for the attractive energy from G_{mix} ($G_{steric} = G_{mix} + G_{elastic}$), and is reminiscent of sterically stabilized material in a poor solvent (Tadros, 2009).

To acquire a surface-active polymer, one needs repeating sections of insoluble and soluble parts. Thus, for an aqueous solvent; an ideal adsorbing polymer

should have hydrophobic sections with $\chi > 0.5$ so that these sections would prefer attaching to the interface than being solvated by the aqueous phase; while hydrophilic sections should have $\chi < 0.5$, so that the chains would swell and expand in the solvent. This is why homo-polymers are not suitable for stabilization of dispersions, since all of the molecule is soluble in either a hydrophobic or hydrophilic solvent. With polymers that have proteins for hydrophobic sections, any parameter that effects protein hydrophobicity (i.e., pH or ionic strength) also effects *Flory-Huggins* parameter and hence, results in variations of surface affinity (Alizadeh-Pasdar and Li-Chan, 2000; Tucker et al., 2015). *Flory-Huggins* parameter also gives information on the extend of solubility, meaning, for $\chi < 0.5$, the smaller it is, the better the solvent is and vice versa (Flory, 1953). The relative solubilities of various sections of a polymer is especially important for food systems where the solvents and constituents are rather diverse and complex (Berton-Carabin et al., 2018). Consequently, comprehension of the interactions of polymer chains with the solvents is the first step towards systematic design of functional molecules with superior interfacial properties.

As previously mentioned, $G_{elastic}$ is always positive and plays a key role in steric stabilization. It is especially dominant when the particle distances get closer than the thickness of the adsorbed layer (δ). A schematic is shown in Fig. 1.16. G_{mix} displays a very sharp increase with a further decrease in h after the point where the adsorbed layers of two particles start to overlap, for $h < 2\delta$. As h decreases, $G_{elastic}$ similarly shows a sharp increase with h after $h < \delta$. At some distance, comparable to 2δ , G_{Total} exhibits a minimum with h , G_{min} . This min is observed in the region $h > 2\delta$, since according to Eqn.1; G_T also displays a rapid increase for $h < 2\delta$. The value of G_{min} is a function of Hamaker constant (A), thickness of the adsorbed layer (δ) and radius of the particle (R). G_{min} increases with increasing A and R . For constant A and R , it decreases with an increase in δ (such as using a surfactant with a higher molecular weight that adsorbs as a thicker layer on particles). Representational energy vs distance

curves with changing δ/R ratios are given in Fig. 1.17. As δ/R values get larger, G_{min} decreases. A lower difference in free energy (ΔG) indicates enhanced thermodynamic stability for the system. This is the reason why, after some point, systems reach thermodynamic stability, such is the case with nano-dispersions with $R < 50$ nm (Fleer, 2010; Kontogiorgos, 2019; T. Tadros et al., 2004).

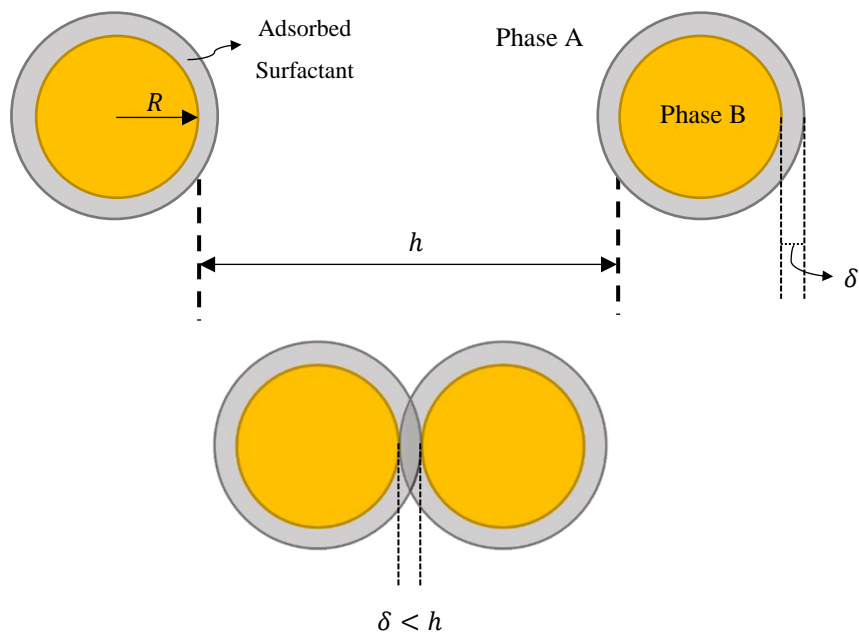


Figure 1.11. Flocculation of droplets in a colloidal system

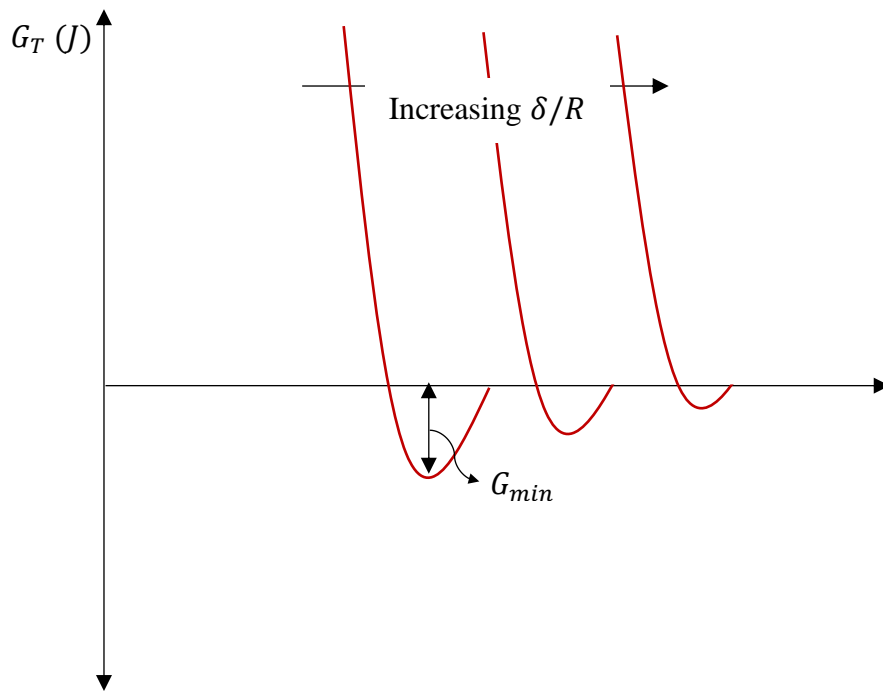


Figure 1.12. Effect of δ/R of Gibbs free energy of a dispersion

1.3.3.3 Strong affinity towards the interface

To act as an emulsifying agent, a polymer should possess sections with interfacial activity. That is, when mixed, it should position itself on the interface and decrease the interfacial tension. This happens spontaneously when polymer-interface interactions are preferred over solvent-interface interactions. There are many established theories that identify interfacial adsorption of small molecule surfactants. Being much larger and more involved in structure, the behavior of polymers is far more unpredictable. Thus, it is much harder to develop approaches that predict polymer behaviors with absolute accuracy (Netz and Andelman, 2003; Pérez-Mosqueda et al., 2013). To treat the problem, two main approaches so far have gained considerable acceptance;

- i. Random Walk Approach
- ii. Statistical Mechanical Approach

Random walk approach bases itself on *Flory's* theories about polymer chain behaviors in bulk solutions where surfaces are considered as reflecting barriers. The most crucial attribute of Statistical Mechanical approach is the distinction of polymer chains into three segments based on their interfacial functionality; trains, loops and tails. Out of these, statistical mechanical method is a more realistic model as, unlike random walk approach, it also considers the possible interactions within the polymer chains itself (Scheutjens and Fler, 1980, 1979). To this day, the most widely accepted and studied theory defining polymer adsorption has been *Scheutjens and Fler (SF) self-consistent field theory* (Ettelaie et al., 2016; Fler et al., 1993; Fler, 2010; Parkinson et al., 2005; Scheutjens and Fler, 1985), which merges ideas from both theories and combines them in a realistic manner. *SF* theory is widely accepted as a useful framework for discussing the relative interactions of commonly used biopolymers (Lips et al., 1991). Therefore, it is *SF* Theory (also referred to as

the step weighted random walk approach) that will be further discussed in this study.

SF theory does not involve any predetermined assumption for segment density distribution. Partition functions for all segments (molecules adsorbed, dissolved, and solvent molecules) were derived in a random approach. All types of chain conformations were represented as step weighted random walks on a quasi-crystalline lattice, which elongates in parallel layers from the interface. A schematic representation is given in Fig. 1.18. According to this approach, the three segments with energy states were identified. Trains are the adsorbed layers, the parts of the molecule that show interfacial activity. These sections are divided by loops and tails that extend to the continuous phase. For an aqueous phase, loops are the hydrophilic section in between the two points of contact with the interface, whereas tails constitute the hydrophilic sections that are free at one end and connected to the interface on the other (Fleer et al., 1993; Scheutjens and Fleer, 1980, 1979).

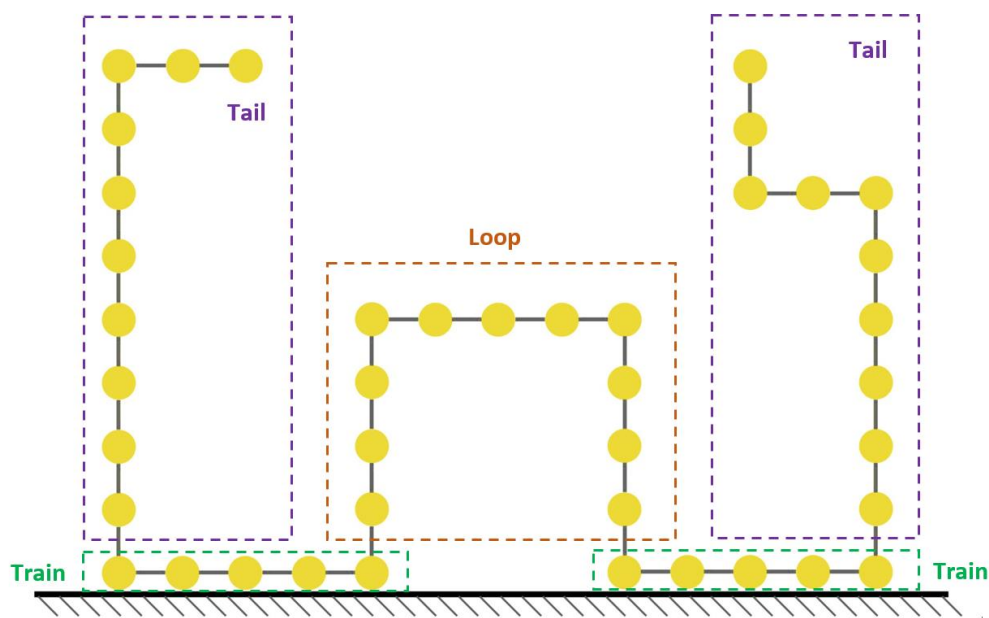


Figure 1.13. Representation of trains-tails-loops configuration of a polymer at an interface

SF theory identifies the different chain conformations that are comprised of varying degrees of the three segments (trains, loops and tails). The partition function is written for different configurations, all of which are treated of connected sequences of segments. Random mixing between the solvent molecules and the polymer segments are assumed in each layer. This approximation is called the mean-field approximation. To calculate the relative amounts of each segment, each step in the random walk is assigned a weighting factor, p_i . This parameter is the result of three contributions;

- (i) Configurational entropy of mixing
- (ii) An adsorption energy, χ^s (=0 for segments far from the interface)
- (iii) Segment-solvent interaction parameter, χ (the *Flory-Huggins* parameter, that was previously mentioned)

Using the weighting factors and a matrix formulation, the statistical probability of the chain taking any conformation can be estimated for any given segment density profile. Eventually, this makes it possible to draw theoretical adsorption isotherms that relate the amount of adsorbed polymer on the interface with respect to bulk concentration (Fleer et al., 1993; Scheutjens and Fleer, 1980, 1979). *SF* theory also confirms the experimental observation of irreversible adsorption of proteins. Proteins, once adsorbed on the interface, even after a washout procedure, were shown to remain attached to the interface (Freer and Radke, 2004). For high chain lengths (as in polymers), the isotherms take the shape called “high-affinity isotherm” that is identified with very low bulk concentrations of polymer in solution (approaching zero) that does not change with desorption (Tadros, 2009). This suggests that almost all of the chains are completely and irreversibly adsorbed.

SF theory provides not only mathematical relations that help predict the interactions between different constituents of dispersed systems, it also builds a fundamental framework of information that helps in explanation of the

underlying mechanism. Some applications include identification of the interactions between mixtures of polymers and colloid particles (Park and Conrad, 2017; Yan et al., 2011; Yang et al., 2006), behavior of weakly charged polyelectrolytes in charged cylindrical systems (Man et al., 2008; Man and Yan, 2010), nucleation in binary polymer blends (Qi and Yan, 2008), self-assembly of diblock copolymers and phase behaviors of diblock copolymer solutions (Suo et al., 2009).

For polymers, *SF* theory gives a very accurate representation of the experimental adsorption isotherm, only except for a difference in shape in the low concentration region. The estimated curves are flat, whereas the real experimentally obtained data results in a more rounded curve. This effect was later identified by Cohen-Stuart et al. and was associated with molecular weight distribution (polydispersity) of polymers (Fleer et al., 1993). The changes in adsorption affinities of smaller and larger molecules in a single polymer solution at varying concentrations result in this irregular behavior. *SF* Theory also makes it possible to predict the relative percentages of each segment in the total distribution for a certain chain length, polymer volume fraction and Flory-Huggins parameter. At low concentrations, fraction of trains (p) is much higher according to *SF* theory. With increasing concentration and surface coverage, p tends to decrease which leaves more room for loops and tails. This case is very similar to typical protein adsorption and is observed in a number of studies (Calero et al., 2010; Davis and Foegeding, 2006; Dickinson, 2018; Padala et al., 2009; Seta et al., 2014). *SF* Theory, being a statistical approach that is made possible by an abundance of assumptions for simplification, may present an idealized case compared to the complex behavior of most biopolymers in nature. However, there is a fairly broad consensus of view, established by extensive experimental proof on well-defined synthetic polymer systems, that the simplified statistical models do indeed present a sound mechanistic foundation for defining the fundamental characteristics of adsorption and colloidal stabilization by all kinds of macromolecules, including natural biopolymers.

Different types of polymers adsorb differently on the interface. The train-loop-tail configuration is more akin for homopolymers and copolymers of block type. For a segment of a molecule to adsorb, the minimum segment adsorption energy, χ^s is required. Though the minimum value of χ^s is fairly small by itself, the overall energy might be high as it is the cumulative energy from all adsorbing segments. For adsorbing homopolymers (i.e., poly(ethylene oxide) (PEO) or polyvinyl pyrrolidone (PVP)), the energy requirement might be exceptionally high due to the abundance of trains segments, and this value is subject to change with molecular conformation (Tadros, 2009).

As previously stated, homopolymers are inferior alternatives as dispersion stabilizers. A literature assessment led us to the conclusion that effective functionality of polymer chains demands a certain degree of repetitive structure similar to that of copolymers. These repetitive segments should be composed of alternating divisions that are either soluble ($\chi < 0.5$) or insoluble ($\chi > 0.5$) in the medium. This definition resembles that of random, block or graft copolymers (Atta et al., 2013; Fleer et al., 1993). There are some synthetic polymers that are especially designed with these properties in mind, such as polyvinyl alcohol (PVA) (Cano et al., 2015). There are also similar copolymers of natural origin. Though natural polymers exhibit somewhat unpredictably patterns of repetition and even with modification of biopolymers, preparation of strictly alternating copolymers are difficult (Voragen et al., 2009; Winning et al., 2009).

The type of polymers that possess the capability to provide effective stabilization to dispersions are of the types $A - B$ (di-block), $A - B - A$ (tri-block), BA_n (graft) and random copolymers. In this representation, A refers to the soluble segments where B are the segments with interfacial affinity. Some examples of A for aqueous media could be polysaccharides, polyethylene oxide, polyvinyl pyrrolidone and examples of B particles that could be inserted into

these chains proteins, polymethylmethacrylate and polystyrene (Guzmán et al., 2016; Tadros, 2009).

Fig. 1.19 illustrates all different types of adsorption based on chain architecture. Most natural polysaccharides tend to have a random copolymer structure. Some examples are cellulose derivatives (i.e. hydroxyl propyl methyl cellulose (HPMC), methyl cellulose (MC), non-blocky pectin). In random copolymers, there is no strict pattern in the distribution of hydrophobic patches; thus, it is more likely for these polymers to have local sections that either contains a higher density of anchoring points or long lateral soluble chains. Consequently, steric stability is hindered (Ettelaie et al., 2003; Voragen et al., 2009; Winning et al., 2009). Chemical and enzymatic modification of polysaccharides by the addition of functionalized groups in between sugar molecules resulting in a random pattern of repetition. Therefore, this type of adsorption is common for polysaccharides with functionalized sugar residues as in chemically modified starches and celluloses (Kontogiorgos, 2019). Polymers with di-block, tri-block or graft type grant more effective steric stabilization. Block copolymers are composed of regions (blocks) of varying lengths that display different affinities towards the solvent. For such a polysaccharide (i.e. citrus pectin) when dissolved in an aqueous-based dispersion, hydrophobic blocks adsorb at the interface while hydrophilic blocks (called “buoy”) extrude laterally towards the solvent, forming a steric stabilization layer (Ettelaie et al., 2003; Voragen et al., 2009; Winning et al., 2009). Graft copolymers, on the other hand, contain side chains or branches whose repeat units have a different composition or configuration than the main chain (Feng et al., 2011). Graft copolymers commonly are the most suitable polymers to grant effective stabilization to dispersions (Liang et al., 1995; Netz and Andelman, 2003; T. F. Tadros et al., 2004). Polymers of BA_n type, where the hydrophilic sections form the side chains, have a brush-like conformation when adsorbed on the interface in an aqueous medium (Fig.5). This mode of adsorption is particularly helpful in steric stabilization, and its efficiency scales with side-chain length (Fleer, 2010;

Marques et al., 1988; Sheiko et al., 2008; Zhao and Brittain, 2000). There are some natural polysaccharides that lie in this category like gum Arabic, mesquite gum and quince seed extract (Ray et al., 1995; Vernon-Carter et al., 2008; Wang et al., 2018). Nevertheless, it should be mentioned that it is quite tricky to assign biopolymers to one of these categories. In reality, most biopolymers of natural origin will fall into an intermediate situation. Even the same biopolymer could change in structure depending on its source. For instance, pectin, exists in forms of either di-block, tri-block or grafted in nature (Voragen et al., 2009; Winning et al., 2009)

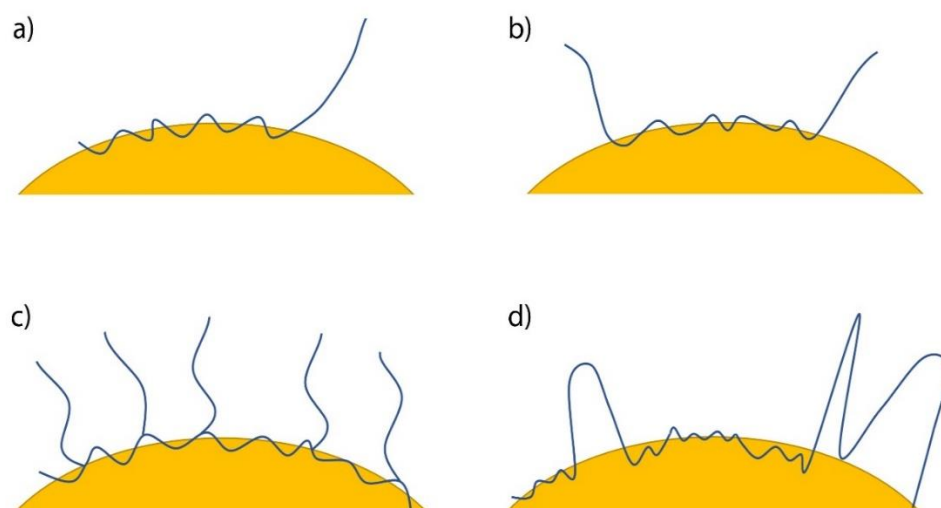


Figure 1.14. Representational adsorption models depending on copolymer type (a) $A - B$ copolymer (b) $A - B - A$ copolymer (c) Graft copolymer (d) Random copolymer

1.3.3.4 Steric Stabilization

Steric stabilization is mainly achieved through the bulky solvated polymer chains that extend laterally into the outer medium. However, the presence of some non-adsorbed material dissolved in the continuous phase can also contribute to dispersion stability through the depletion mechanism (Semenov and Shvets, 2015). As stated before, the soluble regions of the polymer are responsible for this type of stabilization. For polysaccharides conjugated with proteins, the irreversibly adsorbed proteins provide a reliable anchor at the interface for the carbohydrates to execute their steric stabilization functions. Many studies have demonstrated and discussed the importance of carbohydrates in emulsion stabilization (Al-Assaf et al., 2007; Anal et al., 2019; Z. Gao et al., 2017; Jain and Anal, 2018; W. Liu et al., 2018; Shi et al., 2017). A protein-carbohydrate conjugate's stabilization properties were found to be more related to the function of carbohydrates rather than proteins. Many studies on the subject revealed that there was no direct correlation with protein content and emulsion stabilization (Alba et al., 2016; Bai et al., 2017; Huang et al., 2001; Nakamura et al., 2006, 2004; Osano et al., 2014; Sanchez et al., 2018). This led the researchers to the conclusion that protein content, though essential for interfacial activity, was not the determining factor in long term stabilization. Adsorption mechanism, folding patterns of the protein, and length and distribution of polysaccharide chains, all of which determine the extent of steric effects, were found to be more influential for colloidal stabilization.

Here we will focus on stabilization by steric effects, though for systems stabilized by polyelectrolytes, steric effects are complimented by electrostatic mechanisms of stabilization (Napper, 1983; Netz and Andelman, 2003; Rodriguez Patino and Pilosof, 2011). Nevertheless, steric repulsions are the dominant mode of stabilization for all neutral polymers and are common for all adsorbing polymers. Assume two droplets that are entirely covered with a protein-polysaccharide layer of thickness, δ , as shown in Fig. 1.20. If the droplets approach each other so that surface–surface separation distance between the two droplets gets smaller than the thickness of the

sum of the two layers ($h < 2\delta$), the polysaccharide chains start to interact with each other. For such a case, two distinct scenarios could occur;

- (i) Interpenetration without compressions
- (ii) Compression without interpenetration

For the first case, the chains could overlap and penetrate into the gaps (Fig. 1.20a), whereas for the second case, the chains compress each other without overlapping or penetration (Fig. 1.20b) (Flory and Krigbaum, 1950). Both cases create a higher polymer density in the interaction zone ($h < 2\delta$) and influence the conformation of adsorbed polymer. These alterations could trigger changes in the thickness of the polymer layer and fractions of adsorbed segments. In the real case, it is presumably an intermediate between the two, the polymers most likely undergo both interpenetration and compression to varying degrees (Tadros, 2009; T. F. Tadros et al., 2004).

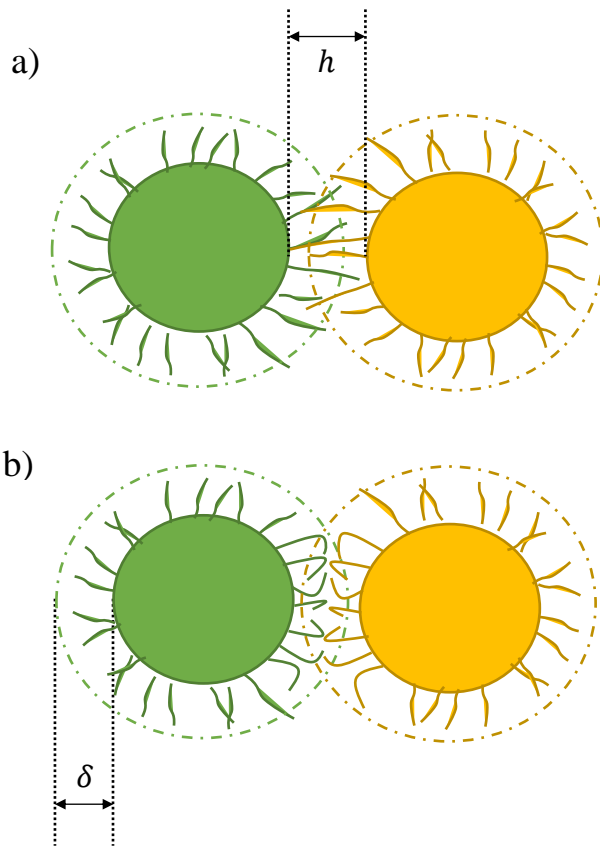


Figure 1.15. Schematic representation of the interaction between particles with adsorbed polymer layers

The local increase in polymer load in the interaction region causes a strong repulsion as a consequence of two effects; (i) A sharp rise in the osmotic pressure in the overlap zone due to unfavorable mixing of polymer chains, assuming the polymer was in favorable solvent conditions. This effect is expressed as osmotic repulsion or mixing interaction, and it is identified with the free energy of interaction, G_{mix} . (ii) Loss of configurational entropy of the overlapping chains. The decrease in entropy is caused by the decrease in available volume for the chains through overlapping or compression. This is termed as volume restriction interaction, entropic or elastic interaction, and it is defined by the free energy of interaction $G_{elastic}$ (Fleer et al., 1993). Remember that steric interaction free energy (G_s) was defined as the combination of G_{mix} and $G_{elastic}$.

$$G_s = G_{mix} + G_{elastic} \quad (1.10)$$

Before the droplet's interactions, there are no steric repulsion effects and assume the chemical potential for the solvent on each droplet layer is defined by μ_i^α , and the volume fraction for the polymer in the layer is ϕ_2 . In the interaction zone (of a volume element dV), the chemical potential of the solvent is changed to μ_i^β where $\mu_i^\beta < \mu_i^\alpha$. This reduction in chemical potential of the solvent is the result of the rise in polymer concentration in the overlap region. In the overlap region, the chemical potential of the polymer chains, on the other hand, displays a sudden rise due to compression or penetration. These changes cause a rise in the local osmotic pressure of the overlap zone; hence the solvent diffuses from the bulk to overlap zone, which sets the particles apart (Kontogiorgos, 2019; Tadros, 2011). The intense repulsive energy born from this effect is calculated by considering the free energy of mixing, G_{mix} which is a function of *Flory-Huggins* (χ) parameter among others. This amounts to the strong influence solubility of the polymer in the solvent plays on steric stabilization (Flory and Krigbaum, 1950).

Van der waals forces, especially when particles are particularly close, become a dominant attractive force that might act against steric stabilization. Van der Waals forces are distance-dependent, weak intermolecular attractions that operate between all molecules and atoms. Three distinct forces contribute to van der Waals interactions: orientation force, induction force, and dispersion force. All these forces are present in interactions between polar molecules. For non-polar molecules, however, the dispersion force is the only interaction existing between molecules (Lu et al., 2005). Ninham and Parsegian (1970) proposed a model for the van der Waals interaction energy for a particle surface covered by an adsorbed layer, given by the following expression;

$$U_A(h) = -\frac{1}{12\pi} \left[\frac{A_{232}}{h^3} + \frac{A_{123}}{(h+\delta)} + \frac{A_{121}}{(h+2\delta)^3} \right] \quad (1.11)$$

Where δ is the thickness of the adsorbed layer, h is the separation distance and A_{232} , A_{123} , A_{121} are distinct Hamaker constants that refer to the characteristics of inter-particle interaction between different particles in vacuum (Ninham and Parsegian, 1970). As seen in Eqn. 7, the relation is strongly dependent on the distance between particles. For particles close enough that $\delta < 2h$, van der Waals forces become very prominent. For polymers however, with the presence of a thick adsorbed layer (a relatively large δ/D ratio), effect of van der Waals forces are less pronounced. It is known that with increasing thickness of the adsorbed layer, molecular attraction energy gradually decreases (Sato and Ruch, 1980). That is why, for systems stabilized by polymeric surfactants, the influence of van der Waals attraction is less notable than other intermolecular interactions.

1.3.3.5 Rate of Adsorption

For effective emulsion stabilization, a hydrocolloid should exhibit surface activity, that is, it should have the capability to reduce interfacial tension. What is just as essential is that, this process should take place over a timescale that is relevant to emulsion preparation. To put it more clearly, the rate of adsorption and the rate of

formation of a transient adsorbed layer should be higher than the rate of droplet collisions, that acts as the primary source of initiation for phase separation (Adams et al., 1998; Walstra, 2002). Observation of the whole process of adsorption from the transient surface tension curves is crucial considering the fact that many surface phenomena occur at distinct time scales. Adsorption process takes place in a number of different steps each identified with distinct rates. From surface tension relaxation curves, it is possible to identify important mechanisms such as diffusion from the bulk phase, relaxation of polymer at the interface, molecular reorientation following adsorption, phase transitions, or even possible retardation of adsorption through steric hindrance (Bos and Van Vliet, 2001; Graham and Phillips, 1980; Serrien et al., 1992; van den Tempel and Lucassen-Reynders, 1983).

Adsorption of macromolecular surfactants generally display a surface tension relaxation profile similar to the one shown in Fig. 1.21. The rate of relaxation follows three distinct regimes, namely;

- i) Induction period (Regime I), region where no change in surface tension is observed
- ii) Monolayer saturation (Regime II), identified as the region of steep tension decline
- iii) Interfacial gelation (Regime III), the final and longest region of relaxation regime with slow decline in ST (Beverung et al., 1999; Freer et al., 2004b).

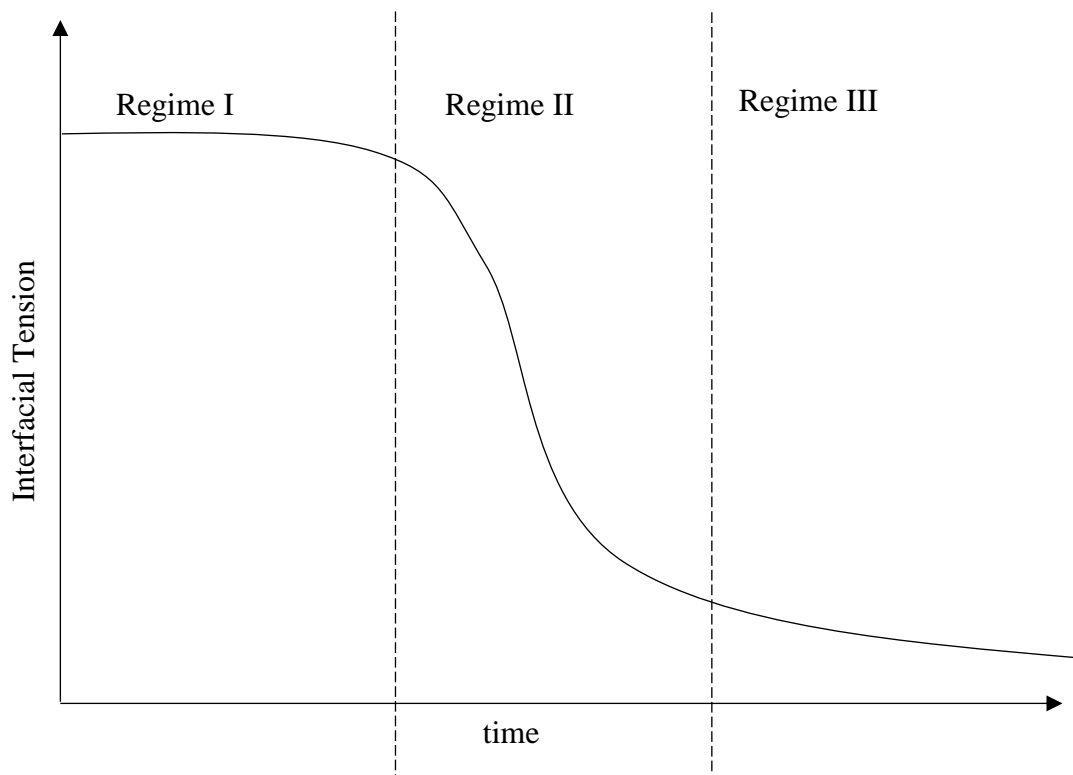


Figure 1.16. A representative curve displaying typical dynamic interfacial tension response of polymeric surfactants in dilute solutions

The duration of initial adsorption of biopolymers onto the void interface is identified as the induction period where the interfacial tension values remain relatively constant at pure fluid values. There is a prevailing effect of the molecular size of the surface-active material on the surface tension, with large molecules like proteins necessitating %99 of monolayer coverage for a surface tension reduction of 1 mN/m. This requirement explains why induction period is only observed for dilute solutions. Many reserachers witnessed induction periods for macromolecular surfactants that have vanished over certain bulk concentrations (Bouyer et al., 2013; Covis et al., 2014; Davis and Foegeding, 2006; Freer and Radke, 2004; Moreira et al., 2012; Pérez-Mosqueda et al., 2013; Wüstneck et al., 1996). After this critical concentration, rate of adsorption increases to a point where adsorption is so rapid that induction finalizes in a duration that exceeds the instrument's limitations, which is perceived as an instant tension decline in relaxation curves.

The presence and duration of an induction period and/or the critical concentration is strongly related to the interfacial affinity of the adsorbing material. The number of surface contacts (trains) also plays a major role in the time it takes for these sections to be exposed to the interface and is one of the reasons behind the induction period (Freer et al., 2004b; Shaw, 1992). Consequently, the differences in induction periods of different protein solutions at the same concentration suggests a difference in protein affinity and/or denaturation kinetics (Beverung et al., 1999). Protein adsorbed in their native state are much more rapid in displaying interfacial activity. Proteins with a random structure were demonstrated to adsorb much faster than globular proteins onto an oil-water interface. Beverung et al. (1999) have reported a much faster rate of adsorption with β -casein than ordered globular proteins and associated this with the irregular structure of the protein that does not require an interfacial unfolding for surface coverage. The lack of an induction period is also a vital requirement for a desirable foaming agent, where an instantly adsorbed material is essential for preventing foam collapse during agitation (Arabadzhieva et al., 2011; Davis and Foegeding, 2006).

Regime II is characterized with a steep decline in interfacial tension and is over within seconds for most proteins (Fig. 1.21) (Beverung et al., 1999). The rapid reduction in surface tension during this period is related to continued loading of the interface accompanied by molecular arrangements within the already adsorbed layer. As proteins relax from their rigid conformations, new side chains from the interior of the protein are exposed to the interface, thereby increasing the number of contacts (trains) between the macromolecular surfactant and the interface. This phenomenon initiates the irreversible adsorption mechanism for proteins (Berg, 2010; Freer et al., 2004b). Another process taking place during this regime that results in reduction in interfacial tension is diffusion of new surfactants from bulk phase. Both routes decrease the interfacial tension by increasing the number of contacts with the surfactant and interface. However, taking into account the induction mechanism in Regime I, it is possible to suspect that denaturation of proteins or conformational changes in the polymer might have a more dominant control over interfacial tension

reduction than diffusion of new surfactants and their initial adsorption. Assuming this is the case, Regime II could be used as an indication of the conformational stability of a polymer (i.e. to measure rate of interfacial unfolding). With protein unfolding the hydrophobic residues are exposed, not only to the interface, but also to some of the adjacent peptide residues that, upon interaction, initiates interfacial gelation (interprotein aggregation) (Anderson et al., 2000). This phase is also the point where initiation of interfacial gelation occurs. Arrangements in the molecular structure of the adsorbed polymer also has a secondary effect. With continued conformational changes, polymer positions itself in such a way that more of the non-adsorbing regions head towards the bulk phase where they are soluble in, which makes room for new molecules to adsorb (Beverung et al., 1999).

Final regime (Regime III) in Fig. 1.21 is characterized by a much slower decline in interfacial tension and can last anywhere between hour to days as evidenced by a number of studies (Cao et al., 2013; Y. Liu et al., 2018; Niño et al., 2001; Sosa-Herrera et al., 2016; Wüstneck et al., 1996). Adsorbed molecules after an initial conformational change to maximize the contact area with the interface, slowly continue to relax to a more energetically favorable conformation. During this period, the final remaining hydrophobic and hydrophilic side chains that are stuck in an unfavorable position, change positions to end in a more energetically favorable environment (Freer et al., 2004b; Shaw, 1992). For an oil-in water emulsion, this causes multiple hydrophilic layers to extrude through the aqueous phase, which causes a more compact adsorbed layer with the molecules getting closer in proximity. As a result, the intermolecular interactions of the adsorbed polymer layer increases. This causes the proteins at the interface to aggregate and form bridges that connect at various points. The resulting crosslinked structure resembles that of an amorphous gel-like network. That explains why Regime III is also called interfacial gelation period. Interprotein aggregation, which initiated in Regime II, finalizes during this stage. For polymers, long-time molecular rearrangements, formation of new interactions between adjacent proteins, breakage and build of non-covalent structure-stabilizing bonds may continue for days which contribute to surface tension

changes, even after surface concentration is saturated. These changes are irreversible and for proteins cause permanent loss of structure and function. For some polymers, the conformational changes might result in attraction between the adsorbed surfactant molecules and those dissolved in bulk phase. This attraction causes additional layers to form over the initial monolayer. Surface tension decline after critical micellization concentration is associated with multilayer formation (Karbaschi et al., 2014; Rühls et al., 2013; Wüstneck et al., 1996).

1.4 Objectives of the Study

Even though first studies on quince seed extract dates back to 1930s (Renfrew and Cretcher, 1932), and there have been several exciting findings (de Escalada Pla et al., 2010; Rakhimov et al., 1985), it is safe to say that this seed with exceptional properties has not received enough attention. To the best of our knowledge, the current literature is still lacking in the number of comprehensive studies regarding the use of quince seed extract for stabilizing dispersions.

In the first part of this dissertation, the goal was to assess the emulsion stabilizing performance of quince seed extract with respect to a commonly used and studied emulsion stabilizer, xanthan gum. The objective was to investigate the physical stability, rheology and microstructure of oil (sunflower oil) in water emulsions, stabilized by 2 % w/v (g/mL) WPI and varying concentrations of xanthan gum and quince seed extracts. This first section of the study made use suspect that the extract might have emulsifying capabilities, which at the time of the study was not yet discovered. Hence, from then on, we focused our efforts on the interfacial activity of this extract.

Next study investigated the air-water interfacial properties of quince seed extract as a representation of how the extract would behave in a real foam application. This study aims to establish how the extract's surface properties (dynamic surface tension and dilatational surface rheology) differ with varying concentrations (between

0.01%-1%), pH's (3, 7, 9, and 11) and ionic strengths (0.1, 0.3, 0.5 M NaCl). The last part of the study concentrates on the examination of the oil-water interfacial properties of quince seed extract, which can serve as a representation of how the extract would function in a real emulsion system. This last part follows a similar experimental design and aims to discover how the extract's interfacial properties (dynamic surface tension and dilatational surface rheology) change with varying concentrations (between 0.01%-1%), pH's (3, 7, 9, and 11) and ionic strengths (0.1, 0.3, 0.5 M NaCl). This way, in a fundamental point of view; the study provides the possibility of gaining more insight on the processes occurring during interfacial adsorption and explaining their mechanism with established theories; as well as, providing the literature with direct information of this novel biopolymer's possible applications and its performance as a stability enhancer in foams and emulsions. We believe the dissertation will also be a great addition to current literature as there currently are no studies that examine interfacial properties of this extract or its potential application in an emulsion or foam system.

CHAPTER 2

MATERIAL & METHODS

2.1 Materials

2.1.1 Characterization of emulsion stabilization properties of quince seed extract as a new source of hydrocolloid

Quinces were of variety *Cydonia oblonga* cultivated in Antalya and was purchased from a local grocery store in Ankara, Turkey. Xanthan gum and sodium azide ($\geq 99.99\%$ trace metals basis) were purchased from Sigma Aldrich. Whey protein isolate having a protein content of 88% (WPI) (*Bipro*, *Hardline* Nutrition, Turkey) was used. Sunflower oil (*Yudum*, Balıkesir, Turkey) was purchased from a local grocery store in Ankara, Turkey. Distilled water was used to prepare all solutions.

2.1.2 Investigation of surface properties of quince seed extract

Quince seed extract (QSE) was obtained from seeds of the quinces purchased from a local grocery store during the winter season in Ankara, Turkey. All solutions were prepared with distilled water further purified using a Milli-Q filtration unit (with a resistivity $\geq 18.2 \text{ M}\Omega \text{ cm}$) (Millipore Co., Bedford, WA). The pH and ionic strength of the solutions were adjusted using HCl (0.1 M at pH1), NaOH (0.1 M at pH13) and NaCl purchased from Sigma-Aldrich Chemie GmbH (Darmstadt, Germany).

2.1.3 Examination of interfacial properties of quince seed extract on a sunflower oil-water interface

Quinces, to prepare the extract, were purchased from a local grocery store during the winter season in Ankara, Turkey. Milli-Q water purified by a Milli-Q filtration unit (with a resistivity > 18.2) (Millipore Co., Bedford, WA) was used for the preparation of all samples. HCl (0.1 M at pH1), NaOH (0.1 M at pH13), and NaCl purchased from Sigma-Aldrich Chemie GmbH (Darmstadt, Germany), were incorporated to adjust the pH and ionic strength of solutions.

2.2 Methods

2.2.1 Characterization of emulsion stabilization properties of quince seed extract as a new source of hydrocolloid

2.2.1.1 Production of quince seed extract

For quince seed extract extraction, a modified version of the method by Abbastabar et al. (2015) was followed. Seeds were removed from the fruit flesh and freeze-dried. In order to maximize surface area for extraction, the seeds were ground prior to soaking into deionized water. Water – ground seed mixture (with a water/solid ratio of 50:1) was continuously agitated at 30°C for 24 hours. The resulting solution was centrifuged, filtered with a cheese cloth and freeze dried to obtain the crude gum extract. The method yielded approximately 8% extract based on dry weight of seeds.

2.2.1.2 Emulsion preparation

Sun flower oil was added into 2.5% w/v (g/ml) WPI solution prepared with distilled water, to obtain dispersions with 2% (w/v) WPI and 20% (w/v) sun flower oil. An O/W emulsion was formed by homogenization at 7500 rpm for 2 min with a high-

speed homogenizer (WiseTis HG-15D, Wertheim, Germany). Xanthan gum (XG) and quince seed extract (QSE) with varying concentrations (0.05%, 0.1%, 0.2%, 0.3%, 0.5%, 0.75% w/v) were added to the emulsions and homogenized at 7500 rpm for 3 min. Sodium azide (0.02% w/v) was added into the final emulsions as an antimicrobial agent. The final compositions of the emulsions are given in Table 2.1. Day 0 measurements were carried out within 1-3 hours of emulsion preparation. For time-dependent measurements, the emulsions were sealed and stored in refrigerator at 4 °C. With a simple chilling test, it was assured that oil did not freeze under refrigeration temperature. No pH adjustments were made to the final emulsions since both WPI concentration and oil-phase volume fraction had little effect on pH. The final pH of the emulsions ranged between 6.5-7.

Table 2.1. Composition of the O/W emulsions

Sample Description	Conc. Of WPI (% w/v)	Conc. of sun flower oil (% v/v)	Conc. of xanthan gum (% w/v)	Conc. of quince seed extract (%w/v)
NOX	2	20	0	0
0.05X	2	20	0.05	0
0.1X	2	20	0.1	0
0.2X	2	20	0.2	0
0.3X	2	20	0.3	0
0.5X	2	20	0.5	0
0.75X	2	20	0.75	0
0.05Q	2	20	0	0.05
0.1Q	2	20	0	0.1

0.2Q	2	20	0	0.2
0.3Q	2	20	0	0.3
0.5Q	2	20	0	0.5
0.75Q	2	20	0	0.75

2.2.1.3 Confocal Microscopy

To study the microstructure of the emulsions, a confocal scanning laser microscope was used (Zeiss LSM 510, Zeiss, Germany). CSLM was operated in fluorescence mode. The samples were excited with an Ar laser at 488 nm, with light emitted back at 585 nm. Nile Red was used to stain the oil phase. In CSLM images, stained oil particles were displayed as bright red spots buried throughout the dark continuous phase.

For staining, a modified version of the method by Sun and Gunasekaran (2009) was followed (Sun and Gunasekaran, 2009). Nile Red was dissolved with acetone to acquire 10% w/v Nile red solution. 20 μ l aliquots of this solution were immediately added to deionized water to obtain a Nile Red concentration of 0.01% w/v. 50 μ l of the dye solution was poured into 5 ml of each emulsion and resulting solution was vortexed for 1 min. The whole staining procedure was carried out with minimal light exposure to dye. Confocal images of samples 0.1X, 0.1Q, 0.5X and 0.5Q were taken within 2 hours of preparation and on day 30.

2.2.1.4 Rheological Characterization

Shear rate ramp and amplitude sweep tests were conducted using a cone-and-plate (40 mm diameter and 4° cone angle, 0.1425 mm gap) dynamic rheometer (Kinexus Dynamic Rheometer, Malvern, UK). For shear rate ramp, shear stress values were recorded for shear rates varying between 0.1 s⁻¹ – 100 s⁻¹, with a total ramp time of

2 min and 20 sample points. Amplitude tests were conducted to measure the linear viscoelastic region of the samples with varying strains of 0.1% - 100% and at a fixed frequency of 1 Hz.

Xanthan gum is known to display shear thinning behavior and its solutions are rheologically characterized with power-law based models (Koocheki et al., 2009a). Observing the shear stress vs shear rate curves and considering the results of previous studies, the samples were fitted to three different models; Newtonian, power-law and Herschel Bulkley model. The only model that consistently yielded good fitting results for all samples ($R^2 > 0.98$) were the power-law model. Thus, for ease of comparison, power-law model was chosen;

$$\tau = K\dot{\gamma}^n \quad (2.1)$$

where τ is shear stress, K is the consistency index, $\dot{\gamma}$ is shear rate, n is flow behaviour index. However, for some of the samples that either display non-negligible values of yield stress (> 1 Pa) or have a flow behavior index (n) higher than 0.9 so that it is almost Newtonian; the results are separately reported inside text (Hosseini-Parvar et al., 2010; Shiroodi et al., 2012). All data All rheological measurements were performed at $25 \pm 0.1^\circ\text{C}$ within 2 hours of emulsion preparation

2.2.1.5 Visual Assessment of Creaming

To assess the relative stability of the emulsions, creaming stability measurements were conducted. The emulsions, within 30 min of preparation, were poured into glass tubes, 10 mm in diameter and 100 mm in height. The tubes were sealed and kept at 4°C , and visually monitored over the course of 5 months. The emulsions displayed a time-dependent separation into a top cream layer and a bottom serum layer. Creaming index was calculated as;

$$CI (\%) = 100 \frac{H_S}{H_T} \quad (2.2)$$

where H_S is the serum layer height, H_T is the total emulsion height (Keowmaneechai and McClements, 2002). Creaming stability data and images were used to evaluate the extent of droplet aggregation in an emulsion. A higher aggregation rate favored particle coalescence, which increased the rate of creaming.

Modified Stokes equation (Gouldby et al., 1991) (Eqn. 2) can be used to predict the creaming rate of non-dilute emulsions with poly-dispersed particles;

$$v = -\frac{\phi_m d_f^2 (\rho_2 - \rho_1) g}{18\eta_1} \times (1 - \phi_f)^{4.65} \quad (2.3)$$

Where d_f is effective floc diameter, ϕ_m is maximum packing volume fraction, ϕ_f is effective volume fraction, g is acceleration due to gravity, ρ_2 is the density of the oil phase, ρ_1 is the aqueous phase, and η_1 is the viscosity of the continuous phase.

2.2.1.6 Particle Size Measurements

A light diffraction based particle size analyzer (Mastersizer 3000, Malvern, UK) was used to analyze the volume–moment mean diameter (d_{43}), calculated as;

$$d_{43} = \frac{\sum n_i d_i^4}{\sum n_i d_i^3} \quad (2.4)$$

where n_i is the number of particles in emulsion with diameter d_i . The refractive index and absorption values used were 1.56 and 0.1, respectively. Emulsions were diluted to between 10^{-4} and 10^{-7} fold with distilled water to prevent possible multiple scattering effects. Particle size measurements were performed at days 0, 4, 7, 10, 14, 20 and 30.

2.2.1.7 Nuclear Magnetic Resonance (NMR) T_2 Relaxometry Experiments

^1H NMR relaxometry experiments were conducted on a 0.5 T NMR spectrometer (SpinCore Inc, Gainesville, FL, USA) operating at a Larmor frequency of 23.2 MHz for ^1H equipped with a 10 mm diameter radio frequency (r.f.) coil. All data were

recorded using a Carr–Purcell–Meiboom–Gill (CPMG) pulse sequence with the repetition delay (TR) set to 5s to minimize the effect of longitudinal relaxation on the signal. The echo delay (TE) was set to 2000 μ s and a total of 16 scans were averaged for each of the 2750 echo maxima points. Mean spin-spin relaxation times (T_2) were calculated by fitting the decaying signal acquired over the 2750 points to the equation;

$$S = M_0 \left(e^{-\frac{TE}{T_2}} \right) \quad (2.5)$$

where S denotes the NMR signal, M_0 is the initial net magnetization. To calculate the T_2 times of distinct compartments, the signal was fit to a bi-exponential curve instead. Samples were poured into 5 mm d. cylindrical tubes and were kept at 4°C until analysis. Approximately 3 hours before measurements, tubes were taken out of the refrigerator and were allowed to equilibrate to room temperature (25°C) before analysis.

2.2.2 Investigation of surface properties of quince seed extract

2.2.2.1 Experimental Design

The experimental design followed is given in Table 2.2.

Table 2.2. Experimental Design for investigation of surface properties of QSE

Sample name	Concentration of QSE (% w/v)	pH	NaCl Concentration (M)
Q0.01	0.01	7	0
Q0.025	0.025	7	0
Q0.05	0.05	7	0
Q0.1	0.1	7	0
Q0.15	0.15	7	0

Q0.175	0.175	7	0
Q0.185	0.185	7	0
Q0.2	0.2	7	0
Q0.3	0.3	7	0
Q0.4	0.4	7	0
Q0.5	0.5	7	0
Q0.6	0.6	7	0
Q0.75	0.75	7	0
Q1	1	7	0
P3	0.3	3	0
P7	0.3	7	0
P11	0.3	11	0
S0	0.3	7	0
S0.1	0.3	7	0.1
S0.3	0.3	7	0.3
S0.5	0.3	7	0.5

Surface-active polymer concentration is one of the most influential factors in determining the system's interfacial properties. Therefore, a wide range of concentrations was investigated. After preliminary trials, the bottom limit was decided as 0.01% (w/v), which is the least amount of polymer that has a notable effect on lowering surface tension. The upper range was chosen as 1% (w/v) since, after this concentration, the viscosity of the solutions was exceedingly high, which is known to hinder the effects of surface relaxation due to molecular diffusion (Pérez-Mosqueda et al., 2013). The concentration span between two consecutive concentrations were narrowed down, getting closer to the identified critical aggregation concentration (CAC=0.165 % w/v). This was done to identify CAC and further examine the properties of the solution at that point.

At a set concentration, the fate of the polysaccharide at the air-water surface, hence the stability of the dispersions, is a function of its molecular characteristics and water-air-polymer interactions. The hydrocolloid's conformation plays a vital role in that regard (Kontogiorgos, 2019). Hydrocolloids dispersed in food systems, that can display a wide range of pHs and ionic strengths similarly can exhibit exceptionally different molecular conformations. Thus, we have prepared solutions with a set amount of QSE (0.3% w/v) and changed pH (3, 7, and 11) and NaCl concentration (0, 0.1, 0.3, and 0.5 M). Samples Q0.3, P7 and S0 are same, yet named differently for ease of comparison of samples with different pHs and salt contents.

2.2.2.2 Quince Seed Extract Preparation

The same procedure from Section 2.2.1.1. was followed for QSE production.

2.2.2.3 Sample Preparation

Pre-determined amounts of QSE were added to Millipore water with pH adjusted (to either 3, 7 or 11), and solutions were mixed with a magnetic stirrer for 3 hours before measurements. QSE was acidic in nature, so to secure the set pHs, a final adjustment was performed after QSE addition. For adjustment of ionic strength of solutions, NaCl was added to Millipore water (pH7) in given amounts to obtain solutions of 0.1, 0.3, and 0.5 M.

2.2.2.4 Dynamic Surface Tension Measurements

For real-time surface tension data acquisition, a Ramé-Hart tensiometer (Ramé-Hart Instrument Co., Netcong, NJ, USA) coupled with an automated dispenser was used. The droplet profile was recorded through a charge-coupled device camera and digitized via a computer with DropImage Advanced software, v.2.2. installed. A schematic of the system is given in Fig. 2.1.

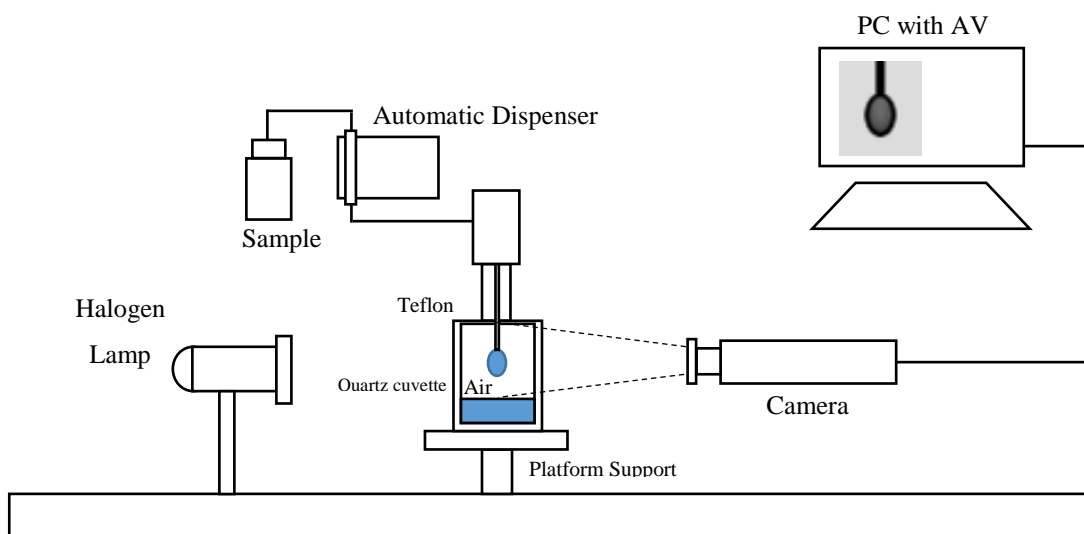


Figure 2.1. Schematic representation of the pendant drop measurement setup for measurement at an air-water interface

Prior to measurements, system was calibrated by a 4 mm diameter spherical standard. Additionally, in-between measurements, syringe and needle were cleaned with ethanol solution followed by an abundant rinse with MilliQ water. Cleanliness of water and the equipment was ensured by measurement of surface tension of MilliQ water. Measurements were pursued if water yielded a constant ST profile at 72 ± 0.5 mN/m for 10 min. Data points were taken each 30 s. The automated pipette system was adjusted to maintain drop volumes constant at 25 μ L.

Pendant drop technique was employed for surface tension measurements. This technique involves the calculation of surface tension from the size and the vertical shape of a drop left hanging under the effect of gravity from the tip of a needle inside a secondary fluid phase (which was air in our case). The needle was connected to a syringe, which was controlled by computer software. Computer automation enables rapid drop image acquisition, edge detection, and fitting of the axisymmetric drop shape to the Young-Laplace equation to find the surface tension. The basic principle of the measurement is based on the variation in pressure across a surface. The two areas of curvature of the surface and surface tension are related to this pressure difference by Young-Laplace equation (Eqn. 1).

$$\Delta P = \gamma \left(\frac{1}{R_1} + \frac{1}{R_2} \right) \quad (2.6)$$

where ΔP is Laplace pressure (the pressure difference across fluid interface), γ is the surface tension, R_1 and R_2 are the orthogonal maximum curvature radii of the elongated drop (Berry et al., 2015; W. Wang et al., 2014). The drop profiles were continuously monitored, hence the reduction in surface tension could be recorded as a function of time.

To distinguish the drop from any outside effects, the tip of the needle was positioned inside a thermostated quartz cuvette at 25 °C, and to keep relative humidity constant inside; the cell was covered with waxed Teflon lids (Fig. 2.1). In order to prevent droplet shrinkage due to evaporation, the cell was filled with 2 ml distilled water. However, even in a saturated atmosphere, monitoring of a single droplet over long periods is limited by evaporation or adsorption effects (Freer et al., 2004a; Wüstneck et al., 1996). Evaporation causes a reduction in surface area, which causes compression and changes in polymer density at the surface.

It was claimed by multiple researchers that it is not possible to identify the real equilibrium of large surface-active polymers (such as proteins). These large molecules, after positioning themselves to the sub-surface (which is the hypothetical layer right beneath the interface), continue to reorient themselves to come up with the most compact and effective conformation that minimizes surface free energy (Beverung et al., 1999; Ward and Tordai, 1946). This procedure might continue even after 24 h (Arabadzhieva et al., 2011; Beverung et al., 1999). However, as previously mentioned, prolonged observation of the same drop is subject to errors due to water evaporation/adsorption effects. For this reason, specimens were subjected to a detailed analysis with a high number of replications for varying time periods. All samples were monitored for 24 h at least twice. Depending on the results of these, we believed reliable dynamic surface tension data could only be taken within the first 2 h. Hence, the remaining replicates were monitored for 60 to 120 min. Due to the large and complex molecular structure of the QSE, relaxation profiles turned out to be quite complicated, and repeatability was rather low. To ensure data reliability, the

total number of replicates varied between 8-10. A two-way analysis of variance was performed (with $\alpha=0.05$).

Within the first 120 min, true adsorption equilibrium, if it really exists, could not be reached. Nevertheless, after a period of 30-60 min, all samples displayed a pseudo-equilibrium where the tension did not change by more than 1 mN/m in 1 h. Equilibrium surface tension data reported are actually these pseudo-equilibrium values. Similar behavior was observed by various researcher studying surface behavior of proteins, and a similar approach was followed (Bouyer et al., 2013; Cao et al., 2013; Sosa-Herrera et al., 2016; Vereyken et al., 2001; Wüstneck et al., 1996).

2.2.2.5 Surface Rheology

2.2.2.5.1 Theoretical Background

Equilibrium surface tension analysis and the rate of surface tension relaxation provides information on surface coverage mechanism. However, viscoelasticity of the interfaces after dilation/compression or shear, being much more sensitive to disturbances in the adsorption layer, gives access to a broader range of information that is not attainable with surface tension analysis only (Karbashi et al., 2014).

In this method, the drop is subjected to a sinusoidal expansion and contraction at a set oscillation frequency. A similar change in surface tension accompanies this infinitesimal periodic change in area. The dilatational surface modulus (ϵ) is defined as the change in surface tension (γ) with a change in surface area (A) (Lucassen and Van Den Tempel, 1972a).

$$E = \frac{d\gamma}{dA} \quad (2.7)$$

There are two contributions to dilatational modulus; dilatational storage modulus (E') and dilatational loss modulus (E'').

$$E = E' + iE'' \quad (2.8)$$

The real part E' (storage modulus) refers to the recoverable elastic energy stored at the interface after a change in surface area. The imaginary part E'' (loss modulus) refers to the energy dissipated through surface tension relaxation by adsorption of surfactants dissolved in the bulk phase. E' and E'' can be calculated independently from the following equations (Cao et al., 2013);

$$E' = \Delta\gamma \frac{A_0}{\Delta A} \cos\theta \quad (2.9)$$

$$E'' = \Delta\gamma \frac{A_0}{\Delta A} \sin\theta \quad (2.10)$$

Where $\Delta\gamma$ is the periodic variation in interfacial stress, ΔA is the periodic variation in interfacial area and θ is the phase angle between the periodic stress and strain curves.

Interfacial stress and surface area are calculated from the following relations;

$$\gamma = \gamma_0 + \Delta\gamma \sin(\omega t + \theta) \quad (2.11)$$

$$A = A_0 + \Delta A \sin(\omega t) \quad (2.12)$$

Where the parameters γ_0 , $\Delta\gamma$, A_0 , ΔA and θ are determined by regression using a least squares method. Once these parameters are found, dilatational storage and loss moduli can be calculated from Eqns. (4) and (5) (Freer et al., 2003). For a more comprehensive review of oscillatory pendant-drop tensiometry theory, readers are advised to refer to (Miller et al., 1996).

2.2.2.5.2 Dilatational Rheology Measurements

Dilatational rheology measurements were carried out with the same Ramé-Hart tensiometer (Ramé-Hart Instrument Co., Netcong, NJ, USA) tensiometer used for dynamic surface tension data acquisition. Oscillation in area was provided by automated dispenser coupled with a gas-tight syringe, capable of oscillating drop area with a maximum frequency of 0.2 Hz. E' and E'' was calculated by fitting of

area, surface tension and time data to the above-mentioned equations using DropImage Advanced Software, v.2.2.

Upon preliminary amplitude sweep measurements, a strain of below %10 was found to be suitable to devoid the samples off non-linear effects (data not shown). For 25 μL sized drops, below %1 strain, the moduli could not be calculated due to instrument restrictions. Other researchers have also stated a strain of below %10 to lie within the linear viscoelastic region (Ravera et al., 2010; Rühls et al., 2013). Nevertheless, most disturbances happening during preparation, storage and transportation of dispersions, cause strains usually higher than this limit. Most interfacial responses in real-life, thus, are non-linear (Mendoza et al., 2014). Eqs. (4) and (5) require the perturbations to be limited to a strain that lies within the linear viscoelastic regime. Consequently, to better represent real life behavior, strain for oscillation measurements was chosen as %8, which lies within the linear region and is close to the upper limit of that. Additionally, in order to maintain a Laplacian shape for the oscillating drop, we restrain attention to drops that are not highly viscous (up to 1% w/v QSE).

Similar to the dynamic-tension measurements, surface rheological response is observed over long time frames. To avoid continually oscillating the same drop for long periods of time, fresh drops are formed for each experiment and aged for 30 min before starting periodic oscillations. Area was varied at a constant strain of 8%, at 10 different frequencies between 0.01-0.1 Hz. 40 points were recorded with a period of 4. Experiments were repeated 5 times for each sample. All experiments were performed at 25 °C.

2.2.2.6 z-Average Particle Size

Quince seed extract mean radius was estimated by calculation of z-average particle sizes using a Malvern Zetasizer (Nano ZS, Malvern, UK). The system was based on dynamic light scattering. The method involves the measurement of self-

diffusion coefficient ($D, m^2/s$) and conversion of it to hydrodynamic diameter (d_H, nm) according to Stokes-Einstein equation.

$$d_H(\times 10^9) = \frac{kT}{3\pi\eta D} \quad (2.13)$$

Where k is the Boltzman's constant and T is the absolute temperature (K) (Y. Yang et al., 2012). Experiments were conducted in standard disposable cuvettes at 25 °C with a refractive index of 1.45 for the biopolymer. To ensure observation of aggregate sizes at the pre-determined concentrations, solutions were not diluted. Nevertheless, as confirmed with the software's data quality section, none of the samples displayed multiple scattering. The results obtained are mean of 100 measurements from three replicates each.

2.2.2.7 Estimation of Diffusion Coefficient from Tensiometer Measurements

Dynamic surface tension can be utilized as a tool for investigating the adsorption mechanism of surface-active material onto interfaces. In the case of low molecular weight surfactants, there are a number of adsorption theories whose accuracy is well-established over many years of research. However, for polymers, no such model exists. In this study, we have used a diffusion-controlled adsorption model. Measurements of the dynamic surface tension are used to define the adsorption process using an approach by Fainerman et al. (1994) to determine the effective diffusion coefficient (Fainerman et al., 1994). The diffusion coefficients found with this approach are D_{eff} values, yet they still provide information about the rate of interfacial layer formation. D_{eff} calculated this way is expected to lie within a certain range. Unrealistically low results would indicate that processes slower than diffusion determines the rate of adsorption, whereas too high values point out to an error in the fitting or the lack of assumptions necessary to identify a process seemingly faster than diffusion (Wüstneck et al., 1996).

To distinguish between the initial and final rate of adsorption, two diffusion coefficients at the time dependencies as $t \rightarrow 0$ and $t \rightarrow \infty$ will be determined. For low protein concentrations and as $t \rightarrow 0$, diffusion coefficients can be estimated solely from $\gamma - t$ dependencies without the requirement of any particular conditions (such as obeying any well-recognized adsorption isotherm).

Calculation of D_{eff} at long times, on the other hand, requires the information of the thermodynamic equilibrium state of the interfacial layer. For proteins that may never reach a true equilibrium, this knowledge does not exist. In our case, the quasi-equilibrium points were used. The identification of these were previously stated in Section 2.2.2.4. Taking all these into account and the fact that polymers behave differently at short and long times, the two diffusion coefficients ($t \rightarrow 0$ and $t \rightarrow \infty$) does not necessarily have to be in good agreement (Freer et al., 2004a; Wüstneck et al., 1996).

$D_{eff\ t \rightarrow 0}$ can be determined from the following relation;

$$D_{eff\ t \rightarrow 0} = \frac{\pi}{4} \left[\frac{1}{RTc} \left(\frac{d\gamma}{dt^{0.5}} \right)_{t \rightarrow 0} \right]^2 \quad (2.14)$$

where T is the temperature (K), c is the concentration (M), R is the gas constant ($\frac{J}{mol.K}$) and γ is surface tension ($\frac{N}{m}$) (Wüstneck et al., 1996). $\frac{d\gamma}{dt^{0.5}}$ is the slope of the initial linear section of γ vs $t^{0.5}$ curve. However, choice of method (pendant drop) limits the acquisition of surface tension at $t = 0$ (where surface concentration $\Gamma = 0$). Even the first measurement taken right after the drop was full formed at the tip of the needle does not give the correct surface tension at $t = 0$. Especially for higher surface-active polymer concentrations, the initial adsorption will presumably be > 0 . Thus, γ was extrapolated to $\gamma = \gamma_0$, where γ_0 is the surface tension of water. The measurements were repeated if the time when $\gamma = \gamma_0$ differed from 0 by more than 3 s. If this prerequisite was met, the results were deemed reliable.

To find $D_{eff\ t \rightarrow \infty}$, the following relation can be used;

$$\left(\frac{d\gamma}{dt^{0.5}}\right)_{t \rightarrow 0} = \frac{2RT\Gamma^2}{c} \left(\frac{\pi}{4D_{eff} t \rightarrow \infty}\right)^{0.5} \quad (2.15)$$

where Γ is the surface excess concentration. Assuming the polymer's adsorption is identified by Gibb's adsorption isotherm, given as;

$$\Gamma = -\frac{c}{RT} \frac{d\gamma}{dc} \quad (2.16)$$

We obtain;

$$D_{eff} t \rightarrow \infty = \pi \frac{\left(\frac{d\gamma}{d\ln c}\right)^4}{\left(RTc \left(\frac{d\gamma}{dt^{0.5}}\right)_{t \rightarrow \infty}\right)^2} \quad (2.17)$$

Though Gibb's equation may not ideally represent polymer adsorption mechanism, there are many approaches used for proteins that are based on Gibb's equation (Radke, 2015, 2014; Wüstneck et al., 1996; Young and Torres, 1989).

2.2.2.8 Estimation of Diffusion Coefficient using NMR Relaxometry Measurements

NMR experiments were conducted on a 0.32 T NMR system (Spin Track SB4, Mary El, Russia). Self-diffusion coefficients (SDCs) of QSE samples were determined using a pulse gradient spin echo sequence with three 22 μ s, 90° pulses. The time intervals between the first and the second pulses and between the second and the third pulses were 2 ms and 60 ms, respectively, with an acquisition time of 500 μ s. The duration of the pulsed gradient field was 1 ms, and the gradient strength was 1.66 x 10⁻² T/m. All NMR measurements were repeated four times for each sample and NMR results (gradient vs amplitude data) were fitted to a suitable equation to estimate self-diffusion coefficients using MATLAB. All fittings resulted in R² > 0.95.

2.2.3 Examination of interfacial properties of quince seed extract on a sunflower oil-water interface

2.2.3.1 Experimental Design

The experimental design is presented in Table 2.3.

Table 2.3. Experimental Design for investigation of interfacial properties of QSE

Sample name	Concentration of QSG (% w/v)	pH	NaCl Concentration (M)
Water	0.01	7	0
Q0.02	0.025	7	0
Q0.05	0.05	7	0
Q0.1	0.1	7	0
Q0.2	0.2	7	0
Q0.3	0.3	7	0
Q0.4	0.4	7	0
Q0.5	0.5	7	0
Q0.75	0.75	7	0
Q1	1	7	0
P3	0.3	3	0
P7	0.3	7	0
P11	0.3	11	0
S0	0.3	7	0
S0.1	0.3	7	0.1
S0.3	0.3	7	0.3
S0.5	0.3	7	0.5

Out of the many factors that shape a system's interfacial properties, surfactant concentration is one of the most influential. Therefore, concentration was determined

as the main parameter for this study. After some preliminary experiments, the bottom and upper limit was chosen as 0.01 and 1% w/v, respectively. Concentrations lower than 0.01% had next to no effect on interfacial tension, whereas concentrations higher than 1% were exceedingly high, which could introduce a viscosity induced hindrance to polymer diffusion.

The molecular conformation is another vital element determining interfacial properties (Kontogiorgos, 2019). Thus, factors such as pH and ionic strength that play a key role in the molecular arrangement were chosen as the other independent variables for the study. For this purpose, solutions were prepared with a constant QSE concentration (0.3% w/v) and adjusted to pHs 3, 7, and 11 and NaCl concentrations of 0.1, 0.3, and 0.5 M.

2.2.3.2 Quince Seed Extract Preparation

The same procedure from Section 2.2.1.1. was followed for QSE production.

2.2.3.3 Sample Preparation

Pre-determined concentrations of QSE were added to Milli-Q water with pH set (to either 3, 7 or 11), and solutions were mixed with a magnetic stirrer for 3 hours prior to analyses. QSE was acidic in nature, so to ensure the set pHs, an additional adjustment was performed after QSE incorporation. For modification of ionic strength of solutions, NaCl was added to Milli-Q water (\cong pH7) in assigned amounts to achieve solutions of 0.1, 0.3, and 0.5 M.

2.2.3.4 Dynamic Interfacial Tension Measurements

For real-time surface tension data acquisition, a Ramé-Hart tensiometer (Ramé-Hart Instrument Co., Netcong, NJ, USA) coupled with an automated dispenser was used. The droplet profile was monitored through a charge-coupled device camera and

digitized via a computer with DropImage Advanced software, v.2.2. installed. A schematic of the system is given in Fig. 2.2. Pendant drop method was employed. This method involves the acquisition of surface tension data by relating the shape that a drop of a primary fluid takes inside a secondary fluid, to interfacial tension by using the Young-Laplace relation (Berry et al., 2015; W. Wang et al., 2014).

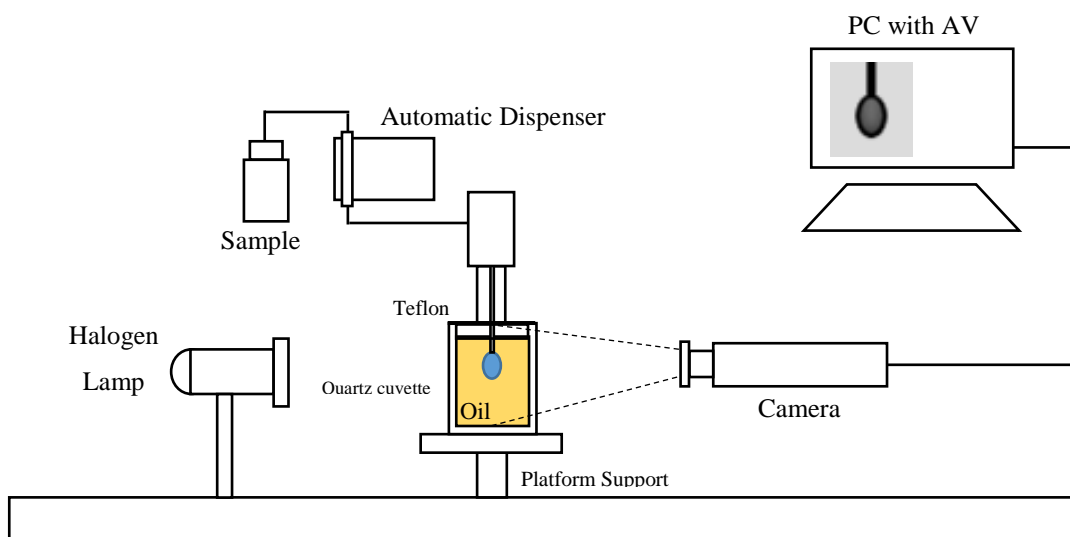


Figure 2.2. Schematic representation of the pendant drop measurement setup for measurement at an oil-water interface

The system was calibrated with a 4 mm diameter spherical standard prior to analyses. In-between measurements, syringe, and needle were washed with ethanol solution followed by an abundant rinse with Milli-Q water. The purity of water and cleanliness of the equipment were assured by measuring surface tension of water used. We have analyzed if water generated a constant ST profile at 72 ± 0.5 mN/m for 10 min. Measurements were taken each 30 s. The automated pipette system was adjusted to maintain drop volumes constant at 25 μ L.

The needle tip was positioned inside a thermostated quartz cuvette at 25 °C (Fig. 2.2). The cuvette was filled with approximately 30 ml of sunflower oil. Sunflower oil was pre-saturated with water by mixing it with water (1:1 ratio) by a magnetic

stirrer for 24 h. The mixture is left to settle, and the separated oil phase is subsequently removed from the water to be used for analysis.

Surface active polymers, with their large and complex molecular structure, continue to reorient, and change their molecular arrangement even after being positioned to the interface. This process could last over a day (Arabadzhieva et al., 2011; Beverung et al., 1999; Ward and Tordai, 1946). However, such a long measurement of droplets might introduce problems of their own. In our case, we could not ever achieve perfect equilibrium. The interfacial tension kept decreasing even after 24 h. What is interesting is that, this continuous reduction was observed even for water. This could be related to the contaminants in oil that exhibit surface activity. A similar behavior was observed by other researchers in the past (Bouyer et al., 2013; Seta et al., 2014). Additionally, even after the pre-saturation of oil, it was able to dissolve water. Though the solubility is minimal, it still caused enough reduction in the interfacial area to affect interfacial tension significantly.

After prolonged monitor of most of the samples for at least 12 h, we have decided that reliable dynamic surface tension data could be taken within the first 60 min for most samples. Within this time, true adsorption equilibrium is not achieved. Nevertheless, the reduction in interfacial tension slowed down to < 1 mN/m per 1 h, which was identified by the researchers as a pseudo-equilibrium state. Equilibrium interfacial tension data shown in Fig. 3.16 are the interfacial tension values that this pseudo-equilibrium state starts. To maximize data reliability, 8-10 measurements were taken from each sample. To identify the statistical significance of the difference between samples, a two-way analysis of variance test was performed (with $\alpha=0.05$). Similar behavior was witnessed by several researchers examining surface behavior of proteins, where a similar approach was pursued (Bouyer et al., 2013; Cao et al., 2013; Miller et al., 1996; Sosa-Herrera et al., 2016; Vereyken et al., 2001).

2.2.3.5 Dilatational Interfacial Rheology

Dilatational rheological measurements were performed with the Ramé-Hart tensiometer (Ramé-Hart Instrument Co., Netcong, NJ, USA) tensiometer likewise used for dynamic surface tension data acquisition. Oscillation in area was provided by automated dispenser coupled with a gas-tight syringe, capable of oscillating drop area with a maximum frequency of 0.2 Hz. Modulus data was calculated by mathematical fitting of area, surface tension and time data with the help of DropImage Advanced Software, v.2.2.

The dilatational interfacial modulus (ε) is described as the change in surface tension (γ) with a change in surface area (A) (Lucassen and Van Den Tempel, 1972a) (Eqn. 1). The method involves the introduction of a sinusoidal expansion and contraction to the drop in order to observe the subsequent change in interfacial tension. Dilatational modulus has two contributors;

$$\varepsilon = \frac{d\gamma}{dA} = \varepsilon' + i\varepsilon'' \quad (2.18)$$

where ε' is dilatational storage modulus and ε'' is dilatational loss modulus. The real part ε' (storage/elastic modulus) is associated with the recoverable energy stored at the interface, whereas the imaginary part ε'' (loss/viscous modulus) is associated with the energy dissipated through relaxation of interfacial tension through adsorption of surfactants dissolved in the bulk phase. (Cao et al., 2013). For an ideally elastic interface, there is an instantaneous change in interfacial stress following the change in interface area without any delay (Mendoza et al., 2014). Nevertheless, for most real systems there is a phase angle (θ) born out of the delay between the periodic oscillations of area and interfacial stress curves (Freer et al., 2004a).

Upon preliminary amplitude sweep measurements, a strain of < %10 was found to be suitable to rid the samples of non-linear effects (data not shown) identified with a modulus dependency on the applied strain. The presence of a strain dependency

invalidates the relations employed to estimate dilatational moduli. Thus, perturbations were carried out at a strain of 8%, which belongs to the linear viscoelastic region, and is close to the upper limit so that it might better represent disturbances occurring in real life (Mendoza et al., 2014).

As in the dynamic-tension measurements, the interfacial rheological response is monitored over long time spans. To avoid continuously oscillating the same drop for extended periods, new drops are formed for each measurement and aged for 30 min prior to analysis. Area was altered at a constant strain of 8%, at 10 different frequencies between 0.01-0.1 Hz. For each frequency, 40 points were measured with a period of 4. Experiments were repeated 5 times for each specimen. All experiments were conducted at 25 °C.

2.2.4 Statistical Analysis

Statistical analyses were performed using statistical analysis software (Minitab v16.0, Pennsylvania, USA). For comparison of the means to identify which groups were significantly different from others, analysis of variance (ANOVA) with Tukey's multiple comparison test was used. Differences were considered significant for $p < 0.05$.

CHAPTER 3

RESULTS & DISCUSSION

As previously stated, the dissertation can be divided into three different studies that, as a whole, compliment each other. Section 3.1 is dedicated to evaluation of stabilization properties of QSE in an oil-in-water emulsion, and comparing it to a non-adsorbing and commonly employed biopolymer, Xanthan Gum. Section 3.2 and 3.3, that follows, are dedicated to the investigation of surface (air-water) and interfacial (oil-water) properties of the biopolymer, respectively.

3.1 Characterization of emulsion stabilization properties of quince seed extract as a new source of hydrocolloid

3.1.1 Rheological Characterization

3.1.1.1 Linear-Viscoelastic Behavior

Rheological characteristics of emulsions are shaped by various interaction forces taking place in the system during creaming, sedimentation, flocculation, coalescence and Ostwald ripening. A number of parameters influence emulsion flow characteristics such as oil volume fraction, chemical composition and viscosities of the dispersed and continuous phases, electrolyte concentration, droplet granulometry as well as interfacial rheology (Tadros, 1994).

Most of the dynamic rheological measurements are carried out in the linear viscoelastic range. The range of linear viscoelastic region is determined by three factors; (a) length of the polymer molecules, (b) elasticity of the molecular chains, and (c) interactions between portions of a polymer molecule with other portions of

the same molecule or other molecules (Rouse, 1953). Storage modulus (G') is insensitive to changes in strain until a critical strain value. In amplitude sweep measurements; if the deviation from linear becomes larger than 5%, the linear viscoelastic region is over (Abbastabar et al., 2015). The length of linear viscoelastic region is associated with the strength of polymer gel and is a crucial indicator determining whether the gel behaves like a particle (strain weakening, short linear region, small rupture strain) or polymer gel (strain hardening, long linear region, and large rupture strain) (Abbastabar et al., 2015; Sun and Gunasekaran, 2009).

Table 3.1. Effect of XG and QSE concentration on consistency (K), flow index (n) and correlation coefficient of power law model (R^2) and length of linear viscoelastic range in 2% (w/v) WPI stabilized emulsions containing 20% v/v O/W.

Sample				Linear Viscoelastic range (% strain)
Description	K (Pa.sⁿ)	n	R²	
0.05Q	0.016 ^g	0.918 ^a	0.994	-
0.1Q	0.029 ^g	0.834 ^{ab}	0.994	3.35 ^e
0.2Q	0.063 ^g	0.770 ^b	0.996	3.90 ^{de}
0.3Q	0.136 ^{fg}	0.618 ^c	0.995	6.40 ^{cd}
0.5Q	0.349 ^e	0.526 ^d	0.997	10.30 ^{ab}
0.75Q	1.012 ^d	0.417 ^e	0.997	10.95 ^a
0.05X	0.051 ^g	0.682 ^c	0.999	-
0.1X	0.225 ^{ef}	0.505 ^d	0.999	2.35 ^e
0.2X	0.889 ^d	0.331 ^f	0.999	4.95 ^{de}
0.3X	2.083 ^c	0.259 ^{fg}	0.999	6.05 ^{cd}

Table 3.1. (continued)

0.5X	5.733 ^b	0.184 ^{gh}	0.999	7.95 ^{bc}
0.75X	9.927 ^a	0.159 ^h	0.998	10.85 ^a

Means within the same column, followed by the different letters (a–h) are significantly different ($p < 0.05$).

The % strain that G' deviates from linear for each sample is given in Table 3.1. No measurements could be taken for control sample (NOX) and 0.05X and 0.05Q samples as they did not display any visible viscoelastic region. The rest of the quince and xanthan emulsions exhibited increasing range in viscoelastic region with an increasing gum concentration. This could be explained with increased polymer gel strength and viscoelastic behavior with gum concentration. Quince and xanthan samples displayed comparable linear viscoelastic ranges for the same concentrations. For 0.75X and 0.75Q, G' deviated from linear at 10.85 % and 10.95 %, respectively. Table 3.2 shows linear region storage (G') and loss modulus (G'') at 1 MHz frequency for all samples. For dilute solutions, G'' and G' were quite close to each other. As gum concentration increased, G' increased more than G'' . At 0.75 % w/v, G' became excessively larger than G'' . This indicated that the gum solution tended to generate macromolecular networks with a more elastic behavior at higher gum concentrations (>0.2% for Xanthan, >0.3% for Quince emulsions). Both G' and G'' for xanthan emulsions were approximately 8 times the magnitude of those of quince emulsions indicating a more elastic behavior, a stronger structure, higher resistance to flow which was also observed through shear rate ramp experiments.

Table 3.2. Effect of XG and QSE concentration on elastic (G') and loss modulus (G'') in 2wt% WPI stabilized emulsions containing 20% v/v O/W.

Sample Description	G' (Pa)	G'' (Pa)
0.1X	0.475 ^b	0.530 ^d

Table 3.2. (continued)

0.2X	1.930 ^b	1.500 ^{cd}
0.3X	6.050 ^b	3.400 ^c
0.5X	17.00 ^a	5.850 ^b
0.75X	26.15 ^a	9.050 ^a
0.1Q	0.055 ^b	0.130 ^d
0.2Q	0.140 ^b	0.195 ^d
0.3Q	0.380 ^b	0.410 ^d
0.5Q	1.225 ^b	0.975 ^d
0.75Q	1.750 ^b	1.070 ^d

Means of each gum type within the same column, followed by the different letters (a–e) are significantly different ($p < 0.05$).

3.1.1.2 Flow Characteristics

Shear thinning behavior, identified with a decreasing apparent viscosity with an increasing shear rate, is probably the most encountered flow behavior in emulsions (Bouyer et al., 2012). Different models have been proposed to define shear-thinning behavior in low, medium, and high shear rate ranges; such as power law, Herschel-Bulkey, Cross, Reiner-Philippoff, Van Wazer, and Powel-Eyring (Abbastabar et al., 2015). A number of studies have utilized Cross model for characterization of rheological behavior of quince seed extract emulsions (Abbastabar et al., 2015, 2014). Cross model, similar to power law model, can be used to describe pseudo plastic behavior, but is valid for a wider range of shear rates (Abbastabar et al., 2015). However, it is quite common for xanthan solutions to be identified with a power law model (Krstonošić et al., 2019; Sun et al., 2007; Sun and Gunasekaran, 2009; Tian

et al., 2015). For ease of comparison, a relatively narrow shear rate range was chosen (0.1 s^{-1} - 100 s^{-1}) and the rheological data were fit to power law, Herschel-Bulkey and Newtonian models depending on the presence of a yield stress and/or shear thinning behavior.

It is common for solutions containing polysaccharides with thickening properties to display Newtonian behavior until a certain polymer concentration (i.e. critical concentration). The critical concentration (C^*) is where the solution shows a transition from dilute to semi-dilute state at which interaction of molecules increases and interpenetration occurs (Hwang and Kokini, 1991; Williams and Phillips, 2009). Below this value, polymer molecules are widely spread and molecule chains have no interaction with each other. As concentration increases, overlapping of polymer chains occur which results in a non-Newtonian behavior (Beckett, 1996). Critical concentration for xanthan gum solutions has been previously defined as 0.1 g solid / 100 ml soln. (Walstra, 2002). However, in this study a significant shear thinning behavior in all xanthan gum emulsions including the one with 0.05 g gum / 100 ml soln (0.05X), was observed. This was most likely related with the synergistic effect of whey protein isolate (WPI) and polysaccharides on the flow characteristics (Bryant and McClements, 2000). 0.05Q emulsion, on the other hand, displayed negligible changes in apparent viscosity values with changing shear rates and yielded a power law index (n) of 0.92 (which is close to 1). Hence, it was more suitable to define 0.05Q with a Newtonian model. Nevertheless, for quince seed extract concentrations $\geq 0.1 \%$ w/v; the emulsions exhibited a shear-thinning behavior. Control sample (NOX) was fit to a Newtonian model with high correlation coefficients ($r^2=0.997$), and demonstrated a viscosity (μ) of 0.007 Pa.s.

There are a number of ways to increase the stability of emulsions such as (a) using an adsorbing biopolymer or small surfactant that decreases interfacial tension, (b) increasing thickness and viscoelastic behavior of the interfacial layer, (c) using a non-adsorbing biopolymer (such as xanthan gum) to increase the viscosity of the continuous phase and minimize particle collisions. A higher viscosity and yield stress

greatly decreases the possibility of phase separation through creaming and sedimentation.

Table 3.1 lists the consistency index (K) and power law index (n) values. For all emulsions, emulsion consistency and shear thinning behavior was more pronounced with increasing gum concentrations. For quince samples, emulsion viscosity was quite insensitive to shear rate changes in dilute concentrations (0.05Q & 0.1Q); this effect was replaced by a dominant shear thinning behavior at increasing concentrations but never reached the levels of xanthan gum emulsions. At 0.75 % w/v gum concentration, 0.75X possessed an extremely larger K (9.93 Pa.sⁿ) and a much smaller n (0.16) compared 0.75Q (K=1.012 Pa.sⁿ, n=0.42). Fig. 3.1 shows the change in apparent viscosity with shear rate for XG and QSE emulsions. As apparent from Fig. 3.1a & 3.1b, all xanthan gum emulsions displayed higher viscosities than their quince counterpart, as well as a higher dependency on shear rate illustrated with a higher negative slope. For xanthan and quince samples that had similar K values, n was smaller in xanthan gum emulsions. This underlines the relative power of xanthan gum in giving shear-thinning characteristic to solutions. Under the effect of an increasing shear rate, the emulsion droplets and polymer chains become more ordered along the direction of flow which decreases the resistance to flow observed as a lower viscosity. Xanthan gum molecules are capable of quickly aligning to direction of flow and decrease the interaction between chains, thus showed better shear thinning capability compared to quince mucilage (Abbastabar et al., 2015; Hosseini-Parvar et al., 2010; McClements, 2004). Yield stress values were negligibly small for most of the emulsions (<0.5 Pa) except 0.5X and 0.75X, which possessed yield stress values of 0.85 Pa and 1.54 Pa, respectively. Xanthan gum solutions overall had much higher viscosities, a more solid behavior when not under any stress and an ease in mixing coming from the higher sensitivity to shear rate. Even for gum concentrations that had similar apparent viscosities for the two gum solutions, the lower n provides xanthan gum samples with a preferred fluidity when under the effect of high shear rates.

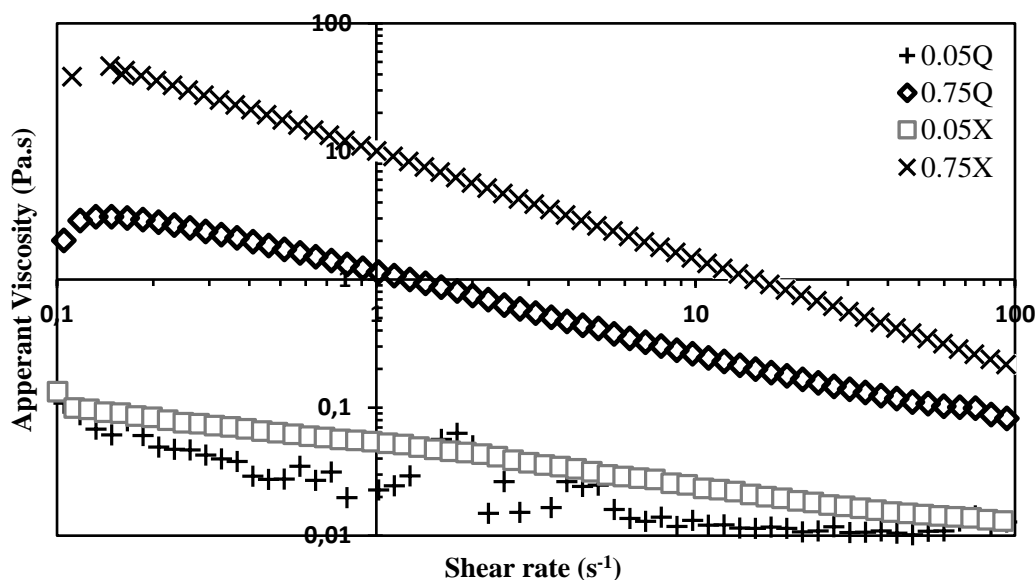


Figure 3.1. Effect of XG and QSE concentration on flow behavior of 2 %w/v WPI stabilized emulsions containing 20% v/v sunflower oil.

3.1.2 Particle Size Distribution

Particle size measurements were performed at days 0, 4, 7, 10, 14, 20 and 30. Day 0 measurements were taken within an hour of sample preparation. Control samples (NOX), and 0.05Q displayed a phase separation approximately 3-4 hours after sample preparation. In the next 24 hours, further phase separations occurred in three other samples with dilute gum concentrations (0.05X, 0.1X and 0.1Q). Hence, these unstable samples were not further analyzed after day 0 measurements.

In contrast to our expectations, the volume-moment mean diameters (d_{43}) of the remaining samples did not change significantly over the course of 30 days ($p > 0.05$) (Fig. 3.2). However, the d_{10} (particle diameter corresponding to 10% of cumulative undersize particle size distribution) of the samples exhibited a slight but significant increase (data not shown) ($p < 0.05$). After the visible disruption in stability of samples with gum concentrations ≤ 0.1 (%w/v), the remaining samples seemed to be stable over the course of 30 days. The experimental time scale was most likely not

sufficient for molecules inside biopolymer network to overcome kinetic energy barriers associated with the restricted movement of the dispersed particles.

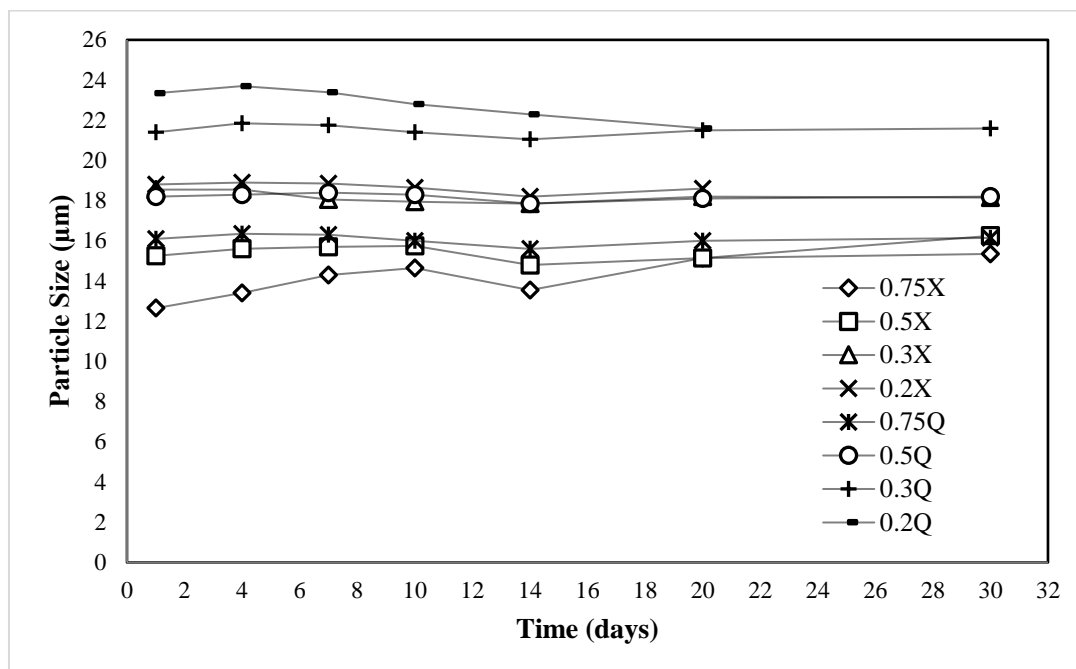


Figure 3.2. Change in volume–moment mean diameter (d_{43}) of 2 %w/v WPI stabilized emulsions containing 20%v/v sunflower oil with respect to storage time and quince seed extract/xanthan gum concentration.

Another explanation is related with the procedure of measurement. Measurements took place in 10^{-4} - 10^{-7} diluted mixtures that were continuously stirred at 2000 rpm. This could have resulted in separation of flocculated particles. Flocculation of oil particles is known to be reversible with mild stirring, whereas coalescence that involves rupture of the thin liquid film of the continuous phase requires much higher energy inputs to be reversed. Thus, coalescence is accepted as irreversible (Damodaran, 2005; Wilde et al., 2004). Stirring during measurements could have reversed particle flocculation. This, coupled with the presence of whey and other proteins in quince mucilage most likely was sufficient to prevent coalescence and a possible change in d_{43} during the 1 month that measurements were taken.

Fig. 3.3 shows day 0 measurements of each sample. d_{43} particles sizes display a decreasing trend with increasing gum concentration. There was a high negative correlation between the particle sizes and gum concentration (Pearson correlation coefficients of 0.90 and 0.91 for quince and xanthan gum emulsions, respectively). As stated by Walstra et al. (1988), the average particle size of droplets achieved by dispersion of oil in water is governed by the following empirical equation;

$$d_{av} \propto \frac{\gamma_i^{\frac{3}{5}}}{E^{\frac{1}{5}} \rho^{\frac{1}{5}}} \quad (3.1)$$

Where E is the energy input per unit volume, γ is the interfacial tension between the two phases and ρ is the density of the continuous phase (Walstra, 1988). Eqn. 4 states that the mean particle size of emulsions prepared by the same method would be higher for a larger density of the continuous phase. This is in agreement with our finding that relates gum concentration with mean particle size. A higher mean particle size increases the creaming rate by increasing the net force acting on the particles, hence, is usually associated with a lower stability. Confocal microscope images and creaming index measurements (Sections 3.4 and 3.5) also suggested at an increased stability with increasing xanthan gum and quince seed extract concentration. Emulsions prepared with xanthan gum had lower particles sizes than quince seed extract emulsions; this could be explained with the possible adsorbing nature of quince seed extract. Quince seed extract contains 10-25 % wt. proteins which are known to adsorb at the oil-water interface due to presence of hydrophobic and hydrophilic sides arbitrarily distributed in their tertiary structure (Ritzoulis et al., 2014).

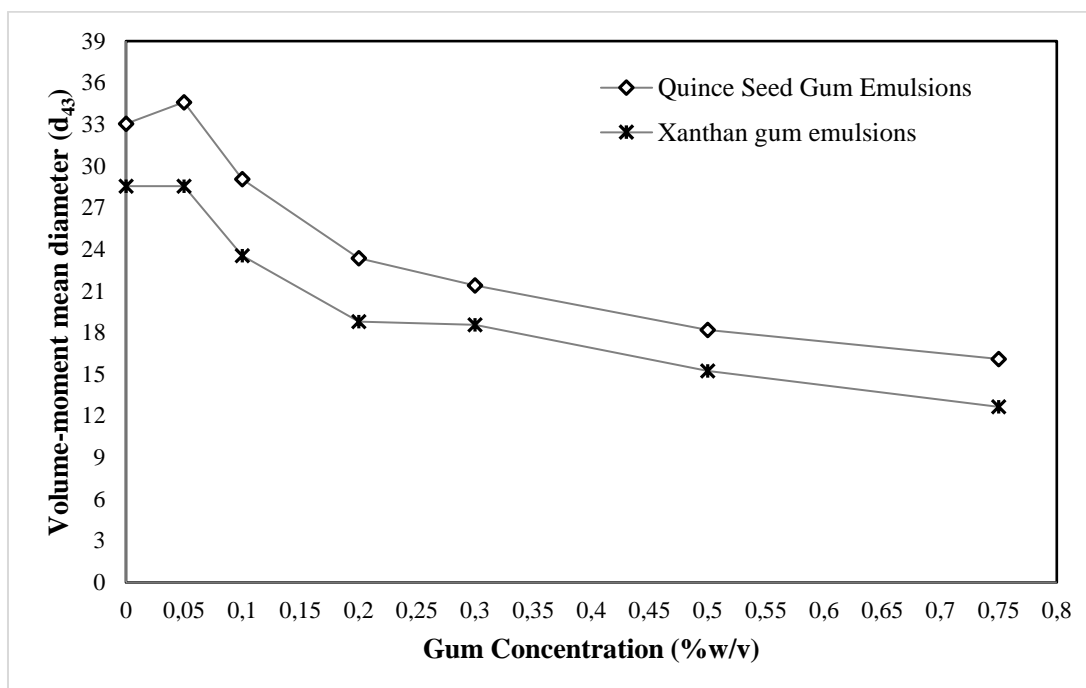


Figure 3.3. Effect of gum type and concentration on Day 0 volume–moment mean diameter (d_{43}) measurements

3.1.3 NMR T_2 Relaxation Measurements

Time domain NMR is a powerful noninvasive method to investigate microstructure of water-based systems. Some applications in emulsions include particles size measurements (Haiduc et al., 2007; Van Duynhoven et al., 2002), evaluation of mobility states (Duval et al., 2006; Le Botlan et al., 2000) and quantification of dispersed phase ratio (DPR) (Bernewitz et al., 2013; Le Botlan et al., 2000; Peña and Hirasaki, 2003).

In ^1H NMR measurements, sample placed in an external magnetic field is disturbed by a secondary momentary magnetic signal that is perpendicular to the previous one. After removal of the secondary signal, the sample relaxes to its former state. The transversal component of the exponential relaxation is governed by the relaxation time, T_2 . Protons of the sample with different environments will relax at different rates, which ensure separation of signal coming from varying proton pools with their

respective relaxation times (Kirtil et al., 2014; E. Kirtil and Oztop, 2016). Transversal relaxation of mobile protons is usually described by an exponential relaxation curve with T_2 relaxation times larger than 2 ms. By setting an echo time (TE) of 2 ms, it was ensured that the signal only comes from the mobile protons; which, in our case, is majorly dominated by protons from oil and water (Duval, et al., 2006). Accordingly, the exponential decaying signal was fit to a mono and bi-exponential curve to observe the changes in overall T_2 times and T_2 times of the water and oil phases.

The measurements were taken for each sample, right after sample preparation and over the course of 30 days. The results are of mono- and bi-exponential fitting of relaxation data is given in Fig. 3.4 and Fig. 3.5, respectively. NOXc and NOXs refer to the cream and serum phases acquired after phase separation of the control sample NOX. As apparent in Fig. 4, all the mean T_2 times reside within the limits set by T_2 times of NOXc and NOXs. NOXs displayed the highest T_2 times ($\cong 1350$ ms). However, this value is still excessively smaller than that of pure water ($\cong 2500$ ms) (Chary & Govil, 2008) most likely due to labile whey protons (such as in $\sim\text{OH}$) increasing the relaxation rate of water protons (Duval et al., 2006). Cream phase, on the other hand, that contains high amounts of sunflower oil displays much faster relaxation rates characterized with the lowest T_2 times overall. Oil protons resonance at a frequency that is close to Larmor frequency for ^1H , thus exhibiting a much higher rate of energy exchange compared to water, and is characterized by short T_2 times ($\cong 150$ ms) (Belton et al., 2003).

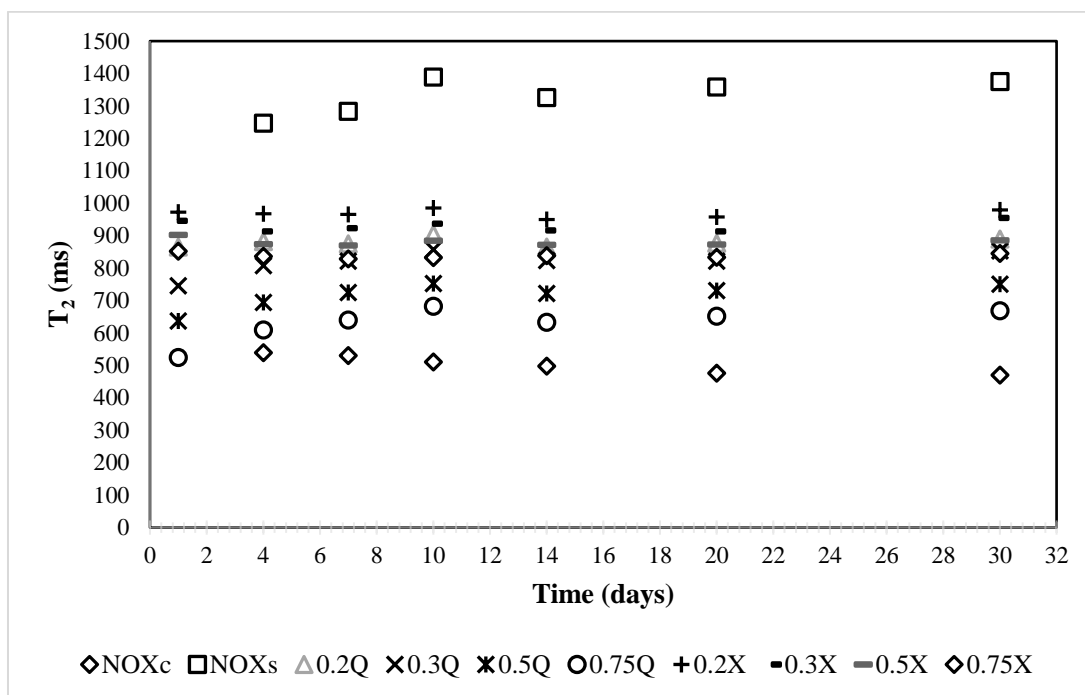


Figure 3.4. Mean NMR T_2 relaxation times of 2 %w/v WPI stabilized emulsions containing 20% v/v sunflower oil with respect to storage time and quince seed extract/xanthan gum concentration

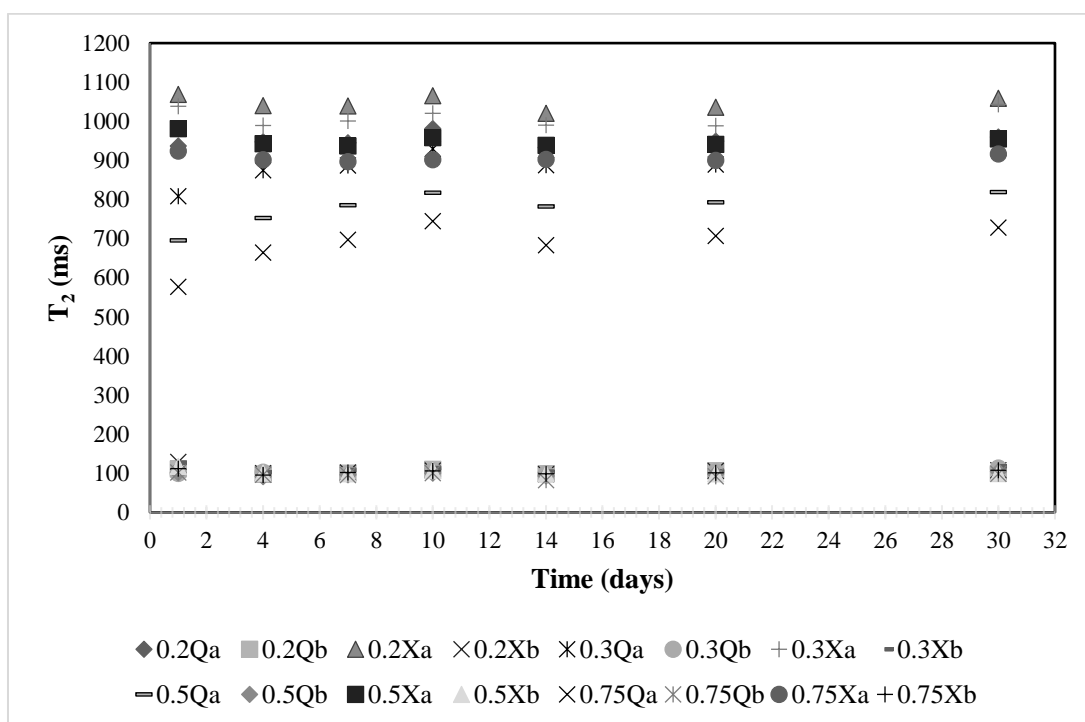


Figure 3.5. T_2 relaxation times acquired through bi-exponential fitting of NMR relaxation data of 2 %w/v WPI stabilized emulsions containing 20% v/v sunflower oil with respect to storage time and quince seed extract/xanthan gum concentration

The fact that mean T_2 of all samples (Fig. 3.4) lies between the extremes of cream and serum T_2 values was an indicator of the increased exchange of protons between the two phases through emulsification. This intermediate relaxation rate could be associated with (a) the increased contact area between the two phases by dispersion of oil into water, (b) the presence of surface active agents adsorbed on the interface (E. Kirtil and Oztop, 2016). In that regard, T_2 relaxation times are expected to decrease with a decreasing particle size and an increasing macromolecule and/or surfactant concentration. As previously discussed, the particle sizes did not display a changing trend with time. In that regard, it is normal for T_2 relaxation time to yield similar results. The chosen time scale coupled with the high random deviation in NMR measurements (caused by momentary changes in frequency) might have hindered the possibility of observing a statistically significant trend with time.

In Fig. 3.5, it is seen that the signal from oil (T_{2b}) is not much affected from gum concentration or type, since the mobility of oil is not affected from gum addition. However, as seen in Fig. 3.4 and Fig. 3.5, gum type and concentration greatly affects relaxation rate of free water and water that is closely associated with protein based biopolymers adsorbed onto the surface of oil. It is apparent that there is a decreasing trend in T_2 times with the increasing gum concentration, owing to the macromolecule network restricting mobility of water.

What is worth noting is that, xanthan gum emulsions, despite the smaller droplet sizes, have longer T_2 times (between 800-1000 ms) whereas quince seed extract emulsions have shorter T_2 times (between 500-850 ms). Xanthan gum is known to decrease the mobility of water by entrapping it into stiff polymer chains of β -(1-4)-D-glucose molecules making single, double or triple helixes that are in strong interaction with one another (Jansson et al., 1975; Melton et al., 1976). This complex network is loosely bound and flexible which gives the solution its shear thinning

properties (Bouyer et al., 2012). However, xanthan gum is a non-adsorbing polysaccharide, meaning it does not adsorb on the oil/water interface when used in emulsions and does not have any interaction with whey protein (Bouyer et al., 2012). Quince mucilage, on the other hand, though there still are not enough studies on its use as a stabilizer in emulsions, is known to be an adsorbing polymer and has emulsifying properties (Ritzoulis et al., 2014). Thus, for quince seed extract emulsions, in addition to restricted mobility of water, the lowering in T_2 is also due to the increased proton exchange at the oil/water interface. Adsorbed quince mucilage molecules act as emulsifiers, and emulsifiers are known to decrease relaxation time by changing the conformation of triglyceride, water and whey molecules at the interface (Le Botlan et al., 2000).

3.1.4 Emulsion Stability

Stability of the emulsions was assessed by visible observations and measurement of the height of the separated serum layer. Creaming profile images and creaming index (% CI) (calculated from Eqn. 1) data as a function of storage time are given in Fig. 3.6 and Fig. 3.7, respectively. The emulsions were monitored over a period of 5 months, with measurements taken at Day 0-10, 30, 45, 150. Upon this period, the samples that displayed a visible phase separation were NOX, 0.05Q, 0.05X, 0.1Q, 0.1X, 0.2Q, 0.2X, 0.3Q. Out of these, NOX, 0.05Q were the first to destabilize. Within 3-4 hours of sample preparation, both started showing signs of separation. Of particular importance is that, 0.05Q was faster to reach the final % CI value of 72% compared to NOX. The rapid creaming rate of 0.05Q was observed multiple times during other measurements and posed a real challenge for us. The amphiphilic characteristic of quince seed mucilage might be the reason behind this observation. Quince seed mucilage is composed of linear chains of glucans, a galactoglucan/manno-glucans or galacto-manno-glucans (Ritzoulis et al., 2014). The structure also shelters around 10-25 % wt of proteins with glutamic acid, aspartic acid and asparagine being the most abundant amino acids (Ritzoulis et al., 2014;

Vignon and Gey, 1998). Assuming the concentration of adsorbing biopolymer was not high enough to saturate the whole interface, the long quince seed molecules might have adsorbed on multiple droplets creating a bridge. This phenomenon, known as bridging flocculation, is responsible for inducing extensive flocculation in the presence of low concentrations of weak emulsifiers and could explain the faster creaming in 0.05Q compared to control (Damodaran, 2005; Ritzoulis et al., 2014; Sun and Gunasekaran, 2009).

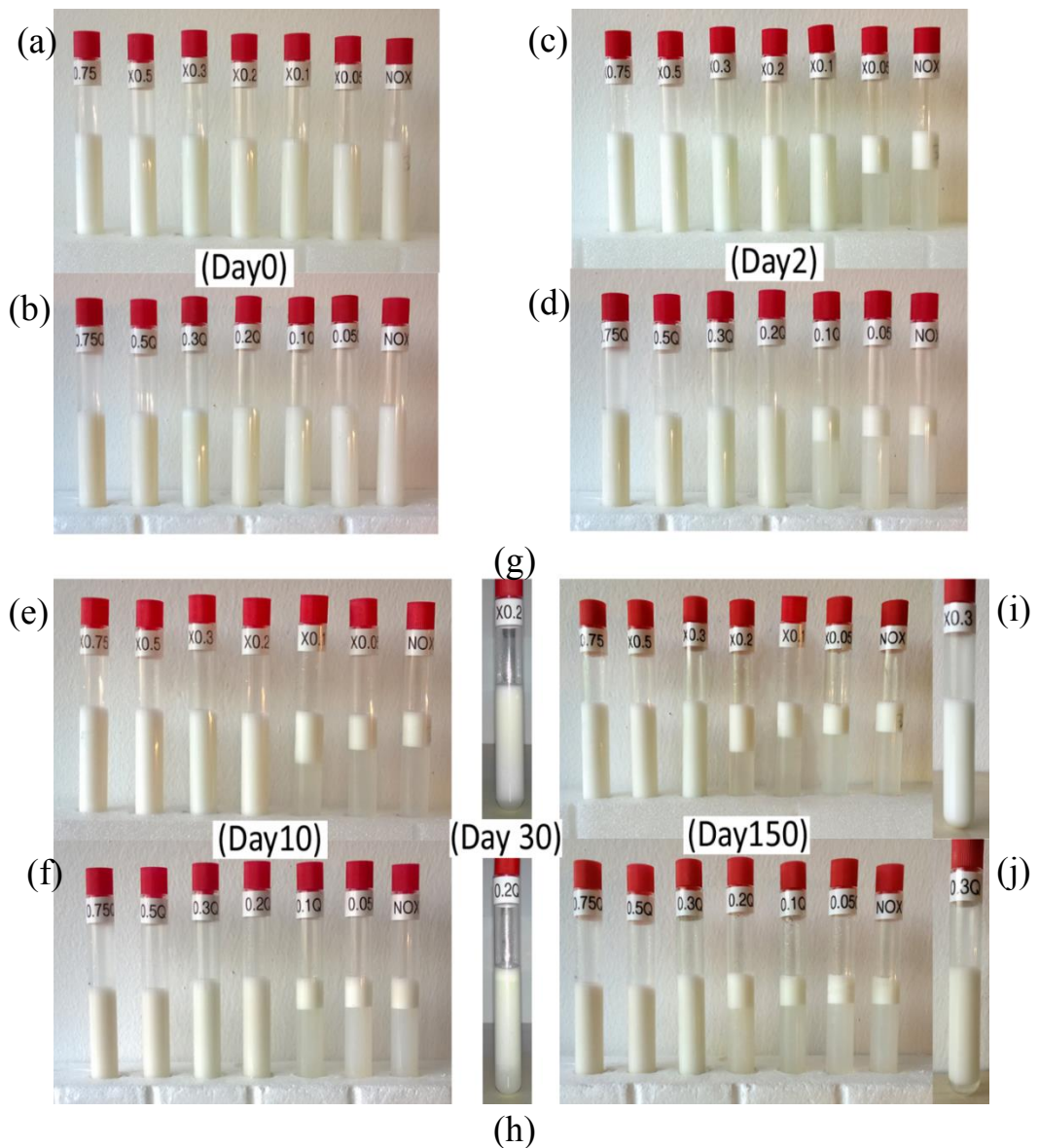


Figure 3.6. Images of (a) emulsions on Day 0 prepared with xanthan gum in decreasing gum concentration from left to right (0.75X, 0.5X, 0.3X, 0.2X, 0.1X, NOX) (b) emulsions on Day 0 prepared with quince seed extract in decreasing gum concentration from left to right (0.75Q, 0.5Q, 0.3Q, 0.2Q, 0.1Q, NOX) (c) emulsions prepared with xanthan gum on Day 2 (d) emulsions prepared with quince seed extract on Day 2 (e) emulsions prepared with xanthan gum on Day 10 (f) emulsions prepared with quince seed extract on Day 10 (g) 0.2X on Day 30 (h) 0.2Q on Day 30 (i) emulsions prepared with xanthan gum on Day 150 (j) emulsions prepared with quince seed extract on Day 150

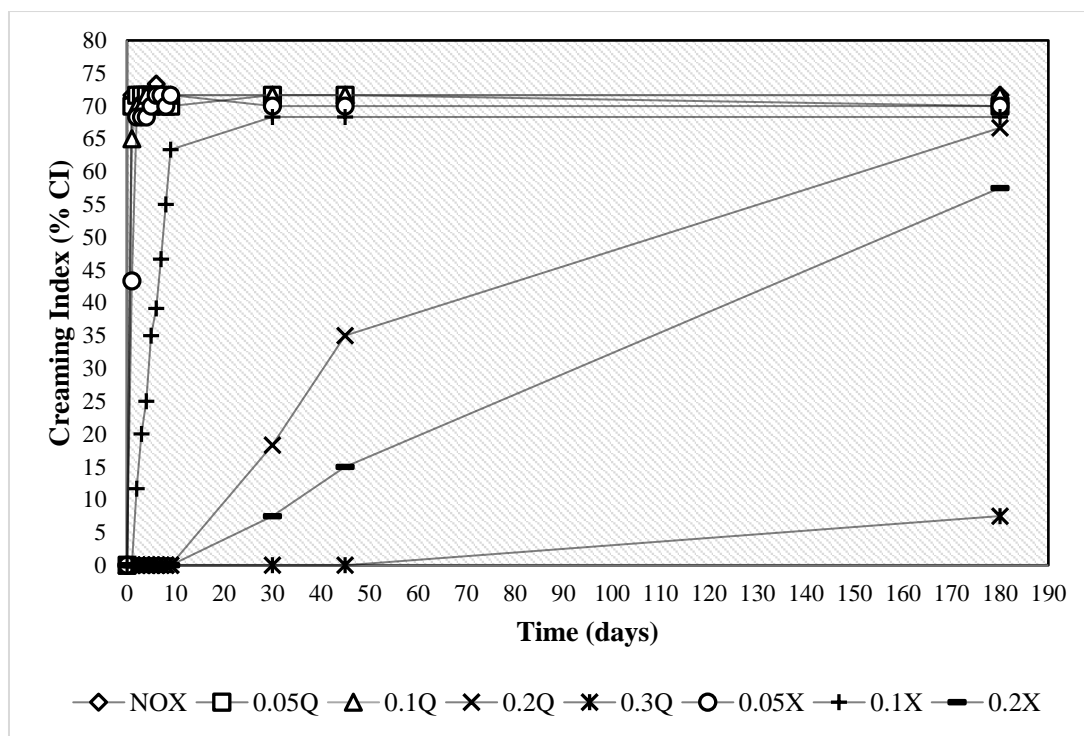


Figure 3.7. Effect of gum type and concentration on creaming index (%CI) of 2wt% WPI stabilized emulsions containing 20%v/v sunflower oil.

0.05X, 0.1Q and 0.1X showed distinct layers of cream and serum within 24 hours of preparation, though 0.1X was much slower to reach equilibrium % CI value. 0.1Q reached equilibrium % CI at day 1, whereas it took more than 10 days for 0.1X to reach equilibrium. The rapid phase separation in 0.1Q could again be attributed to bridging flocculation. This is further supported by the fact that after the 0.1 % w/v

limit, quince and xanthan emulsions started displaying comparable stabilities. At the 30-day mark, 0.2X and 0.2Q both had visible creaming with % CI's of 7.5% and 18.3%, respectively. Unlike the sharp layer of 0.2X, 0.2Q showed a much vaguer boundary layer (Fig 3.6g and Fig. 3.6h). This vague appearance suggests a more poly-dispersed droplet distribution close to the cream boundary. In case the particles are not under a yield stress that prevents free movement, large droplets cream faster than small ones as indicated by the modified Stokes equation (Eqn. 2). One common observation for all unstable quince samples was that, there was no clear boundary at the beginning of creaming. The boundary layer gradually became sharper as all small droplets eventually rose to the cream layer. In the presence of a yield stress, large particles cannot cream faster than smaller ones as they are agglomerated or flocculated to form a weak gel-like network throughout the system. However, with time due to Brownian motion and effect of gravity this weakly flocculated system goes through a restructuring which might reduce the interaction between flocs and cause collapse of the gel network (Hemar et al., 2001). This latter mechanism was previously associated with emulsions containing xanthan gum (Sun et al., 2007) and explains the destabilization seen in xanthan gum emulsions with gum concentrations ≥ 0.1 % w/v, whereas quince seed extract emulsions with low viscosities and yield stress displayed creaming behaviors more closely identified with modified Stokes equation (Sun et al., 2007).

At the 5-month mark, 0.3Q had formed a phase boundary with a % CI of 7.5% while 0.3X did not display any visible phase boundary. As previously mentioned, the stabilization mechanism of xanthan gum was through increasing the viscosity of the solution and hindering droplet collisions. Quince seed is not as effective in increasing the viscosity of the emulsion for the same concentrations. Actually, there is an order of magnitude difference in apparent viscosities of same concentration of quince and xanthan gum emulsions (for gum concentration ≥ 0.2 % wt/v). However, despite the 10-fold difference in apparent viscosities; emulsion-stabilizing effect of quince seed extract was comparable to xanthan gum at same concentrations. Quince seed extract, similar to gum arabic, is an adsorbing biopolymer (Damodaran, 2005; Ritzoulis et

al., 2014). In addition to its thickening properties, the amphiphilic characteristic of quince seed extract provides it with emulsification capabilities. Quince seed proteins adsorb along with the whey proteins on the surface of droplets; and the steric and/or electrostatic repulsions caused by the adsorbed proteins prevent flocculation. Additionally, the presence of polymers on the surfactant layer increases the thickness and flexibility of the lamella film, making it harder for flocculated particles to merge (Evans et al., 2013; Ritzoulis et al., 2014; Tcholakova et al., 2005; Vignon and Gey, 1998).

3.1.5 Emulsion Microstructure

Microstructure of the emulsions can be seen as a function of storage time for samples 0.1X, 0.1Q, 0.5X and 0.5Q in Fig 3.8. Day 0 images were acquired within approximately 2 hours of sample preparation. Initial microscope images revealed that, 2% WPI and xanthan gum stabilized emulsions, 0.1X and 0.5X, had a similar microstructure with the exception of 0.1X showing occasional signs of flocculation. The ongoing flocculation that had begun within hours of preparation caused 0.1X to generate a phase boundary within 24 hours (Fig. 3.7). Both 0.5X and 0.5Q had individual droplets that seem to be stably suspended in the polymer network. At Day 0, confocal microscope images of quince seed extract and WPI stabilized sample, 0.1Q, consisted of very large particles surrounded by a rather blank continuous phase. Even within 2 hours of preparation, 0.1Q exhibits signs of creaming. This rapid disruption in stability could be associated with bridging flocculation as previously explained.

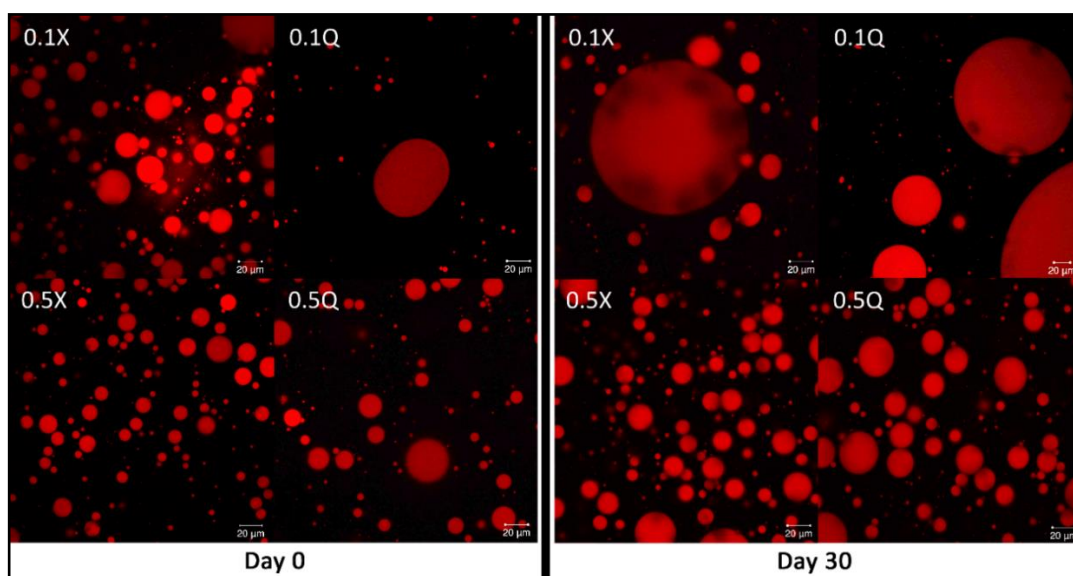


Figure 3.8. Confocal microscopy images of samples 0.1X, 0.1Q, 0.5X, 0.5Q on day 0 (left) and day 30 (right).

0.1X and 0.1Q had completely phase separated by day 30 (Fig. 3.8). Therefore, they were mildly agitated before a portion of the samples was taken from the middle of the tubes and placed onto the coverslip for examination. Upon agitation, both samples were easily distinguishable from their initial states displaying enormous oil patches. However even after mild agitation, oil phase in 0.1X had a higher tendency to be dispersed into the serum phase generating a greater number of small micro-sized particles compared to 0.1Q, which confirms the dominant role viscosity play in emulsion stability. Unsurprisingly, not much of a change was observed in 0.5X and 0.5Q after 30 days since these samples proved to be stable in emulsion stability measurements even after 150 days (Fig. 3.7).

3.2 Investigation of surface properties of quince seed extract

3.2.1 Equilibrium Surface Tension & z-Average Particle Size

Equilibrium surface tension (ST) measurement is the most accessible and commonly employed surface measurement and is defined as the capillary force per unit length acting on the interface (mostly reported in mN/m) after the adsorption of the surfactant is finalized (Berg, 2010; Shaw, 1992). Despite its immense popularity in colloidal studies, the measurement of equilibrium surface tension alone provides no information on the dynamic interfacial behavior, which leaves out important interfacial phenomena like rate and mechanism of adsorption, the interface's resistance to shear and dilatational disturbances (Karbaschi et al., 2014). The impact of these complimenting surface processes is established by research that confirms that a reduction in interfacial tension is not the only parameter that defines the stability of a dispersion. Emulsions of certain paraffin hydrocarbons exhibit poor kinetic stabilities despite displaying considerably low surface tensions, yet emulsions stabilized by some large molecular surfactants (such as asphaltenes and resins) show prolonged stability under physical disturbances and even years after their formation (Z. Wang et al., 2014). Nevertheless, equilibrium surface tension is directly proportional to Gibb's free energy of the interface, and any reduction in ST is recognized as a reduction in excess surface energy, which confers dispersions higher thermodynamic stability (Berg, 2010; Z. Wang et al., 2014). Consequently, the use of a single value like ST eases comparison of different surfactants by presenting scientists and the industry with a quantitative indicator of "performance" of the surfactant on the employed interface.

For large molecular surfactants like quince seed extract, the process of adsorption takes a long time to be finalized. Adsorption process will be examined in more detail in the Section 3.2; however, at this point, we believe it is essential to talk about the challenges we came across in identification of an equilibrium. All samples were

subjected to a total of 10 measurements, with 2 of them lasting longer than 12 hours (overnight), and the other 8 data were measured for 120 minutes. Samples continued to relax (especially the ones with concentrations < 0.3 % w/v) even after 2 hours. However, after 2 hours ST relaxation process was extremely slow ($\cong 0.5 \frac{mN}{m}$ per hour). The droplets were measured inside sealed cuvettes, whose inner % RH was preserved close to saturation, which was ensured by filling approximately $\frac{1}{4}$ of the cuvette with water. The objective of this design was to minimize evaporation and subsequent particle shrinkage. Nevertheless, despite our best efforts, we were not able to completely stop evaporation. The disperser used was automated and was adjusted to keep the particle area constant at all times. Still we believe, considering the loss in total solution volume in syringe, evaporation was in place and after a certain amount of time, relaxation processes become so slow that it was not possible to certainly relate the reduction in surface tension with adsorption. ST reduction due to evaporation induced shrinkage could start to dominate over the adsorption considering the slower rates. For higher concentrations (< 0.5 % w/v), interestingly, we observed an opposite trend. There was a very slow increase in ST ($\cong 0.2 \frac{mN}{m}$ per hour) after the initial decrease. This behavior started after around 1-2 hours of droplet formation and was explained with the extract's highly hygroscopic structure. Upon conformational changes during relaxation due to formation of new free adsorption sites on the air-water surface, some of the water vapor in the cuvette could be attached to the droplet and adsorb on the particle surface. This hypothesis was confirmed with marginal increases in syringe volume in overnight measurements. That is why we found it most suitable to report equilibrium ST data as the minimum ST achieved within 120 minutes of particle formation. Similar challenges were encountered by other researchers as well; it was reported by some that interfacial properties continue to drift even after days of formation for polymeric surfactants (Bantchev and Schwartz, 2003; Beverung et al., 1999; Cascão Pereira et al., 2003; Freer et al., 2004b; Tupy et al., 1998).

Fig. 3.9a shows the surface tension isotherms that relate the change in quince seed extract concentration with equilibrium surface tension values. QSE, to our surprise, was very effective in displaying a significant reduction in surface tension even in concentrations as low as 0.025 % w/v. At 0.025 % w/v, QSE managed to reduce ST of water from 72 mN/m down to 58.9 mN/m. Expectedly, higher bulk concentrations also increase the amount of surfactant on the interface, which further reduces surface tension. By increasing QSE concentration, it was possible to decrease ST down to around 36.5 mN/m. As analyzed in detail in the previous section, QSE is a large branched polysaccharide that mainly consists of a xylose backbone, with proteins attached to the glucuronic and galacturonic acid molecules on the branches and it is these proteins that are mainly responsible for the extract's surface affinity. There are very few biopolymers that naturally contain proteins that have such high accessibility to the surface. Gum Arabic, which is a benchmark emulsifying and stabilizing agent, contains around 1-2% protein and concentration of up to 3% w/v of the gum can decrease ST of pure water down to the range of 46-55 mN/m as reported in multiple studies (Bouyer et al., 2013; Cao et al., 2013; Huang et al., 2001). This value is also lower than most other polysaccharide based stabilizers such as guar gum (52.95 mN/m @ 1% w/v concentration), tragacanth gum (47.4 mN/m @ 0.85 % w/v) (Moreira et al., 2012), Acacia tortuosa gum (42.6 mN/m @ 0.5 % w/v concentration)(Muñoz et al., 2007), Sterculia apetala gum (56 mN/m @ 0.5% w/v) (Pérez-Mosqueda et al., 2013), Acacia Senegal gum (57.4 mN/m @ 0.5 % w/v) (Castellani et al., 2010b), okra gum (47.9 mN/m @ 0.5 % w/v) (Yuan et al., 2019). QSE shows an exceptional reduction in surface tension compared to similar biopolymers. This behavior could be explained with the high hydrophobicity of the gum. As explained in Section A.1.4 (See Appendix), the extract's proteins are composed of 37 % of hydrophobic amino acids, and the hydrophobic portions of the protein also possesses high accessibility to the surface, as is apparent in the gum's high surface hydrophobicity.

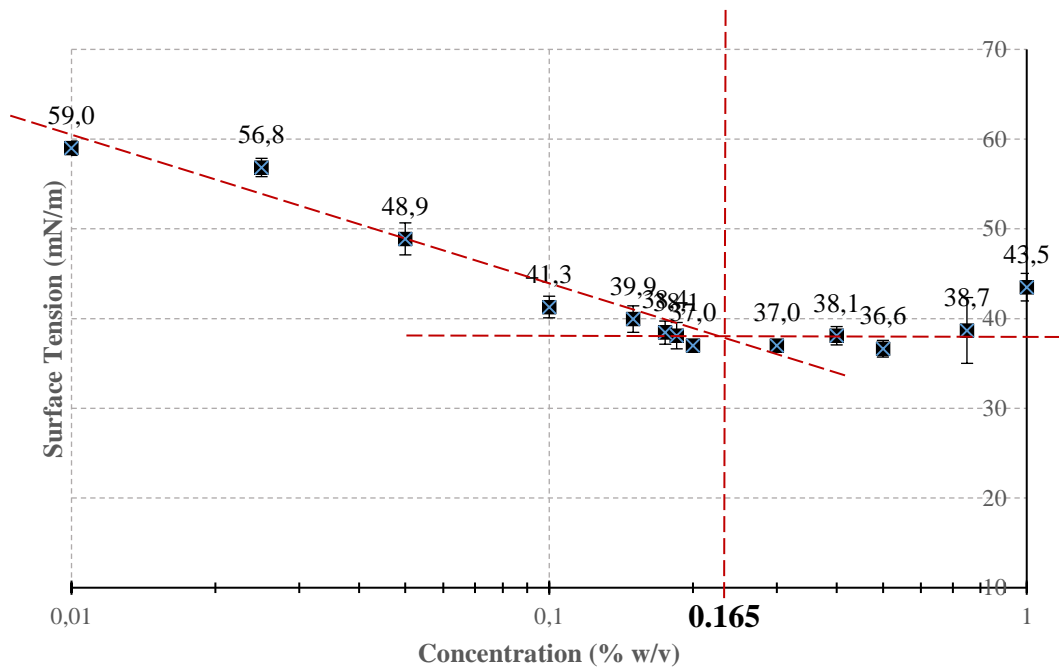
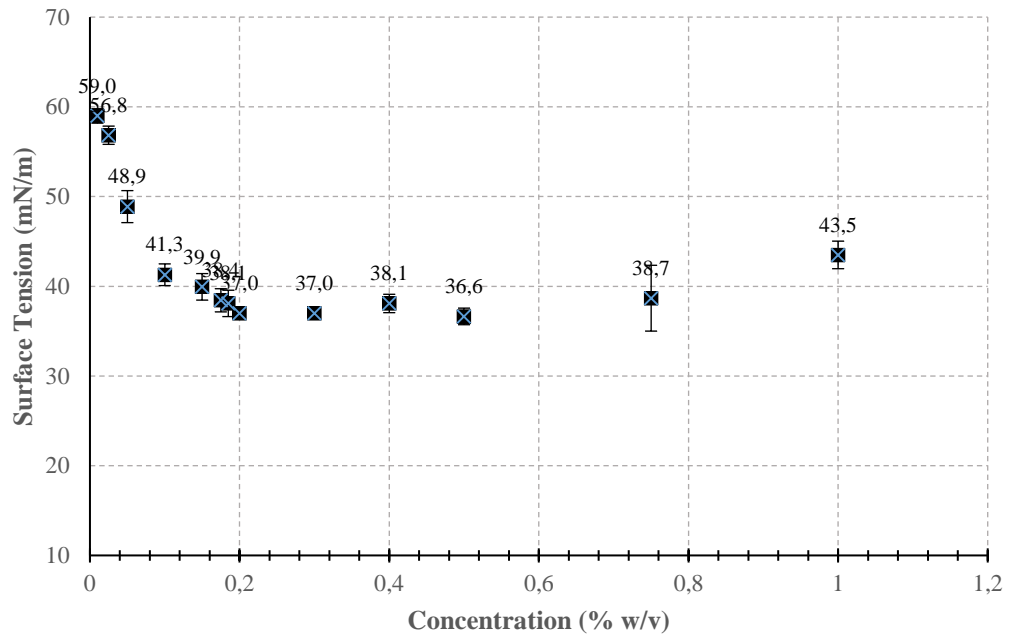


Figure 3.9. (a) Equilibrium Surface Tension Isotherm (b) Equilibrium Surface Tension Isotherms (x-axis drawn at a logarithmic scale)

As demonstrated in Fig. 3.9a, ST values decrease down to a plateau (~ 36 mN/m), after which concentration has no effect on ST. This could be explained by total

monolayer coverage of the interface. The concentration where this occurs is reminiscent of critical micellization concentration for small molecular surfactants. Critical micellization concentration (CMC) is defined as the concentration for a specific surfactant-solvent combination at which the surface becomes saturated, and any added surfactant would exist in micelles in bulk (Arabadzhieva et al., 2011; Shaw, 1992). Similar behavior is also witnessed in polymeric surfactants, at which after a certain polymer concentration (critical aggregation concentration, CAC), further polymer addition produces polymeric aggregates (Krstonošić et al., 2019; Tadros, 2009). Similarly, in our findings, after CAC, QSE addition had no effect on eq. STs. To identify CAC, most utilized method is to draw linear curves over ST vs. $\log C$ curve, and label the point of intersection as CAC (Bu et al., 2004; Dal-Bó et al., 2011; Rub et al., 2013). Fig. 3.9b, is the ST vs. C curve drawn on a logarithmic scale. The linear trend curves for the decreasing and constant ST sections intersect at a concentration of around 0.165 % w/v. This sharp kink point of slope change in ST isotherm curves (Fig. 3.9a and 3.9b) was defined as CAC for QSE at an air-water interface. This means further polymer addition after a concentration of 0.165 % w/v does not confer increased thermodynamic stability to an emulsion/foam or help facilitate its initial formation. 0.165 % w/v is a relatively low concentration to provide surface saturation. In comparison, Gum Arabic continues to decrease eq ST. up to concentrations of 3% w/v (Cao et al., 2013). Consequently, it is safe to say that QSE can provide similar emulsification properties for much lower concentrations than most similar biopolymers, or ensures much higher stability for the same concentration. The highly hydrophobic nature of the protein and the unique structure that these hydrophobic residues are positioned could be the reason for this. It is already well-known for block and graft type copolymers like QSE to have much lower CACs compared to homopolymers or other copolymers (Tadros, 2009).

Table 3.3. z-average diameters of QSE aggregates

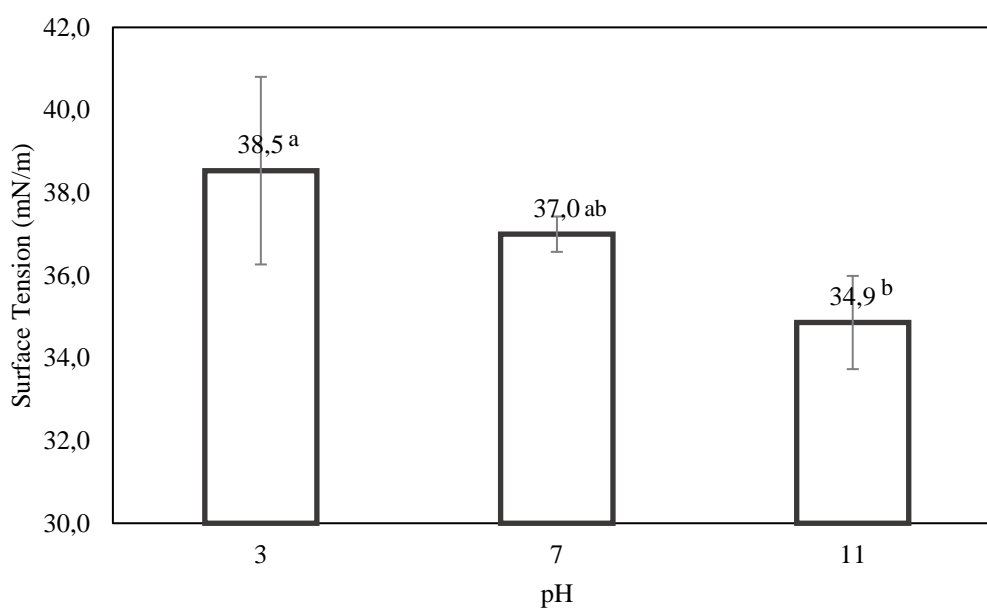
Concentration (% w/v)	z-ave (d.nm)
Control	481±68 ^d
0.05	891±92 ^{cd}
0.1	989±81 ^d
0.2	2772.5±251 ^b
0.3	2287±195 ^{bc}
0.4	2795±253 ^a
0.5	3013±193 ^b
0.6	2619±228 ^b
0.75	2643±230 ^b
1	3124±378 ^b

Table 3.3 shows the zeta-sizer measurement results for QSE solutions at various concentrations. Measurement of hydrodynamic radius, determined by dynamic light scattering measurements, is one of the most useful methods in determining the size and conformation of polymers. Hydrodynamic radius (R_h) is a measure of the effective size of a polymer and described as the radius of an equivalent hard-sphere diffusing at the same rate as the molecule under observation (Wilkins et al., 1999). The size of a molecule could change depending on external conditions, as is strongly related to the solute-solvent and solute-solute interactions (Tadros, 2011). QSE chain size seems to be around 900 nm when solvated in water (Table 3.3). However, for concentrations above <0.2% w/v, the polymer sizes suddenly increase to <2500 nm, which indicates aggregate formation composed of clusters of several QSE molecules. These polymer aggregates occur as a result of close association of hydroxyl groups (abundant in QSE molecule) that have strong hydrogen bonding capacity and are

reversible via dilution (Burchard, 2001). The sudden jump in polymer size between concentrations 0.1 – 0.2 % w/v, is in agreement with the CAC identified as 0.165 % w/v by eq. ST measurements. QSE aggregates sizes go up to ~3100 nm. Protein aggregates can range in size from nanometers to hundreds of micrometers, yet the size of QSE aggregates is larger than aggregates of commonly employed proteins and protein-polysaccharide combinations. Gelatin- hsiang-tiao gum aggregates showed aggregate sizes up to a maximum of 1500 nm (You et al., 2020), major portion of gum Arabic aggregates peaked at around 1000 nm (Isobe et al., 2020), casein micelles peaked around 550 nm (M. Chen et al., 2018), soy protein aggregates showed maximum aggregate sizes of 525 nm (Wu et al., 2019), and acid aggregated whey proteins reached a maximum aggregate size of ~2500 nm. QSE's larger molecular weight and highly branched structure could be the reason behind the large aggregate sizes. Molecules with larger sizes, though tend to adsorb more slowly on the interfaces, once adsorbed, form more stable dispersions as a result of the thick gel-like network they form on the interface (Bouyer et al., 2013; Davis and Foegeding, 2006; Freer et al., 2004b).

The effect of pH and salt content on equilibrium STs are depicted in Fig. 3.10a and 3.10b, respectively. Eq. ST of QSE decreased from 38.5 mN/m to 34.5 mN/m as pH increases from 3 to 11. As stated in Section 1.1, the isoelectric point of QSE is pH 4.2 (Deng et al., 2019). So out of the chosen pHs, pH3 is the one closest to the extract's isoelectric point, where the net surface charge of the gum is zero. QSE is a polyelectrolyte and contains a significant amount of charged groups such as sugar acids and amino acids. These acids are located on the branches, and as we go further away from the isoelectric point of pH 4.2 to basic pHs, more and more of these groups are negatively charged, which increases the overall charge of the molecule up to -38.1 mv at pH10 (Deng et al., 2019). The increased charge at the interface may have promoted electrostatic attraction between polysaccharide and protein molecules, which reduced competition for the interface and yielded more closely packed and thicker, denser interfaces. Higher surface excess concentration is known to result in lower STs. This result seems to be in line with findings of other studies

that have demonstrated an increase in QSE's emulsifying and foaming properties as pH moves further away from the isoelectric point (Deng et al., 2019). STs were also significantly effected from the ionic strength of the medium, as seen in Fig. 3.10b. There was no significant difference between eq. STs. of S0.1, S0.3, and S0.5 (lying around ~34.5 mN/m), yet ST without any NaCl for the same concentration was 37.0 mN/m. This means, salt addition decreases equilibrium STs. The concentrations used are within the “salting in” range for QSE, as shown by previous studies (Ashraf et al., 2017; Deng et al., 2019; Rezagholi et al., 2019), which means adding more NaCl increases protein solubility. Protein chains are better solvated by water in the presence of Na⁺ and Cl⁻ ions, hence polymer chains spread out more with charged and polar groups extruding through the aqueous phase in well-separated lateral chains. This conformational change eases unfolding of the proteins, which better exposes the hydrophobic residues to the interface, decreasing surface tension.



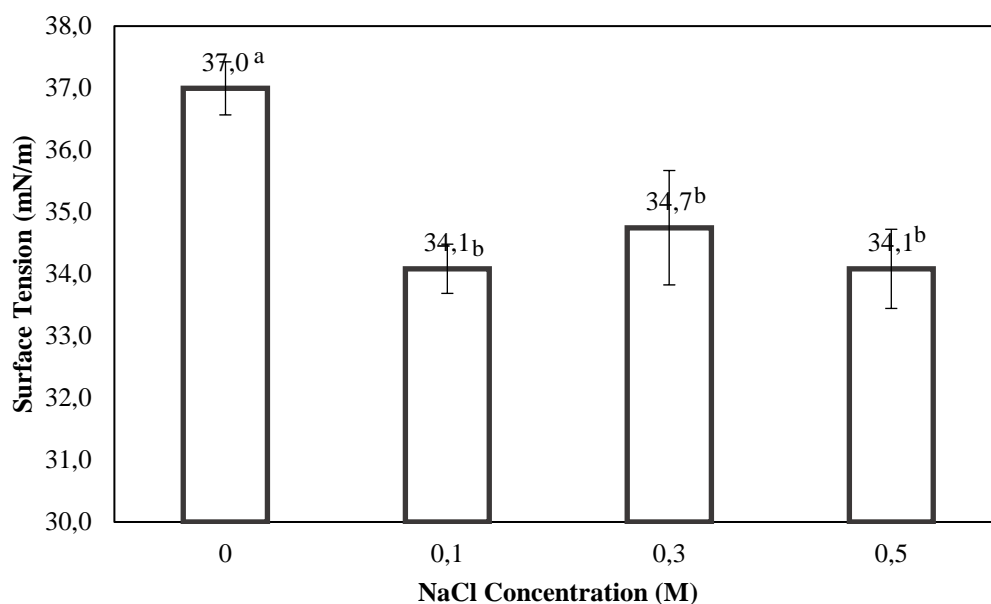


Figure 3.10. (a) Equilibrium surface tension of QSE solutions at different pHs (b) Equilibrium surface tension of QSE solutions at different NaCl concentrations

3.2.2 Dynamic Surface Tension Curves

For a biopolymer to be an effective foaming/emulsifying agent, in addition to showing surface activity, it should also have the capacity to lower surface tension within the time scales that are relevant to the emulsification process (Walstra, 2002; Walstra and Smulders, 2007). The rate of adsorption as well as the adsorption profile is just as important in assessment of emulsification properties of a surfactant. Especially for polymers, due to their large molecular weight, the rate of adsorption is usually slower than small molecular surfactants and also some processes, such as foaming, requires a rapid positioning on the interface, which further necessitates the investigation of adsorption dynamics (Cao et al., 2013; Freer et al., 2004b; Seta et al., 2014; Wüstneck et al., 1996).

Interfacial adsorption of surface active materials is governed by the change in surface pressure with adsorbent concentration on the surface. According to *Le-Chatelier*

principle, the direction of equilibrium would shift in the direction which stress can be relieved. For surface active biopolymers dissolved in solution bulk, interactions between polysaccharides and the interface is more favorable than that of solvent and the interface (Wüstneck et al., 1996). Consequently, adsorption occurs spontaneously and causes increasing surface pressure up to an equilibrium value. For low-molecular weight surfactants there are well-established adsorption theories, yet in the case of polymers no such model exists (Kontogiorgos, 2019; Wüstneck et al., 1996). Langmuir isotherm, however, is demonstrated to be a close approximation to real protein adsorption process and was used for estimation of diffusion coefficient in surface studies (Santini et al., 2007b; Tadros, 2009; Wüstneck et al., 1996).

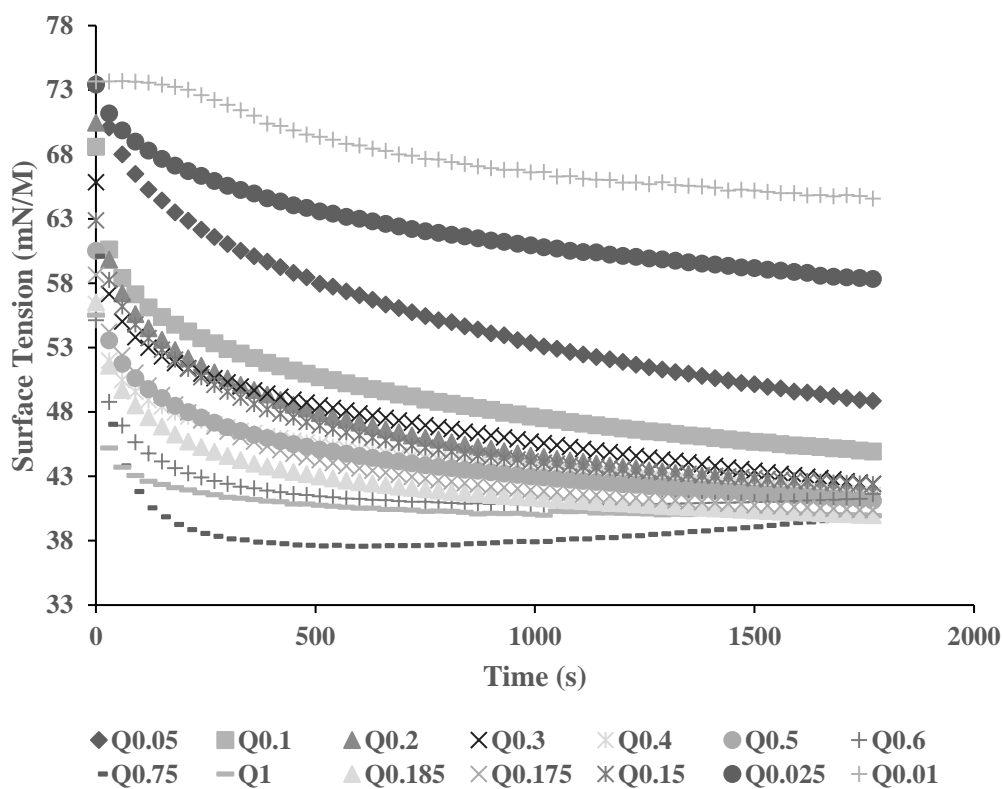


Figure 3.11. Effect of concentration on the surface tension profile of QSE solutions

The dynamic ST vs concentration curves can be seen in Fig. 3.11. For ease of comparison, only the first 30 minutes were shown on the graph. As previously discussed, the data reliability decreases for longer times. As the rate of relaxation

rate decreases, other processes such as evaporation of adsorption of water, becomes more dominant which makes the curves harder to interpret. As seen in Fig. 3.11, the adsorption curves for the first 30 minutes, seems to consist of two regions with distinctly different slopes, with an initially high relaxation rate that greatly decreases after around the 200-400 s mark. This kink in slope refers to a change in mechanism of ST relaxation. Only one of the samples (Q0.01), follows a different relaxation profile that contains an additional lag phase where ST does not drop within the initial 200 s. This behavior is reminiscent of typical protein adsorption that occurs in three different regimes. A representative curve is given in Fig.1.21. The first of these, Regime I, is only observed for dilute concentrations. During this period, because of the possible existence of kinetic barriers to surfactant adsorption over the measured time scale, there occurs no drop in ST (Adamczyk et al., 2009; Beverung et al., 1999; Macleod and Radke, 1994; Pérez-Mosqueda et al., 2013). This regime, also called induction or lag period. This phenomenon is interpreted in several ways. Such a mechanism proposes a phase transition related to intermolecular attraction supplemented by diffusion and adsorption of additional surfactant molecules that do not create changes in surface tension. Another such mechanism explains this behavior, co-operative adsorption caused by intermolecular attractions which causes the activation energy for desorption to increase faster than adsorption. The presence of interaction due to co-operative adsorption reduces surface pressure which compensates for the ST reduction owing to the increase in surface concentration (Calero et al., 2010). In any case, due to the slow rate of diffusion, or interfacial unfolding and rearrangement of globular proteins, ST's do not drop appreciably during this period (Beverung et al., 1999; Nahringbauer, 1995; Pérez-Mosqueda et al., 2013).

We have only observed an induction period for a concentration of 0.01%, at which the equilibrium ST was around 63 mN/m. At such low concentrations, owing to the scarcity of QSE in bulk, the effective diffusion coefficient which is a function of concentration is so small that a period of constant ST is observed. For concentrations larger than 0.025 % w/v, the relaxation curves proceed to Regime II so quickly that

it cannot be observed within the time scale of pendant drop method. For foams, rapid interfacial acquisition is necessary. Molecules that do not require an unfolding to show interfacial activity, have been demonstrated to be better suited for foam formation. These molecules that can directly adsorb on the interface in their native state, have shown no induction period and this attribute was reported to contribute to their foamability (Davis and Foegeding, 2006; Zhu and Damodaran, 1994). With a rapid adsorption, the interface acquires higher resistance against disturbances in the form of energy input introduced during foam formation, which hinders foam collapse. Due to differences in surface affinity and denaturation kinetics, different polymers display vastly different relaxation profiles (Beverung et al., 1999). The fact that QSE does not display an induction period for concentrations over 0.025 % w/v, designates its strong potential as a foaming agent.

For concentrations over 0.025 % w/v, relaxation of ST starts within the first few seconds of particle formation. A higher concentration of the surfactant polymer in bulk results in an almost instant acquisition of an interfacial concentration above the critical value necessary to observe ST reduction. The next relaxation phase (Regime II in Fig. 1.21) is identified with a sudden decline in ST and for all QSE concentrations was over within the first 200 s. During this phase, molecules diffused to the interface partially expose hydrophobic residues to the air-water surface and irreversibly adsorb (Macritchie, 1978; Vrij, 1976). The steep decline in surface tension is explained with two mechanisms that act simultaneously. Adsorbed molecules relax from their rigid conformation that makes room for more of the hydrophobic sections of the molecule to adsorb, increasing the number of contacts for each molecule. At the same time, new molecules continue to diffuse from the bulk aqueous phase and adsorb, either in their native state or with minimal conformational change. This process continues until interfacial saturation (Beverung et al., 1999).

The lack of an induction period and the very steep ST decline is a rare observation in surfactant biopolymers. For globular proteins for instance, a lag period is commonly observed and Regime II ST reduction progresses at a slower rate

(Beverung et al., 1999; Covis et al., 2014; Dickinson, 2018; Karbaschi et al., 2014; Sosa-Herrera et al., 2016). This finding implies that QSE proteins, even in their native state, and the polysaccharide chains solvated in water, contain hydrophobic residues that have instant access to an interface. The high surface hydrophobicity of QSE implies that the tertiary structure of the proteins is aligned such that the hydrophobic amino acids are not embedded into the molecule interior. Protein surface hydrophobicity was found to be directly related to the rate of tension decline in Regime II by Beverung et al. (1999) who have shown casein and BSA that displays the greatest rates of ST decline to also possess the highest surface hydrophobicities out of the proteins investigated. As summarized in Section A.1.3 in Appendix, QSE is composed of three different polysaccharide-protein complexes with some of them being smaller than others. The smaller glycoproteins, could have rapidly diffused to the interface and started ST decline which could have been supported by subsequent irreversible adsorption of the much larger QSG2. A similar observation was made for Gum Arabic. The consensus is that the AGP (arabinogalactan-protein) component is the fraction mostly responsible for Gum Arabic's interfacial properties with the glycoprotein fraction taking a supplementary role (Evans et al., 2013; Funami et al., 2007; Kontogiorgos, 2019; Sanchez et al., 2018). It is known that with polydisperse polymers, the larger molecular weight fractions, adsorb preferentially over smaller ones and with time, especially at higher concentrations, they replace smaller fractions that are much quicker to be positioned on the interface (Cao et al., 2013; Tadros, 2009). Rate of relaxation in Regime II, expectedly, increases with increasing concentration. With higher concentration of surfactant in bulk, the molecules' accessibility to the surface increases. The rate of diffusion also increases owing to the shortened mean free path for diffusion. A more crowded solution also increases the rate and probability of molecular collisions that also increases interfacial positioning of the protein molecules (Young and Torres, 1989). Many other researchers have also reported increasing relaxation rate with surfactant concentration (Arabadzhieva et al., 2011; Bouyer et al., 2013; Moreira et al., 2012;

Pérez-Mosqueda et al., 2013; Sosa-Herrera et al., 2016; W. Wang et al., 2014; Young and Torres, 1989).

The final regime starts around the 200 s mark and continues up until the end of time dependent measurements. As previously discussed, QSE at the air-water interface never displayed a true equilibrium. The slower gradual decline in Regime III (Fig. 1.21) is associated with conformational changes in the adsorbed layer, and the resulting interfacial skin formation (Benjamins and van Voorst Vader, 1992; Cascão Pereira et al., 2003). With ongoing slow rearrangements, adsorbed molecules tend to seek the most energetically favorable positions for their hydrophobic and hydrophilic side chains. During this process more and more of the hydrophobic sections are exposed to the interface, whereas the rest of the molecule, through increased intermolecular attractions, form aggregates, branches and protein-polysaccharide complexes (Freer et al., 2004b; Krstonošić et al., 2019; Sosa-Herrera et al., 2016). The enhanced degree of entanglements form bridges that connect at various points, resulting in an amorphous gel-like network at the interface (Beverung et al., 1999; Freer et al., 2004b). For surfactant polymers, this stage goes on for such a long time at such a slow rate that makes it hard to distinguish a true equilibrium ST. Multilayer adsorption, long-time molecular rearrangements, breakage and generation of non-covalent stabilizing bonds and interactions between adjacent proteins in solution bulk continue to contribute to ST changes, sometimes over a period of days (Ward and Tordai, 1946; Wüstneck et al., 1996). Slope of ST decline in Regime III, decreases with increasing concentration (Fig. 3.11). This was quite opposite to our observation with the relaxation in Regime II. Relaxation rate in Regime II had increased with increasing concentration. After the critical aggregation concentration of 0.165 % w/v, all samples equilibrated at the same ST plateau (38 mN/m). However, as the QSE concentrations increased, it took longer to reach that equilibrium. This behavior may be related to restriction of molecular mobilities by enhanced viscosity of the solution. As previously examined by the authors, QSE causes significant increases in viscosity and a shift from Newtonian to a non-

Newtonian flow behavior over a concentration of 0.05 % w/v (Emrah Kirtil and Oztop, 2016).

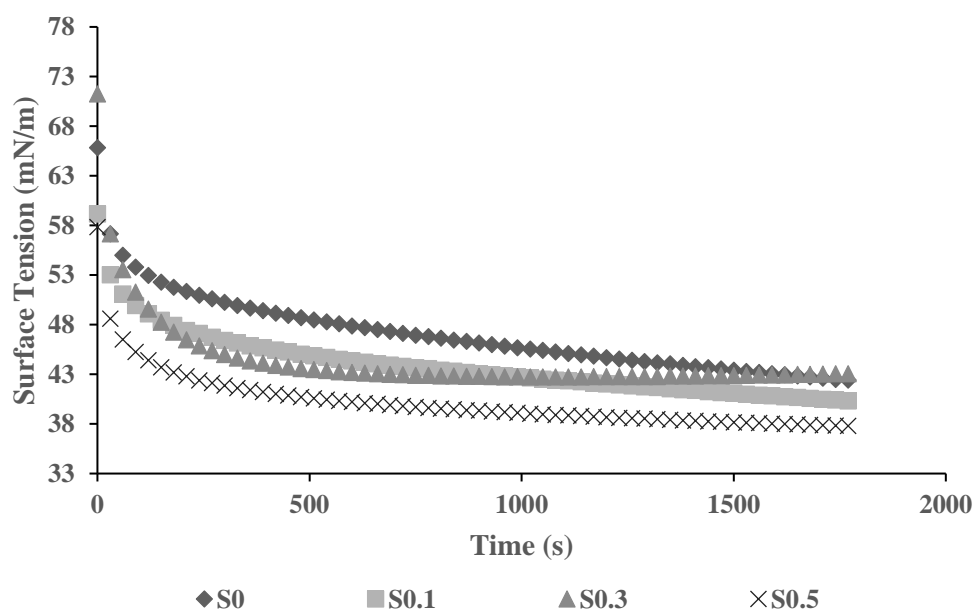
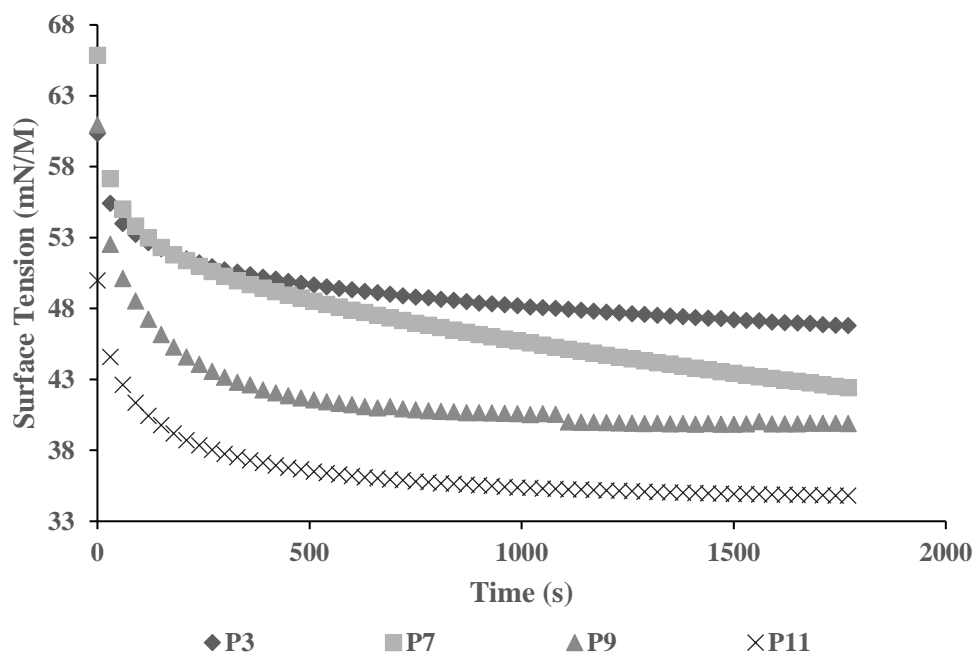


Figure 3.12. (a) Effect of pH on the surface tension profile of QSE solutions (b) Effect of NaCl concentration on the surface tension profile of QSE solutions

Electrostatic effect also plays a major role in conformation of the adsorbed layer. The relative contribution of these electrostatic effects is obviously dependent on the pH and the ionic strength of the aqueous medium. Fig. 3.12a shows the dynamic ST relaxation curves for solutions at different pHs. There is an obvious increasing trend in the rate of relaxation as the pH increases from 3 to 11. The isoelectric point of the proteins of the extract is pH 4.2 (Deng et al., 2019). Thus, out of the pHs examined pH3 is the one closest to the isoelectric point, thus moving to higher pHs, we get further from the isoelectric point. QSE has a high charge density, owing to an abundance of glucuronic and galacturonic acid residues as well as the high protein content. At pH10, the zeta potential of the extract is -38.4 mV. Fig. 3.13 shows an idealized illustration of an adsorbed layer of QSE for pHs near isoelectric point (Fig. 3.13a) and further from it (Fig. 3.13b). Over a pH of 4.2 proteins are negatively charged, this is also higher than the pKa's of both galacturonic (pKa of 3.5) (Dickinson, 2018) and gulucuronic acid (pKa of 3.12) (Wang et al., 1991). At pH values close to 4.0, uncharged polymer chains readily self-associate and due to a lack of electrostatic repulsion, molecules tend to locate in close proximity where hydrophobic interactions become dominant. This causes a thinner and denser adsorbed layer with decreased interactions with the aqueous phase (Fig. 3.13a). For this case, the free volume associated with each chain is lower and the reduced conformational entropy restricts the addition of new polymer chains on the interface. The dense packing also makes it harder for the already adsorbed chains to relocate and increases the time it takes for the molecules to relax to their most energetically favourable state (Alba et al., 2016; Castellani et al., 2010a). This hindering effect of pH in protein unfolding and the resulting diminished surface activity was also encountered by Deng et al. 2019, who have discovered QSE to show lowest emulsifying ability index (EAI), emulsion stability index (ESI) and foaming capacity for pHs near 4.0 (Deng et al. 2019).

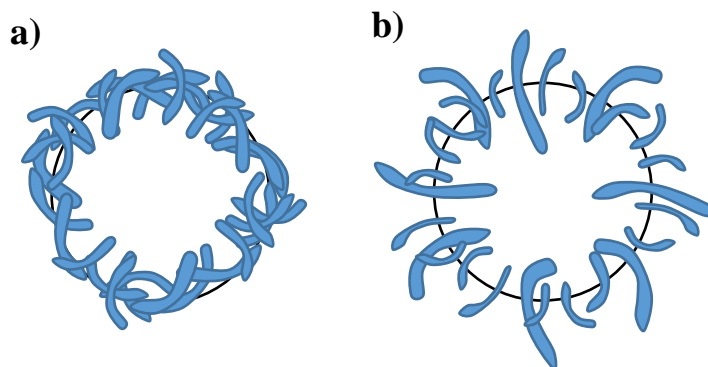


Figure 3.13. Idealized illustration of the effect of pH on the adsorbed QSE layer (a) pH close to 4.2 (b) when $\text{pH} \ll$ or $\gg 4.2$.

For pH values well above 4.2, as illustrated in Fig. 3.13b, electrostatic repulsion between the negatively charged carboxylic acid groups and the proteins cause the polymer chains to extend further from the interface, increasing water-QSE interactions, which is also supported by increased protein solubility at higher pHs (Deng et al., 2019). As a result, hydrophilic molecule fractions extrude through the bulk phase in a more wide-spread manner, providing more room for fresh molecules to adsorb. Additionally, the reduced hydrophobic interactions within the molecule itself results in an accelerated structural flexibility that increases the molecular mobility which facilitates molecular rearrangements. All these increase the rate of relaxation of the polymer for pHs higher than 4.2. At pH11, the equilibrium ST is also significantly lower than other pHs by around 2 mN/m. This implies that, with the increased negative charge, after a certain point, not only the rate of unfolding, also the final state of the molecule changes. QSE is abundant in disulfide bonds (19.79 $\mu\text{M/g}$ as identified by method) which is known to provide high structural stability of proteins and can act as a barrier against protein denaturation (Beverung et al., 1999; Du et al., 2012; Karbaschi et al., 2014; Tang et al., 2006). The high charge at pH11 presumably was sufficient to break the final remaining disulfide bonds and overcome other possible intermolecular attractions that prevent complete unfolding. As a result, final remaining hydrophobic residues are exposed to the air-water interface resulting in a decline in ST. Other researchers have similarly

observed increased surface activity of proteins further from the isoelectric point (Mundi and Aluko, 2012; Tang et al., 2006).

Fig. 3.12b shows the ST relaxation profiles of QSE solution with differing amounts of NaCl (S0: control, S0.1: 0.1 M, S0.3: 0.3 M, S0.5: 0.5 M). Addition of a background electrolyte species (e.g. NaCl) to a polyelectrolyte solution results in the formation of an ionic double layer. All these ions are only soluble in the aqueous phase and simultaneous transport of each species is finalized when surface-active ions (e.g. QSE anions), are completely covered by its associated indifferent counter-ion (e.g. sodium cations) which is surrounded by an indifferent co-ion (e.g. chloride anions). Ions within the double layer are anchored to their positions surrounding the interface by a series of electrostatic attractions and repulsions (Z. Gao et al., 2017; Macleod and Radke, 1994). This later could act as a shield against transport of nonionic surfactants in particular. For charged polymers, the salt screening effect can facilitate adsorption (Young and Torres, 1989). For our case, the presence of an ionic double layer enhanced the rate of transport of surfactant and its adsorption. A higher ionic strength solvent is known to reduce the Debye length of charged protein side chains (Beverung et al., 1999). As a result, electrostatic repulsion decreases which allows for faster interfacial saturation and helps the proteins to pack in a more efficient way. Similarly, the charged sugar acids, that are not adsorbed but extrude through the aqueous phase, being negatively charged at neutral pH, can form a layer of charge-charge repulsion that acts against the movement of surfactants towards the interface. The accumulation of Na⁺ cations around the surfactant-laden interface decreases electrostatic repulsion and accelerates the adsorption of fresh polymers. Similar finding were reported by other researchers studying the effect of ionic strength on surface properties of charged surfactants (Beverung et al., 1999; Hayase and Tsubota, 1986; Ishimuro and Ueberreiter, 1980; Young and Torres, 1989).

3.2.3 Surface Rheology Measurements

Despite surface affinity being a necessity in the formation of a dispersed system with a large interfacial area, actual long term stability is enabled through improved resistance of interfaces from surrounding dispersing phases (Bos and Van Vliet, 2001; Dickinson, 2001, 1999, 1998). Especially for systems stabilized by macromolecular surface-active species, this resistance is more pronounced. The gel-like network formed by adsorbed thick polymer layer results in the generation of an elastic interfacial-skin (Freer et al., 2004a) that act as a barrier against droplet coalescence (Santini et al., 2007b). However, a simple visual analysis doesn't provide much quantitative information on the interfacial skin's mechanical properties, formation kinetics, and relaxation rates. This ambiguity is overcome by interfacial rheological measurements that convey information on the interface's response to both the compressional and shear deformation (Langevin, 2000). A highly stable interface should be able to dampen external disturbances both normal and tangential to the interface; that way, film rupture can be prevented. Unlike surface tension that is a measure of forces normal to the interface, dilatational surface rheology is related to forces operating tangentially, which further underlines its significance (Santini et al., 2007b). The theory is also supported by experimental data that shows a direct relation between surface dilatational properties with foam and emulsion stability (Beverung et al., 1999; Cao et al., 2013; Cascão Pereira et al., 2001; Davis and Foegeding, 2006; Freer et al., 2004b; Kontogiorgos, 2019; Mendoza et al., 2014; Pérez-Mosqueda et al., 2013; Santini et al., 2007b; Vernon-Carter et al., 2008; Zhang et al., 2011).

Table 3.4. Average E' , E'' and $\tan\Delta$ values for QSE at an air-water surface

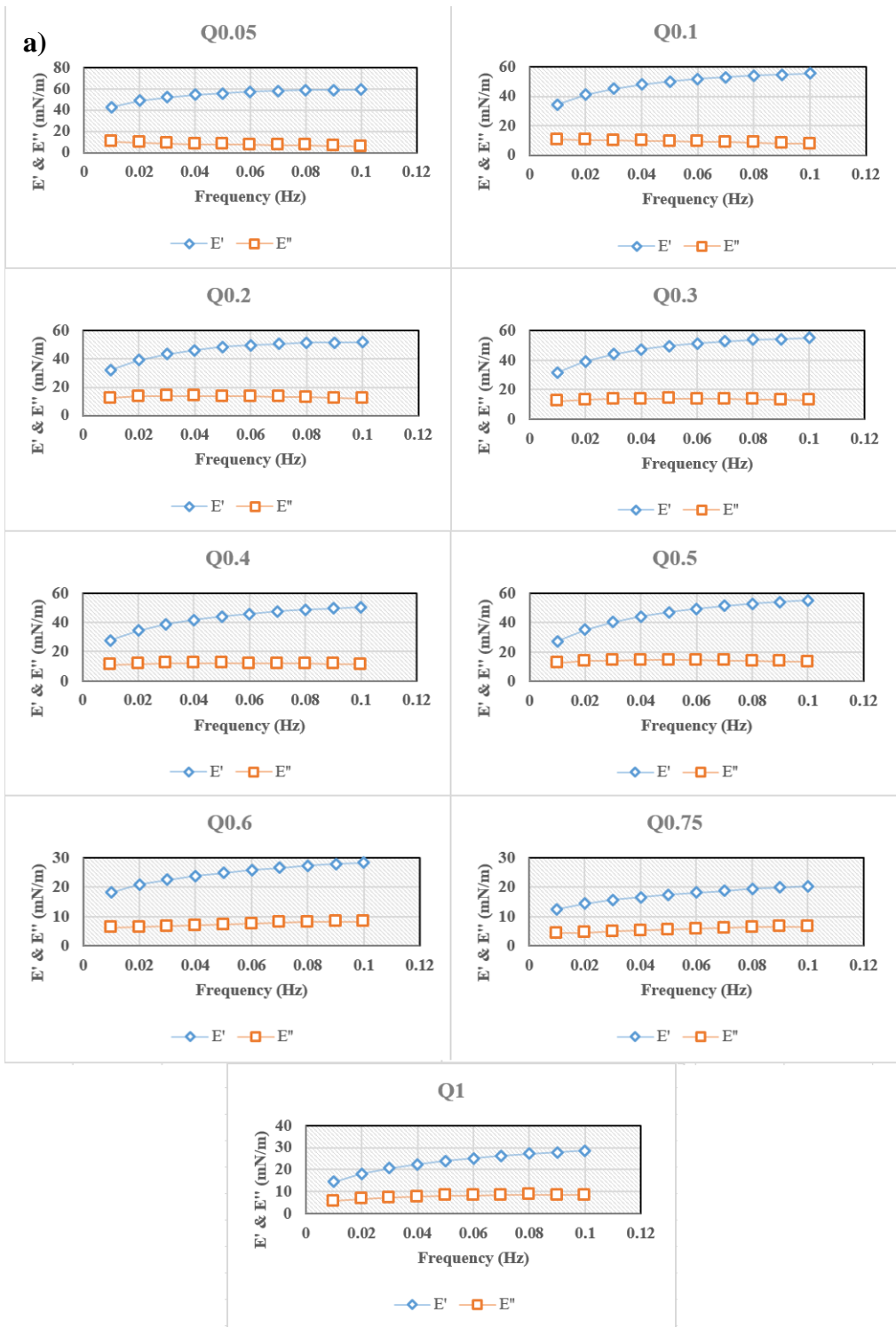
Concentration			
(% w/v)	E' (mN/m)	E'' (mN/m)	$\tan\Delta$ (°)
0.05	58.18±9.41 ^a	8.71±2.07 ^a	0.15±0.01 ^c
0.1	48.5±2.09 ^{ab}	9.55±0.26 ^a	0.20±0.01 ^c
0.2	46.52±1.74 ^{abc}	13.12±3.17 ^a	0.29±0.07 ^b
0.3	47.99±1.54 ^{abc}	13.42±1.61 ^a	0.29±0.03 ^{ab}
0.4	42.85±5.02 ^{bc}	11.83±1.96 ^a	0.28±0.02 ^b
0.5	45.72±3.75 ^{abc}	13.98±2.34 ^a	0.32±0.03 ^{ab}
0.6	24.63±4.63 ^{bc}	7.41±0.87 ^a	0.31±0.02 ^{ab}
0.75	22.35±7.88 ^c	7.08±2.26 ^a	0.33±0.04 ^{ab}
1	23.48±1.91 ^{bc}	7.89±1.01 ^a	0.34±0.04 ^a
pH			
3	40.77±1.97 ^a	7.23±0.29 ^b	0.18±0.01 ^b
7	47.99±1.54 ^a	13.42±1.61 ^a	0.29±0.03 ^{ab}
11	29.79±8.08 ^a	9.44±1.96 ^{ab}	0.36±0.11 ^a
Salt Content (M)			
0	47.99±1.54 ^a	13.42±1.61 ^a	0.29±0.03 ^a
0.1	37.80±1.77 ^a	11.11±1.61 ^a	0.30±0.03 ^a
0.3	28.68±7.00 ^a	7.29±1.88 ^a	0.26±0.01 ^a
0.5	41.21±0.68 ^a	10.26±1.31 ^a	0.26±0.03 ^a

Table 3.4 lists the average values for E' and E'' of 10 different frequencies (from 0.01 to 0.1 Hz). E' (dilatational storage modulus) is a measure of the elastic counterforce of the surface to a possible deformation, whereas E'' (dilatational loss modulus) defines how fast the initial values of ST is restored after deformation (Mendoza et al., 2014; Seta et al., 2014). For all concentrations, elastic behavior is more prominent on the air-water interface. This implies that the viscoelastic interface formed by QSE adsorption behaves more like an elastic solid than a viscous fluid, which bestows the surface a higher resistance to deformation. This behavior is typical for viscoelastic polymer layers (Pérez-Mosqueda et al., 2013). Perfectly elastic interfaces store all of the energy input by deformation, later to release it without loss. Consequently, with higher elasticity, the interface gains a higher resistance against deformation (Freer et al., 2004b). A film subjected to stretching by external disturbances increases in surface area, which results in a reduction in surface excess concentration of the foaming agent (called *Gibbs* effect). If enough time passes for surfactants soluble in bulk phase to diffuse to the surface, original ST can be restored (*Marangoni* effect). The *Gibbs-Marangoni* effect is necessary for foam formation, and the absence of this mechanism is the reason pure liquids do not foam (Shaw, 1992).

For foams, one of the most dominant destabilization mechanisms is film rupture. The process always proceeds by local thinning on the fluid surface formed by a greater expansion of the surface area in a certain region of the interface. This leads to a dilution of surfactant on the thinning region and results in a surface tension gradient (Karbachi et al., 2014; Santini et al., 2007b). It takes time for the surfactant to be transported from the rest of the interface and the bulk to the thinning region. During this time, the thinning region is considerably more susceptible to rupture than the rest of the interface. Surfactant diffuses to this region, carrying a significant amount of underlying solution, which nullifies the thinning process. The interface requires a high *Gibbs* elasticity to counter the effects of local thinning during the surfactant transport process. Nevertheless, a highly viscous surface (identified by a higher dilatational loss modulus) acts opposingly to this mechanism. High bulk viscosity is

expected to retard the rate of foam collapse; on the contrary, high surface viscosity can strongly inhibit bulk fluid and surfactant transport at and close to surfaces, which causes more rapid film drainage (Arabadzhieva et al., 2011; Shaw, 1992). Thus, a highly elastic and less viscous surface provides the highest possible stability against foam collapse. This essentiate the importance of phase angle ($\tan\Delta$), which depicts the ratio of the loss to storage modulus. Hence, the lower $\tan\Delta$ the more stable a foam formed by this surfactant will be. The fact that $\tan\Delta$ values are below 0.36 for all samples, suggests that the interface exhibits a higher elastic character, which implies that QSE would be a potentially effective foaming agent.

Fig. 3.14 shows the frequency dependence of all E' and E'' of all samples. Surface elasticity (ε_r) and surface viscosity (η) is are a function of both bulk surfactant concentration (c) and frequency (ν). The extend of these dependences are also known according the equations of $\varepsilon_r(\nu, c)$ and $\eta(\nu, c)$ identified by van den Tempel and Lucassen (Lucassen and Van Den Tempel, 1972a, 1972b). Studying frequency dependence is crucial as it provides information on the relative importance of relaxation processes like diffusion-adsorption and/or molecular rearrangements (Santini et al., 2007b). E' and E'' of all QSE solutions displayed very similar trends with frequency. E' was higher than E'' for all frequencies. E' for all concentrations, pHs and ionic strength, displayed an increasing trend with increasing frequency. E'' , on the other hand, stayed constant within the frequency range studied (0.01-0.1 Hz). The increase in E' with frequency is non-linear, with an initially higher dependence on frequency that seems to decrease for frequencies over 0.04 Hz.



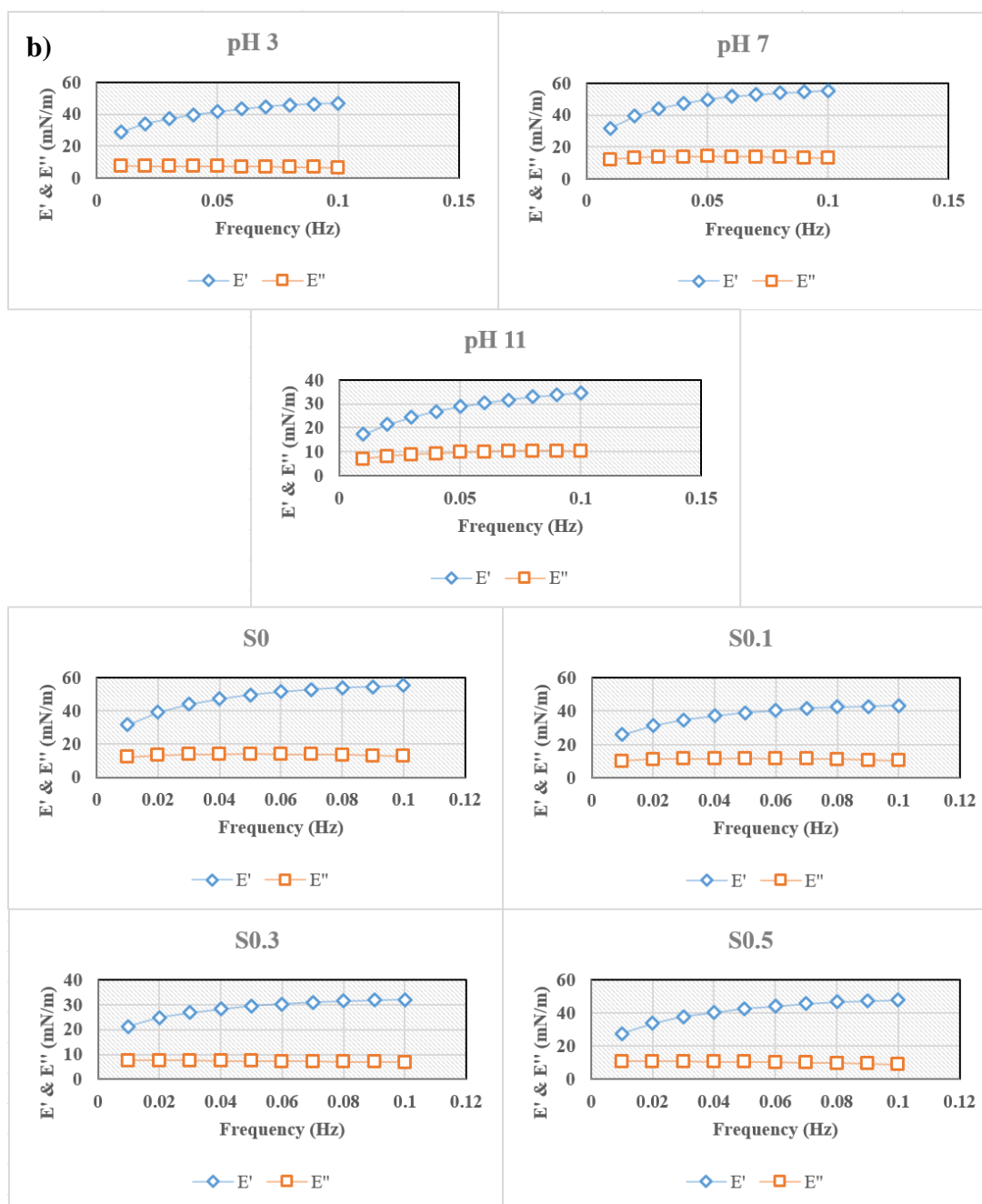


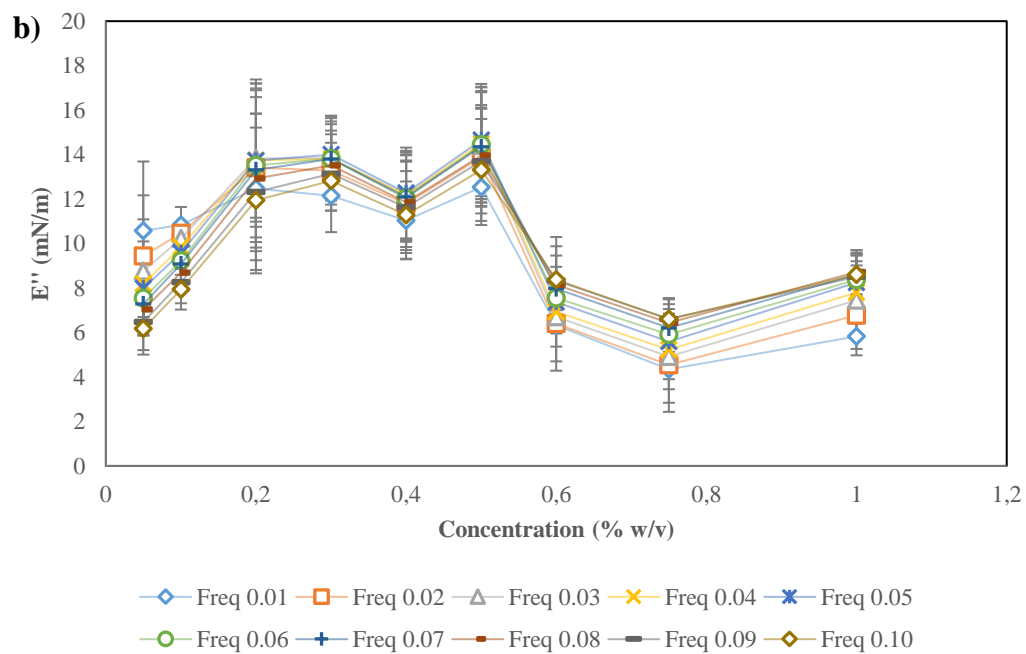
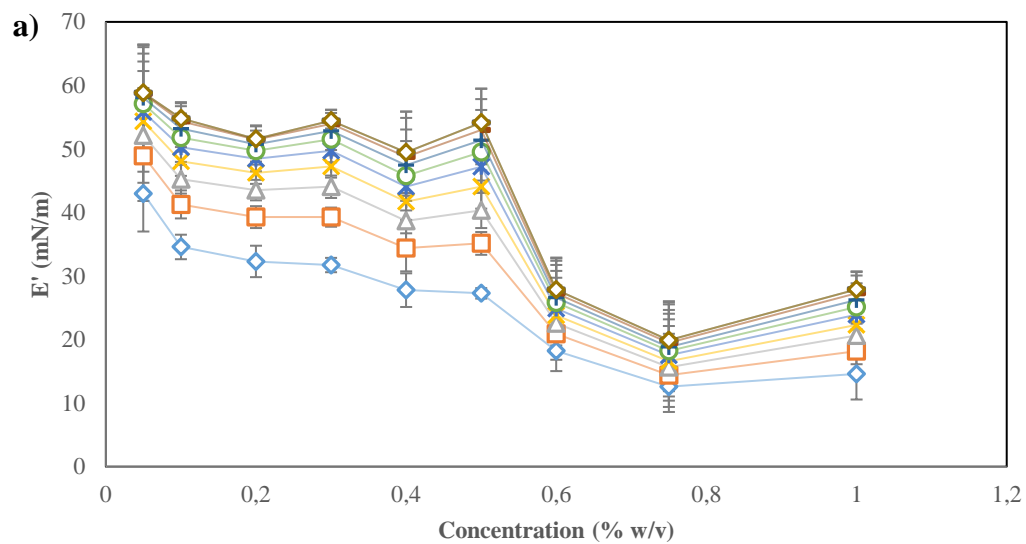
Figure 3.14. (a) Frequency dependence of E' and E'' of QSE solutions with varying concentrations (b) Frequency dependence of E' and E'' of QSE solutions with varying pHs and NaCl concentrations

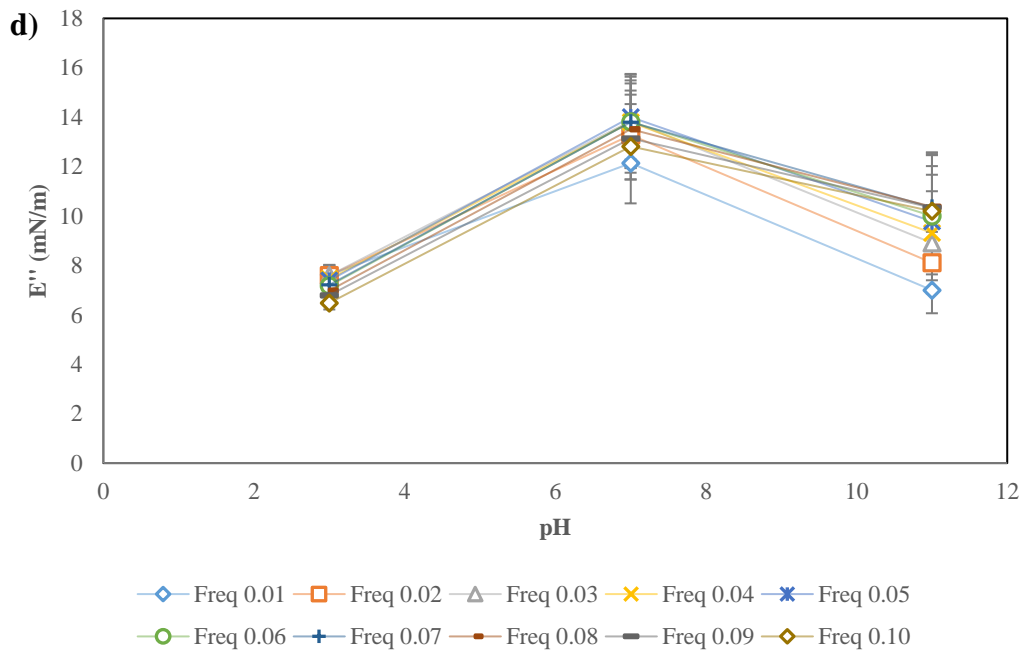
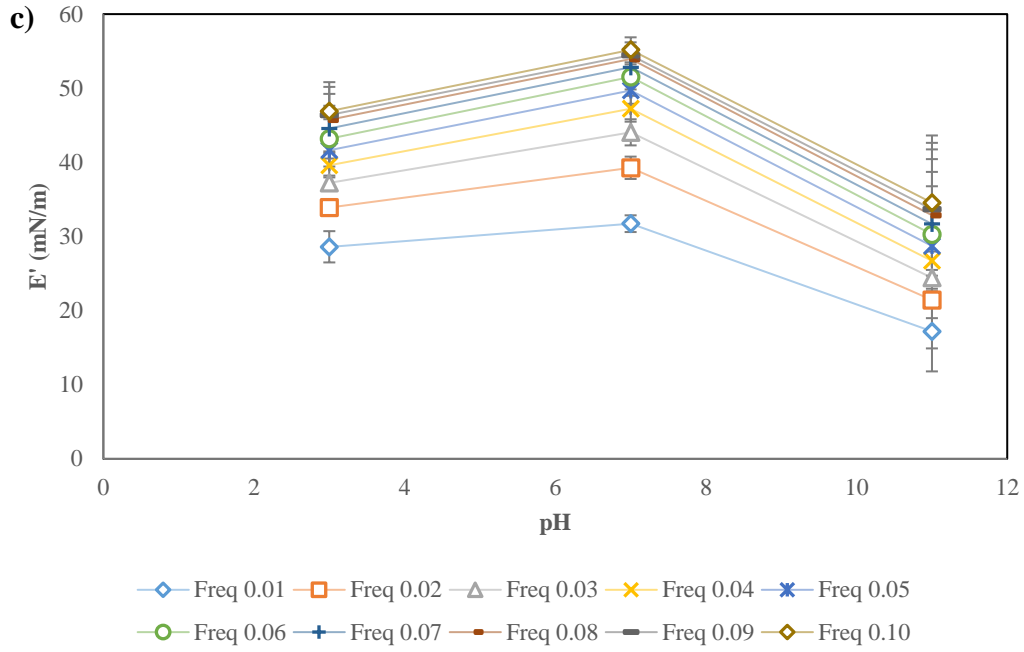
As the surface monolayer is directly in contact with a bulk surfactant solution, the surface rheological properties are strongly influenced by adsorption and desorption

processes. Expanding (compressing) the monolayer causes adsorption (desorption) of the polymeric surfactants to diffuse from (to) the bulk phase in order to re-achieve its equilibrium state (Cao et al., 2013; Santini et al., 2007b). Real behavior lies within two extreme cases. When surface deformation is slow (low frequencies), the monolayer has enough time to reach equilibrium, so much so that deformation has almost no effect on ST. For this case, there is no resistance to expansion ($\varepsilon \rightarrow 0$). When the deformation is so rapid (high frequencies) that the monolayer has no time to respond, it behaves like an insoluble layer, and a change in surface area is directly observed as a similar change in ST (perfectly elastic case). The frequency range obviously lies within these two extremities. According to this mechanism, it is expected for E' to increase with increasing rate of area deformation until a certain plateau is reached (Cao et al., 2013; Ma et al., 2011; Ravera et al., 2005; Wang et al., 2011). The reason of the change in slope with increasing frequency shows E' approaching the plateau value. The initial high dependency of E' on ν , suggest that effect of diffusion of molecules between the bulk and interface on dilatational rheological properties of the surfactant monolayer is more dominant for low frequencies ($\leq 0.4 \text{ Hz}$).

E'' staying constant within the frequency range studied indicates that the characteristic frequency of the relaxation process at the surface layer is higher than the highest oscillating frequency used in measurements (0.1 Hz) (Cao et al., 2013; Ma et al., 2011; Ravera et al., 2005; Wang et al., 2011). The frequency range chosen was restricted by the instrument's limitations. This means surface relaxation is dominated by rapid relaxation processes, those with characteristic frequencies higher than 0.1 Hz. Since QSE molecules are very bulky, molecular rearrangements would take place at lower frequencies, as observed by Cao et al. on silwet408 which is a surfactant with a much smaller molecular weight than QSE (Cao et al., 2013). If the effect of molecular rearrangements were dominant, the opposing effects of diffusion and surface repositioning would presumably cause a local maximum within the frequency range studied (Pérez-Mosqueda et al., 2013; Rühls et al., 2013). Consequently, it is safe to say diffusion of fresh surfactant molecules to void sites on

the interface is the basic mechanism of relaxation for frequencies between 0.01 and 0.1 Hz.





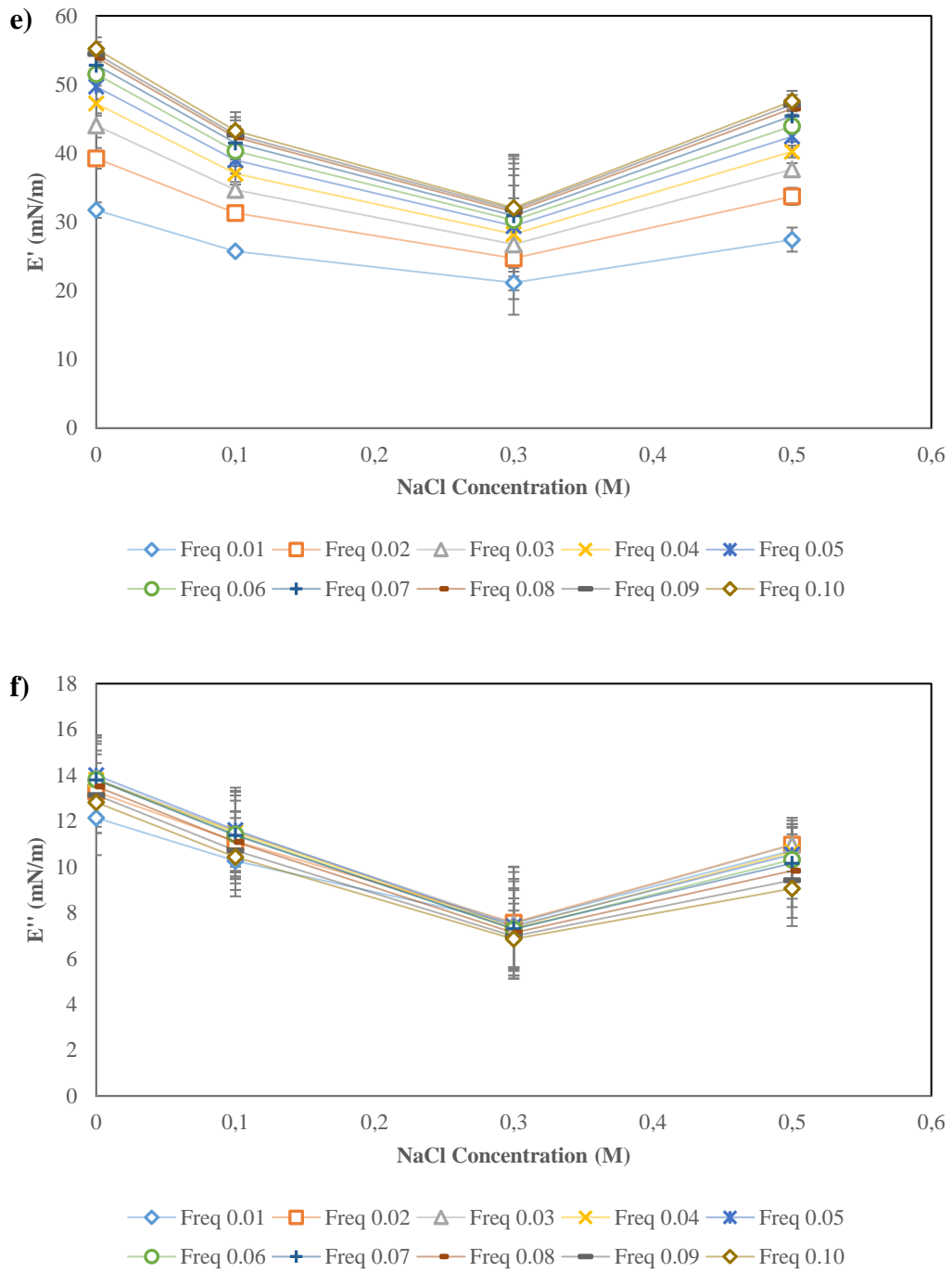
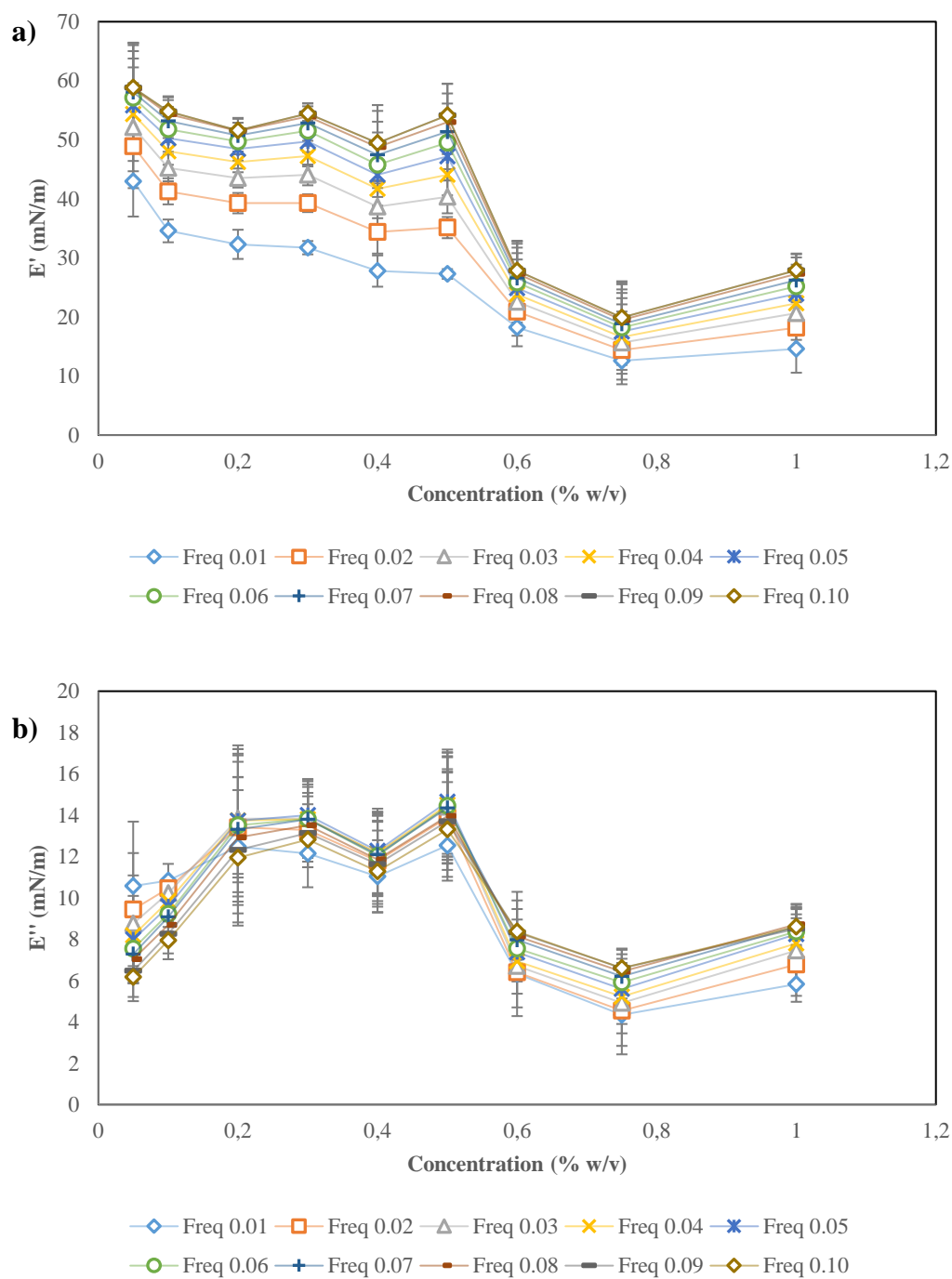
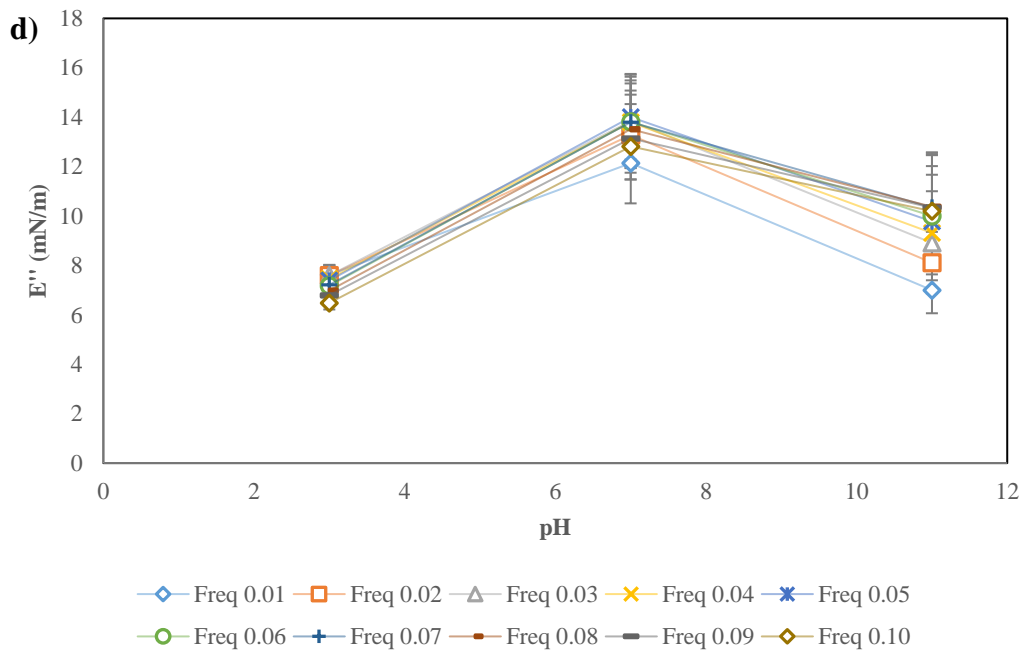
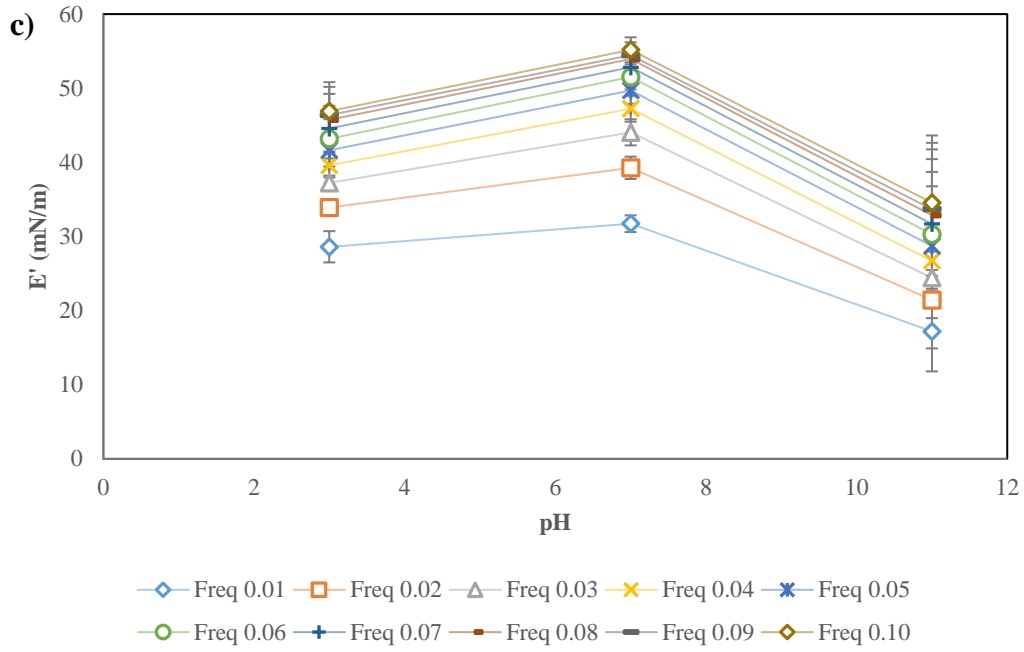


Figure 3.15. Concentration dependence of (a) E' (storage modulus) (b) E'' (loss modulus), pH dependence of (c) E' (storage modulus) (d) E'' (loss modulus), NaCl concentration dependence of (e) E' (storage modulus) (f) E'' (loss modulus) for frequencies 0.01-0.1 Hz.

Fig. 3.15 shows the concentration, pH, and ionic strength dependence of surface dilatational rheological properties of QSE. With concentration, all frequencies follow a similar trend. The results are the average of at least eight different measurements. Despite the strange zig-zag behavior, the fact that all frequencies follow the same trend implies that the behavior should be the result of a conflict between opposing mechanisms, one of which becomes more dominant for concentrations over 0.5 w/v. The effect of bulk surfactant concentration on dilatational modulus was explained by *van den Tempel and Lucassen* model (Ma et al., 2011). One of the mechanisms is related to the molecular interactions between the surface and adjacent bulk phase; the other is related to the surfactant concentration on the surface. With an increase in concentration, more and more molecules are available to the interface, which results in formation of a thicker interfacial network with stronger intermolecular interactions. The thick polymer layer is associated with a higher dilatational modulus and dilatational elasticity. However, on the other hand, higher bulk concentration causes increased molecular exchange between bulk and the interface, which decreases the interfacial tension gradients and thus, results in a reduction in dilatational modulus and elasticity. As a result, as the interface becomes saturated with polymer, the elasticity-enhancing effect of a thicker polymer layer is compensated and finally dominated by the decreased elasticity related to an increased molecular exchange. For this reason, it is to be expected to observe a number of maxima up until a concentration where one of the mechanisms prominently dominates. Multiple other researchers have similarly reported the presence of one or a few maxima and the presence of a sharp kink in slope E' vs c curves (Arabadzhieva et al., 2011; Cao et al., 2013; Rühls et al., 2013; Santini et al., 2007b; W. Wang et al., 2014). As depicted in Fig. 3.15a, the dominance of molecular exchange occurs at a concentration of 0.5 % w/v, after which surface dilatational storage modulus decreases significantly (less than half of its initial value). As previously discussed, there is a strong relation between foam stability and E' values, demonstrated in a number of studies (Beverung et al., 1999; Cao et al., 2013; Cascão Pereira et al., 2001; Davis and Foegeding, 2006; Freer et al., 2004b; Kontogiorgos, 2019; Mendoza

et al., 2014; Pérez-Mosqueda et al., 2013; Santini et al., 2007b; Vernon-Carter et al., 2008; Zhang et al., 2011). Consequently, a concentration of 0.5 % w/v is the highest bulk concentration for a QSE stabilized dispersion, where the interface possesses the highest stability against deformation and the resulting foam collapse or coalescence.





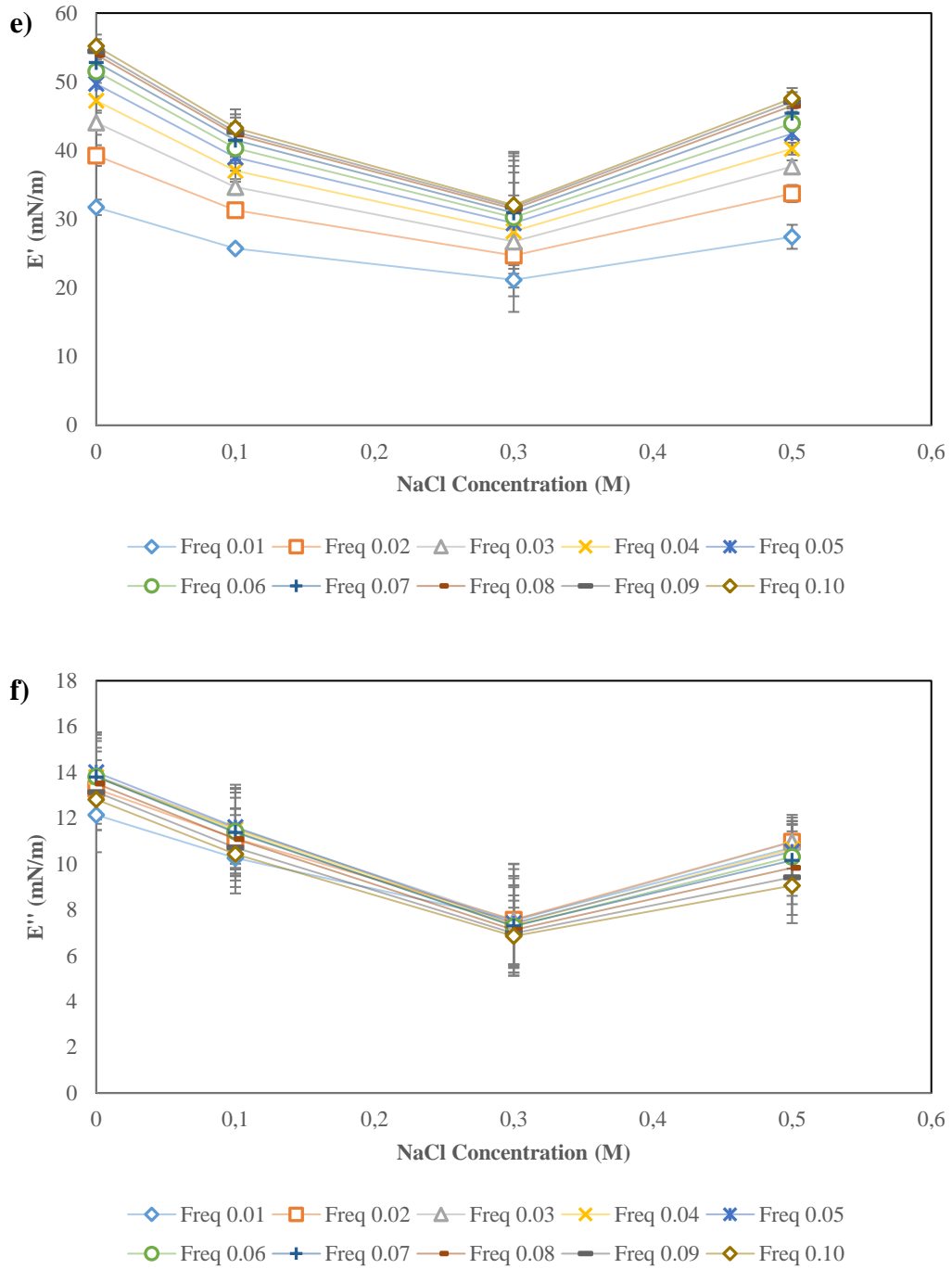


Figure 3.15. Concentration dependence of (a) E' (storage modulus) (b) E'' (loss modulus), pH dependence of (c) E' (storage modulus) (d) E'' (loss modulus), NaCl concentration dependence of (e) E' (storage modulus) (f) E'' (loss modulus) for frequencies 0.01-0.1 Hz.

There also seems to be a frequency dependent shift in local maximum at E' vs c curve (Fig. 3.15a). Maximum is shifted to higher concentrations with increasing frequency. For frequencies over 0.04 Hz, the maximum concentration that displays the highest loss modulus is 0.05 % w/v. For lower frequencies, loss modulus starts following a linearly decreasing trend, with the slope increasing as the frequencies go lower. When discussing surface rheological properties, as previously mentioned, there are two different frequencies that need to be considered, namely, the frequency of molecular exchange (μ) and the disturbance frequency (ν). If the frequency of molecular exchange does not lie within the disturbance frequencies applied (0.01 – 0.1 Hz), it is not possible to see a maximum. The maximum modulus value is actually the cross-over point where the change from $\mu < \nu$ to $\mu > \nu$ takes place (Stubenrauch and Miller, 2004). This shows that with increasing frequencies, the surfactant concentration needed for the crossover increases. Similarly for dilatational loss modulus (E''), surfactant bulk concentration initiates two opposing mechanisms. With an increase in bulk concentration, surface concentration also increases resulting in enhanced relaxation between the two phases that facilitates the release of excess surface energy by ST relaxation, thus increasing loss modulus. However, increasing bulk concentration also increases surface's resistance to deformation that decreases the ST gradient generated by dilatational deformation. This process, on the other hand, results in a reduction in dilatational loss modulus (Huang et al., 2008; Z. Wang et al., 2014). As shown in Fig. 3.15b., E'' values display a maximum at 0.5 % w/v after which it decreases sharply. This indicates that, similar to storage modulus, 0.5 % w/v makes up the critical limit where the effect of one of the opposing mechanisms start to dominate. For E'' , after 0.5 % w/v, the decrease in loss modulus related to the decrease in ST gradient becomes more dominant.

The effect of pH and ionic strength on surface rheological properties can be seen in Fig. 3.15c, d, e, f. Both E' and E'' follows a similar trend, where dilatational modulus displays a local maximum at pH7 and a minimum at a NaCl concentration of 0.3 M. Changes in pH and ionic strength of the medium, causes changes in conformation of polymer chains both at bulk and polymer chains. Bulk conformational changes effect

the ease and rate of adsorption whereas surface changes effect properties like equilibrium ST and dilatational modulus (Karbaschi et al., 2014; Kontogiorgos, 2019). As previously discussed, a thicker and more extensively bonded network on the interface results in increased surface elasticity, which is observed as an increase in dilatational modulus. The effect of molecular conformation on surface rheology was investigated in a number of studies. Karbaschi et al. 2014 came to the conclusion that for increasing number of hydrophobic chains exposed to the surface, dilatational modulus values increased. Additionally, Covis et al. 2014 reported that a more thoroughly unfolded protein chain causes more of the molecule to adsorb, and also increases the length of the loops (non-adsorbed sections of a polymer chain positioned between two points of contact with the interface). With an increasing number of loops, upon surface expansion or compression, non-adsorbed hydrophobic residues could be positioned such that they merge with the hydrophobic aggregates within the adsorbed layer and vice versa, therefore reducing the elasticity of the surface and lowering E^* (Covis et al., 2014). The local maxima and minima in these curves presumably represent the points where either of these processes dominates.

3.2.4 Diffusion Coefficients Governing the Adsorption Process

Table 3.5 lists the diffusion coefficients governing the adsorption process of quince seed extract dissolved in solution bulk onto the interface. There is a major difference between the initial and final rates of diffusion as displayed by the difference between D_0 and D_∞ values. For most samples, the initial rates are a few orders of magnitude larger than the final diffusion rates close to equilibrium. This demonstrates that the process cannot be described by a classical diffusion model and an elaborate analysis requires distinguishing the initial and final adsorption processes, that are obviously controlled by their own distinct subprocesses (Möbius et al., 2001; Senkel et al., 1998). The difference between the initial and final rates of diffusion get particularly

larger as QSE concentration increases. For lower concentrations, the difference is much less significant.

Table 3.5. Diffusion coefficients estimated from tensiometer measurements and NMR Relaxometry data

	Tensiometer		NMR
	D_0 (m ² /s)	D_∞ (m ² /s)	SDC (m ² /s)
Concentrations			
Q0.01	1.79 x10 ^{-05a}	1.16 x10 ^{-04a}	2.59 x10 ^{-09a}
Q0.025	2.62 x10 ^{-05a}	2.03 x10 ^{-05b}	2.53 x10 ^{-09a}
Q0.05	2.30 x10 ^{-05a}	1.44 x10 ^{-06b}	2.56 x10 ^{-09a}
Q0.1	2.81 x10 ^{-05a}	7.39 x10 ^{-08b}	2.50 x10 ^{-09a}
Q0.2	8.65 x10 ^{-06b}	1.5 x10 ^{-08bc}	2.44 x10 ^{-09a}
Q0.3	5.50 x10 ^{-06b}	4.65 x10 ^{-09c}	2.45 x10 ^{-09a}
Q0.4	4.89 x10 ^{-06b}	1.66 x10 ^{-09c}	2.64 x10 ^{-09a}
Q0.5	4.53 x10 ^{-06b}	7.32 x10 ^{-10cd}	2.48 x10 ^{-09a}
Q0.6	4.99 x10 ^{-06b}	3.21 x10 ^{-10d}	2.46 x10 ^{-09a}
Q0.75	3.72 x10 ^{-06b}	1.76 x10 ^{-10d}	2.45 x10 ^{-09a}
Q1	2.53 x10 ^{-06b}	8.2 x10 ^{-11de}	2.53 x10 ^{-09a}
pHs			
P3	1.06 x10 ^{-06a}	2.42 x10 ^{-08a}	2.52 x10 ^{-09a}
P7	5.50 x10 ^{-06b}	4.65 x10 ^{-09b}	2.45 x10 ^{-09a}
P11	1.48 x10 ^{-06b}	1.73 x10 ^{-09b}	2.49 x10 ^{-09a}
NaCl Content			
S0	5.50 x10 ^{-06a}	4.65 x10 ^{-09a}	2.45 x10 ^{-09a}
S0.1	1.64 x10 ^{-06b}	1.56 x10 ^{-08b}	2.58 x10 ^{-09a}
S0.3	3.74 x10 ^{-06bc}	6.85 x10 ^{-09b}	2.45 x10 ^{-09a}
S0.5	8.70 x10 ^{-06c}	2.94 x10 ^{-09b}	2.43 x10 ^{-09a}

Let us now discuss why the rates of diffusion are significantly altered with time. For short time range, the interface is devoid of any surfactants. For proteins, it is known that for adsorption to occur, first proteins should unfold which starts after proteins position themselves onto the subsurface. This hypothetical subsurface layer, where molecular repositioning takes place, is initially empty and the molecules are free to occupy a large area. The mechanism of molecular rearrangement for proteins can be expressed by the *Braun-Le-Chatelier* principle of adsorption (Möbius et al., 2001; Serrien et al., 1992). For low surface pressures (such as at initial times and/or low concentrations), the area per molecules (J) is maximum; which also results in the highest frequency for of conformational changes at the interface. As subsurface is populated by more and more adsorbing molecules (at longer times and/or high concentrations), J decreases, which hinders the rearrangements and the subsequent interfacial adsorption. For low surfactant concentrations, the it takes longer for the subsurface to be populated, and sometimes it never is so crowded that molecules restrict eachothers' rearrangements. In those cases, the rate of adsorption is controlled by the rate of diffusion of surfactant from the bulk to the subsurface. However, as concentration increases, more surfactants are readily available to the interface and initial diffusion rate is very quickly replaced by the second slower rate of diffusion (Wüstneck et al., 1996). This also explains why Regime II (mentioned in Section 3.2.2) is over more quickly as surfactant concentration in bulk gets higher. For these cases, the rate of overall process is governed by the rate of molecular rearrangements, which explains the decrease in D_{∞} with increasing concentration. The trends in D_0 and D_{∞} with pH and NaCl concentration is very similar to what was observed in Section 3.2.2 in Dynamic Surface Tension curves, with the rates of ST relaxation increasing as pH moves from 3 to 11 and as salt content increases. The mechanism behind this observation is already explain in Section 3.2.2.

Self diffusion coefficient for solutions prepared with said amounts of QSE, at specified pH and salt concentrations, measured using NMR Relaxometry, are placed next to the diffusion coefficients of tensiometer measurements for ease of comparison. As apparent from Table 3.5, no significant difference is introduced to

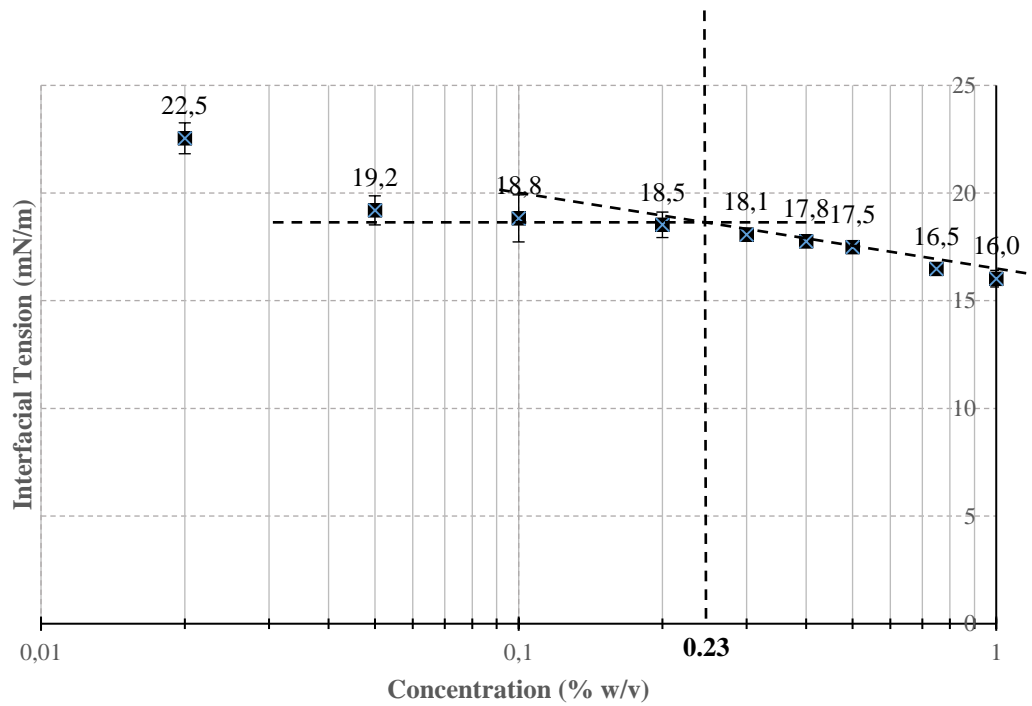
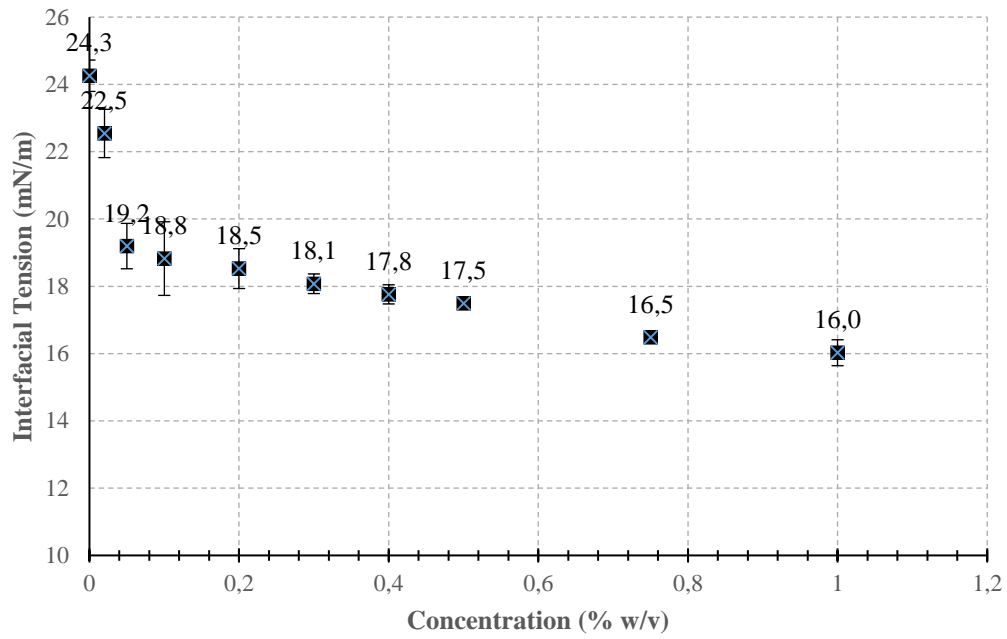
the SDS of solutions with changes in concentration, pH and salt concent. NMR SDCs are diffusion coefficients measured in absence of an interface and rather than being a measure of the rate of adsorption, they represent the rate of *Brownian motion* of the molecules in the water-QSE mixture, which gives insight on the restriction of the molecular mobility by addition of QSE, salt and modification of pH (Dellarosa et al., 2015; Johns, 2009). In absence of an interface, the molecular mobility of the solution itself seems to be constant regardless of the changes made. The diffusion coefficient calculated from tensiometer measurements (will be called D_T from now on) is a complex quantity that is characteristic for both the diffusion and the crossing of the barrier between subsurface and surface (which possesses an activation barrier to overcome). The NMR measurements are key here being the true diffusion coefficients (D) without an interfacial barrier and help determine the process of adsorption that assumes the controlling role. If $D_T \gg D$ or they are of the same order of magnitude, we can say that the presence of an interface accelerated the molecular movements by the spontaneous adsorption of already exposed hydrophobic sections of the surfactants. For this case, diffusion is the rate determining step in adsorption, and there is no additional barrier at the subsurface and it is safe to say adsorption is almost instantaneous once the molecules diffuse to the interface (Ward and Tordai, 1946). If $D_T \ll D$, it is evident that the barrier against adsorption at the subsurface is the rate-determining step. If D is more than a few orders of magnitude smaller than D_T , the diffusion process can be completely neglected and the system could be visualized as an instantaneous diffusion of subsurface followed by a slow molecular rearrangement process (Ward and Tordai, 1946). Considering these, up until QSE concentrations of 0.04 % w/v, diffusion seems to be the determining step for overall rate of adsorption, which means molecules at the subsurface do not experience a barrier to adsorption caused by the population of this layer. However, for concentrations of 0.05 % w/v and higher; the rate of molecular rearrangements slows down and assumes the controlling role for adsorption. For all pH and salt contents; D_T and D were of the same order of magnitude, which indicates that concentration

of surfactant had a more influential effect on diffusion rate than the other factors modified.

3.3 Examination of interfacial properties of quince seed extract on a sunflower oil-water interface

3.3.1 Equilibrium Interfacial Tension

The primary function of a surfactant is to facilitate emulsification by decreasing interfacial tension. This is related to the reduced Gibbs free energy as the amphiphilic surfactant molecules fill the oil-water interface (W. Wang et al., 2014). It takes time for surfactant molecules to diffuse and adsorb on the interface; hence, after forming a fresh interface, interfacial tension starts to decrease down until it reaches a certain plateau at equilibrium. This value is defined as equilibrium surface tension (Berg, 2010; Shaw, 1992). Equilibrium interfacial tension, being an easy and accessible measure of surfactant's performance on the particular oil-water system, is the most widely studied interfacial property (Karbaschi et al., 2014). Fig. 3.16 shows equilibrium interfacial tension values of QSE at a sunflower oil-water interface for increasing concentrations.



S

Figure 3.16. (a) Equilibrium Interfacial Tension Isotherm (b) Equilibrium Interfacial Tension Isotherm (x-axis drawn at a logarithmic scale)

Before moving on to discussion of the results, we believe it is necessary to explain some of the challenges encountered during measurements. To calibrate the system, we tried to make sure the interfacial tension value of pure water- sunflower oil interface is close to its literature value of ~ 25 mN/m (Fisher et al., 1985). However, it was observed that interfacial tension of water was never fully equilibrated. The water was purified of contaminants (Milli-Q water) and the purity was confirmed with a surface tension of ~ 74 mN/m at the air-water interface that remains constant over 24 h. Therefore, the decrease in interfacial tension could not be related to the adsorption processes that this study focuses on, meaning there are other processes that cause interfacial reduction which could get in the way of accurately interpreting the results. Overnight measurement of pure water- sunflower oil interface showed that tension values decrease down to 8 mN/m, with the particle shrinking down to $\sim 20\%$ of its initial volume. This indicated that water was soluble in oil. Though the solubility of water in oil is very low at 25°C (ranging between 0.1-0.25 v/v at saturation) (Hilder, 1968), considering the difference in the volume of oil in the cuvette (~ 30 ml) and the volume of water particle (~ 25 μl), it is not surprising to see most of the particle dissolved after 24 h. To prevent this, oil was pre-saturated with water which decreased the shrinkage considerably ($\sim 80\%$ of its initial volume after 24 h). With a pre-saturated oil and water interface, the interfacial tension started at 24.2 ± 0.2 mN/m and decreased to 18.3 ± 0.7 mN/m in 24 h, which implies a tension reduction rate of ~ 0.25 mN/m/h on average. This is most likely the result of adsorption of surface-active oil contaminants. Other researchers have also encountered a similar trend when measuring dynamic interfacial tension at a water-oil interface (Bouyer et al., 2013; Kontogiorgos, 2019; Seta et al., 2014). Equilibrium surface tension values were identified as the point where the interfacial tension relaxation rate decreases down to the relaxation rate of pure water (~ 0.25 mN/m/h). Most samples acquired this value within the first 2 h of interface formation. The QSE concentration dependence of equilibrium interfacial tension values are depicted in Fig. 3.16. The data in figure is the mean ten different measurements with two overnight and eight 2 h long measurements.

QSE bulk concentration dependence of interfacial tension is depicted in Fig. 3.16a. Upon trials, 0.02 % w/v was chosen as the lowest concentration, resulting in a statistically significant reduction in interfacial tension (IT) (from 24.2 mN/m down to 22.5 mN/m). 0.02 % w/v is a considerably low hydrocolloid concentration to have any effect on the interface. QSE is a graft copolymer whose main polysaccharide fraction consists of a xylose backbone with high amounts of glucuronic and galacturonic acid residues at the branches. The extract also has a very high protein content (~20 % by wt. (Emrah Kirtil and Oztop, 2016)). The proteins are supposedly attached covalently to the main polysaccharide chain. The proteins, being amphiphilic in nature, act as the system's emulsifiers, whereas polysaccharides contribute to the thickness and elasticity of the adsorption layer as well as providing steric stabilization (Tadros, 2009). There is a growing trend in designing polysaccharide-protein conjugate polymers to develop a structure similar to QSE's native state (Anal et al., 2019; Jain and Anal, 2018; Kontogiorgos, 2019). Emulsions stabilized by these Maillard conjugates have preserved their structural stability for more extended periods than emulsions stabilized than the hydrocolloids alone or in combination (Anal et al., 2019; Anvari and Joyner (Melito), 2017; Z. Gao et al., 2017; Y. Liu et al., 2018). Another natural biopolymer that is considered a benchmark emulsifying and stabilizing agent in food and cosmetic industry is Gum Arabic, which also is a graft copolymer with proteins covalently attached to one of the polysaccharide fractions (Alfrén et al., 2012; Bouyer et al., 2013; Kontogiorgos, 2019). As a comparison, Gum Arabic, exhibited a similar equilibrium interfacial tension of ~21 mN/m at a concentration of 5 % w/v (Isobe et al., 2020). Another polysaccharide chitosan at a concentration of 0.1 % w/v decreased interfacial tension for a sunflower oil-water interface from 26.37 ± 0.01 mN/m to 21.51 ± 0.31 mN/m (Lopes et al., 2020). The fact that QSE solutions can significantly affect tension at a concentration of 0.02% w/v, demonstrates the gum's effectiveness as an emulsion stabilizer.

For the concentration range studied (0.02-1 % w/v), the lowest interfacial tension acquired was 16.02 ± 0.38 mN/m. The lowest IT was observed at the 0.75 – 1 % w/v

range. This indicates a 34% reduction in IT by addition of QSE. (Vélez-Erazo et al., 2020) studied the interfacial properties of some macromolecular stabilizers (i.e. pea protein, xanthan gum, sodium alginate, carrageenan, pectin, gellan gum, locust bean gum, tara gum and gum Arabic) at a sunflower oil-water interface. The macromolecular surfactants investigated displayed equilibrium interfacial tension values that ranged between 17 and 22 mN/m. This implies that QSE could prove to be a very effective emulsifier, and help ease emulsion preparation with its high surface affinity and considerable tension reduction functions. This coupled with the viscosity enhancing, and steric stabilizing effect of the gum could make it a very good natural alternative to other widely employed stabilizers. This unusual behavior could be related to the extract's high hydrophobicity. The amino acid profile of QSE reveals that 33.27% of the amino acids in the gums proteins were hydrophobic (Deng et al., 2019). The high hydrophobicity is also accompanied by a high surface hydrophobicity, which indicates that the hydrophobic portions of the proteins have high accessibility to the interface even at their native conformation.

As clearly observed in Fig. 3.16a, there is a sharp kink in the interfacial tension isotherm curve. For the initial three concentrations, there is a very steep slope implying an initially strong dependence of IT on bulk QSE concentration, which later on is replaced by a much less gradual reduction. This behavior is reminiscent of critical micellization concentration (CMC) encountered in solutions of small molecular surfactants. CMC is described as the bulk surfactant concentration at which the interface is saturated with the surfactant; hence, further addition of surfactants would cause them to form micelles in solution bulk rather than being positioned on the interface (Arabadzhieva et al., 2011; Shaw, 1992). Polymeric surfactants like proteins also exhibit a similar behavior where after a critical concentration (Critical aggregation concentration, CAC), polymers tend to form aggregates in bulk and not directly contribute to surface excess concentration (Krstonošić et al., 2019; Tadros, 2009). A standard method for specifying CMC/CAC is to draw linear curves over IT vs logC curves and mark the point of intersection as CAC (Bu et al., 2004; Dal-Bó et al., 2011; Rub et al., 2013). Fig.

3.16b is the ST vs. C curve with the horizontal axis drawn on a logarithmic scale. The curves intersect at a concentration of ~ 0.23 % w/v. Therefore, 0.23% w/v is the CAC for QSE at a sunflower oil-water interface. This concentration is quite low, which means QSE provides monolayer saturation at very low concentrations. Though significantly slower, the decrease in IT continues even after the identified CAC. Similarly, a decrease of IT after CMC/CAC was observed by other researchers and was associated with concentration induced changes in molecular aggregates in bulk and/or multilayer formation resulting from the attraction of bulk surfactants and the adsorbed layer (Beverung et al., 1999; Gashua et al., 2016; Krstonošić et al., 2019; Semenov and Shvets, 2015; W. Wang et al., 2014; Wüstneck et al., 1996).

Fig. 3.17a depicts the change of equilibrium IT for three different pHs, 3, 7, and 11. The solution at pH11 displayed a considerably lower IT than the others. QSE molecules are abundant in sugar acids (uronic acid content of 20 % by wt (Vignon & Gey, 1998)), which are negatively charged at basic pHs. QSE also contains ~ 21 % by wt of proteins that are also negatively charged over the isoelectric point. Out of the pHs examined, pH11 is the one that is furthest from the isoelectric point of the extract, reported as pH 4.2 by (Deng et al., 2019). Sugar acids are positioned on the branches of the molecules, and pH-induced increase in the negative charge of these residues presumably caused the branches to be more widely spread and position themselves farther from the adsorption layer with chains elongated through the aqueous phase. This could have made more room for proteins to adsorb, and with increased protein concentration at the interface, interfacial tension decreased. This result is in line with another study by Deng et al (2019), who have demonstrated increased emulsifying and foaming properties as solution pHs get further from the isoelectric point.

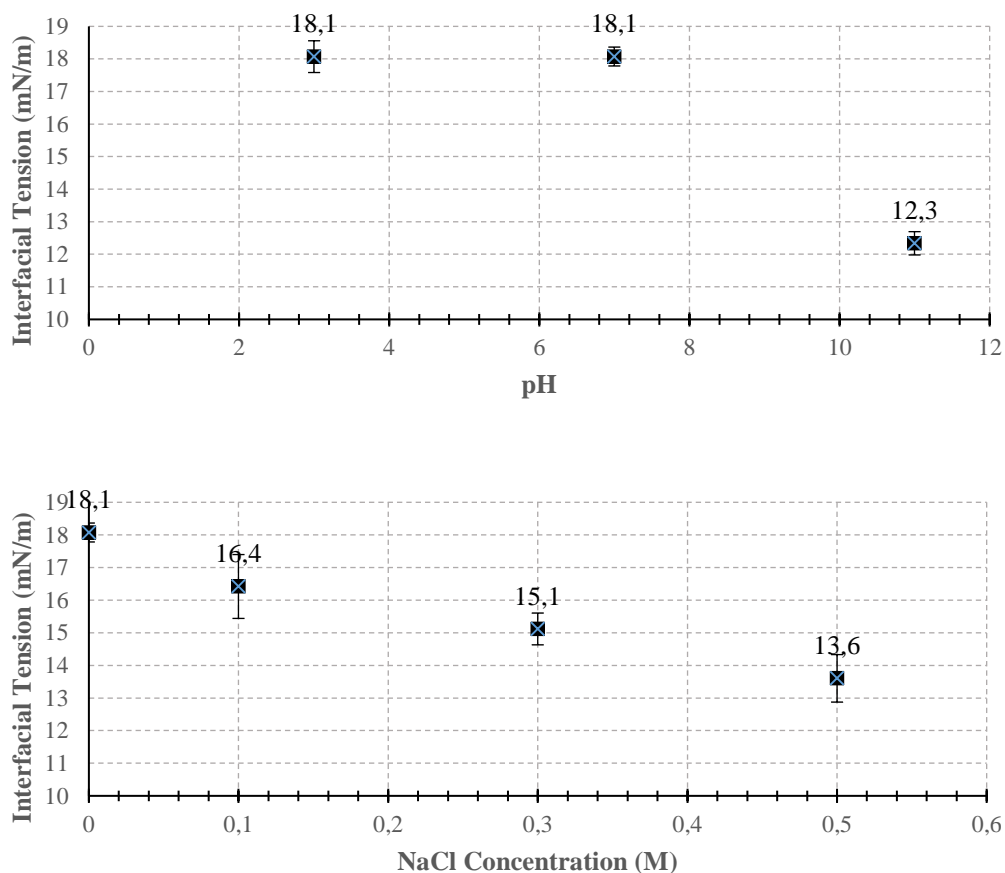
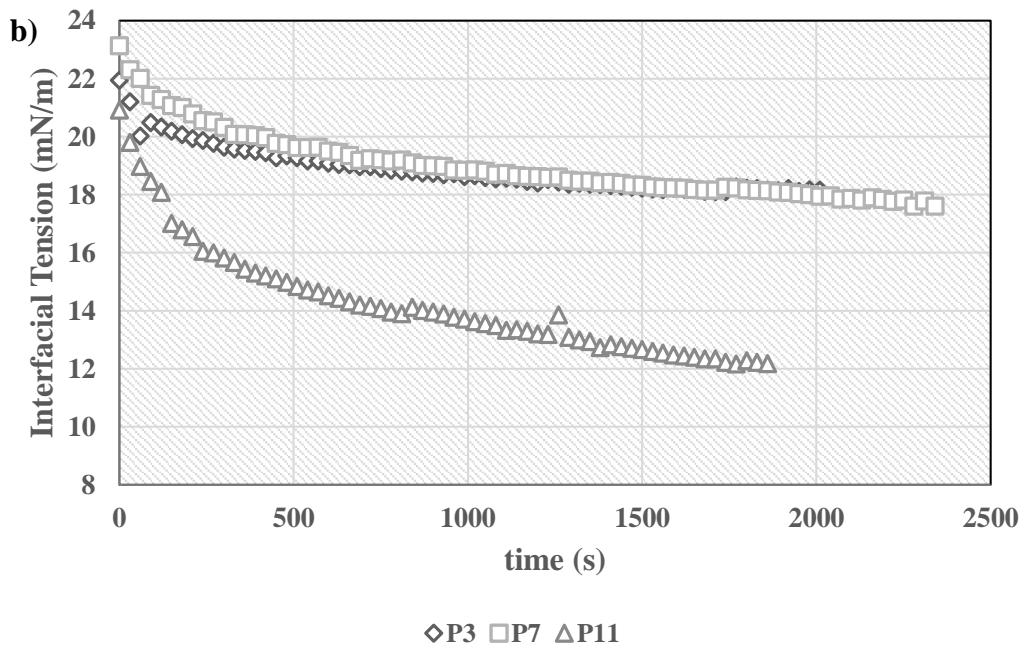
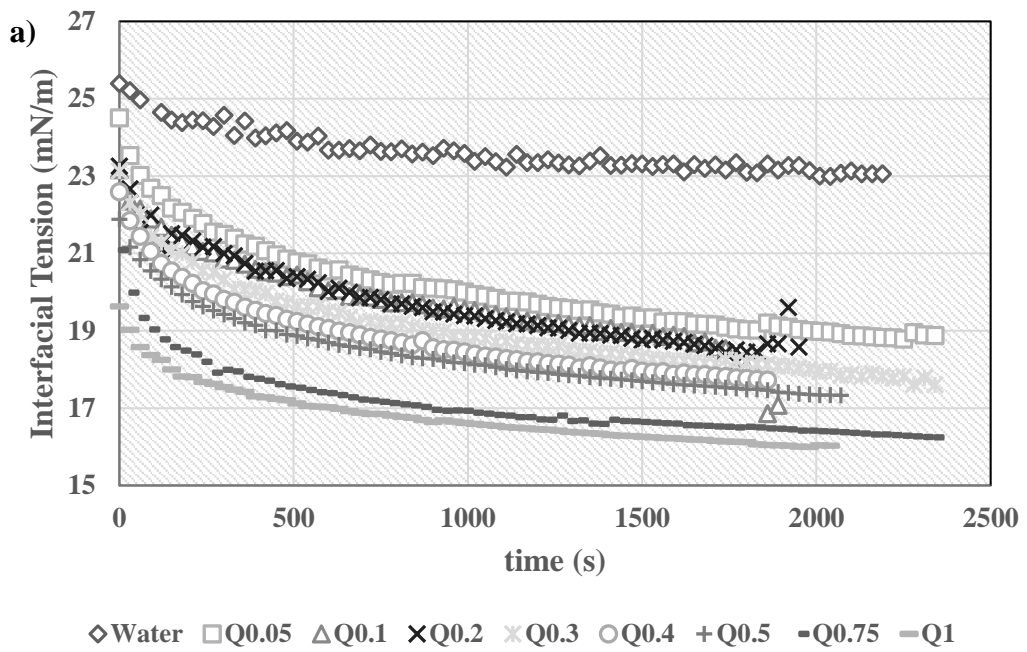


Figure 3.17. (a) Equilibrium interfacial tension of QSE solutions at different pHs (b) Equilibrium interfacial tension of QSE solutions at different NaCl concentrations

As apparent in Fig. 3.17b, IT values were significantly affected by the ionic strength of the medium. There is an obvious negative correlation between NaCl concentration and equilibrium ITs. The concentration range studied (0-0.5 M) is within the “salting in” range for QSE, as shown by other researchers (Ashraf et al., 2017; Deng et al., 2019; Rezagholi et al., 2019), meaning an increase in NaCl concentration increases protein solubility. In the presence of Na^+ and Cl^- ions, protein chains are better solvated by water, which supports increased interactions between water molecules and the polymer. As a result, hydrophilic fractions of the proteins spread out more towards the aqueous phase, which will ease protein unfolding and result in hydrophobic groups to be better exposed to the interface, thus decreasing interfacial tension.

3.3.2 Dynamic Interfacial Tension

Though the reduction in interfacial tension at equilibrium is necessary for effective emulsification, it is not the only parameter governing the process. The adsorbing process and the resulting reduction in interfacial tension should occur in a timescale relevant to the process of emulsion formation (Walstra, 2002; Walstra and Smulders, 2007). Consequently, monitoring the adsorption dynamics is just as crucial in assessing the potential of a surfactant as an emulsifier. This is particularly substantial for polymeric surfactants, which are slower to adsorb on interfaces than small molecular surfactants owing to the retarded diffusion and molecular rearrangements with a larger molecular weight (Seta et al., 2014). The investigation of dynamic interfacial tension at an oil-water interface is particularly characteristic as it mimics the adsorption of lipase enzyme, which is a protein that shows activity on an oil-water interface. There is a growing trend to decrease the caloric contribution of fats in foods, either by hindering lipase activity at the interface or replacing bile salts that facilitate emulsification by other irreversible solid nano-particles (Kontogiorgos, 2019). Examination of the rate and mechanism of adsorption makes up a fundamental step for such surface studies.



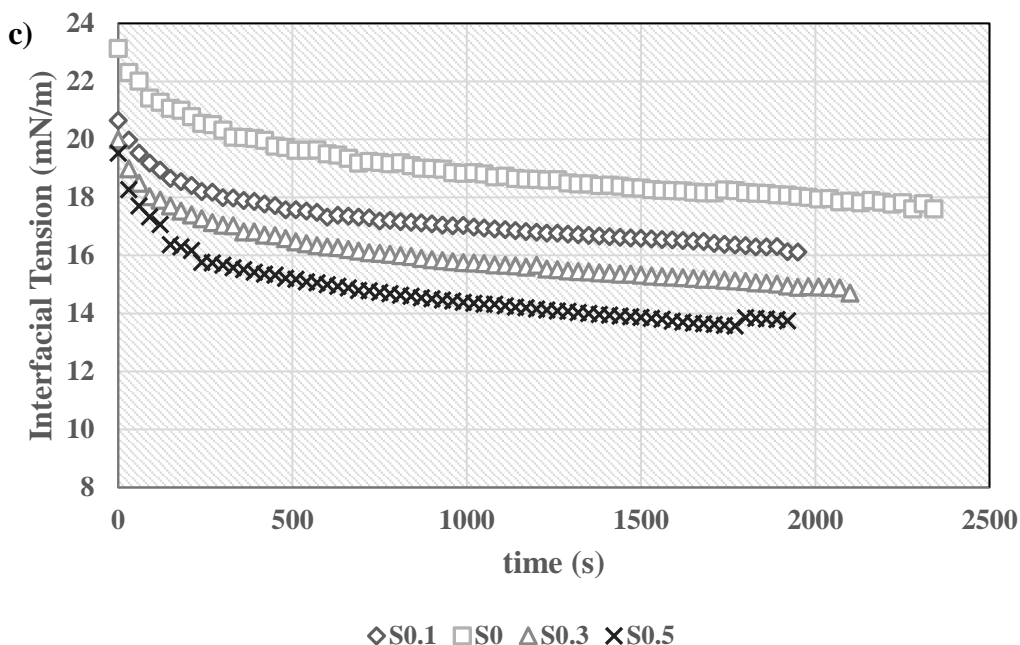


Figure 3.18. (a) Effect of concentration on the surface tension profile of QSE solutions (b) Effect of pH on the surface tension profile of QSE solutions (c) Effect of NaCl concentration on the surface tension profile of QSE solutions

Fig. 3.18a depicts the change in interfacial tension for the first 2000 s for each concentration. After the 2000 s mark, the IT relaxation rate of all the samples slowed down to the relaxation rate of pure water; hence, we believe it is not relevant for the study. As clearly observed in Fig. 3.18a, the initial IT (IT @ t=0) seems to decrease with concentration. For an ideally instant measurement, we expect the IT to start from the equilibrium IT of pure water (~ 24.3 mN/m). The first measurement of each concentration was taken within 10 s of droplet formation. The increased rate of IT reduction with increasing concentration explains this behavior. Observing the relaxation profile in Fig. 3.18 clearly shows a non-linear relaxation regardless of concentration. Upon QSE addition, the solutions relax in two distinct regimes. Up to the 200 s mark, there is an initial steep negative slope, which is later replaced by a much slower relaxation rate that continues on up to ~ 2000 s. Such a relaxation profile is reminiscent of typical protein adsorption. Protein adsorption is made up of three distinct regimes with different relaxation rates; (i) induction/lag period

(Regime I), (ii) monolayer saturation (Regime II), and (iii) interfacial gelation (Regime III). The first of these, Regime I, is associated with the period where there is no visible drop in IT from its initial value and is only observed for dilute protein concentrations. We have not observed such an induction region even for the most dilute concentration employed (0.05 % w/v). This lag period encountered in protein adsorption is the result of the presence of kinetic barriers to surfactant adsorption, either due to the slow rate of diffusion or the time it takes for the molecules at sub-surface (the hypothetical layer right beneath the surface (Ward and Tordai, 1946) to take a favorable conformation to adsorb (Calero et al., 2010; Freer et al., 2004b). The fact that QSE solutions do not exhibit such a lag in relaxation implies that the surface-active fractions are quick to diffuse and adsorb without any unfolding necessity. The high surface accessibility of hydrophobic residues of proteins in QSE is supported by the high surface hydrophobicity of the extract, as reported by Deng et al. (2019). QSE has a weight-average molecular weight of 9.61×10^6 Da, thus it is interesting to see that QSE does not display a lag period, despite most biopolymers with smaller molecular weights (i.e. sodium caseinate (Sosa-Herrera et al., 2016), Sterculia apetala gum (Pérez-Mosqueda et al., 2013), ovalbumin (Beverung et al., 1999), lysozyme (Freer et al., 2004b, 2004a), β -lactoglobulin & β -casein (Wüstneck et al., 1996) display a lag period at similar concentrations. It was shown by (Wang et al., 2018) that QSE consists of three different polysaccharide fractions, with the two of these being much lower in molecular weight (1250 Da and 1529 Da) than the major fraction (1.4×10^6 Da). These smaller glycoproteins could have almost diffused to and adsorb on the interface before the initial measurement took place. The absence of a lag period implies that QSE decreases interfacial tension almost instantly after interface formation, shortening the time it takes for emulsification processes (such as homogenization).

Regime II is characterized by a rapid decline in IT and for QSE samples in Fig. 3.18, it began at $t=0$ and was finalized within the initial 200 s for all concentrations. During this period, molecules positioned at the sub-surface go through molecular rearrangements to partially expose the hydrophobic regions to the oil-water interface

and adsorb irreversibly (Macritchie, 1978). The steep decline in interfacial tension is the result of two different mechanisms operating simultaneously; the increase of the number of contacts with the interface for each molecule through relaxation of the polymer from the initial rigid conformation, diffusion and adsorption of new molecules to fresh and recently emptied sites on the interface. These processes continue until monolayer coverage (Beverung et al., 1999). For QSE, during this phase, the initially adsorbed glycoproteins with smaller molecular weights are presumably replaced by the major QSE fraction, which is a very bulky and branched polymer of a xylose based backbone with galactose, glucose, galacturonic and glucuronic acid molecules and proteins attached to the branches (Hakala et al., 2014; Rezagholi et al., 2019; Wang et al., 2018). For polydisperse polymers, fractions with larger molecular weights adsorb preferentially over smaller ones. With time and particularly for higher concentrations, the larger fractions replace smaller ones, which are much faster to be positioned on the interface (Cao et al., 2013; Tadros, 2009). Comparing the effect of concentration on the relaxation profiles, it is possible to see a positive correlation between the relaxation rate in Regime II and bulk QSE concentration. As the amount of surfactant in bulk increases, more molecules become readily accessible to the interface. The closer the molecules are to the interface, the shorter the mean free path for diffusion, which decreases diffusion time. A denser solution also increases the probability of molecular collisions that initiates interfacial positioning of the molecules (Young and Torres, 1989). This phenomenon is observed by many other researchers studying the interfacial dynamics of macromolecular surfactants (Arabadzhieva et al., 2011; Bouyer et al., 2013; Moreira et al., 2012; Pérez-Mosqueda et al., 2013; Sosa-Herrera et al., 2016; W. Wang et al., 2014; Young and Torres, 1989).

The final regime for all QSE concentrations starts around the 200 s mark and lasts until the end of time-dependent measurements. Most protein and polymeric surfactants almost never display a true equilibrium, owing to the slow and ongoing changes in structure of the adsorbed layer. Two processes govern the gradual and slow decline during Regime III; increased interfacial molecular packing due to

ongoing molecular rearrangements and multilayer adsorption (Benjamins and van Voorst Vader, 1992; Cascão Pereira et al., 2003; Freer et al., 2004b). The unfolded and adsorbed protein layer continues to relax to the most energetically favorable state, exposing more and more of the hydrophobic sections to the interface. This process is accompanied by the repositioning of the hydrophilic side chains away from the adsorbed layer. As a result, the interface is populated exclusively by surface-active fractions, resulting in a more compactly packed interfacial layer of amphiphilic residues, which reduces the interfacial tension. Meanwhile, the non-adsorbed sections of the molecule, due to the increased proximity, display stronger intermolecular interactions which results in formation of molecular aggregates and protein-polysaccharide complexes (Freer and Radke, 2004; Krstonošić et al., 2019; Sosa-Herrera et al., 2016). The enhanced degree of entanglements form bridges that connect at various points, resulting in an amorphous gel-like network at the interface (Beverung et al., 1999; Freer et al., 2004b, 2003). This explains why this period is also called interfacial gelation. For some surfactants, the changes in the adsorbed layer in this regime introduces an attraction between surfactants in bulk and interface, which might result in multiple layers of surfactant to adsorb. Multilayer adsorption is another reason for the slow decline in IT after monolayer surfactant coverage. For QSE samples, the relaxation of IT for prolonged times was related to molecular conformation changes and the resulting increase in interfacial concentration. Unlike Regime II, we have not observed a significant relation between relaxation rates and bulk QSE concentration for Regime III. This implies that bulk concentration had a minimal effect on the rate of molecular rearrangements at the interface. The fact that the relaxation rate in Regime II was dominantly influenced by bulk surfactant concentration, proves that the primary controlling mechanism in that step was the diffusion of new molecules to void interfacial sites. After monolayer coverage, concentration did not seem to have such a prominent effect on rate of IT decline.

QSE is a polyelectrolyte with a high charge density due to a high fraction of galacturonic and glucuronic acid residues and contains ~20% by wt. proteins. The

electrostatic effect plays a significant role in defining the rate and the state of the molecular conformations at the adsorbed layer. The crucial role molecular conformation play on interfacial activity was discussed by Kontogiorgos et al. (2019) who have noted that a polysaccharide or protein's emulsification potential is not only a function of its concentration but also of its conformation. The relative contribution of these electrostatic effects is obviously dependent on the pH and the ionic strength of the aqueous medium. Fig. 3.18b depicts the transient interfacial tension profiles for three different pHs; 3, 7 and, 11. As similarly observed in equilibrium IT values (Fig. 3.17a), the relaxation profile of QSE solution at pH3 and 7 was almost identical. The isoelectric point of QSE proteins was identified as 4.2 by Deng et al. (2019). According to Deng et al. (2019), the zeta potential of QSE molecules were 23.0 mV at pH3 and it was -22.7 mV at pH7. This indicates that, though opposite in charge, the QSE proteins display similar electrostatic potentials for the pHs, 3 and 7. The zeta potential at pH10 (which was the highest pH investigated by the researchers) was reported as -38.1 mV. This proves the expected outcome that the further one gets from the solution's isoelectric point, the higher the zeta potential becomes. At pH11, as clearly evident from Fig. 3.18b, QSE molecules relax to their equilibrium at a much faster rate, and additionally, this equilibrium is 33% less than the equilibrium IT at a neutral pH. These results imply a more rapid unfolding of the molecule as well as a different final conformational that presumably provides more efficient interfacial packing. Out of the pHs studied, pH11 is also the furthest from the pKa's of both galacturonic (pKa of 3.5) (Dickinson, 2018) and gulucuronic acid (pKa of 3.12) (Wang et al., 1991), which implies that a major fraction of the carboxylic acid groups will be negatively charged at pH11. When solution pH is close to the isoelectric point of the proteins, owing to the lack of electrostatic repulsion, molecule-molecule interactions dominate. Intermoleculer attractions between protein chains is ever present at any pH, yet with a decrease in overall charge of the molecule, molecules that were principally kept apart by electrostatic repulsion move closer to one another. With increasing proximity of the molecules, hydrophobic interactions such as Van der Waals forces start to dominate over

protein-water interactions, hence, the molecules start to form aggregates. The aggregation in the adsorbed layer causes generation of a denser interface that hangs close to the droplet surface. The reduction in conformational entropy of the polymer chains both make it harder for new polymer chains to be incorporated to the interfacial layer, and it also inhibits the ability of the already adsorbed molecules to reposition themselves to a more energetically favorable state (Alba et al., 2016; Castellani et al., 2010a). The decreased interactions between QSE and water molecules and the low electrostatic charges at pHs close to pH4.2 also inhibit the extract's steric stabilization potential. The diminished interfacial activity and steric stabilization potential of QSE were supported by Deng et al. (2019) findings that demonstrated QSE to exhibit the lowest emulsifying ability index (EAI), emulsion stability index (ESI) and foaming capacity at it pHs close to its isoelectric point of 4.2 (Deng et al., 2019).

At pH11, due to high negative-negative charge repulsions, polymer chains in order to maximize the distance between charged groups, tend to stay as widely spread as possible. As a result, polar and charged groups extrude through the bulk phase in a more wide-spread manner, providing more room for fresh molecules to adsorb. Additionally, the decreased hydrophobic interactions within the molecule provide better structural flexibility that enhances the molecular mobility, which, in return, accelerates molecular rearrangements (Alba and Kontogiorgos, 2017). These occurrences together contribute to the increased relaxation rate of interfacial tension at pH11. The equilibrium IT at pH11 is also considerably lower than the other pHs by ~ 6 mN/m. As previously stated, this suggests an increased number of contacts with surfactant and the interface, either resulting from an increased surfactant concentration or a more complete unfolding of the proteins that maximizes interfacial activity (Fleer et al., 1993; Fleer, 2010; Parkinson et al., 2005). QSE is abundant in disulfide bonds ($19.79 \mu\text{M/g}$ as identified by method) which is one of the most important structure stabilizing bonds in proteins (Du et al., 2012; Tang et al., 2006). The increasingly negative charge repulsion at increasing pHs, was after some point, sufficiently strong to overcome the final remaining disulfide bonds and

other intermolecular attractions that prevented total unfolding. There are other studies in the literature that have reported increased interfacial activity as the pH of the medium gets further from the isoelectric point of proteins (Deng et al., 2019; Mundi and Aluko, 2012; Tang et al., 2006).

The transient interfacial tension profiles of QSE solutions with differing amounts of NaCl was shown in Fig. 3.18c (S0: control, S0.1: 0.1 M, S0.3: 0.3 M, S0.5: 0.5 M). As clearly evident from the figure, IT relaxation rates considerably increases with increasing salt content. When a background electrolyte is present in an emulsion (e.g., NaCl) stabilized by a polyelectrolyte surfactant, an ionic double layer surrounds the interface. QSE is negatively charged at neutral pH; thus Na^+ ions simultaneously transport to the interface and surround QSE anions, which is surrounded by a secondary layer of Cl^- ions (Z. Gao et al., 2017; Macleod and Radke, 1994). For QSE molecules, the presence of a double layer accelerated the rate of adsorption. There could be two possible mechanisms behind this behavior. With increasing ionic strength of the medium, the Debye length of charged protein side chains decreases. Consequently, electrostatic repulsion decreases, resulting in a quicker interfacial saturation and better interfacial packing of proteins (Beverung et al., 1999). Additionally, charged sugar acids positioned at the branches extrude through the aqueous medium, while the rest of the molecule adsorbs. These negatively charged groups can inhibit the diffusion of new molecules by forming a layer of charge-charge repulsion. The ionic interaction of Na^+ ions and these charged fractions decreases electrostatic repulsion and facilitates the adsorption of fresh polymers onto the oil-water interface. Other researchers have similarly reported an acceleration in the adsorption rate of charged surfactants with increasing ionic strength of the medium (Beverung et al., 1999; Hayase and Tsubota, 1986; Ishimuro and Ueberreiter, 1980).

3.3.3 Dilatational Interfacial Rheology Measurements

Dilatational interfacial rheology focuses on the change in interfacial tension in case of an expansion/contraction on interfacial area, and the data acquired can indicate the interface's resistance to external perturbations (Bos and Van Vliet, 2001; Dickinson, 2001, 1999, 1998). Therefore, investigation of interfacial rheology is just as essential as interfacial tension. The contribution to long term emulsion stability is particularly more pronounced for systems stabilized by polymeric surfactants, such as QSE. The adsorption of these large macromolecules results in the formation of an interfacial gel-like skin network (Freer et al., 2004a) that dampens breakage of droplets and functions as a barrier against coalescence (Santini et al., 2007b; W. Wang et al., 2014). Many studies have found a strong correlation between interface dilatational properties and stability of dispersions (Beverung et al., 1999; Cao et al., 2013; Cascão Pereira et al., 2001; Davis and Foegeding, 2006; Freer et al., 2004b; Kontogiorgos, 2019; Mendoza et al., 2014; Pérez-Mosqueda et al., 2013; Santini et al., 2007b; Vernon-Carter et al., 2008; Zhang et al., 2011).

Table 3.6. Average E' , E'' and $\tan\Delta$ values for QSE at an oil-ware interface

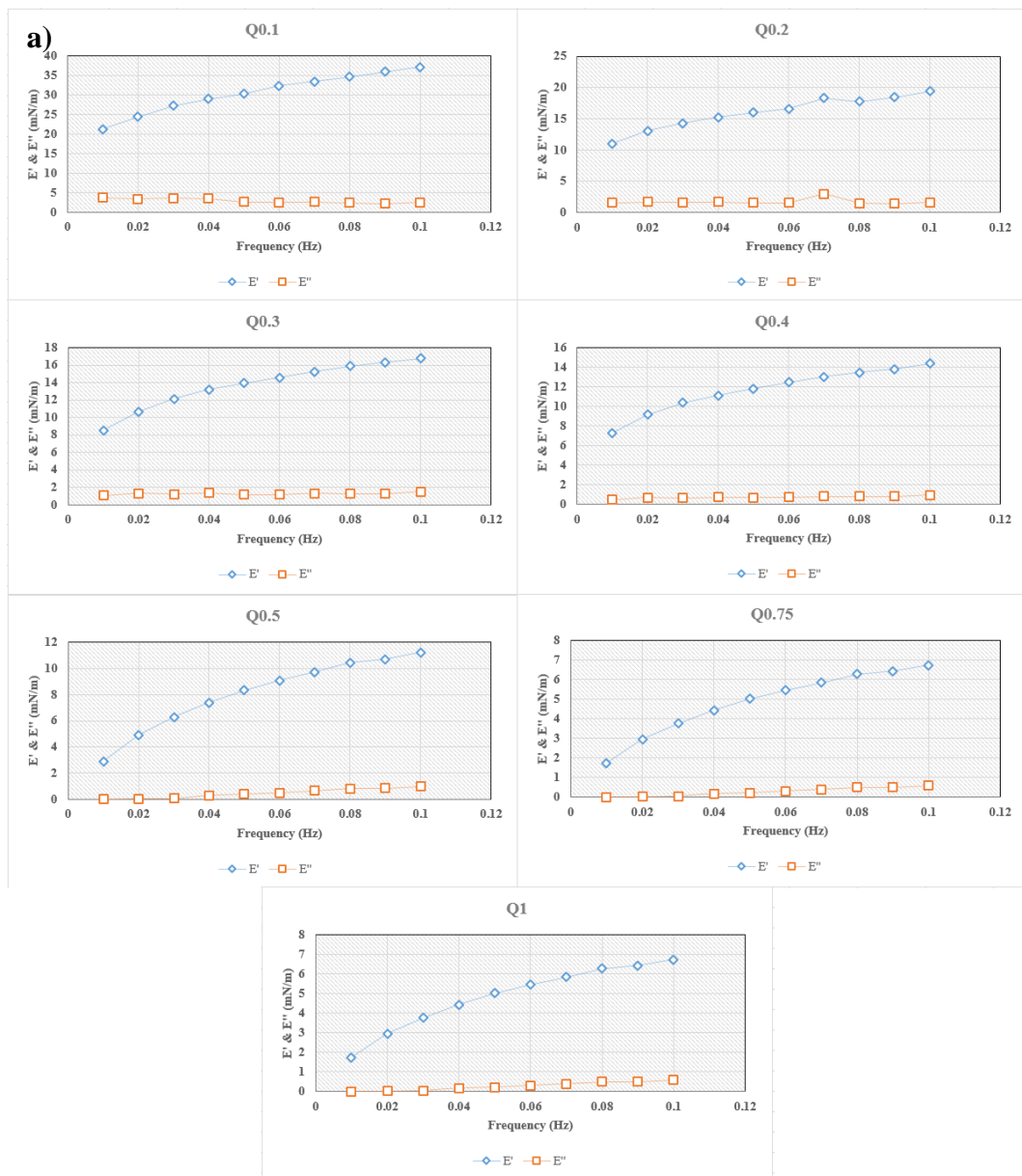
Concentration (%)	E' (mN/m)	E'' (mN/m)	$\tan\Delta$ (°)
0.1	30.61±5.03 ^a	2.93±0.80 ^a	0.10±0.02 ^a
0.2	16.17±2.50 ^b	1.75±0.37 ^{ab}	0.11±0.02 ^{ab}
0.3	14.79±3.39 ^b	1.32±0.31 ^b	0.09±0.02 ^{ab}
0.4	11.69±1.24 ^b	0.76±0.20 ^b	0.07±0.02 ^{ab}
0.5	9.09±2.26 ^b	0.25±0.36 ^{bc}	0.03±0.09 ^{ab}
0.75	5.45±2.07 ^c	0.15±0.14 ^{cd}	0.03±0.08 ^{ab}
1	3.00±1.95 ^d	0.08±0.37 ^d	0.03±0.01 ^b
pH			
3	10.00±1.92 ^a	0.73±0.19 ^a	0.07±0.01 ^a
7	14.79±2.39 ^b	1.32±0.31 ^{ab}	0.09±0.02 ^a
11	20.08±1.19 ^c	1.45±0.43 ^b	0.08±0.01 ^a
Salt Content			
0	14.79±3.39 ^a	1.32±0.31 ^a	0.09±0.02 ^a
0.1	15.16±3.39 ^a	1.45±0.28 ^a	0.10±0.01 ^a
0.3	9.95±1.53 ^{ab}	1.20±0.04 ^a	0.13±0.02 ^a
0.5	9.35±1.73 ^b	0.92±0.30 ^a	0.10±0.04 ^a

E' and E'' was measured for 10 different frequencies (within the range 0.01 – 0.1 Hz). Table 3.6 displays the averages of these frequencies for differing concentrations, pHs and salt contents. E' (dilatational storage modulus) is a measure

of the elastic counterforce of the surface to a possible deformation, whereas E'' (dilatational loss modulus) defines how fast the initial values of ST is restored after deformation (Mendoza et al., 2014; Seta et al., 2014). Regardless of solution conditions and QSE concentration, all oil-water interfaces were prominently elastic rather than viscous, as identified by the much higher E' values ($E' \gg E''$). This indicates that the viscoelastic later formed by QSE adsorption on an oil-water interface acts more like an elastic solid rather than a viscous fluid. This result is typical for viscoelastic polymer layers and is one of the advantages of polymeric surfactants over small molecular ones as it bestows the interface higher resistance against deformation (Pérez-Mosqueda et al., 2013). Upon disturbance to the interface, an ideally elastic interface can store all the mechanical energy, later release it without loss, and return to its original shape and form (Freer et al., 2004b). Interfacial elasticity increases the interface's ability to store energy; hence, a higher storage modulus is preferable for interfaces as it provides the dispersed particles with higher resistance against rupture that could occur in the possibly turbulent conditions of emulsion formation, processing and transportation or merging of particles during long term storage (Seta et al., 2014; W. Wang et al., 2014). This behavior can be explained by Marangoni effect. Assuming an interface saturated with surfactant has lost its original shape and size and is elongated due to an external disturbance, this causes the generation of an interfacial tension gradient. To recover the droplet to its initial state, excess surfactants in bulk diffuses to the depleted region (Marangoni effect). However, until this process is finalized, the droplet is susceptible to rupture from its weakened regions. A profoundly elastic interface resists deformation and generates a greater driving force for surfactants to diffuse to the depleted region, reducing film compressibility and improving the resistance to the change in interfacial area that takes place in droplet breakage and coalescence (D'Aubeterre et al., 2005).

For emulsions, in particular, the effect of interfacial dilatational rheology is widely recognized (Aksenenko et al., 2007; Cui et al., 2010; Derkach et al., 2009; Santini et al., 2007a; Vernon-Carter et al., 2008; W. Wang et al., 2014). Many researchers have

even demonstrated that interfacial rheological properties are the dominant factor in determining emulsions' stability, even more so than interfacial tension (Angle and Hua, 2012; Fruhner et al., 2000; Reichert and Walker, 2013; Urbina-Villalba, 2004). However, most of the droplet breakage occurs during emulsion formation, which is one reason why the application of an overly long homogenization procedure can cause phase separation. The enhanced resistance facilitates the emulsification process by contributing to the droplet size distribution in a turbulently stirred system (W. Wang 2014). Bak et al. (2012) investigated the effect of interfacial tension and rheological properties on droplet breakage in an oil-in-water emulsion prepared by Tween 20 and Tween 80. The researchers have concluded that it is interfacial dilatational properties, dilatational elasticity, in particular, that mainly governs this process. Higher dilatational elasticity was associated with better resistance against rupture of droplets due to the mechanical energy input during emulsification (Bak and Podgórska, 2012). Consequently, the relatively high elastic character that QSE adsorption layers display implies that it would be a very effective emulsion stabilizer. It was demonstrated that flexible proteins tend to form films with low levels of viscoelasticity. As the rigidity of the protein structure increases, the interfacial layer elasticity increases (Seta et al., 2014). QSE proteins are structurally very stable as identified by the high denaturation temperature (103.4 °C), a high number of free sulfhydryl (SH) groups (9.73 $\mu\text{M/g}$), and disulfide (SS) bonds (19.79 $\mu\text{M/g}$) (Deng et al., 2019). This structural rigidity could be one of the reasons behind the relatively high interfacial elasticity. Casein for one, though is a very surface active molecule, due to its flexible structure, shows inferior emulsion stabilization properties compared globular proteins such as β -lactoglobulin and ovalbumin (Graham and Phillips, 1979; Pezennec et al., 2000).



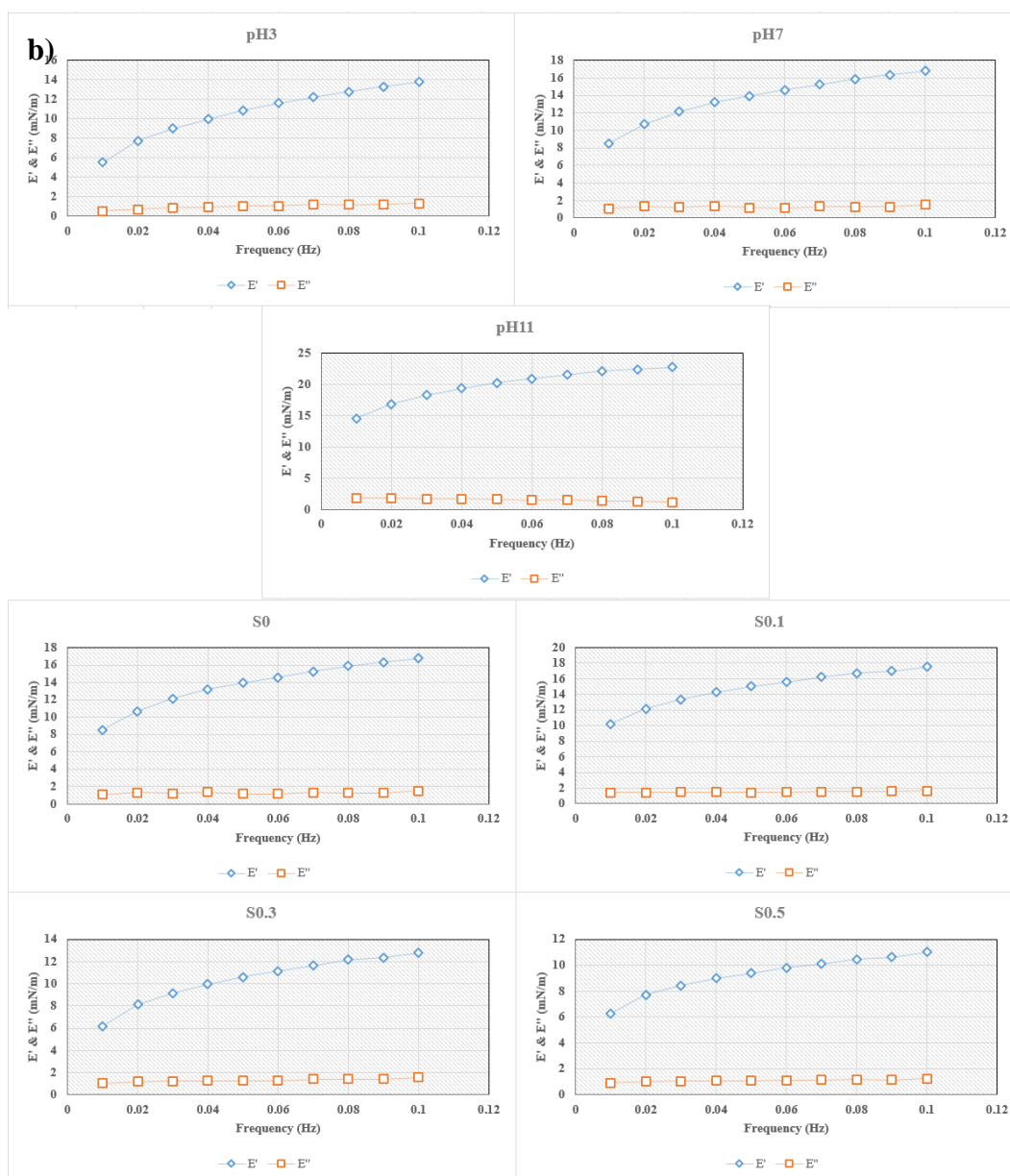


Figure 3.19. (a) Frequency dependence of E' and E'' of QSE at an oil-water interface with varying concentrations (b) Frequency dependence of E' and E'' of QSE at an oil-water interface with varying pHs and NaCl concentrations

The frequency dependence of E' and E'' of all samples are displayed in Fig. 3.19. Regardless of surfactant concentration, pH and salt content, E' and E'' displayed similar trend with frequency. E' increased in a non-linear fashion with increasing frequency, whereas E'' was not substantially affected and remained relatively

constant for the frequency range studied (0.01 – 0.1 Hz). The initial higher rate of increase in E' seems to decrease to a more linear profile after 0.04 Hz. With increasing frequency, the rate of deformation in interfacial area increases, which decreases the time for the interfacial monolayer to respond to these perturbations. The change in interfacial tension is compensated by the adsorption or desorption of surfactant from the adjacent bulk phase (Marangoni effect). However, for frequencies where the rate of area expansion/contraction is faster than the rate of adsorption, the monolayer starts to behave like an insoluble surfactant layer where a change in interfacial area is accompanied by a similar change in interfacial tension (Gibb's effect)(D'Aubeterre et al., 2005). As Gibb's effect becomes more dominant, the interface becomes more elastic, which is observed as an increase in dilatational storage modulus values (E'). The increase in E' with frequency continues until a certain plateau is reached (Cao et al., 2013; Ma et al., 2011; Ravera et al., 2005; Wang et al., 2011). The visible change in slope at around 0.4 Hz, indicates E' approaching this plateau, yet it could not be observed within the frequency range employed.

E'' , on the other hand, was not significantly affected by a 10-fold increase in frequency (from 0.01 to 0.1 Hz). This indicates that the characteristic frequency of the relaxation process at the interfacial layer is greater than the maximum oscillating frequency, which was restricted by instrument limitations (Cao et al., 2013; Ma et al., 2011; Ravera et al., 2005; Wang et al., 2011). What this implies is that, interfacial relaxation is governed by rapid processes with characteristic frequencies larger than 0.1 Hz. For a bulky molecule such as QSE, molecular rearrangements would occur slowly, and competition between the two mechanisms of relaxation; diffusion, and interfacial repositioning would result in the observation of a local maximum in E'' within the frequency range measured, as demonstrated in several other studies (Pérez-Mosqueda et al., 2013; Rühls et al., 2013). Hence, this brings us to the conclusion that adsorption of fresh QSE molecules in solution bulk to empty regions on the interface is the dominant mechanism of relaxation between the frequencies 0.01 - 0.1 Hz.

Concentration, pH, and ionic strength dependence of interfacial dilatational rheological properties are given in Table 3.6. With increasing concentration the average E' and E'' values both decreased, with E'' approaching 0 as concentration increases. The evident decline in dilatational complex modulus, E^* , implies the loss of viscoelastic character of the adsorbed film layer with increasing bulk QSE concentration. It is quite common to observe maximum or minimum modulus values with changing surfactant concentration. Interfacial rheological properties are governed by two different frequencies, namely, the frequency of molecular exchange (μ) and the disturbance frequency (ν). To observe a local extremity, the frequency of molecular exchange should lie within the range of disturbance frequencies applied, because the maximum/minimum modulus value is the cross over point where $\mu < \nu$ to $\mu > \nu$ takes place (Stubenrauch and Miller, 2004). The fact that, no such local extremity is observed in either of the modulus values indicated that the disturbance frequency range does not cover the molecular exchange frequency.

For the storage modulus, E' , the effect of bulk surfactant concentration is governed by two opposing mechanisms (Ma et al., 2011). Normally one would expect an increase in interfacial elasticity as more and more surfactants become available to the interface. An increase in surfactant concentration could lead to the formation of a thicker interfacial network with higher levels of crosslinking between chains, resulting in a more solid-like behavior, hence the higher elasticity. However, the effect of increasing surfactant concentration is limited by interfacial monolayer saturation. If the polymer does not have the capability to form multiple layers, the addition of surfactant after CAC would not significantly alter the interfacial configuration. The CAC for QSE on an oil-water interface was identified as 0.23 % w/v. Particularly after this concentration, a secondary mechanism becomes more dominant. With higher bulk surfactant concentration, the rate of molecular exchange between the interface and bulk increases, as demonstrated by the dynamic interfacial tension curves (Fig. 3.18). Increased molecular exchange decreases the interfacial gradient generated by expansion/contraction of the interfacial area. This decreases the interface's ability to respond to the changes in area (ΔA) with a similar change in

interfacial tension ($\Delta\gamma$), which is observed as a reduction in dilatational storage modulus (Santini et al., 2007). For QSE adsorbing at an oil-water interface, the second mechanism is obviously much more dominant within the concentration range examined (0.1-1 % w/v). Many other researchers have observed similar declines in E' with concentration and explained it with the effect of increased molecular exchange (Arabadzhieva et al., 2011; Cao et al., 2013; R hls et al., 2013; Santini et al., 2007b; W. Wang et al., 2014). As discussed before, the strong relation between dispersion stability and E' was shown in multiple studies (Beverung et al., 1999; Cao et al., 2013; Casc o Pereira et al., 2001; Davis and Foegeding, 2006; Freer et al., 2004b; Kontogiorgos, 2019; Mendoza et al., 2014; P rez-Mosqueda et al., 2013; Santini et al., 2007b; Vernon-Carter et al., 2008; Zhang et al., 2011). Thus, according to our findings, lower concentrations could prove better stabilization in emulsion, only considering the interfacial elasticity. However, many other factors such as interfacial tension and viscosity of the continuous phase play prominent roles in determining overall system stability. Hence, further analysis in a real emulsion system is necessary for a definite interpretation.

As seen in Table 3.6, there seems to be a negative correlation E' and QSE concentration as well. There are normally two opposing mechanisms at play here, yet obviously, one of them strictly dominates for our samples. With a higher bulk surfactant concentration, there is enhanced molecular exchange between bulk and the interface, which promotes the release of excess energy at the interface by interfacial tension relaxation, hence increasing dilatational loss modulus. By an increase in bulk concentration, the resistance of the interface to deformation also increases, which hinders the formation of a tension gradient by the deformation during measurement modulus, which decreases dilatational loss modulus (Huang et al., 2008; Z. Wang et al., 2014). E'' values seem to approach 0 as solution concentration increases, which is also similar for E' values. This implies the loss of viscoelastic character of the interface at concentrations higher than 1 % w/v. The increased rate of adsorption and the loss of interfacial tension gradient seem to be mechanisms responsible for the diminishing interfacial viscoelasticity. The effect of

pH and ionic strength on interfacial rheological properties can also be seen in Table 3.6. Both dilatational moduli increase with increasing pH, whereas they seem to decrease with increasing ionic strength of the medium. The amount of free Na^+ and Cl^- ions and pH of the medium is the dominant factor in defining the interfacial conformation of the adsorbed polymer. These conformation changes can considerably influence interfacial packing (increasing/decreasing surface excess concentration) and or change the number of contact points with the interface as well as defining the extend of polymer-polymer interactions on the adsorption layer (Karbaschi et al., 2014; Kontogiorgos, 2019). As previously mentioned, a thicker and more extensively bonded network of surfactants on the interface leads to higher interfacial elasticity (identified by higher E' values). As pH gets further from the isoelectric point of proteins (pH 4.2) and the pKa of the sugar acids (pH 3.12 and 3.5) responsible for the charge on the polysaccharide chains, the interfacial layer gets more negatively charged. We had previously discussed how increasing negative charge on QSE resulted in a more compactly packed interfacial layer, as supported by a much lower equilibrium interfacial tension values at pH 11 than at neutral pH. With more polymer available at the interface, the interfacial layer gets thicker, and the closer packing lead to increased intermolecular attractions, which caused the interfacial layer to display higher modulus values. On the other hand, increasing ionic strength had the opposite effect. With Na^+ ions surrounding the anions on QSE layer, the charge-charge repulsion within the polymer chains is neutralized, which seems to result in decreased interfacial viscoelasticity. A conformational change is responsible for this result, but it is not possible with current knowledge to give a definite explanation. Covis et al. (2014), considering their findings, hypothesized that with an increasing number of loops (non-adsorbed sections of a polymer chain positioned between two points of contact with the interface), the viscoelastic character of the interface is diminished. Karbaschi et al. (2014), found a direct relationship between the number of hydrophobic residues exposed to the surface and dilatational modulus values. Both these studies demonstrate the strong impact of

molecular conformation on interfacial rheology, as we have observed in QSE samples.

CHAPTER 4

CONCLUSION & RECOMMENDATIONS

Quince seed extract, with its chemically complex and diverse structure, is a challenging biopolymer to work with, but has so far shown promising results in stabilization of emulsions and foams. Some substantial findings were acquired by the use of quince seed extract (QSE) in an oil-in-water emulsion and comparing it with emulsions stabilized by similar concentrations of xanthan gum. Physical properties of the emulsions such as viscosity and droplet size influenced the creaming rate. Quince seed extract resulted in emulsions with smaller low-shear viscosities and shear thinning capabilities compared to same concentrations of xanthan gum. Still, the emulsion thickening properties of QSE were significant. Particle sizes were shown to decrease with increasing gum concentration related with the higher entrapment capability of an increasing yield stress and viscosity. NMR T_2 relaxation results indicated the dominant effect of serum layer mobility on physical stability. The lower T_2 values of QSE solutions were suggestive of the gum's emulsification properties. In future studies, the microstructure of the emulsions and the physico-chemical dynamics behind destabilization mechanisms could be further analyzed by NMR T_2 relaxation spectra acquired through Non-Negative Least square transformation of NMR data. Overall, gum concentrations >0.3 w/v yielded physically stable emulsions even after 5 months. Quince seed extract was demonstrated to be a good natural alternative to emulsion thickening stabilizers that provided comparable stabilization power for lower viscosities, owing to its surface-active properties.

Investigation of surface properties of QSE revealed the extract's interfacial activity and the concentrations, pH and salt content for the biopolymer to fold into its most effective interfacial conformation. QSE was effective in lowering surface tension at

an air-water interface even at concentrations as low as 0.025 % w/v (reduction of eq. ST from 72 mN/m to 58.9 mN/m). By QSE addition alone equilibrium surface tension could be lowered to ~ 36 mN/m, which is lower than the lowest ST that can be achieved with many other surface active biopolymers. Critical aggregation concentration (CAC) was identified as 0.165 % w/v, which is also lower compared to similar hydrocolloids, meaning a relatively low concentration of the extract was sufficient to provide complete surface coverage. *Z*-average particle size data supported this claim by displaying an abrupt increase in mean particle diameter (from ~ 900 nm to >2500 nm) as bulk QSE concentration exceeds the CAC of 0.165 % w/v. Dynamic surface tension curves revealed an almost instantaneous adsorption of polymer for concentrations over 0.01 % w/v, which demonstrates the strong potential of the gum as a foaming agent. Surface tension relaxation rates increased with increasing concentration. Dilatational surface rheology measurements revealed that, regardless of concentration, air-water interface was prominently elastic, that implies a high resistance against deformation. Dilatational modulus is highest at a concentration range of 0.3 – 0.5 % w/v for all frequencies investigated. As solution pHs get further from the isoelectric point of QSE proteins, the rate of adsorption of QSE molecules on to the interface and the equilibrium surface pressures increased. Surface properties were also significantly affected by ionic strength of the medium, with eq. STs decreasing with increasing QSE concentration. pH and ionic strength induced conformational changes in the interfacial layer also lead to the formation of local minima and maxima in dilatational elastic and loss modulus within the pH and NaCl concentration studied.

At an sunflower oil-water interface, the lowest concentration that yielded a statistically significant drop in interfacial was found as 0.02 % w/v (reduction of eq. ST from 24.2 mN/m to 22.5 mN/m). QSE dropped interfacial tension down to ~ 16 mN/m at the highest concentration examined (1% w/v). Critical aggregation concentration (CAC) was identified as 0.23 % w/v, which is a relatively low concentration compared to hydrocolloids of similar nature. Dynamic interfacial tension results revealed that the interfacial tension relaxation occurs in two distinct

regimes; monolayer saturation and interfacial gelation, with total surface coverage over within the first 200 s for all samples. None of the samples exhibited a lag phase. This rapid adsorption is a significant indicator of the quick stabilizing effect of the polymer that could initiate even during emulsification where most of the particle breakage occurs. Dilatational interfacial rheology measurements showed that, on all samples, the oil-water interface was prominently elastic, which is associated with increased physical stabilization in emulsions. Changes in pH and ionic strength of the medium, resulted in conformational changes in the adsorption layer prominent enough to influence interfacial properties. The solution at pH11 yielded the lowest equilibrium interfacial tension (12.3 mN/m). Similarly, with increasing NaCl, the equilibrium interfacial tension values decreased; down to 13.6 mN/m at 0.5 M NaCl, which was explained by increasing protein solubility within the range of 0-0.5 M NaCl.

Despite the few studies in literature that have demonstrated quince seed extract to be a promising dispersion stabilizer, the mechanism of adsorption and the interfacial behavior of this biopolymer on an oil-water interface was never explored. This dissertation with clear findings not only proves the significant emulsifying potential of the extract, it also provides quantitative information on the interfacial properties of QSE on an oil-water interface, as well as explaining the mechanism behind the interfacial behavior of this complex and unique biopolymer. Taking all these into account, it would be safe to say, with this study, QSE is proven to be a potentially effective natural alternative to other polymeric surfactants and stabilizers commonly employed in the food, cosmetic and pharmaceutical industries.

REFERENCES

- Abbastabar, B., Azizi, M.H., Abbasi, S., 2014. Optimization of Extraction Yield of Quince Seed Gum and Rheological Characteristics Under the Optimum Extraction Conditions. *J. Nutr. Sci. Food Technol.* 9, 29–38.
- Abbastabar, B., Azizi, M.H., Adnani, A., Abbasi, S., 2015. Determining and modeling rheological characteristics of quince seed gum. *Food Hydrocoll.* 43, 259–264. <https://doi.org/10.1016/j.foodhyd.2014.05.026>
- Adamczyk, Z., Nattich, M., Barbasz, J., 2009. Deposition of colloid particles at heterogeneous and patterned surfaces. *Adv. Colloid Interface Sci.* <https://doi.org/10.1016/j.cis.2008.12.003>
- Adams, F., Walstra, P., Brooks, B.W., Richmond, H.N., Zerfa, M., Bibette, J., Hibberd, D.J., Robins, M.M., Weers, J.G., Kabalnov, A.S., Petsev, D.N., Obey, T., Vincent, B., Kunieda, H., Pons, R., Solans, C., Forster, T.H., Von Rybinski, W., Smulders, P., Iwanaga, T., Deminiere, B., Colin, A., Calderon, F., 1998. *Modern Aspects of Emulsion Science*. The Royal Society of Chemistry. <https://doi.org/10.1039/9781847551474>
- Akhtar, M., Dickinson, E., Mazoyer, J., Langendorff, V., 2002. Emulsion stabilizing properties of depolymerized pectin. *Food Hydrocoll.* 16, 249–256. [https://doi.org/10.1016/S0268-005X\(01\)00095-9](https://doi.org/10.1016/S0268-005X(01)00095-9)
- Aksenenko, E. V., Kovalchuk, V.I., Fainerman, V.B., Miller, R., 2007. Surface dilational rheology of mixed surfactants layers at liquid interfaces. *J. Phys. Chem. C.* <https://doi.org/10.1021/jp073904g>
- Al-Assaf, S., Phillips, G.O., Aoki, H., Sasaki, Y., 2007. Characterization and properties of Acacia senegal (L.) Willd. var. senegal with enhanced properties (Acacia (sen) SUPER GUM™): Part 1-Controlled maturation of Acacia senegal var. senegal to increase viscoelasticity, produce a hydrogel form and

- convert a poor into a good emulsifier. *Food Hydrocoll.* 21, 319–328.
<https://doi.org/10.1016/j.foodhyd.2006.04.011>
- Al-Hakkak, J., Al-Hakkak, F., 2010. Functional egg white-pectin conjugates prepared by controlled Maillard reaction. *J. Food Eng.* 100, 152–159.
<https://doi.org/10.1016/j.jfoodeng.2010.03.040>
- Alba, K., Bingham, R.J., Gunning, P.A., Wilde, P.J., Kontogiorgos, V., 2018. Pectin Conformation in Solution. *J. Phys. Chem. B* 122, 7286–7294.
<https://doi.org/10.1021/acs.jpccb.8b04790>
- Alba, K., Kontogiorgos, V., 2017. Pectin at the oil-water interface: Relationship of molecular composition and structure to functionality. *Food Hydrocoll.* 68, 211–218. <https://doi.org/10.1016/j.foodhyd.2016.07.026>
- Alba, K., Sagis, L.M.C., Kontogiorgos, V., 2016. Engineering of acidic O/W emulsions with pectin. *Colloids Surfaces B Biointerfaces* 145, 301–308.
<https://doi.org/10.1016/j.colsurfb.2016.05.016>
- Alfrén, J., Peñarrieta, J.M., Bergenståhl, B., Nilsson, L., 2012. Comparison of molecular and emulsifying properties of gum arabic and mesquite gum using asymmetrical flow field-flow fractionation. *Food Hydrocoll.* 26, 54–62.
<https://doi.org/10.1016/j.foodhyd.2011.04.008>
- Alizadeh-Pasdar, N., Li-Chan, E.C.Y., 2000. Comparison of protein surface hydrophobicity measured at various pH values using three different fluorescent probes. *J. Agric. Food Chem.* 48, 328–334.
<https://doi.org/10.1021/jf990393p>
- Alizadeh Behbahani, B., Tabatabaei Yazdi, F., Shahidi, F., Hesarinejad, M.A., Mortazavi, S.A., Mohebbi, M., 2017. Plantago major seed mucilage: Optimization of extraction and some physicochemical and rheological aspects. *Carbohydr. Polym.* 155, 68–77. <https://doi.org/10.1016/j.carbpol.2016.08.051>
- Anal, A.K., Shrestha, S., Sadiq, M.B., 2019. Biopolymeric-based emulsions and

their effects during processing, digestibility and bioaccessibility of bioactive compounds in food systems. *Food Hydrocoll.* 87, 691–702.

<https://doi.org/10.1016/j.foodhyd.2018.09.008>

Anderson, R.E., Pande, V.S., Radke, C.J., 2000. Dynamic lattice Monte Carlo simulation of a model protein at an oil/water interface. *J. Chem. Phys.* 112, 9167–9185. <https://doi.org/10.1063/1.481537>

Angle, C.W., Hua, Y., 2012. Dilational interfacial rheology for increasingly deasphalted bitumens and n -C5 asphaltenes in toluene/NaHCO₃ solution. *Energy and Fuels.* <https://doi.org/10.1021/ef300846z>

Anvari, M., Joyner (Melito), H.S., 2017. Effect of fish gelatin-gum arabic interactions on structural and functional properties of concentrated emulsions. *Food Res. Int.* 102, 1–7. <https://doi.org/10.1016/j.foodres.2017.09.085>

Arabadzhieva, D., Mileva, E., Tchoukov, P., Miller, R., Ravera, F., Liggieri, L., 2011. Adsorption layer properties and foam film drainage of aqueous solutions of tetraethyleneglycol monododecyl ether. *Colloids Surfaces A Physicochem. Eng. Asp.* 392, 233–241. <https://doi.org/10.1016/j.colsurfa.2011.09.061>

Ashraf, M.U., Hussain, M.A., Muhammad, G., Haseeb, M.T., Bashir, S., Hussain, S.Z., Hussain, I., 2017. A superporous and superabsorbent glucuronoxylan hydrogel from quince (*Cydonia oblonga*): Stimuli responsive swelling, on-off switching and drug release. *Int. J. Biol. Macromol.* 95, 138–144. <https://doi.org/10.1016/j.ijbiomac.2016.11.057>

Atta, A.M., El-Sherbiny, S.I., Salah, A.M., Abd El-hafiez Ahmed, A.R., 2013. Surface and Adsorption Parameters of Water Soluble Polymeric Surfactants Based on Ethoxylated Schiff Base Polymers in Aqueous Medium. *J. Dispers. Sci. Technol.* 34, 1113–1123. <https://doi.org/10.1080/01932691.2012.738103>

Bai, L., Huan, S., Li, Z., McClements, D.J., 2017. Comparison of emulsifying properties of food-grade polysaccharides in oil-in-water emulsions: Gum

- arabic, beet pectin, and corn fiber gum. *Food Hydrocoll.* 66, 144–153.
<https://doi.org/10.1016/j.foodhyd.2016.12.019>
- Bak, A., Podgórska, W., 2012. Investigation of drop breakage and coalescence in the liquid-liquid system with nonionic surfactants Tween 20 and Tween 80. *Chem. Eng. Sci.* <https://doi.org/10.1016/j.ces.2012.02.021>
- Bantchev, G.B., Schwartz, D.K., 2003. Surface shear rheology of β -casein layers at the air/solution interface: Formation of a two-dimensional physical gel. *Langmuir* 19, 2673–2682. <https://doi.org/10.1021/la0262349>
- Beckett, S.T., 1996. *Physico-Chemical Aspects of Food Processing*, Physico-Chemical Aspects of Food Processing. <https://doi.org/10.1007/978-1-4613-1227-7>
- Belton, P.S., Gil, A.M., Webb, G.A., Rutledge, D., 2003. *Magnetic Resonance in Food Science*, Special Publications. The Royal Society of Chemistry, Cambridge, UK. <https://doi.org/10.1039/9781847551269>
- BeMiller, J.N., Whistler, R.L., 2009. *Starch: Chemistry and Technology*, ISSN. Elsevier Science.
- Benjamins, J., Cagna, A., Lucassen-Reynders, E.H., 1996. Viscoelastic properties of triacylglycerol/water interfaces covered by proteins, in: *Colloids and Surfaces A: Physicochemical and Engineering Aspects*. Elsevier Science B.V., pp. 245–254. [https://doi.org/10.1016/0927-7757\(96\)03533-9](https://doi.org/10.1016/0927-7757(96)03533-9)
- Benjamins, J., van Voorst Vader, F., 1992. the determination of the surface shear properties of adsorbed protein layers. *Colloids and Surfaces*. [https://doi.org/10.1016/0166-6622\(92\)80271-3](https://doi.org/10.1016/0166-6622(92)80271-3)
- Benmouffok-Benbelkacem, G., Caton, F., Baravian, C., Skali-Lami, S., 2010. Non-linear viscoelasticity and temporal behavior of typical yield stress fluids: Carbopol, Xanthan and Ketchup. *Rheol. Acta.* <https://doi.org/10.1007/s00397-010-0430-4>

- Berg, J.C., 2010. *An Introduction to Interfaces & Colloids: The Bridge to Nanoscience*. World Scientific.
- Bernewitz, R., Dalitz, F., Köhler, K., Schuchmann, H.P., Guthausen, G., 2013. Characterisation of multiple emulsions by NMR spectroscopy and diffusometry. *Microporous Mesoporous Mater.* 178, 69–73.
<https://doi.org/10.1016/j.micromeso.2013.02.049>
- Bernstein, M.A., King, K.F., Zhou, X.J., Glover, G.H., 2005. Handbook of MRI pulse sequences. *NMR Biomed.* 18, 202–203.
<https://doi.org/10.1002/nbm.947>
- Berry, J.D., Neeson, M.J., Dagastine, R.R., Chan, D.Y.C., Tabor, R.F., 2015. Measurement of surface and interfacial tension using pendant drop tensiometry. *J. Colloid Interface Sci.*
<https://doi.org/10.1016/j.jcis.2015.05.012>
- Berton-Carabin, C.C., Sagis, L., Schroën, K., 2018. Formation, Structure, and Functionality of Interfacial Layers in Food Emulsions. *Annu. Rev. Food Sci. Technol.* 9, 551–587. <https://doi.org/10.1146/annurev-food-030117-012405>
- Beverung, C.J., Radke, C.J., Blanch, H.W., 1999. Protein adsorption at the oil/water interface: Characterization of adsorption kinetics by dynamic interfacial tension measurements. *Biophys. Chem.* 81, 59–80.
[https://doi.org/10.1016/S0301-4622\(99\)00082-4](https://doi.org/10.1016/S0301-4622(99)00082-4)
- Bi, B., Yang, H., Fang, Y., Nishinari, K., Phillips, G.O., 2017. Characterization and emulsifying properties of β -lactoglobulin-gum Acacia Seyal conjugates prepared via the Maillard reaction. *Food Chem.* 214, 614–621.
<https://doi.org/10.1016/j.foodchem.2016.07.112>
- Bos, M.A., Van Vliet, T., 2001. Interfacial rheological properties of adsorbed protein layers and surfactants: A review. *Adv. Colloid Interface Sci.*
[https://doi.org/10.1016/S0001-8686\(00\)00077-4](https://doi.org/10.1016/S0001-8686(00)00077-4)

- Bouyer, E., Mekhloufi, G., Huang, N., Rosilio, V., Agnely, F., 2013. β -Lactoglobulin, gum arabic, and xanthan gum for emulsifying sweet almond oil: Formulation and stabilization mechanisms of pharmaceutical emulsions. *Colloids Surfaces A Physicochem. Eng. Asp.* 433, 77–87. <https://doi.org/10.1016/j.colsurfa.2013.04.065>
- Bouyer, E., Mekhloufi, G., Rosilio, V., Grossiord, J.L., Agnely, F., 2012. Proteins, polysaccharides, and their complexes used as stabilizers for emulsions: Alternatives to synthetic surfactants in the pharmaceutical field? *Int. J. Pharm.* 436, 359–378. <https://doi.org/10.1016/j.ijpharm.2012.06.052>
- Bu, H., Kjøniksen, A.L., Nyström, B., 2004. Rheological characterization of photochemical changes of ethyl(hydroxyethyl)cellulos dissolved in water in the presence of an ionic surfactant and a photosensitizer. *Biomacromolecules* 5, 610–617. <https://doi.org/10.1021/bm034443h>
- Buffo, R.A., Reineccius, G.A., Oehlert, G.W., 2001. No Title, *Food Hydrocolloids*. Elsevier. [https://doi.org/10.1016/S0268-005X\(00\)00050-3](https://doi.org/10.1016/S0268-005X(00)00050-3)
- Burchard, W., 2001. Structure formation by polysaccharides in concentrated solution. *Biomacromolecules*. <https://doi.org/10.1021/bm0001291>
- Calero, N., Muñoz, J., Ramírez, P., Guerrero, A., 2010. Flow behaviour, linear viscoelasticity and surface properties of chitosan aqueous solutions. *Food Hydrocoll.* 24, 659–666. <https://doi.org/10.1016/j.foodhyd.2010.03.009>
- Cano, A., Fortunati, E., Cháfer, M., Kenny, J.M., Chiralt, A., González-Martínez, C., 2015. Properties and ageing behaviour of pea starch films as affected by blend with poly(vinyl alcohol). *Food Hydrocoll.* 48, 84–93. <https://doi.org/10.1016/j.foodhyd.2015.01.008>
- Cao, C., Zhang, L., Zhang, X.X., Du, F.P., 2013. Effect of gum arabic on the surface tension and surface dilational rheology of trisiloxane surfactant. *Food Hydrocoll.* 30, 456–462. <https://doi.org/10.1016/j.foodhyd.2012.07.006>

- Capron, I., Cathala, B., 2013. Surfactant-free high internal phase emulsions stabilized by cellulose nanocrystals. *Biomacromolecules* 14, 291–296. <https://doi.org/10.1021/bm301871k>
- Cascão Pereira, L.G., Johansson, C., Blanch, H.W., Radke, C.J., 2001. A bike-wheel microcell for measurement of thin-film forces. *Colloids Surfaces A Physicochem. Eng. Asp.* 186, 103–111. [https://doi.org/10.1016/S0927-7757\(01\)00488-5](https://doi.org/10.1016/S0927-7757(01)00488-5)
- Cascão Pereira, L.G., Théodoly, O., Blanch, H.W., Radke, C.J., 2003. Dilatational rheology of BSA conformers at the air/water interface. *Langmuir* 19, 2349–2356. <https://doi.org/10.1021/la020720e>
- Castel, V., Rubiolo, A.C., Carrara, C.R., 2017. Droplet size distribution, rheological behavior and stability of corn oil emulsions stabilized by a novel hydrocolloid (Brea gum) compared with gum arabic. *Food Hydrocoll.* 63, 170–177. <https://doi.org/10.1016/j.foodhyd.2016.08.039>
- Castellani, O., Al-Assaf, S., Axelos, M., Phillips, G.O., Anton, M., 2010a. Hydrocolloids with emulsifying capacity. Part 2 - Adsorption properties at the n-hexadecane-Water interface. *Food Hydrocoll.* 24, 121–130. <https://doi.org/10.1016/j.foodhyd.2009.07.006>
- Castellani, O., Guibert, D., Al-Assaf, S., Axelos, M., Phillips, G.O., Anton, M., 2010b. Hydrocolloids with emulsifying capacity. Part 1 - Emulsifying properties and interfacial characteristics of conventional (*Acacia senegal* (L.) Willd. var. *senegal*) and matured (*Acacia* (sen) SUPER GUM™) *Acacia senegal*. *Food Hydrocoll.* 24, 193–199. <https://doi.org/10.1016/j.foodhyd.2009.09.005>
- Chen, H. ming, Fu, X., Luo, Z. gang, 2016. Effect of molecular structure on emulsifying properties of sugar beet pulp pectin. *Food Hydrocoll.* 54, 99–106. <https://doi.org/10.1016/j.foodhyd.2015.09.021>
- Chen, H., Qiu, S., Liu, Y., Zhu, Q., Yin, L., 2018. Emulsifying properties and

functional compositions of sugar beet pectins extracted under different conditions. *J. Dispers. Sci. Technol.* 39, 484–490.

<https://doi.org/10.1080/01932691.2016.1151360>

Chen, M., Feijen, S., Sala, G., Meinders, M.B.J., van Valenberg, H.J.F., van Hooijdonk, A.C.M., van der Linden, E., 2018. Foam stabilized by large casein micelle aggregates: The effect of aggregate number in foam lamella. *Food Hydrocoll.* 74, 342–348. <https://doi.org/10.1016/j.foodhyd.2017.08.026>

Colnago, L.A., Moraes, T.B., Monaretto, T., Andrade, F.D., 2015. Rapid Determination of Food Quality Using Steady State Free Precession Sequences in TD-MNR Spectroscopy, in: *Magnetic Resonance in Food Science: Defining Food by Magnetic Resonance*. The Royal Society of Chemistry, pp. 1–16. <https://doi.org/10.1039/9781782622741-00001>

Consoli, L., Dias, R.A.O., Rabelo, R.S., Furtado, G.F., Sussulini, A., Cunha, R.L., Hubinger, M.D., 2018. Sodium caseinate-corn starch hydrolysates conjugates obtained through the Maillard reaction as stabilizing agents in resveratrol-loaded emulsions. *Food Hydrocoll.* 84, 458–472. <https://doi.org/10.1016/j.foodhyd.2018.06.017>

Cornillon, P., Salim, L.C., 2000. Characterization of water mobility and distribution in low- and intermediate-moisture food systems. *Magn. Reson. Imaging* 18, 335–341. [https://doi.org/10.1016/S0730-725X\(99\)00139-3](https://doi.org/10.1016/S0730-725X(99)00139-3)

Corzo-Martínez, M., Carrera-Sánchez, C., Villamiel, M., Rodríguez-Patino, J.M., Moreno, F.J., 2012a. Assessment of interfacial and foaming properties of bovine sodium caseinate glycosylated with galactose. *J. Food Eng.* 113, 461–470. <https://doi.org/10.1016/j.jfoodeng.2012.06.025>

Corzo-Martínez, M., Carrera Sánchez, C., Moreno, F.J., Rodríguez Patino, J.M., Villamiel, M., 2012b. Interfacial and foaming properties of bovine β -lactoglobulin: Galactose Maillard conjugates. *Food Hydrocoll.* 27, 438–447. <https://doi.org/10.1016/j.foodhyd.2011.11.003>

- Covis, R., Desbrieres, J., Marie, E., Durand, A., 2014. Dilational rheology of air/water interfaces covered by nonionic amphiphilic polysaccharides. Correlation with stability of oil-in-water emulsions. *Colloids Surfaces A Physicochem. Eng. Asp.* 441, 312–318.
<https://doi.org/10.1016/j.colsurfa.2013.09.027>
- Cserhádi, T., Forgács, E., Oros, G., 2002. Biological activity and environmental impact of anionic surfactants. *Environ. Int.* 28, 337–348.
[https://doi.org/10.1016/S0160-4120\(02\)00032-6](https://doi.org/10.1016/S0160-4120(02)00032-6)
- Cui, X.H., Zhang, Lei, Luo, L., Zhang, Lu, Zhao, S., Yu, J.Y., 2010. Interfacial dilational properties of model oil and chemical flooding systems by relaxation measurements. *Colloids Surfaces A Physicochem. Eng. Asp.*
<https://doi.org/10.1016/j.colsurfa.2010.08.012>
- Cullen, P.J., Duffy, A.P., O'Donnell, C.P., O'Callaghan, D.J., 2001. Process viscometry for the food industry. *Trends Food Sci. Technol.* 11, 451–457.
[https://doi.org/10.1016/S0924-2244\(01\)00034-6](https://doi.org/10.1016/S0924-2244(01)00034-6)
- D'Aubeterre, A., Da Silva, R., Aguilera, M.E., 2005. Experimental study on Marangoni effect induced by heat and mass transfer. *Int. Commun. Heat Mass Transf.* <https://doi.org/10.1016/j.icheatmasstransfer.2004.06.012>
- D'Avila, M.A., Powell, R.L., Phillips, R.J., Shapley, N.C., Walton, J.H., Dungan, S.R., d'Avila, M.A., Powell, R.L., Phillips, R.J., Shapley, N.C., Walton, J.H., Dungan, S.R., 2005. Magnetic resonance imaging (MRI): A technique to study flow an microstructure of concentrated emulsions. *Brazilian J. Chem. Eng.* 22, 49–60. <https://doi.org/10.1590/S0104-66322005000100006>
- Dal-Bó, A.G., Laus, R., Felipe, A.C., Zanette, D., Minatti, E., 2011. Association of anionic surfactant mixed micelles with hydrophobically modified ethyl(hydroxyethyl)cellulose. *Colloids Surfaces A Physicochem. Eng. Asp.* 380, 100–106. <https://doi.org/10.1016/j.colsurfa.2011.02.028>
- Dalgleish, D.G., 2006. Food emulsions - Their structures and structure-forming

- properties, in: *Food Hydrocolloids*. Elsevier, pp. 415–422.
<https://doi.org/10.1016/j.foodhyd.2005.10.009>
- Damodaran, S., 2005. Protein Stabilization of Emulsions and Foams. *Food Sci.* 70, 54–66.
- Davis, J.P., Foegeding, E.A., 2006. Foaming and Interfacial Properties of Polymerized Whey Protein Isolate. *J. Food Sci.* 69, C404–C410.
<https://doi.org/10.1111/j.1365-2621.2004.tb10706.x>
- de Escalada Pla, M.F., Uribe, M., Fissore, E.N., Gerschenson, L.N., Rojas, A.M., 2010. Influence of the isolation procedure on the characteristics of fiber-rich products obtained from quince wastes. *J. Food Eng.* 96, 239–248.
<https://doi.org/10.1016/j.jfoodeng.2009.07.018>
- Dellarosa, N., Ragni, L., Laghi, L., Tylewicz, U., Rocculi, P., Dalla Rosa, M., 2015. Time domain nuclear magnetic resonance to monitor mass transfer mechanisms in apple tissue promoted by osmotic dehydration combined with pulsed electric fields. *Innov. Food Sci. Emerg. Technol.*
<https://doi.org/10.1016/j.ifset.2016.01.009>
- Deng, Y., Huang, L., Zhang, C., Xie, P., Cheng, J., Wang, X., Li, S., 2019. Physicochemical and functional properties of Chinese quince seed protein isolate. *Food Chem.* 283, 539–548.
<https://doi.org/10.1016/j.foodchem.2019.01.083>
- Derkach, S.R., Krägel, J., Miller, R., 2009. Methods of measuring rheological properties of interfacial layers (Experimental methods of 2D rheology). *Colloid J.* <https://doi.org/10.1134/S1061933X09010013>
- Desbrières, J., López-Gonzalez, E., Aguilera-miguel, A., Sadtler, V., Marchal, P., Castel, C., Choplin, L., Durand, A., 2017. Dilational rheology of oil/water interfaces covered by amphiphilic polysaccharides derived from dextran. *Carbohydr. Polym.* 177, 460–468.
<https://doi.org/10.1016/j.carbpol.2017.09.011>

- Dickinson, E., 2018. Hydrocolloids acting as emulsifying agents – How do they do it? *Food Hydrocoll.* 78, 2–14. <https://doi.org/10.1016/j.foodhyd.2017.01.025>
- Dickinson, E., 2017. Biopolymer-based particles as stabilizing agents for emulsions and foams. *Food Hydrocoll.* 68, 219–231. <https://doi.org/10.1016/j.foodhyd.2016.06.024>
- Dickinson, E., 2009. Hydrocolloids and emulsion stability, in: *Handbook of Hydrocolloids: Second Edition*. Elsevier Inc., pp. 23–49. <https://doi.org/10.1533/9781845695873.23>
- Dickinson, E., 2008a. Interfacial structure and stability of food emulsions as affected by protein-polysaccharide interactions. *Soft Matter* 4, 932–942. <https://doi.org/10.1039/b718319d>
- Dickinson, E., 2008b. Emulsification and emulsion stabilization with protein-polysaccharide complexes, in: *Gums and Stabilisers for the Food Industry 14*. Royal Society of Chemistry, pp. 221–232.
- Dickinson, E., 2003. Hydrocolloids at interfaces and the influence on the properties of dispersed systems. *Food Hydrocoll.* [https://doi.org/10.1016/S0268-005X\(01\)00120-5](https://doi.org/10.1016/S0268-005X(01)00120-5)
- Dickinson, E., 2001. Milk protein interfacial layers and the relationship to emulsion stability and rheology. *Colloids Surfaces B Biointerfaces*. [https://doi.org/10.1016/S0927-7765\(00\)00204-6](https://doi.org/10.1016/S0927-7765(00)00204-6)
- Dickinson, E., 1999. Adsorbed protein layers at fluid interfaces: Interactions, structure and surface rheology. *Colloids Surfaces B Biointerfaces*. [https://doi.org/10.1016/S0927-7765\(99\)00042-9](https://doi.org/10.1016/S0927-7765(99)00042-9)
- Dickinson, E., 1998. Proteins at interfaces and in emulsions. Stability, rheology and interactions. *J. Chem. Soc. - Faraday Trans.* 94, 1657–1669. <https://doi.org/10.1039/a801167b>
- Dickinson, E., 1993. Towards more natural emulsifiers. *Trends Food Sci. Technol.*

[https://doi.org/10.1016/0924-2244\(93\)90103-H](https://doi.org/10.1016/0924-2244(93)90103-H)

- Djordjevic, D., Kim, H.J., McClements, D.J., Decker, E.A., 2004. Physical stability of whey protein-stabilized oil-in-water emulsions at pH 3: Potential ω -3 fatty acid delivery systems (Part A). *J. Food Sci.* <https://doi.org/10.1111/j.1365-2621.2004.tb10696.x>
- Doublier, J.L., Launay, B., 1981. Rheology of Galactomannan Solutions: Comparative Study of Guar Gum and Locust Bean Gum. *J. Texture Stud.* 12, 151–172. <https://doi.org/10.1111/j.1745-4603.1981.tb01229.x>
- Du, Y., Jiang, Y., Zhu, X., Xiong, H., Shi, S., Hu, J., Peng, H., Zhou, Q., Sun, W., 2012. Physicochemical and functional properties of the protein isolate and major fractions prepared from *Akebia trifoliata* var. *australis* seed. *Food Chem.* 133, 923–929. <https://doi.org/10.1016/j.foodchem.2012.02.005>
- Duval, F.P., Van Duynhoven, J.P.M., Bot, A., Duynhoven, J.P.M. Van, Bot, A., 2006. Practical implications of the phase-compositional assessment of lipid-based food products by time-domain NMR. *JAOCS, J. Am. Oil Chem. Soc.* 83, 905–912. <https://doi.org/10.1007/s11746-006-5045-7>
- Duvallet, S., Fenyo, J.C., Vandeveld, M.C., 1989. Meaning of molecular weight measurements of gum arabic, *Polymer Bulletin*.
- Effendy, I., Maibach, H.I., 1995. Surfactants and experimental irritant contact dermatitis, *Contact Dermatitis*. John Wiley & Sons, Ltd. <https://doi.org/10.1111/j.1600-0536.1995.tb00470.x>
- Ettelaie, R., Holmes, M., Chen, J., Farshchi, A., 2016. Steric stabilising properties of hydrophobically modified starch: Amylose vs. amylopectin. *Food Hydrocoll.* 58, 364–377. <https://doi.org/10.1016/j.foodhyd.2016.03.004>
- Ettelaie, R., Murray, B.S., James, E.L., 2003. Steric interactions mediated by multiblock polymers and biopolymers: Role of block size and addition of hydrophilic side chains, in: *Colloids and Surfaces B: Biointerfaces*. Elsevier,

pp. 195–206. [https://doi.org/10.1016/S0927-7765\(03\)00140-1](https://doi.org/10.1016/S0927-7765(03)00140-1)

- Evans, M., Ratcliffe, I., Williams, P. a., 2013. Emulsion stabilisation using polysaccharide-protein complexes. *Curr. Opin. Colloid Interface Sci.* 18, 272–282. <https://doi.org/10.1016/j.cocis.2013.04.004>
- Fainerman, V.B., Makievski, A. V., Miller, R., 1994. The analysis of dynamic surface tension of sodium alkyl sulphate solutions, based on asymptotic equations of adsorption kinetic theory. *Colloids Surfaces A Physicochem. Eng. Asp.* [https://doi.org/10.1016/0927-7757\(94\)02747-1](https://doi.org/10.1016/0927-7757(94)02747-1)
- Farahmandfar, R., Asnaashari, M., Salahi, M.R., Khosravi Rad, T., 2017. Effects of basil seed gum, Cress seed gum and Quince seed gum on the physical, textural and rheological properties of whipped cream. *Int. J. Biol. Macromol.* 98, 820–828. <https://doi.org/10.1016/j.ijbiomac.2017.02.046>
- Feng, C., Li, Y., Yang, D., Hu, J., Zhang, X., Huang, X., 2011. Well-defined graft copolymers: From controlled synthesis to multipurpose applications. *Chem. Soc. Rev.* 40, 1282–1295. <https://doi.org/10.1039/b921358a>
- Fisher, L.R., Mitchell, E.E., Parker, N.S., 1985. Interfacial Tensions of Commercial Vegetable Oils with Water. *J. Food Sci.* 50, 1201–1202. <https://doi.org/10.1111/j.1365-2621.1985.tb13052.x>
- Fleer, G., Stuart, M.A.C., Scheutjens, J.M.H.M., Cosgrove, T., Vincent, B., 1993. *Polymers at Interfaces*. Springer Netherlands.
- Fleer, G.J., 2010. Polymers at interfaces and in colloidal dispersions. *Adv. Colloid Interface Sci.* 159, 99–116. <https://doi.org/10.1016/j.cis.2010.04.004>
- Flory, P.J., 1953. *Principles of Polymer Chemistry*, Baker lectures 1948. Cornell University Press.
- Flory, P.J., Krigbaum, W.R., 1950. Statistical mechanics of dilute polymer solutions. II. *J. Chem. Phys.* 18, 1086–1094. <https://doi.org/10.1063/1.1747866>

- Freer, E.M., Radke, C.J., 2004. Relaxation of asphaltenes at the toluene/water interface: Diffusion exchange and surface rearrangement. *J. Adhes.* 80, 481–496. <https://doi.org/10.1080/00218460490477143>
- Freer, E.M., Svitova, T., Radke, C.J., 2003. The role of interfacial rheology in reservoir mixed wettability. *J. Pet. Sci. Eng.* 39, 137–158. [https://doi.org/10.1016/S0920-4105\(03\)00045-7](https://doi.org/10.1016/S0920-4105(03)00045-7)
- Freer, E.M., Yim, K.S., Fuller, G.G., Radke, C.J., 2004a. Shear and dilatational relaxation mechanisms of globular and flexible proteins at the hexadecane/water interface. *Langmuir* 20, 10159–10167. <https://doi.org/10.1021/la0485226>
- Freer, E.M., Yim, K.S., Fuller, G.G., Radke, C.J., 2004b. Interfacial Rheology of Globular and Flexible Proteins at the Hexadecane/Water Interface: Comparison of Shear and Dilatation Deformation. *J. Phys. Chem. B* 108, 3835–3844. <https://doi.org/10.1021/jp037236k>
- Fruhner, H., Wantke, K.D., Lunkenheimer, K., 2000. Relationship between surface dilational properties and foam stability. *Colloids Surfaces A Physicochem. Eng. Asp.* [https://doi.org/10.1016/S0927-7757\(99\)00202-2](https://doi.org/10.1016/S0927-7757(99)00202-2)
- Funami, T., Zhang, G., Hiroe, M., Noda, S., Nakauma, M., Asai, I., Cowman, M.K., Al-Assaf, S., Phillips, G.O., 2007. Effects of the proteinaceous moiety on the emulsifying properties of sugar beet pectin. *Food Hydrocoll.* 21, 1319–1329. <https://doi.org/10.1016/j.foodhyd.2006.10.009>
- Gao, C., Tang, F., Gong, G., Zhang, J., Hoi, M.P.M., Lee, S.M.Y., Wang, R., 2017. PH-Responsive prodrug nanoparticles based on a sodium alginate derivative for selective co-release of doxorubicin and curcumin into tumor cells. *Nanoscale* 9, 12533–12542. <https://doi.org/10.1039/c7nr03611f>
- Gao, Z., Fang, Y., Cao, Y., Liao, H., Nishinari, K., Phillips, G.O., 2017. Hydrocolloid-food component interactions. *Food Hydrocoll.* 68, 149–156. <https://doi.org/10.1016/j.foodhyd.2016.08.042>

- Gashua, I.B., Williams, P.A., Baldwin, T.C., 2016. Molecular characteristics, association and interfacial properties of gum Arabic harvested from both *Acacia senegal* and *Acacia seyal*. *Food Hydrocoll.* 61, 514–522.
<https://doi.org/10.1016/j.foodhyd.2016.06.005>
- Gooch, J.W., 2012. *Encyclopedic Dictionary of Polymers*. Springer New York.
- Gouldby, S.J., Gunning, P.A., Hibberd, D.J., Robins, M.M., 1991. Creaming in Flocculated Oil-in-Water Emulsions, in: *Food Polymers, Gels and Colloids*.
<https://doi.org/10.1533/9781845698331.244>
- Goycoolea, F.M., Calderón De La Barca, A.M., Balderrama, J.R., Valenzuela, J.R., 1997. Immunological and functional properties of the exudate gum from northwestern Mexican mesquite (*Prosopis* spp.) in comparison with gum arabic. *Int. J. Biol. Macromol.* 21, 29–36. [https://doi.org/10.1016/S0141-8130\(97\)00037-8](https://doi.org/10.1016/S0141-8130(97)00037-8)
- Graham, D.E., Phillips, M.C., 1980. Proteins at liquid interfaces. IV. Dilatational properties. *J. Colloid Interface Sci.* 76, 227–239. [https://doi.org/10.1016/0021-9797\(80\)90289-1](https://doi.org/10.1016/0021-9797(80)90289-1)
- Graham, D.E., Phillips, M.C., 1979. Proteins at liquid interfaces. III. Molecular structures of adsorbed films. *J. Colloid Interface Sci.*
[https://doi.org/10.1016/0021-9797\(79\)90050-X](https://doi.org/10.1016/0021-9797(79)90050-X)
- Guthausen, G., 2016. Analysis of food and emulsions. *Trends Anal. Chem.* 10–13.
<https://doi.org/10.1016/j.trac.2016.02.011>
- Guzey, D., McClements, D.J., 2006. Formation, stability and properties of multilayer emulsions for application in the food industry, *Advances in Colloid and Interface Science*. Elsevier. <https://doi.org/10.1016/j.cis.2006.11.021>
- Guzmán, E., Llamas, S., Maestro, A., Fernández-Peña, L., Akanno, A., Miller, R., Ortega, F., Rubio, R.G., 2016. Polymer-surfactant systems in bulk and at fluid interfaces. *Adv. Colloid Interface Sci.* 233, 38–64.

<https://doi.org/10.1016/j.cis.2015.11.001>

- Gwartney, E.A., Larick, D.K., Foegeding, E.A., 2004. Sensory texture and mechanical properties of stranded and particulate whey protein emulsion gels. *J. Food Sci.* <https://doi.org/10.1111/j.1365-2621.2004.tb09945.x>
- Ha, M.A., Apperley, D.C., Evans, B.W., Max Huxham, I., Gordon Jardine, W., Viëtor, R.J., Reis, D., Vian, B., Jarvis, M.C., 1998. Fine structure in cellulose microfibrils: NMR evidence from onion and quince. *Plant J.* 16, 183–190. <https://doi.org/10.1046/j.1365-313X.1998.00291.x>
- Haiduc, A.M., van Duynhoven, J.P.M.M., Heussen, P., Reszka, A.A., Reiffers-Magnani, C., 2007. Multivariate modelling of the microstructural quality of food emulsions based on NMR. *Food Res. Int.* 40, 425–434. <https://doi.org/10.1016/j.foodres.2006.05.010>
- Hakala, T.J., Saikko, V., Arola, S., Ahlroos, T., Helle, A., Kuosmanen, P., Holmberg, K., Linder, M.B., Laaksonen, P., 2014. Structural characterization and tribological evaluation of quince seed mucilage. *Tribol. Int.* 77, 24–31. <https://doi.org/10.1016/j.triboint.2014.04.018>
- Hamdani, A.M., Wani, I.A., Bhat, N.A., Siddiqi, R.A., 2018. Effect of guar gum conjugation on functional, antioxidant and antimicrobial activity of egg white lysozyme. *Food Chem.* 240, 1201–1209. <https://doi.org/10.1016/j.foodchem.2017.08.060>
- Han, J.R., Gu, L.P., Zhang, R.J., Shang, W.H., Yan, J.N., McClements, D.J., Wu, H.T., Zhu, B.W., Xiao, H., 2019. Bioaccessibility and cellular uptake of β -carotene in emulsion-based delivery systems using scallop (*Patinopecten yessoensis*) gonad protein isolates: Effects of carrier oil. *Food Funct.* 10, 49–60. <https://doi.org/10.1039/c8fo01390j>
- Hashemi, R.H., Bradley, W.G., Lisanti, C.J., 2010. *MRI: The Basics, The Basics Series*. Lippincott Williams & Wilkins.

- Hayase, K., Tsubota, H., 1986. Monolayer properties of sedimentary humic acid at the air-water interface. *J. Colloid Interface Sci.* [https://doi.org/10.1016/0021-9797\(86\)90255-9](https://doi.org/10.1016/0021-9797(86)90255-9)
- Hemar, Y., Tamehana, M., Munro, P.A., Singh, H., 2001. Influence of xanthan gum on the formation and stability of sodium caseinate oil-in-water emulsions, in: *Food Hydrocolloids*. [https://doi.org/10.1016/S0268-005X\(01\)00075-3](https://doi.org/10.1016/S0268-005X(01)00075-3)
- Hilder, M.H., 1968. The solubility of water in edible oils and fats. *J. Am. Oil Chem. Soc.* 45, 703–707. <https://doi.org/10.1007/BF02541262>
- Hosseini-Parvar, S.H., Matia-Merino, L., Goh, K.K.T., Razavi, S.M.A., Mortazavi, S.A., 2010. Steady shear flow behavior of gum extracted from *Ocimum basilicum* L. seed: Effect of concentration and temperature. *J. Food Eng.* <https://doi.org/10.1016/j.jfoodeng.2010.06.025>
- Hu, B., Han, L., Kong, H., Nishinari, K., Phillips, G.O., Yang, J., Fang, Y., 2019. Preparation and emulsifying properties of trace elements fortified gum arabic. *Food Hydrocoll.* 88, 43–49. <https://doi.org/10.1016/j.foodhyd.2018.09.027>
- Hu, X.Z., Cheng, Y.Q., Fan, J.F., Lu, Z.H., Yamaki, K., Li, L. Te, 2010. Effects of drying method on physicochemical and functional properties of soy protein isolates. *J. Food Process. Preserv.* 34, 520–540. <https://doi.org/10.1111/j.1745-4549.2008.00357.x>
- Huang, X., Kakuda, Y., Cui, W., 2001. Hydrocolloids in emulsions: Particle size distribution and interfacial activity. *Food Hydrocoll.* 15, 533–542. [https://doi.org/10.1016/S0268-005X\(01\)00091-1](https://doi.org/10.1016/S0268-005X(01)00091-1)
- Huang, Z., Boubriak, I., Osborne, D.J., Dong, M., Gutterman, Y., 2008. Possible role of pectin-containing mucilage and dew in repairing embryo DNA of seeds adapted to desert conditions. *Ann. Bot.* 101, 277–283. <https://doi.org/10.1093/aob/mcm089>

- Hwang, J., Kokini, J.L., 1991. Structure and Rheological Function of Side Branches of Carbohydrate Polymers. *J. Texture Stud.* 22, 123–167. <https://doi.org/10.1111/j.1745-4603.1991.tb00011.x>
- Ishimuro, Y., Ueberreiter, K., 1980. The surface tension of poly(acrylic acid) in aqueous solution. *Colloid Polym. Sci. Kolloid-Zeitschrift Zeitschrift für Polym.* <https://doi.org/10.1007/BF01584922>
- Isobe, N., Sagawa, N., Ono, Y., Fujisawa, S., Kimura, S., Kinoshita, K., Miuchi, T., Iwata, T., Isogai, A., Nishino, M., Deguchi, S., 2020. Primary structure of gum arabic and its dynamics at oil/water interface. *Carbohydr. Polym.* 249, 116843. <https://doi.org/10.1016/j.carbpol.2020.116843>
- Jain, S., Anal, A.K., 2018. Preparation of eggshell membrane protein hydrolysates and culled banana resistant starch-based emulsions and evaluation of their stability and behavior in simulated gastrointestinal fluids. *Food Res. Int.* 103, 234–242. <https://doi.org/10.1016/j.foodres.2017.10.042>
- Jansson, P. erik, Kenne, L., Lindberg, B., 1975. Structure of the extracellular polysaccharide from *xanthomonas campestris*. *Carbohydr. Res.* [https://doi.org/10.1016/S0008-6215\(00\)85885-1](https://doi.org/10.1016/S0008-6215(00)85885-1)
- Jasniewski, J., Keramat, J., Nasirpour, A., Desobry, S., Pirestani, S., 2016. Effect of glycosylation with gum Arabic by Maillard reaction in a liquid system on the emulsifying properties of canola protein isolate. *Carbohydr. Polym.* 157, 1620–1627. <https://doi.org/10.1016/j.carbpol.2016.11.044>
- Jindal, N., Singh Khattar, J., 2018. Microbial Polysaccharides in Food Industry, in: *Biopolymers for Food Design*. Elsevier Inc., pp. 95–123. <https://doi.org/10.1016/B978-0-12-811449-0.00004-9>
- Jing, H., Yap, M., Wong, P.Y.Y., Kitts, D.D., 2011. Comparison of Physicochemical and Antioxidant Properties of Egg-White Proteins and Fructose and Inulin Maillard Reaction Products. *Food Bioprocess Technol.* 4, 1489–1496. <https://doi.org/10.1007/s11947-009-0279-7>

- Johns, M.L., 2009. NMR studies of emulsions. *Curr. Opin. Colloid Interface Sci.* 14, 178–183. <https://doi.org/10.1016/j.cocis.2008.10.005>
- Jouki, M., Yazdi, F.T., Mortazavi, S.A., Koocheki, A., 2014. Quince seed mucilage films incorporated with oregano essential oil: Physical, thermal, barrier, antioxidant and antibacterial properties. *Food Hydrocoll.* 36, 9–19. <https://doi.org/10.1016/j.foodhyd.2013.08.030>
- Karbaschi, M., Lotfi, M., Krägel, J., Javadi, A., Bastani, D., Miller, R., 2014. Rheology of interfacial layers. *Curr. Opin. Colloid Interface Sci.* 19, 514–519. <https://doi.org/10.1016/j.cocis.2014.08.003>
- Kasran, M., Cui, S.W., Goff, H.D., 2013a. Covalent attachment of fenugreek gum to soy whey protein isolate through natural Maillard reaction for improved emulsion stability. *Food Hydrocoll.* 30, 552–558. <https://doi.org/10.1016/j.foodhyd.2012.08.004>
- Kasran, M., Cui, S.W., Goff, H.D., 2013b. Emulsifying properties of soy whey protein isolate-fenugreek gum conjugates in oil-in-water emulsion model system. *Food Hydrocoll.* 30, 691–697. <https://doi.org/10.1016/j.foodhyd.2012.09.002>
- Keowmaneechai, E., McClements, D.J., 2002. Influence of EDTA and citrate on physicochemical properties of whey protein-stabilized oil-in-water emulsions containing CaCl₂. *J. Agric. Food Chem.* <https://doi.org/10.1021/jf020489a>
- Khouryieh, H.A., Herald, T.J., Aramouni, F., Alavi, S., 2007. Intrinsic viscosity and viscoelastic properties of xanthan/guar mixtures in dilute solutions: Effect of salt concentration on the polymer interactions. *Food Res. Int.* 40, 883–893. <https://doi.org/10.1016/j.foodres.2007.03.001>
- Kirtil, Emrah, Oztop, M.H., 2016. Characterization of emulsion stabilization properties of quince seed extract as a new source of hydrocolloid. *Food Res. Int.* 85, 84–94. <https://doi.org/10.1016/j.foodres.2016.04.019>

- Kirtil, E., Oztop, M.H., 2016. ^1H Nuclear Magnetic Resonance Relaxometry and Magnetic Resonance Imaging and Applications in Food Science and Processing. *Food Eng. Rev.* 8. <https://doi.org/10.1007/s12393-015-9118-y>
- Kirtil, E., Oztop, M.H.M.H., Sirijariyawat, A., Ngamchuachit, P., Barrett, D.M.D.M., McCarthy, M.J.M.J., 2014. Effect of pectin methyl esterase (PME) and CaCl_2 infusion on the cell integrity of fresh-cut and frozen-thawed mangoes: An NMR relaxometry study. *Food Res. Int.* 66, 409–416. <https://doi.org/10.1016/j.foodres.2014.10.006>
- Kock, F.V.C., Colnago, L.A., 2016. Rapid method for monitoring chitosan coagulation using low-field NMR relaxometry. *Carbohydr. Polym.* 150, 1–4. <https://doi.org/10.1016/j.carbpol.2016.05.007>
- Kokubun, S., Ratcliffe, I., Williams, P.A., 2018. The interfacial, emulsification and encapsulation properties of hydrophobically modified inulin. *Carbohydr. Polym.* 194, 18–23. <https://doi.org/10.1016/j.carbpol.2018.04.018>
- Konez, O., 2011. Manyetik Rezonans Görüntüleme: Temel Bilgiler [WWW Document]. URL <http://konez.com/>
- Kontogiorgos, V., 2019. Polysaccharides at fluid interfaces of food systems. *Adv. Colloid Interface Sci.* 270, 28–37. <https://doi.org/10.1016/j.cis.2019.05.008>
- Koocheki, A., Ghandi, A., Razavi, S.M.A., Mortazavi, S.A., Vasiljevic, T., 2009a. The rheological properties of ketchup as a function of different hydrocolloids and temperature. *Int. J. Food Sci. Technol.* 44, 596–602. <https://doi.org/10.1111/j.1365-2621.2008.01868.x>
- Koocheki, A., Taherian, A.R., Razavi, S.M.A., Bostan, A., 2009b. Response surface methodology for optimization of extraction yield, viscosity, hue and emulsion stability of mucilage extracted from *Lepidium perfoliatum* seeds. *Food Hydrocoll.* 23, 2369–2379. <https://doi.org/10.1016/j.foodhyd.2009.06.014>

- Koshani, R., Aminlari, M., Niakosari, M., Farahnaky, A., Mesbahi, G., 2015. Production and properties of tragacanthin-conjugated lysozyme as a new multifunctional biopolymer. *Food Hydrocoll.* 47, 69–78.
<https://doi.org/10.1016/j.foodhyd.2014.12.023>
- Kpodo, F.M., Agbenorhevi, J.K., Alba, K., Bingham, R.J., Oduro, I.N., Morris, G.A., Kontogiorgos, V., 2017. Pectin isolation and characterization from six okra genotypes. *Food Hydrocoll.* 72, 323–330.
<https://doi.org/10.1016/j.foodhyd.2017.06.014>
- Krstonošić, V., Milanović, M., Dokić, L., 2019. Application of different techniques in the determination of xanthan gum-SDS and xanthan gum-Tween 80 interaction. *Food Hydrocoll.* 87, 108–118.
<https://doi.org/10.1016/j.foodhyd.2018.07.040>
- Langevin, D., 2000. Influence of interfacial rheology on foam and emulsion properties. *Adv. Colloid Interface Sci.* 88, 209–222.
[https://doi.org/10.1016/S0001-8686\(00\)00045-2](https://doi.org/10.1016/S0001-8686(00)00045-2)
- Le Botlan, D., Wennington, J., Cheftel, J.C., 2000. Study of the state of water and oil in frozen emulsions using time domain nmr. *J. Colloid Interface Sci.* 226, 16–21. <https://doi.org/10.1006/jcis.2000.6785>
- Lee, M.Y., Hong, K.J., Kajiuchi, T., Yang, J.W., 2005. Synthesis of chitosan-based polymeric surfactants and their adsorption properties for heavy metals and fatty acids. *Int. J. Biol. Macromol.* 36, 152–158.
<https://doi.org/10.1016/j.ijbiomac.2005.05.004>
- Leroux, J., Langendorff, V., Schick, G., Vaishnav, V., Mazoyer, J., 2003. Emulsion stabilizing properties of pectin, in: *Food Hydrocolloids*. Elsevier, pp. 455–462. [https://doi.org/10.1016/S0268-005X\(03\)00027-4](https://doi.org/10.1016/S0268-005X(03)00027-4)
- Li, S., Zhang, B., Li, C., Fu, X., Huang, Q., 2020. Pickering emulsion gel stabilized by octenylsuccinate quinoa starch granule as lutein carrier: Role of the gel network. *Food Chem.* 305, 125476.

<https://doi.org/10.1016/j.foodchem.2019.125476>

- Li, Y., Zhong, F., Ji, W., Yokoyama, W., Shoemaker, C.F., Zhu, S., Xia, W., 2013. Functional properties of Maillard reaction products of rice protein hydrolysates with mono-, oligo- and polysaccharides. *Food Hydrocoll.* 30, 53–60. <https://doi.org/10.1016/j.foodhyd.2012.04.013>
- Liang, W., Bognolo, G., Tadros, T.F., 1995. Stability of Dispersions in the Presence of Graft Copolymer. 1. Adsorption of Graft Copolymers on Latex Dispersions and the Stability and Rheology of the Resulting Dispersions. *Langmuir* 11, 2899–2904. <https://doi.org/10.1021/la00008a010>
- Liggieri, L., Attolini, V., Ferrari, M., Ravera, F., 2002. Measurement of the Surface Dilational Viscoelasticity of Adsorbed Layers with a Capillary Pressure Tensiometer. *J. Colloid Interface Sci.* 255, 225–235. <https://doi.org/10.1006/jcis.2002.8665>
- Lindberg, B., Mosihuzzaman, M., Nahar, N., Abeysekera, R.M., Brown, R.G., Willison, J.H.M., 1990. An unusual (4-O-methyl-d-glucurono)-d-xylan isolated from the mucilage of seeds of the quince tree (*Cydonia oblonga*). *Carbohydr. Res.* 207, 307–310. [https://doi.org/10.1016/0008-6215\(90\)84057-2](https://doi.org/10.1016/0008-6215(90)84057-2)
- Ling, N.N.A., Haber, A., Fridjonsson, E.O., May, E.F., Johns, M.L., 2016. Shear-induced emulsion droplet diffusion studies using NMR. *J. Colloid Interface Sci.* 464, 229–237. <https://doi.org/10.1016/j.jcis.2015.11.013>
- Lips, A., Campbell, I.J., Pelan, E.G., 1991. Aggregation Mechanisms in Food Colloids and the Role of Biopolymers, in: *Food Polymers, Gels and Colloids*. Elsevier, pp. 1–21. <https://doi.org/10.1533/9781845698331.1>
- Liu, W., Li, Y., Chen, M., Xu, F., Zhong, F., 2018. Stabilizing Oil-in-Water Emulsion with Amorphous and Granular Octenyl Succinic Anhydride Modified Starches. *J. Agric. Food Chem.* 66. <https://doi.org/10.1021/acs.jafc.8b02733>

- Liu, W.Y., Feng, M.Q., Wang, M., Wang, P., Sun, J., Xu, X.L., Zhou, G.H., 2018. Influence of flaxseed gum and NaCl concentrations on the stability of oil-in-water emulsions. *Food Hydrocoll.* 79, 371–381. <https://doi.org/10.1016/j.foodhyd.2018.01.010>
- Liu, Y., Yadav, M.P., Yin, L., 2018. Enzymatic catalyzed corn fiber gum-bovine serum albumin conjugates: Their interfacial adsorption behaviors in oil-in-water emulsions. *Food Hydrocoll.* 77, 986–994. <https://doi.org/10.1016/j.foodhyd.2017.11.048>
- Liwarska-Bizukojc, E., Miksch, K., Malachowska-Jutysz, A., Kalka, J., 2005. Acute toxicity and genotoxicity of five selected anionic and nonionic surfactants. *Chemosphere* 58, 1249–1253. <https://doi.org/10.1016/j.chemosphere.2004.10.031>
- Lopes, I.S., Michelon, M., Duarte, L.G.R., Prediger, P., Cunha, R.L., Picone, C.S.F., 2020. Effect of chitosan structure modification and complexation to whey protein isolate on oil/water interface stabilization. *Chem. Eng. Sci.* 116124. <https://doi.org/10.1016/j.ces.2020.116124>
- López-Castejón, M.L., Bengoechea, C., Espinosa, S., Carrera, C., 2019. Characterization of prebiotic emulsions stabilized by inulin and β -lactoglobulin. *Food Hydrocoll.* 87, 382–393. <https://doi.org/10.1016/j.foodhyd.2018.08.024>
- Lu, S., Pugh, R.J., Forssberg, E., 2005. Chapter 4 Particle-particle interactions. *Stud. Interface Sci.* 20, 172–244. [https://doi.org/10.1016/S1383-7303\(05\)80005-5](https://doi.org/10.1016/S1383-7303(05)80005-5)
- Lucassen, J., Van Den Tempel, M., 1972a. Dynamic measurements of dilational properties of a liquid interface. *Chem. Eng. Sci.* 27, 1283–1291. [https://doi.org/10.1016/0009-2509\(72\)80104-0](https://doi.org/10.1016/0009-2509(72)80104-0)
- Lucassen, J., Van Den Tempel, M., 1972b. Longitudinal waves on visco-elastic surfaces. *J. Colloid Interface Sci.* 41, 491–498. <https://doi.org/10.1016/0021->

9797(72)90373-6

- Ma, B.D., Zhang, Lei, Gao, B.Y., Zhang, Lu, Zhao, S., Yu, J.Y., 2011. Interfacial dilational rheological property and lamella stability of branched alkyl benzene sulfonates solutions. *Colloid Polym. Sci.* 289, 911–918.
<https://doi.org/10.1007/s00396-011-2415-y>
- Macleod, C.A., Radke, C.J., 1994. * I 3555–3566.
- Macritchie, F., 1978. Proteins at Interfaces. *Adv. Protein Chem.*
[https://doi.org/10.1016/S0065-3233\(08\)60577-X](https://doi.org/10.1016/S0065-3233(08)60577-X)
- Man, X., Yan, D., 2010. Charge inversion by flexible polyelectrolytes adsorbed onto charged cylindrical surfaces within self-consistent-field theory. *Macromolecules* 43, 2582–2588. <https://doi.org/10.1021/ma9022263>
- Man, X., Yang, S., Yan, D., Shi, A.C., 2008. Adsorption and depletion of polyelectrolytes in charged cylindrical system within self-consistent field theory. *Macromolecules* 41, 5451–5456. <https://doi.org/10.1021/ma8003482>
- Marques, C., Joanny, J.F., Leibler, L., 1988. Adsorption of Block Copolymers in Selective Solvents. *Macromolecules* 21, 1051–1059.
<https://doi.org/10.1021/ma00182a035>
- McClements, D.J., 2009. Biopolymers in Food Emulsions, in: *Modern Biopolymer Science*. Elsevier Inc., pp. 129–166. <https://doi.org/10.1016/B978-0-12-374195-0.00004-5>
- McClements, D.J., 2004. *Food emulsions: Principles, practices, and techniques: Second edition, Food Emulsions: Principles, Practices, and Techniques, Second Edition.*
- Melton, L.D., Mindt, L., Rees, D.A., 1976. Covalent structure of the extracellular polysaccharide from *Xanthomonas campestris*: evidence from partial hydrolysis studies. *Carbohydr. Res.* [https://doi.org/10.1016/S0008-6215\(00\)84296-2](https://doi.org/10.1016/S0008-6215(00)84296-2)

- Mendoza, A.J., Guzmán, E., Martínez-Pedrero, F., Ritacco, H., Rubio, R.G., Ortega, F., Starov, V.M., Miller, R., 2014. Particle laden fluid interfaces: Dynamics and interfacial rheology. *Adv. Colloid Interface Sci.* 206, 303–319. <https://doi.org/10.1016/j.cis.2013.10.010>
- Miller, R., Wüstneck, R., Krägel, J., Kretzschmar, G., 1996. Dilational and shear rheology of adsorption layers at liquid interfaces. *Colloids Surfaces A Physicochem. Eng. Asp.* 111, 75–118. [https://doi.org/10.1016/0927-7757\(95\)03492-7](https://doi.org/10.1016/0927-7757(95)03492-7)
- Mitchell, J., Gladden, L.F., Chandrasekera, T.C., Fordham, E.J., 2014. Progress in Nuclear Magnetic Resonance Spectroscopy Low-field permanent magnets for industrial process and quality control. *Prog. Nucl. Magn. Reson. Spectrosc.* 76, 1–60. <https://doi.org/10.1016/j.pnmrs.2013.09.001>
- Möbius, D., Miller, R., Fainerman, V.B., 2001. *Surfactants: Chemistry, Interfacial Properties, Applications*, ISSN. Elsevier Science.
- Moreira, R., Chenlo, F., Silva, C., Torres, M.D., Díaz-Varela, D., Hilliou, L., Argence, H., 2012. Surface tension and refractive index of guar and tragacanth gums aqueous dispersions at different polymer concentrations, polymer ratios and temperatures. *Food Hydrocoll.* 28, 284–290. <https://doi.org/10.1016/j.foodhyd.2012.01.007>
- Mulcahy, E.M., Mulvihill, D.M., O'Mahony, J.A., 2016. Physicochemical properties of whey protein conjugated with starch hydrolysis products of different dextrose equivalent values. *Int. Dairy J.* 53, 20–28. <https://doi.org/10.1016/j.idairyj.2015.09.009>
- Mundi, S., Aluko, R.E., 2012. Physicochemical and functional properties of kidney bean albumin and globulin protein fractions. *Food Res. Int.* <https://doi.org/10.1016/j.foodres.2012.04.006>
- Muñoz, J., Rincón, F., Carmen Alfaro, M., Zapata, I., de la Fuente, J., Beltrán, O., León de Pinto, G., 2007. Rheological properties and surface tension of Acacia

- tortuosa gum exudate aqueous dispersions. *Carbohydr. Polym.* 70, 198–205.
<https://doi.org/10.1016/j.carbpol.2007.03.018>
- Nahringbauer, I., 1995. Dynamic Surface Tension of Aqueous Polymer Solutions, I: Ethyl(hydroxyethyl)cellulose (BERMOCOLL cst-103). *J. Colloid Interface Sci.* 176, 318–328. <https://doi.org/10.1006/jcis.1995.9961>
- Nakamura, A., Yoshida, R., Maeda, H., Corredig, M., 2006. Soy soluble polysaccharide stabilization at oil-water interfaces, in: *Food Hydrocolloids*. Elsevier, pp. 277–283. <https://doi.org/10.1016/j.foodhyd.2005.02.018>
- Nakamura, A., Yoshida, R., Maeda, H., Furuta, H., Corredig, M., 2004. Study of the role of the carbohydrate and protein moieties of soy soluble polysaccharides in their emulsifying properties. *J. Agric. Food Chem.* 52, 5506–5512. <https://doi.org/10.1021/jf049728f>
- Napper, D.H., 1983. *Polymeric stabilization of colloidal dispersions, Colloid Science : A Series of Monographs*. 2. Academic Press Incorporated.
- Netz, R.R., Andelman, D., 2003. Neutral and charged polymers at interfaces. *Phys. Rep.* [https://doi.org/10.1016/S0370-1573\(03\)00118-2](https://doi.org/10.1016/S0370-1573(03)00118-2)
- Ninham, B.W., Parsegian, V.A., 1970. Van der waals interactions in multilayer systems. *J. Chem. Phys.* 53, 3398–3402. <https://doi.org/10.1063/1.1674507>
- Niño, M.R.R., Sánchez, C.C., Fernández, M.C., Patino, J.M.R., 2001. Protein and lipid films at equilibrium at air-water interface. *J. Am. Oil Chem. Soc.* 78, 873–879. <https://doi.org/10.1007/s11746-001-0358-0>
- Orozco-Villafuerte, J., Cruz-Sosa, F., Ponce-Alquicira, E., Vernon-Carter, E.J., 2003. Mesquite gum: Fractionation and characterization of the gum exuded from *Prosopis laevigata* obtained from plant tissue culture and from wild trees. *Carbohydr. Polym.* 54, 327–333. [https://doi.org/10.1016/S0144-8617\(03\)00187-5](https://doi.org/10.1016/S0144-8617(03)00187-5)
- Osano, J.P., Hosseini-Parvar, S.H., Matia-Merino, L., Golding, M., 2014.

- Emulsifying properties of a novel polysaccharide extracted from basil seed (*Ocimum bacilicum* L.): Effect of polysaccharide and protein content. *Food Hydrocoll.* 37, 40–48. <https://doi.org/10.1016/j.foodhyd.2013.09.008>
- Padala, S.R., Williams, P.A., Phillips, G.O., 2009. Adsorption of Gum Arabic, Egg White Protein, and Their Mixtures at the Oil-Water Interface in Limonene Oil-in-Water Emulsions. *J. Agric. Food Chem.* 57, 4964–4973. <https://doi.org/10.1021/jf803794n>
- Pan, Y., Wu, Z., Zhang, B., Li, X.M., Meng, R., Chen, H.Q., Jin, Z.Y., 2019. Preparation and characterization of emulsion stabilized by octenyl succinic anhydride-modified dextrin for improving storage stability and curcumin encapsulation. *Food Chem.* 294, 326–332. <https://doi.org/10.1016/j.foodchem.2019.05.053>
- Park, N., Conrad, J.C., 2017. Phase behavior of colloid-polymer depletion mixtures with unary or binary depletants. *Soft Matter* 13, 2781–2792. <https://doi.org/10.1039/C6SM02891H>
- Parkinson, E.L., Ettelaie, R., Dickinson, E., 2005. Using self-consistent-field theory to understand enhanced steric stabilization by casein-like copolymers at low surface coverage in mixed protein layers. *Biomacromolecules* 6, 3018–3029. <https://doi.org/10.1021/bm050329i>
- Peña, A.A., Hirasaki, G.J., 2003. Enhanced characterization of oilfield emulsions via NMR diffusion and transverse relaxation experiments. *Adv. Colloid Interface Sci.* 105, 103–150. [https://doi.org/10.1016/S0001-8686\(03\)00092-7](https://doi.org/10.1016/S0001-8686(03)00092-7)
- Pérez-Mosqueda, L.M., Ramírez, P., Alfaro, M.C., Rincón, F., Muñoz, J., 2013. Surface properties and bulk rheology of *Sterculia apetala* gum exudate dispersions. *Food Hydrocoll.* 32, 440–446. <https://doi.org/10.1016/j.foodhyd.2013.02.007>
- Pezennec, S., Gauthier, F., Alonso, C., Graner, F., Croguennec, T., Brulé, G., Renault, A., 2000. The protein net electric charge determines the surface

- rheological properties of ovalbumin adsorbed at the air-water interface. *Food Hydrocoll.* [https://doi.org/10.1016/S0268-005X\(00\)00026-6](https://doi.org/10.1016/S0268-005X(00)00026-6)
- Phillips, G.O., 2008. Giving nature a helping hand, in: *Gums and Stabilisers for the Food Industry 14*. Royal Society of Chemistry, pp. 3–26.
- Qi, S., Yan, D., 2008. Nucleation in polydisperse polymer mixtures. *J. Chem. Phys.* 129, 204902. <https://doi.org/10.1063/1.3020355>
- Radke, C.J., 2015. Gibbs adsorption equation for planar fluid-fluid interfaces: Invariant formalism. *Adv. Colloid Interface Sci.* 222, 600–614. <https://doi.org/10.1016/j.cis.2014.01.001>
- Radke, C.J., 2014. Film and membrane-model thermodynamics of free thin liquid films. *J. Colloid Interface Sci.* 449, 462–479. <https://doi.org/10.1016/j.jcis.2014.12.079>
- Rahimi, R., Shams-Ardekani, M.R., Abdollahi, M., 2010. A review of the efficacy of traditional Iranian medicine for inflammatory bowel disease. *World J. Gastroenterol.* <https://doi.org/10.3748/wjg.v16.i36.4504>
- Rakhimov, D.A., Yuldasheva, N.P., Khamidkhozhaev, S.A., Kondratenko, E.S., 1985. Polysaccharides from the wastes of some fruit and berry, vegetable, and technical crops. *Chem. Nat. Compd.* 21, 19–21. <https://doi.org/10.1007/BF00574241>
- Ravera, F., Ferrari, M., Santini, E., Liggieri, L., 2005. Influence of surface processes on the dilational visco-elasticity of surfactant solutions, in: *Advances in Colloid and Interface Science*. Elsevier, pp. 75–100. <https://doi.org/10.1016/j.cis.2005.06.002>
- Ravera, F., Loglio, G., Kovalchuk, V.I., 2010. Interfacial dilational rheology by oscillating bubble/drop methods. *Curr. Opin. Colloid Interface Sci.* <https://doi.org/10.1016/j.cocis.2010.04.001>
- Ray, A.K., Bird, P.B., Iacobucci, G.A., Clark, B.C., 1995. Functionality of gum

- arabic. Fractionation, characterization and evaluation of gum fractions in citrus oil emulsions and model beverages. *Top. Catal.* 9, 123–131. [https://doi.org/10.1016/S0268-005X\(09\)80274-9](https://doi.org/10.1016/S0268-005X(09)80274-9)
- Reichert, M.D., Walker, L.M., 2013. Interfacial tension dynamics, interfacial mechanics, and response to rapid dilution of bulk surfactant of a model oil-water-dispersant system. *Langmuir*. <https://doi.org/10.1021/la4000395>
- Reid, R., 2018. *Inorganic Chemistry*. EDTECH.
- Renfrew, A.G., Cretcher, L.H., 1932. Quince seed mucilage. *J. Biol. Chem.* 97, 503–510. [https://doi.org/10.1016/s0016-0032\(32\)90829-1](https://doi.org/10.1016/s0016-0032(32)90829-1)
- Rezaghali, F., Hashemi, S.M.B., Gholamhosseinpour, A., Sherahi, M.H., Hesarinejad, M.A., Ale, M.T., 2019. Characterizations and rheological study of the purified polysaccharide extracted from quince seeds. *J. Sci. Food Agric.* 99, 143–151. <https://doi.org/10.1002/jsfa.9155>
- Ritzoulis, C., Marini, E., Aslanidou, A., Georgiadis, N., Karayannakidis, P.D., Koukiotis, C., Filotheou, A., Lousinian, S., Tzimpilis, E., 2014. Hydrocolloids from quince seed: Extraction, characterization, and study of their emulsifying/stabilizing capacity. *Food Hydrocoll.* 42, 178–186. <https://doi.org/10.1016/j.foodhyd.2014.03.031>
- Rodríguez Patino, J.M., Pilosof, A.M.R., 2011. Protein-polysaccharide interactions at fluid interfaces. *Food Hydrocoll.* 25. <https://doi.org/10.1016/j.foodhyd.2011.02.023>
- Rodríguez Patino, J.M., Rodríguez Niño, M.R., 1999. Interfacial characteristics of food emulsifiers (proteins and lipids) at the air-water interface. *Colloids Surfaces B Biointerfaces* 15, 235–252. [https://doi.org/10.1016/S0927-7757\(99\)00012-6](https://doi.org/10.1016/S0927-7757(99)00012-6)
- Rouse, P.E., 1953. A theory of the linear viscoelastic properties of dilute solutions of coiling polymers. *J. Chem. Phys.* <https://doi.org/10.1063/1.1699180>

- Rub, M.A., Asiri, A.M., Khan, J.M., Khan, R.H., Kabir-Ud Din, 2013. Interaction of gelatin with promethazine hydrochloride: Conductimetry, tensiometry and circular dichroism studies. *J. Mol. Struct.* 1050, 35–42.
<https://doi.org/10.1016/j.molstruc.2013.07.010>
- Rühs, P.A., Scheuble, N., Windhab, E.J., Fischer, P., 2013. Protein adsorption and interfacial rheology interfering in dilatational experiment. *Eur. Phys. J. Spec. Top.* 222, 47–60. <https://doi.org/10.1140/epjst/e2013-01825-0>
- Saeidy, S., Nasirpour, A., Djelveh, G., Ursu, A.V., Marcati, A., Gardarin, C., Laroche, C., Delattre, C., Pierre, G., Keramat, J., Michaud, P., 2018. Rheological and functional properties of asafoetida gum. *Int. J. Biol. Macromol.* 118, 1168–1173. <https://doi.org/10.1016/j.ijbiomac.2018.06.177>
- Sanchez, C., Nigen, M., Mejia Tamayo, V., Doco, T., Williams, P., Amine, C., Renard, D., 2018. Acacia gum: History of the future. *Food Hydrocoll.* 78, 140–160. <https://doi.org/10.1016/j.foodhyd.2017.04.008>
- Santini, E., Liggieri, L., Sacca, L., Clause, D., Ravera, F., 2007a. Interfacial rheology of Span 80 adsorbed layers at paraffin oil-water interface and correlation with the corresponding emulsion properties. *Colloids Surfaces A Physicochem. Eng. Asp.* <https://doi.org/10.1016/j.colsurfa.2006.11.041>
- Santini, E., Ravera, F., Ferrari, M., Stubenrauch, C., Makievski, A., Krägel, J., 2007b. A surface rheological study of non-ionic surfactants at the water-air interface and the stability of the corresponding thin foam films. *Colloids Surfaces A Physicochem. Eng. Asp.* 298, 12–21.
<https://doi.org/10.1016/j.colsurfa.2006.12.004>
- Sato, T., Ruch, R., 1980. *Stabilization of Colloidal Dispersions by Polymer Adsorption*, Surfactant science series. Dekker.
- Scheutjens, J.M.H.M., Fler, G.J., 1985. Interaction between Two Adsorbed Polymer Layers. *Macromolecules* 18, 1882–1900.
<https://doi.org/10.1021/ma00152a016>

- Scheutjens, J.M.H.M., Fler, G.J., 1980. Statistical theory of the adsorption of interacting chain molecules. 2. Train, loop, and tail size distribution. *J. Phys. Chem.* 84, 178–190. <https://doi.org/10.1021/j100439a011>
- Scheutjens, J.M.H.M., Fler, G.J., 1979. Statistical theory of the adsorption of interacting chain molecules. 1. Partition function, segment density distribution, and adsorption isotherms. *J. Phys. Chem.* 83, 1619–1635. <https://doi.org/10.1021/j100475a012>
- Semenov, A.N., Shvets, A.A., 2015. Theory of colloid depletion stabilization by unattached and adsorbed polymers. *Soft Matter* 11, 8863–8878. <https://doi.org/10.1039/c5sm01365h>
- Senkel, O., Miller, R., Fainerman, V.B., 1998. Relaxation studies of surfactant adsorption layers at the liquid/air interface by a funnel method. *Colloids Surfaces A Physicochem. Eng. Asp.* 143, 517–528. [https://doi.org/10.1016/S0927-7757\(98\)00586-X](https://doi.org/10.1016/S0927-7757(98)00586-X)
- Serrien, G., Geeraerts, G., Ghosh, L., Joos, P., 1992. Dynamic surface properties of adsorbed protein solutions: BSA, casein and buttermilk. *Colloids and Surfaces* 68, 219–233. [https://doi.org/10.1016/0166-6622\(92\)80208-J](https://doi.org/10.1016/0166-6622(92)80208-J)
- Seta, L., Baldino, N., Gabriele, D., Lupi, F.R., Cindio, B. de, 2014. Rheology and adsorption behaviour of β -casein and β -lactoglobulin mixed layers at the sunflower oil/water interface. *Colloids Surfaces A Physicochem. Eng. Asp.* 441, 669–677. <https://doi.org/10.1016/j.colsurfa.2013.10.041>
- Setiowati, A.D., Saeedi, S., Wijaya, W., Van der Meeren, P., 2017. Improved heat stability of whey protein isolate stabilized emulsions via dry heat treatment of WPI and low methoxyl pectin: Effect of pectin concentration, pH, and ionic strength. *Food Hydrocoll.* 63, 716–726. <https://doi.org/10.1016/j.foodhyd.2016.10.025>
- Shaw, D.J., 1992. *Introduction to Colloid and Surface Chemistry*, Chemical, Petrochemical & Process. Butterworth-Heinemann.

- Sheiko, S.S., Sumerlin, B.S., Matyjaszewski, K., 2008. Cylindrical molecular brushes: Synthesis, characterization, and properties. *Prog. Polym. Sci.* <https://doi.org/10.1016/j.progpolymsci.2008.05.001>
- Shi, Y., Li, C., Zhang, L., Huang, T., Ma, D., Tu, Z. cai, Wang, H., Xie, H., Zhang, N. hai, Ouyang, B. ling, 2017. Characterization and emulsifying properties of octenyl succinate anhydride modified Acacia seyal gum (gum arabic). *Food Hydrocoll.* 65, 10–16. <https://doi.org/10.1016/j.foodhyd.2016.10.043>
- Shiroodi, S.G., Mohammadifar, M.A., Gorji, E.G., Ezzatpanah, H., Zohouri, N., 2012. Influence of gum tragacanth on the physicochemical and rheological properties of kashk. *J. Dairy Res.* 79, 93–101. <https://doi.org/10.1017/S0022029911000872>
- Siew, C.K., Williams, P.A., 2008. Role of protein and ferulic acid in the emulsification properties of sugar beet pectin. *J. Agric. Food Chem.* 56, 4164–4171. <https://doi.org/10.1021/jf073358o>
- Silva, B.M., Andrade, P.B., Ferreres, F., Seabra, R.M., Beatriz, M., Oliveira, P.P., Ferreira, M.A., 2005. Composition of Quince (*Cydonia oblonga* Miller) seeds: phenolics, organic acids and free amino acids. *Nat. Prod. Res.* 19, 275–281. <https://doi.org/10.1080/14786410410001714678>
- Siow, H.L., Gan, C.Y., 2014. Functional protein from cumin seed (*Cuminum cyminum*): Optimization and characterization studies. *Food Hydrocoll.* 41, 178–187. <https://doi.org/10.1016/j.foodhyd.2014.04.017>
- Sosa-Herrera, M.G., Martínez-Padilla, L.P., Delgado-Reyes, V.A., Torres-Robledo, A., 2016. Effect of agave fructans on bulk and surface properties of sodium caseinate in aqueous media. *Food Hydrocoll.* 60, 199–205. <https://doi.org/10.1016/j.foodhyd.2016.03.033>
- Stubenrauch, C., Miller, R., 2004. Stability of foam films and surface rheology: An oscillating bubble study at low frequencies. *J. Phys. Chem. B* 108, 6412–6421. <https://doi.org/10.1021/jp049694e>

- Sun, C., Gunasekaran, S., 2009. Effects of protein concentration and oil-phase volume fraction on the stability and rheology of menhaden oil-in-water emulsions stabilized by whey protein isolate with xanthan gum. *Food Hydrocoll.* 23, 165–174. <https://doi.org/10.1016/j.foodhyd.2007.12.006>
- Sun, C., Gunasekaran, S., Richards, M.P., 2007. Effect of xanthan gum on physicochemical properties of whey protein isolate stabilized oil-in-water emulsions. *Food Hydrocoll.* 21, 555–564. <https://doi.org/10.1016/j.foodhyd.2006.06.003>
- Suo, T., Yan, D., Yang, S., Shi, A.C., 2009. A theoretical study of phase behaviors for diblock copolymers in selective solvents. *Macromolecules* 42, 6791–6798. <https://doi.org/10.1021/ma900939u>
- Sworn, G., Kasapis, S., 1998. Effect of conformation and molecular weight of co-solute on the mechanical properties of gellan gum gels. *Food Hydrocoll.* 12, 283–290. [https://doi.org/10.1016/S0268-005X\(98\)00016-2](https://doi.org/10.1016/S0268-005X(98)00016-2)
- Tadros, T., 2011. Interaction forces between adsorbed polymer layers. *Adv. Colloid Interface Sci.* <https://doi.org/10.1016/j.cis.2011.02.002>
- Tadros, T., 2009. Polymeric surfactants in disperse systems. *Adv. Colloid Interface Sci.* 147–148, 281–299. <https://doi.org/10.1016/j.cis.2008.10.005>
- Tadros, T., Izquierdo, P., Esquena, J., Solans, C., 2004. Formation and stability of nano-emulsions. *Adv. Colloid Interface Sci.* 108–109, 303–318. <https://doi.org/10.1016/j.cis.2003.10.023>
- Tadros, T.F., 2006. *Applied Surfactants: Principles and Applications*. Wiley.
- Tadros, T.F., 1994. Fundamental principles of emulsion rheology and their applications. *Colloids Surfaces A Physicochem. Eng. Asp.* [https://doi.org/10.1016/0927-7757\(93\)02709-N](https://doi.org/10.1016/0927-7757(93)02709-N)
- Tadros, T.F., Vandamme, A., Leveck, B., Booten, K., Stevens, C. V., 2004. Stabilization of emulsions using polymeric surfactants based on inulin. *Adv.*

- Colloid Interface Sci. 108–109, 207–226.
<https://doi.org/10.1016/j.cis.2003.10.024>
- Tang, C.H., Ten, Z., Wang, X.S., Yang, X.Q., 2006. Physicochemical and functional properties of hemp (*Cannabis sativa* L.) protein isolate. *J. Agric. Food Chem.* <https://doi.org/10.1021/jf0619176>
- Tcholakova, S., Denkov, N.D., Sidzhakova, D., Ivanov, I.B., Campbell, B., 2005. Effects of electrolyte concentration and pH on the coalescence stability of β -lactoglobulin emulsions: Experiment and interpretation. *Langmuir* 21, 4842–4855. <https://doi.org/10.1021/la046891w>
- Tian, M., Fang, B., Jin, L., Lu, Y., Qiu, X., Jin, H., Li, K., 2015. Rheological and drag reduction properties of hydroxypropyl xanthan gum solutions. *Chinese J. Chem. Eng.* <https://doi.org/10.1016/j.cjche.2015.04.003>
- Trigueros, L., Pérez-Alvarez, J.A., Viuda-Martos, M., Sendra, E., 2011. Production of low-fat yogurt with quince (*Cydonia oblonga* Mill.) scalding water. *LWT - Food Sci. Technol.* 44, 1388–1395. <https://doi.org/10.1016/j.lwt.2011.01.012>
- Tucker, I.M., Petkov, J.T., Penfold, J., Thomas, R.K., Cox, A.R., Hedges, N., 2015. Adsorption of hydrophobin-protein mixtures at the air-water interface: The impact of pH and electrolyte. *Langmuir* 31, 10008–10016.
<https://doi.org/10.1021/acs.langmuir.5b02403>
- Tupy, M.J., Blanch, H.W., Radke, C.J., 1998. Total internal reflection fluorescence spectrometer to study dynamic adsorption phenomena at liquid/liquid interfaces. *Ind. Eng. Chem. Res.* 37, 3159–3168.
<https://doi.org/10.1021/ie9709244>
- Urbina-Villalba, G., 2004. Effect of dynamic surfactant adsorption on emulsion stability. *Langmuir.* <https://doi.org/10.1021/la030327o>
- van den Tempel, M., Lucassen-Reynders, E.H., 1983. Relaxation processes at fluid interfaces. *Adv. Colloid Interface Sci.* 18, 281–301.

[https://doi.org/10.1016/0001-8686\(83\)87004-3](https://doi.org/10.1016/0001-8686(83)87004-3)

- Van Duynhoven, J.P.M., Goudappel, G.J.W., Van Dalen, G., Van Bruggen, P.C., Blonk, J.C.G., Eijkelenboom, A.P.A.M., 2002. Scope of droplet size measurements in food emulsions by pulsed field gradient NMR at low field. *Magn. Reson. Chem.* <https://doi.org/10.1002/mrc.1115>
- Vélez-Eraza, E.M., Bosqui, K., Rabelo, R.S., Kurozawa, L.E., Hubinger, M.D., 2020. High internal phase emulsions (HIPE) using pea protein and different polysaccharides as stabilizers. *Food Hydrocoll.* 105, 105775. <https://doi.org/10.1016/j.foodhyd.2020.105775>
- Vereyken, I.J., Chupin, V., Demel, R.A., Smeekens, S.C.M., De Kruijff, B., 2001. Fructans insert between the headgroups of phospholipids. *Biochim. Biophys. Acta - Biomembr.* 1510, 307–320. [https://doi.org/10.1016/S0005-2736\(00\)00363-1](https://doi.org/10.1016/S0005-2736(00)00363-1)
- Vernon-Carter, E.J., Pérez-Orozco, J.P., Jiménez-Alvarado, R., Román-Guerrero, A., Orozco-Villafuerte, J., Cruz-Sosa, F., 2008. Application and evaluation of mesquite gum and its fractions as interfacial film formers and emulsifiers of orange peel-oil. *Food Hydrocoll.* 23, 708–713. <https://doi.org/10.1016/j.foodhyd.2008.06.005>
- Vignon, M.R., Gey, C., 1998. Isolation, ¹H and ¹³C NMR studies of (4-O-methyl-D-glucurono)-D- xylans from luffa fruit fibres, jute bast fibres and mucilage of quince tree seeds. *Carbohydr. Res.* 307, 107–111. [https://doi.org/10.1016/S0008-6215\(98\)00002-0](https://doi.org/10.1016/S0008-6215(98)00002-0)
- Voragen, A.G.J., Coenen, G.J., Verhoef, R.P., Schols, H.A., 2009. Pectin, a versatile polysaccharide present in plant cell walls. *Struct. Chem.* 20, 263–275. <https://doi.org/10.1007/s11224-009-9442-z>
- Vrij, A. V., 1976. *Polymers At Interfaces And The Interactions in Colloidal Dispersions.* *Pure Appl. Chem.* <https://doi.org/10.1351/pac197648040471>

- Walstra, P., 2002. *Physical Chemistry of Foods*, Food Science and Technology. CRC Press.
- Walstra, P., 1988. The role of proteins in the stabilization of emulsions, in: *Gums and Stabilizers for the Food Industry*.
- Walstra, P., Smulders, P.E.A., 2007. Chapter 2. Emulsion Formation, in: *Modern Aspects of Emulsion Science*. <https://doi.org/10.1039/9781847551474-00056>
- Wang, H.M., Loganathan, D., Linhardt, R.J., 1991. Determination of the pK(a) of glucuronic acid and the carboxy groups of heparin by ¹³C-nuclear-magnetic-resonance spectroscopy. *Biochem. J.* <https://doi.org/10.1042/bj2780689>
- Wang, L., Liu, H.M., Xie, A.J., Wang, X. De, Zhu, C.Y., Qin, G.Y., 2018. Chinese quince (*Chaenomeles sinensis*) seed gum: Structural characterization. *Food Hydrocoll.* 75, 237–245. <https://doi.org/10.1016/j.foodhyd.2017.08.001>
- Wang, W., Li, K., Wang, P., Hao, S., Gong, J., 2014. Effect of interfacial dilational rheology on the breakage of dispersed droplets in a dilute oil-water emulsion. *Colloids Surfaces A Physicochem. Eng. Asp.* 441, 43–50. <https://doi.org/10.1016/j.colsurfa.2013.08.075>
- Wang, Z., Zhou, J., Wang, X. xuan, Zhang, N., Sun, X. xiu, Ma, Z. su, 2014. The effects of ultrasonic/microwave assisted treatment on the water vapor barrier properties of soybean protein isolate-based oleic acid/stearic acid blend edible films. *Food Hydrocoll.* <https://doi.org/10.1016/j.foodhyd.2013.07.006>
- Wang, Z.L., Li, Z.Q., Zhang, Lei, Huang, H.Y., Zhang, Lu, Zhao, S., Yu, J.Y., 2011. Dilational properties of sodium 2,5-dialkyl benzene sulfonates at air-water and decane-water interfaces. *J. Chem. Eng. Data* 56, 2393–2398. <https://doi.org/10.1021/je1013312>
- Ward, A.F.H., Tordai, L., 1946. Time-dependence of boundary tensions of solutions I. The role of diffusion in time-effects. *J. Chem. Phys.* 14, 453–461. <https://doi.org/10.1063/1.1724167>

- Wei, Y., Xie, Y., Cai, Z., Guo, Y., Wu, M., Wang, P., Li, R., Zhang, H., 2020. Interfacial and emulsion characterisation of chemically modified polysaccharides through a multiscale approach. *J. Colloid Interface Sci.* 580, 480–492. <https://doi.org/10.1016/j.jcis.2020.07.048>
- Whistler, R.L., BeMiller, J.N., 1973. *Industrial Gums, Polysaccharides and Their Derivatives*. Academic Press.
- Wilde, P., Mackie, A., Husband, F., Gunning, P., Morris, V., 2004. Proteins and emulsifiers at liquid interfaces. *Adv. Colloid Interface Sci.* <https://doi.org/10.1016/j.cis.2003.10.011>
- Wilkins, D.K., Grimshaw, S.B., Receveur, V., Dobson, C.M., Jones, J.A., Smith, L.J., 1999. Hydrodynamic radii of native and denatured proteins measured by pulse field gradient NMR techniques. *Biochemistry* 38, 16424–16431. <https://doi.org/10.1021/bi991765q>
- Williams, P.A., Phillips, G.O., 2009. Gum arabic, in: *Handbook of Hydrocolloids: Second Edition*. Elsevier Inc., pp. 252–273. <https://doi.org/10.1533/9781845695873.252>
- Winning, H., Viereck, N., Salomonsen, T., Larsen, J., Engelsen, S.B., 2009. Quantification of blockiness in pectins-A comparative study using vibrational spectroscopy and chemometrics. *Carbohydr. Res.* 344, 1833–1841. <https://doi.org/10.1016/j.carres.2008.10.015>
- Wong, B.T., Day, L., Augustin, M.A., 2011. Deamidated wheat protein-dextran Maillard conjugates: Effect of size and location of polysaccharide conjugated on steric stabilization of emulsions at acidic pH. *Food Hydrocoll.* 25, 1424–1432. <https://doi.org/10.1016/j.foodhyd.2011.01.017>
- Wu, C., Ma, W., Chen, Y., Navicha, W.B., Wu, D., Du, M., 2019. The water holding capacity and storage modulus of chemical cross-linked soy protein gels directly related to aggregates size. *LWT* 103, 125–130. <https://doi.org/10.1016/j.lwt.2018.12.064>

- Wüstneck, R., Krägel, J., Miller, R., Fainerman, V.B., Wilde, P.J., Sarker, D.K., Clark, D.C., 1996. Dynamic surface tension and adsorption properties of β -casein and β -lactoglobulin. *Food Hydrocoll.* 10, 395–405.
[https://doi.org/10.1016/S0268-005X\(96\)80018-X](https://doi.org/10.1016/S0268-005X(96)80018-X)
- Xiao, R., Grinstaff, M.W., 2017. Chemical synthesis of polysaccharides and polysaccharide mimetics. *Prog. Polym. Sci.*
<https://doi.org/10.1016/j.progpolymsci.2017.07.009>
- Yadav, M.P., Strahan, G.D., Mukhopadhyay, S., Hotchkiss, A.T., Hicks, K.B., 2012. Formation of corn fiber gum-milk protein conjugates and their molecular characterization. *Food Hydrocoll.* 26, 326–333.
<https://doi.org/10.1016/j.foodhyd.2011.02.032>
- Yan, D., Suo, T., Zhang, X., Man, X., Miao, B., 2011. Self-consistent field theory and its applications in polymer systems. *Front. Chem. China.*
<https://doi.org/10.1007/s11458-011-0251-8>
- Yang, J.S., Jiang, B., He, W., Xia, Y.M., 2012. Hydrophobically modified alginate for emulsion of oil in water. *Carbohydr. Polym.* 87, 1503–1506.
<https://doi.org/10.1016/j.carbpol.2011.09.046>
- Yang, S., Yan, D., Tan, H., Shi, A.C., 2006. Depletion interaction between two colloidal particles in a nonadsorbing polymer solution. *Phys. Rev. E - Stat. Nonlinear, Soft Matter Phys.* 74, 041808.
<https://doi.org/10.1103/PhysRevE.74.041808>
- Yang, Y., Anvari, M., Pan, C.H., Chung, D., 2012. Characterisation of interactions between fish gelatin and gum arabic in aqueous solutions. *Food Chem.* 135, 555–561. <https://doi.org/10.1016/j.foodchem.2012.05.018>
- Ye, F., Miao, M., Jiang, B., Campanella, O.H., Jin, Z., Zhang, T., 2017. Elucidation of stabilizing oil-in-water Pickering emulsion with different modified maize starch-based nanoparticles. *Food Chem.* 229, 152–158.
<https://doi.org/10.1016/j.foodchem.2017.02.062>

- You, G., Niu, G., Long, H., Zhang, C., Liu, X., 2020. Elucidation of interactions between gelatin aggregates and hsian-tsao gum in aqueous solutions. *Food Chem.* 319, 126532. <https://doi.org/10.1016/j.foodchem.2020.126532>
- Young, S.L., Torres, J.A., 1989. Xanthan: effect of molecular conformation on surface tension properties. *Top. Catal.* 3, 365–377. [https://doi.org/10.1016/S0268-005X\(89\)80011-6](https://doi.org/10.1016/S0268-005X(89)80011-6)
- Yu, M., Zeng, M., Qin, F., He, Z., Chen, J., 2017. Physicochemical and functional properties of protein extracts from *Torreyia grandis* seeds. *Food Chem.* 227, 453–460. <https://doi.org/10.1016/j.foodchem.2017.01.114>
- Yuan, B., Ritzoulis, C., Wang, X., Pan, W., Chen, J., 2019. Interactions between mucin and okra gum during pH cycling. *Food Hydrocoll.* 95, 1–9. <https://doi.org/10.1016/j.foodhyd.2019.03.050>
- Zha, F., Dong, S., Rao, J., Chen, B., 2019. Pea protein isolate-gum Arabic Maillard conjugates improves physical and oxidative stability of oil-in-water emulsions. *Food Chem.* 285, 130–138. <https://doi.org/10.1016/j.foodchem.2019.01.151>
- Zhang, J.B., Wu, N.N., Yang, X.Q., He, X.T., Wang, L.J., 2012. Improvement of emulsifying properties of Maillard reaction products from β -conglycinin and dextran using controlled enzymatic hydrolysis. *Food Hydrocoll.* 28, 301–312. <https://doi.org/10.1016/j.foodhyd.2012.01.006>
- Zhang, L., McCarthy, M.J., 2013. Assessment of pomegranate postharvest quality using nuclear magnetic resonance. *Postharvest Biol. Technol.* 77, 59–66. <https://doi.org/10.1016/j.postharvbio.2012.11.006>
- Zhang, L., McCarthy, M.J., 2012. Black heart characterization and detection in pomegranate using NMR relaxometry and MR imaging. *Postharvest Biol. Technol.* 67, 96–101. <https://doi.org/10.1016/j.postharvbio.2011.12.018>
- Zhang, L.L., Sun, H.Q., Zhang, L.L., Li, Z.Q., Luo, L., Zhao, S., 2011. Interfacial

dilational rheology related to enhance oil recovery. *Soft Matter*.

<https://doi.org/10.1039/c1sm05234a>

Zhang, Y., Lin, J., Zhong, Q., 2016. S/O/W emulsions prepared with sugar beet pectin to enhance the viability of probiotic *Lactobacillus salivarius* NRRL B-30514. *Food Hydrocoll.* 52, 804–810.

<https://doi.org/10.1016/j.foodhyd.2015.08.020>

Zhao, B., Brittain, W.J., 2000. Polymer brushes: Surface-immobilized macromolecules. *Prog. Polym. Sci.* [https://doi.org/10.1016/S0079-6700\(00\)00012-5](https://doi.org/10.1016/S0079-6700(00)00012-5)

Zhao, Y., Khalid, N., Shu, G., Neves, M.A., Kobayashi, I., Nakajima, M., 2017. Formulation and characterization of O/W emulsions stabilized using octenyl succinic anhydride modified kudzu starch. *Carbohydr. Polym.* 176, 91–98.

<https://doi.org/10.1016/j.carbpol.2017.08.064>

Zhu, H., Damodaran, S., 1994. Heat-Induced Conformational Changes in Whey Protein Isolate and Its Relation to Foaming Properties. *J. Agric. Food Chem.*

<https://doi.org/10.1021/jf00040a002>

APPENDICES

A. Statistical Analysis

Quince and Xanthan Emulsions Rheological Analysis

One-way ANOVA: K versus Sample

* NOTE * Cannot draw the interval plot for the Tukey procedure. Interval plots for comparisons are illegible with more than 45 intervals.

Method

Null hypothesis	All means are equal
Alternative hypothesis	Not all means are equal
Significance level	$\alpha = 0.05$
Rows unused	2

Equal variances were assumed for the analysis.

Factor Information

Factor	Levels	Values
Sample	12	0.05Q; 0.05X; 0.1Q; 0.1X; 0.2Q; 0.2X; 0.3Q; 0.3X; 0.5Q; 0.5X; 0.75Q; 0.75X

Analysis of Variance

Source	DF	Adj SS	Adj MS	F-Value	P-Value
Sample	11	205.414	18.6740	15301.09	0.000
Error	12	0.015	0.0012		
Total	23	205.429			

Model Summary

S	R-sq	R-sq(adj)	R-sq(pred)
0.0349348	99.99%	99.99%	99.97%

Means

Sample	N	Mean	StDev	95% CI
0.05Q	2	0.01639	0.00173	(-0.03743; 0.07022)
0.05X	2	0.05155	0.00916	(-0.00227; 0.10537)
0.1Q	2	0.029395	0.000700	(-0.024427; 0.083217)
0.1X	2	0.22555	0.00474	(0.17173; 0.27937)
0.2Q	2	0.06285	0.00738	(0.00903; 0.11667)
0.2X	2	0.8895	0.0601	(0.8357; 0.9433)
0.3Q	2	0.13560	0.00651	(0.08178; 0.18942)
0.3X	2	2.08350	0.00636	(2.02968; 2.13732)
0.5Q	2	0.3488	0.0785	(0.2950; 0.4026)
0.5X	2	5.7335	0.0219	(5.6797; 5.7873)
0.75Q	2	1.0121	0.0635	(0.9583; 1.0659)
0.75X	2	9.92750	0.01061	(9.87368; 9.98132)

Pooled StDev = 0.0349348

Tukey Pairwise Comparisons

Grouping Information Using the Tukey Method and 95% Confidence

Sample	N	Mean	Grouping
0.75X	2	9.92750	A
0.5X	2	5.7335	B
0.3X	2	2.08350	C

0.75Q	2	1.0121	D
0.2X	2	0.8895	D
0.5Q	2	0.3488	E
0.1X	2	0.22555	E F
0.3Q	2	0.13560	F G
0.2Q	2	0.06285	G
0.05X	2	0.05155	G
0.1Q	2	0.029395	G
0.05Q	2	0.01639	G

Means that do not share a letter are significantly different.

One-way ANOVA: n versus Sample

* NOTE * Cannot draw the interval plot for the Tukey procedure. Interval plots for comparisons are illegible with more than 45 intervals.

Method

Null hypothesis	All means are equal
Alternative hypothesis	Not all means are equal
Significance level	$\alpha = 0.05$
Rows unused	2

Equal variances were assumed for the analysis.

Factor Information

Factor	Levels Values
Sample	12 0.05Q; 0.05X; 0.1Q; 0.1X; 0.2Q; 0.2X; 0.3Q; 0.3X; 0.5Q; 0.5X; 0.75Q; 0.75X

Analysis of Variance

Source	DF	Adj SS	Adj MS	F-Value	P-Value
Sample	11	1.36452	0.124048	274.59	0.000
Error	12	0.00542	0.000452		
Total	23	1.36994			

Model Summary

S	R-sq	R-sq(adj)	R-sq(pred)
0.0212545	99.60%	99.24%	98.42%

Means

Sample	N	Mean	StDev	95% CI
0.05Q	2	0.8781	0.0559	(0.8454; 0.9109)
0.05X	2	0.6825	0.0308	(0.6497; 0.7152)
0.1Q	2	0.834050	0.001344	(0.801304; 0.866796)
0.1X	2	0.50480	0.00156	(0.47205; 0.53755)
0.2Q	2	0.7706	0.0337	(0.7378; 0.8033)
0.2X	2	0.331450	0.001061	(0.298704; 0.364196)
0.3Q	2	0.61820	0.00552	(0.58545; 0.65095)
0.3X	2	0.25915	0.00615	(0.22640; 0.29190)
0.5Q	2	0.52575	0.01054	(0.49300; 0.55850)
0.5X	2	0.18430	0.00368	(0.15155; 0.21705)
0.75Q	2	0.41735	0.00318	(0.38460; 0.45010)
0.75X	2	0.159550	0.000778	(0.126804; 0.192296)

Pooled StDev = 0.0212545

Tukey Pairwise Comparisons

Grouping Information Using the Tukey Method and 95% Confidence

Sample	N	Mean	Grouping
0.05Q	2	0.8781	A
0.1Q	2	0.834050	A B
0.2Q	2	0.7706	B
0.05X	2	0.6825	C
0.3Q	2	0.61820	C
0.5Q	2	0.52575	D
0.1X	2	0.50480	D
0.75Q	2	0.41735	E
0.2X	2	0.331450	F
0.3X	2	0.25915	F G
0.5X	2	0.18430	G H
0.75X	2	0.159550	H

Means that do not share a letter are significantly different.

One-way ANOVA: LVR versus Sample

Method

Null hypothesis	All means are equal
Alternative hypothesis	Not all means are equal
Significance level	$\alpha = 0.05$
Rows unused	6

Equal variances were assumed for the analysis.

Factor Information

Factor	Levels	Values
Sample	10	0.1Q; 0.1X; 0.2Q; 0.2X; 0.3Q; 0.3X; 0.5Q; 0.5X; 0.75Q; 0.75X

Analysis of Variance

Source	DF	Adj SS	Adj MS	F-Value	P-Value
Sample	9	182.734	20.3038	44.38	0.000
Error	10	4.575	0.4575		
Total	19	187.309			

Model Summary

S	R-sq	R-sq(adj)	R-sq(pred)
0.676387	97.56%	95.36%	90.23%

Means

Sample	N	Mean	StDev	95% CI
0.1Q	2	3.350	0.919	(2.284; 4.416)
0.1X	2	2.350	0.354	(1.284; 3.416)
0.2Q	2	3.900	0.566	(2.834; 4.966)
0.2X	2	4.950	0.212	(3.884; 6.016)
0.3Q	2	6.400	0.849	(5.334; 7.466)
0.3X	2	6.050	0.919	(4.984; 7.116)
0.5Q	2	10.300	0.424	(9.234; 11.366)
0.5X	2	7.950	0.919	(6.884; 9.016)
0.75Q	2	10.950	0.212	(9.884; 12.016)
0.75X	2	10.850	0.778	(9.784; 11.916)

Pooled StDev = 0.676387

Tukey Pairwise Comparisons

Grouping Information Using the Tukey Method and 95% Confidence

Sample	N	Mean	Grouping
0.75Q	2	10.950	A
0.75X	2	10.850	A
0.5Q	2	10.300	A B
0.5X	2	7.950	B C
0.3Q	2	6.400	C D
0.3X	2	6.050	C D
0.2X	2	4.950	D E
0.2Q	2	3.900	D E
0.1Q	2	3.350	E
0.1X	2	2.350	E

Means that do not share a letter are significantly different.

One-way ANOVA: Shear Viscosity versus Sample

Method

Null hypothesis	All means are equal
Alternative hypothesis	Not all means are equal
Significance level	$\alpha = 0.05$
Rows unused	16

Equal variances were assumed for the analysis.

Factor Information

Factor	Levels	Values
Sample	5	0.05Q; 0.1Q; 0.2Q; 0.3Q; NOX

Analysis of Variance

Source	DF	Adj SS	Adj MS	F-Value	P-Value
Sample	4	0.001455	0.000364	210.84	0.000
Error	5	0.000009	0.000002		
Total	9	0.001463			

Model Summary

S	R-sq	R-sq(adj)	R-sq(pred)
0.0013133	99.41%	98.94%	97.64%

Means

Sample	N	Mean	StDev	95% CI
0.05Q	2	0.010985	0.000728	(0.008598; 0.013372)
0.1Q	2	0.016655	0.001138	(0.014268; 0.019042)
0.2Q	2	0.028365	0.000106	(0.025978; 0.030752)
0.3Q	2	0.04004	0.00258	(0.03766; 0.04243)
NOX	2	0.007150	0.000354	(0.004763; 0.009537)

Pooled StDev = 0.00131332

Tukey Pairwise Comparisons

Grouping Information Using the Tukey Method and 95% Confidence

Sample	N	Mean	Grouping
0.3Q	2	0.04004	A
0.2Q	2	0.028365	B
0.1Q	2	0.016655	C
0.05Q	2	0.010985	D
NOX	2	0.007150	D

Means that do not share a letter are significantly different.

One-way ANOVA: G* versus Sample

Method

Null hypothesis	All means are equal
Alternative hypothesis	Not all means are equal
Significance level	$\alpha = 0.05$
Rows unused	6

Equal variances were assumed for the analysis.

Factor Information

Factor	Levels	Values
Sample	10	0.1Q; 0.1X; 0.2Q; 0.2X; 0.3Q; 0.3X; 0.5Q; 0.5X; 0.75Q; 0.75X

Analysis of Variance

Source	DF	Adj SS	Adj MS	F-Value	P-Value
Sample	9	1427.80	158.644	29.69	0.000
Error	10	53.43	5.343		
Total	19	1481.23			

Model Summary

S	R-sq	R-sq(adj)	R-sq(pred)
2.31157	96.39%	93.15%	85.57%

Means

Sample	N	Mean	StDev	95% CI
0.1Q	2	0.05500	0.00707	(-3.58696; 3.69696)
0.1X	2	0.47500	0.00707	(-3.16696; 4.11696)
0.2Q	2	0.1400	0.0283	(-3.5020; 3.7820)
0.2X	2	1.9300	0.0283	(-1.7120; 5.5720)
0.3Q	2	0.3800	0.0283	(-3.2620; 4.0220)
0.3X	2	6.050	0.636	(2.408; 9.692)
0.5Q	2	1.2250	0.0354	(-2.4170; 4.8670)
0.5X	2	17.00	1.41	(13.36; 20.64)
0.75Q	2	1.750	0.141	(-1.892; 5.392)
0.75X	2	26.15	7.14	(22.51; 29.79)

Pooled StDev = 2.31157

Tukey Pairwise Comparisons

Grouping Information Using the Tukey Method and 95% Confidence

Sample	N	Mean	Grouping
0.75X	2	26.15	A
0.5X	2	17.00	A
0.3X	2	6.050	B
0.2X	2	1.9300	B
0.75Q	2	1.750	B
0.5Q	2	1.2250	B
0.1X	2	0.47500	B
0.3Q	2	0.3800	B
0.2Q	2	0.1400	B
0.1Q	2	0.05500	B

Means that do not share a letter are significantly different.

One-way ANOVA: G** versus Sample

Method

Null hypothesis	All means are equal
Alternative hypothesis	Not all means are equal
Significance level	$\alpha = 0.05$
Rows unused	6

Equal variances were assumed for the analysis.

Factor Information

Factor	Levels	Values
Sample	10	0.1Q; 0.1X; 0.2Q; 0.2X; 0.3Q; 0.3X; 0.5Q; 0.5X; 0.75Q; 0.75X

Analysis of Variance

Source	DF	Adj SS	Adj MS	F-Value	P-Value
Sample	9	156.911	17.4346	67.47	0.000
Error	10	2.584	0.2584		
Total	19	159.495			

Model Summary

S	R-sq	R-sq(adj)	R-sq(pred)
0.508340	98.38%	96.92%	93.52%

Means

Sample	N	Mean	StDev	95% CI
0.1Q	2	0.1300	0.0141	(-0.6709; 0.9309)
0.1X	2	0.5300	0.0141	(-0.2709; 1.3309)
0.2Q	2	0.1950	0.0212	(-0.6059; 0.9959)
0.2X	2	1.5000	0.0707	(0.6991; 2.3009)
0.3Q	2	0.4100	0.0141	(-0.3909; 1.2109)
0.3X	2	3.40	1.56	(2.60; 4.20)
0.5Q	2	0.9750	0.1061	(0.1741; 1.7759)
0.5X	2	5.850	0.354	(5.049; 6.651)
0.75Q	2	1.0700	0.0424	(0.2691; 1.8709)
0.75X	2	9.000	0.141	(8.199; 9.801)

Pooled StDev = 0.508340

Tukey Pairwise Comparisons

Grouping Information Using the Tukey Method and 95% Confidence

Sample	N	Mean	Grouping
0.75X	2	9.000	A
0.5X	2	5.850	B
0.3X	2	3.40	C
0.2X	2	1.5000	C D
0.75Q	2	1.0700	D
0.5Q	2	0.9750	D
0.1X	2	0.5300	D
0.3Q	2	0.4100	D
0.2Q	2	0.1950	D
0.1Q	2	0.1300	D

Means that do not share a letter are significantly different.

Particle Size Analysis of QSE and XG Emulsions

One-way ANOVA: d(43) versus Sample

* NOTE * Cannot draw the interval plot for the Tukey procedure. Interval plots for comparisons are illegible with more than 45 intervals.

Method

Null hypothesis All means are equal
 Alternative hypothesis Not all means are equal
 Significance level $\alpha = 0.05$

Equal variances were assumed for the analysis.

Factor Information

Factor	Levels	Values
Sample	13	0.05Q; 0.05X; 0.1Q; 0.1X; 0.2Q; 0.2X; 0.3Q; 0.3X; 0.5Q; 0.5X; 0.75Q; 0.75X; NOX

Analysis of Variance

Source	DF	Adj SS	Adj MS	F-Value	P-Value
Sample	12	1157.10	96.4254	3298.76	0.000
Error	13	0.38	0.0292		
Total	25	1157.48			

Model Summary

S	R-sq	R-sq(adj)	R-sq(pred)
0.170970	99.97%	99.94%	99.87%

Means

Sample	N	Mean	StDev	95% CI
0.05Q	2	34.600	0.141	(34.339; 34.861)
0.05X	2	28.5500	0.0707	(28.2888; 28.8112)
0.1Q	2	29.0500	0.0707	(28.7888; 29.3112)
0.1X	2	23.5500	0.0707	(23.2888; 23.8112)
0.2Q	2	23.3500	0.0707	(23.0888; 23.6112)
0.2X	2	18.800	0.141	(18.539; 19.061)
0.3Q	2	21.40	0.00	(21.14; 21.66)
0.3X	2	18.550	0.495	(18.289; 18.811)
0.5Q	2	18.20	0.00	(17.94; 18.46)
0.5X	2	15.2500	0.0707	(14.9888; 15.5112)
0.75Q	2	16.100	0.141	(15.839; 16.361)
0.75X	2	12.650	0.212	(12.389; 12.911)
NOX	2	33.0500	0.0707	(32.7888; 33.3112)

Pooled StDev = 0.170970

Tukey Pairwise Comparisons

Grouping Information Using the Tukey Method and 95% Confidence

Sample	N	Mean	Grouping
0.05Q	2	34.600	A
NOX	2	33.0500	B
0.1Q	2	29.0500	C
0.05X	2	28.5500	C
0.1X	2	23.5500	D
0.2Q	2	23.3500	D
0.3Q	2	21.40	E
0.2X	2	18.800	F
0.3X	2	18.550	F
0.5Q	2	18.20	F
0.75Q	2	16.100	G
0.5X	2	15.2500	H
0.75X	2	12.650	I

Means that do not share a letter are significantly different.

z-Ave Diameter of QSE Aggregates

One-way ANOVA: z-ave versus Sample

Method

Null hypothesis	All means are equal
Alternative hypothesis	Not all means are equal
Significance level	$\alpha = 0.05$
Rows unused	12

Equal variances were assumed for the analysis.

Factor Information

Factor	Levels	Values
Sample	9	0.05Q; 0.1Q; 0.2Q; 0.3Q; 0.4Q; 0.5Q; 0.6Q; 0.75Q; NOX

Analysis of Variance

Source	DF	Adj SS	Adj MS	F-Value	P-Value
Sample	8	27283319	3410415	40.50	0.000
Error	9	757805	84201		
Total	17	28041123			

Model Summary

S	R-sq	R-sq(adj)	R-sq(pred)
290.173	97.30%	94.90%	89.19%

Means

Sample	N	Mean	StDev	95% CI
0.05Q	2	1380	390	(916; 1844)
0.1Q	2	1011.6	117.9	(547.5; 1475.8)
0.2Q	2	2813	576	(2348; 3277)
0.3Q	2	2391	257	(1926; 2855)
0.4Q	2	4880	295	(4415; 5344)
0.5Q	2	3017	258	(2552; 3481)
0.6Q	2	2730	158	(2265; 3194)
0.75Q	2	2830.0	123.0	(2365.8; 3294.2)
NOX	2	481.00	1.41	(16.84; 945.16)

Pooled StDev = 290.173

Tukey Pairwise Comparisons

Grouping Information Using the Tukey Method and 95% Confidence

Sample	N	Mean	Grouping
0.4Q	2	4880	A
0.5Q	2	3017	B
0.75Q	2	2830.0	B
0.2Q	2	2813	B
0.6Q	2	2730	B
0.3Q	2	2391	B C
0.05Q	2	1380	C D
0.1Q	2	1011.6	D
NOX	2	481.00	D

Means that do not share a letter are significantly different.

Equilibrium STs for different pHs and Salt Contents

One-way ANOVA: Eq. ST versus Sample

Method

Null hypothesis	All means are equal
Alternative hypothesis	Not all means are equal
Significance level	$\alpha = 0.05$

Equal variances were assumed for the analysis.

Factor Information

Factor	Levels	Values
Sample	3	P11; P3; P7

Analysis of Variance

Source	DF	Adj SS	Adj MS	F-Value	P-Value
Sample	2	53.20	26.598	9.15	0.002
Error	17	49.40	2.906		
Total	19	102.60			

Model Summary

S	R-sq	R-sq(adj)	R-sq(pred)
1.70475	51.85%	46.18%	38.07%

Means

Sample	N	Mean	StDev	95% CI
P11	7	34.857	1.128	(33.498; 36.217)
P3	9	38.532	2.270	(37.333; 39.731)
P7	4	36.995	0.428	(35.197; 38.793)

Pooled StDev = 1.70475

Tukey Pairwise Comparisons

Grouping Information Using the Tukey Method and 95% Confidence

Sample	N	Mean	Grouping
P3	9	38.532	A
P7	4	36.995	A B
P11	7	34.857	B

Means that do not share a letter are significantly different.

One-way ANOVA: Eq. ST. versus Sample

Method

Null hypothesis	All means are equal
Alternative hypothesis	Not all means are equal
Significance level	$\alpha = 0.05$

Equal variances were assumed for the analysis.

Factor Information

Factor	Levels Values
Sample	4 S0; S0.1; S0.3; S0.5

Analysis of Variance

Source	DF	Adj SS	Adj MS	F-Value	P-Value
Sample	3	28.79	9.5975	12.01	0.000
Error	18	14.39	0.7994		
Total	21	43.18			

Model Summary

S	R-sq	R-sq(adj)	R-sq(pred)
0.894085	66.68%	61.12%	52.12%

Means

Sample	N	Mean	StDev	95% CI
S0	4	36.995	0.428	(36.056; 37.934)
S0.1	6	34.767	1.174	(34.000; 35.534)
S0.3	7	34.653	0.947	(33.943; 35.363)
S0.5	5	33.430	0.626	(32.590; 34.270)

Pooled StDev = 0.894085

Tukey Pairwise Comparisons

Grouping Information Using the Tukey Method and 95% Confidence

Sample	N	Mean	Grouping
S0	4	36.995	A
S0.1	6	34.767	B
S0.3	7	34.653	B
S0.5	5	33.430	B

Means that do not share a letter are significantly different.

Surface Rheology Results

SR CONC

One-way ANOVA: E* versus Samples

Method

Null hypothesis	All means are equal
Alternative hypothesis	Not all means are equal
Significance level	$\alpha = 0.05$

Equal variances were assumed for the analysis.

Factor Information

Factor	Levels Values
Samples	9 Q0.05; Q0.1; Q0.2; Q0.3; Q0.4; Q0.5; Q0.6; Q0.75; Q1

Analysis of Variance

Source	DF	Adj SS	Adj MS	F-Value	P-Value
Samples	8	4861	607.7	4.64	0.001
Error	35	4587	131.1		
Total	43	9448			

Model Summary

S	R-sq	R-sq(adj)	R-sq(pred)
11.4480	51.45%	40.36%	24.04%

Means

Samples	N	Mean	StDev	95% CI
Q0.05	4	58.18	9.41	(46.56; 69.80)
Q0.1	6	45.31	9.01	(35.82; 54.79)
Q0.2	5	37.59	12.84	(27.20; 47.98)
Q0.3	5	41.53	14.50	(31.14; 51.93)
Q0.4	5	32.41	14.83	(22.02; 42.80)
Q0.5	5	36.15	13.69	(25.76; 46.54)
Q0.6	5	25.17	11.46	(14.77; 35.56)
Q0.75	5	22.35	7.88	(11.96; 32.74)
Q1	4	23.475	1.914	(11.855; 35.096)

Pooled StDev = 11.4480

Tukey Pairwise Comparisons

Grouping Information Using the Tukey Method and 95% Confidence

Samples	N	Mean	Grouping
Q0.05	4	58.18	A
Q0.1	6	45.31	A B
Q0.3	5	41.53	A B C
Q0.2	5	37.59	B C
Q0.5	5	36.15	A B C
Q0.4	5	32.41	B C
Q0.6	5	25.17	B C
Q1	4	23.475	B C
Q0.75	5	22.35	C

Means that do not share a letter are significantly different.

SR CONC

One-way ANOVA: E** versus Samples

Method

Null hypothesis	All means are equal
Alternative hypothesis	Not all means are equal
Significance level	$\alpha = 0.05$

Equal variances were assumed for the analysis.

Factor Information

Factor	Levels	Values
Samples	9	Q0.05; Q0.1; Q0.2; Q0.3; Q0.4; Q0.5; Q0.6; Q0.75; Q1

Analysis of Variance

Source	DF	Adj SS	Adj MS	F-Value	P-Value
Samples	8	95.05	11.88	1.00	0.453
Error	35	415.51	11.87		
Total	43	510.57			

Model Summary

S	R-sq	R-sq(adj)	R-sq(pred)
3.44555	18.62%	0.02%	0.00%

Means

Samples	N	Mean	StDev	95% CI
Q0.05	4	8.71	2.07	(5.22; 12.21)
Q0.1	6	8.669	1.852	(5.813; 11.524)

Q0.2	5	10.35	4.64	(7.22; 13.48)
Q0.3	5	11.53	4.44	(8.40; 14.66)
Q0.4	5	8.77	4.44	(5.64; 11.90)
Q0.5	5	11.01	4.42	(7.89; 14.14)
Q0.6	5	7.61	3.15	(4.49; 10.74)
Q0.75	5	7.08	2.26	(3.96; 10.21)
Q1	4	7.891	1.006	(4.394; 11.389)

Pooled StDev = 3.44555

Tukey Pairwise Comparisons

Grouping Information Using the Tukey Method and 95% Confidence

Samples	N	Mean	Grouping
Q0.3	5	11.53	A
Q0.5	5	11.01	A
Q0.2	5	10.35	A
Q0.4	5	8.77	A
Q0.05	4	8.71	A
Q0.1	6	8.669	A
Q1	4	7.891	A
Q0.6	5	7.61	A
Q0.75	5	7.08	A

Means that do not share a letter are significantly different.

SR CONC

One-way ANOVA: tand versus Samples

Method

Null hypothesis	All means are equal
Alternative hypothesis	Not all means are equal
Significance level	$\alpha = 0.05$

Equal variances were assumed for the analysis.

Factor Information

Factor	Levels	Values
Samples	9	Q0.05; Q0.1; Q0.2; Q0.3; Q0.4; Q0.5; Q0.6; Q0.75; Q1

Analysis of Variance

Source	DF	Adj SS	Adj MS	F-Value	P-Value
Samples	8	0.14326	0.017908	17.70	0.000
Error	35	0.03541	0.001012		
Total	43	0.17867			

Model Summary

S	R-sq	R-sq(adj)	R-sq(pred)
0.0318088	80.18%	75.65%	68.56%

Means

Samples	N	Mean	StDev	95% CI
Q0.05	4	0.15253	0.01272	(0.12024; 0.18481)
Q0.1	6	0.19648	0.01191	(0.17012; 0.22285)
Q0.2	5	0.2737	0.0601	(0.2448; 0.3026)
Q0.3	5	0.2790	0.0281	(0.2501; 0.3079)
Q0.4	5	0.2701	0.0250	(0.2412; 0.2989)

Q0.5	5	0.3124	0.0244	(0.2835; 0.3413)
Q0.6	5	0.31056	0.02137	(0.28168; 0.33944)
Q0.75	5	0.3265	0.0389	(0.2977; 0.3554)
Q1	4	0.3449	0.0359	(0.3127; 0.3772)

Pooled StDev = 0.0318088

Tukey Pairwise Comparisons

Grouping Information Using the Tukey Method and 95% Confidence

Samples	N	Mean	Grouping
Q1	4	0.3449	A
Q0.75	5	0.3265	A B
Q0.5	5	0.3124	A B
Q0.6	5	0.31056	A B
Q0.3	5	0.2790	A B
Q0.2	5	0.2737	B
Q0.4	5	0.2701	B
Q0.1	6	0.19648	C
Q0.05	4	0.15253	C

Means that do not share a letter are significantly different.

One-way ANOVA: E* versus Sample

Method

Null hypothesis	All means are equal
Alternative hypothesis	Not all means are equal
Significance level	$\alpha = 0.05$

Equal variances were assumed for the analysis.

Factor Information

Factor	Levels	Values
Sample	3	P11; P3; P7

Analysis of Variance

Source	DF	Adj SS	Adj MS	F-Value	P-Value
Sample	2	467.7	233.9	2.10	0.166
Error	12	1339.5	111.6		
Total	14	1807.2			

Model Summary

S	R-sq	R-sq(adj)	R-sq(pred)
10.5652	25.88%	13.53%	0.00%

Means

Sample	N	Mean	StDev	95% CI
P11	5	28.16	7.89	(17.86; 38.45)
P3	5	37.33	7.90	(27.03; 47.62)
P7	5	41.53	14.50	(31.24; 51.83)

Pooled StDev = 10.5652

Tukey Pairwise Comparisons

Grouping Information Using the Tukey Method and 95% Confidence

Sample	N	Mean	Grouping
P7	5	41.53	A
P3	5	37.33	A

P11 5 28.16 A

Means that do not share a letter are significantly different.

One-way ANOVA: E** versus Sample

Method

Null hypothesis All means are equal
 Alternative hypothesis Not all means are equal
 Significance level $\alpha = 0.05$

Equal variances were assumed for the analysis.

Factor Information

Factor	Levels	Values
Sample	3	P11; P3; P7

Analysis of Variance

Source	DF	Adj SS	Adj MS	F-Value	P-Value
Sample	2	64.35	32.175	3.78	0.053
Error	12	102.14	8.512		
Total	14	166.49			

Model Summary

S	R-sq	R-sq(adj)	R-sq(pred)
2.91751	38.65%	28.43%	4.14%

Means

Sample	N	Mean	StDev	95% CI
P11	5	9.441	1.708	(6.598; 12.283)
P3	5	6.480	1.698	(3.638; 9.323)
P7	5	11.53	4.44	(8.69; 14.37)

Pooled StDev = 2.91751

Tukey Pairwise Comparisons

Grouping Information Using the Tukey Method and 95% Confidence

Sample	N	Mean	Grouping
P7	5	11.53	A
P11	5	9.441	A B
P3	5	6.480	B

Means that do not share a letter are significantly different.

One-way ANOVA: tand versus Sample

Method

Null hypothesis All means are equal
 Alternative hypothesis Not all means are equal
 Significance level $\alpha = 0.05$

Equal variances were assumed for the analysis.

Factor Information

Factor	Levels	Values
Sample	3	P11; P3; P7

Analysis of Variance

Source	DF	Adj SS	Adj MS	F-Value	P-Value
Sample	2	0.08753	0.043767	11.51	0.002
Error	12	0.04564	0.003803		
Total	14	0.13317			

Model Summary

S	R-sq	R-sq(adj)	R-sq(pred)
0.0616714	65.73%	60.02%	46.45%

Means

Sample	N	Mean	StDev	95% CI
P11	5	0.3630	0.1019	(0.3029; 0.4231)
P3	5	0.17616	0.01560	(0.11607; 0.23625)
P7	5	0.2790	0.0281	(0.2189; 0.3391)

Pooled StDev = 0.0616714

Tukey Pairwise Comparisons

Grouping Information Using the Tukey Method and 95% Confidence

Sample	N	Mean	Grouping
P11	5	0.3630	A
P7	5	0.2790	A B
P3	5	0.17616	B

Means that do not share a letter are significantly different.

One-way ANOVA: E* versus Sample

Method

Null hypothesis	All means are equal
Alternative hypothesis	Not all means are equal
Significance level	$\alpha = 0.05$

Equal variances were assumed for the analysis.

Factor Information

Factor	Levels	Values
Sample	4	S0; S0.1; S0.3; S0.5

Analysis of Variance

Source	DF	Adj SS	Adj MS	F-Value	P-Value
Sample	3	1066	355.2	3.31	0.047
Error	16	1716	107.2		
Total	19	2782			

Model Summary

S	R-sq	R-sq(adj)	R-sq(pred)
10.3558	38.31%	26.75%	3.61%

Means

Sample	N	Mean	StDev	95% CI
S0	5	41.53	14.50	(31.72; 51.35)
S0.1	5	33.66	9.38	(23.84; 43.47)
S0.3	5	25.30	9.69	(15.49; 35.12)
S0.5	5	43.91	6.07	(34.10; 53.73)

Pooled StDev = 10.3558

Tukey Pairwise Comparisons

Grouping Information Using the Tukey Method and 95% Confidence

Sample	N	Mean	Grouping
S0.5	5	43.91	A
S0	5	41.53	A
S0.1	5	33.66	A
S0.3	5	25.30	A

Means that do not share a letter are significantly different.

One-way ANOVA: E** versus Sample

Method

Null hypothesis	All means are equal
Alternative hypothesis	Not all means are equal
Significance level	$\alpha = 0.05$

Equal variances were assumed for the analysis.

Factor Information

Factor	Levels	Values
Sample	4	S0; S0.1; S0.3; S0.5

Analysis of Variance

Source	DF	Adj SS	Adj MS	F-Value	P-Value
Sample	3	69.63	23.21	2.24	0.123
Error	16	165.79	10.36		
Total	19	235.42			

Model Summary

S	R-sq	R-sq(adj)	R-sq(pred)
3.21902	29.58%	16.37%	0.00%

Means

Sample	N	Mean	StDev	95% CI
S0	5	11.53	4.44	(8.48; 14.58)
S0.1	5	9.52	3.81	(6.47; 12.58)
S0.3	5	6.50	2.42	(3.44; 9.55)
S0.5	5	10.387	1.166	(7.336; 13.439)

Pooled StDev = 3.21902

Tukey Pairwise Comparisons

Grouping Information Using the Tukey Method and 95% Confidence

Sample	N	Mean	Grouping
S0	5	11.53	A
S0.5	5	10.387	A
S0.1	5	9.52	A
S0.3	5	6.50	A

Means that do not share a letter are significantly different.

One-way ANOVA: tand versus Sample

Method

Null hypothesis	All means are equal
-----------------	---------------------

Alternative hypothesis Not all means are equal
 Significance level $\alpha = 0.05$

Equal variances were assumed for the analysis.

Factor Information

Factor	Levels	Values
Sample	4	S0; S0.1; S0.3; S0.5

Analysis of Variance

Source	DF	Adj SS	Adj MS	F-Value	P-Value
Sample	3	0.003201	0.001067	0.75	0.538
Error	16	0.022733	0.001421		
Total	19	0.025933			

Model Summary

S	R-sq	R-sq(adj)	R-sq(pred)
0.0376935	12.34%	0.00%	0.00%

Means

Sample	N	Mean	StDev	95% CI
S0	5	0.2790	0.0281	(0.2433; 0.3148)
S0.1	5	0.2772	0.0568	(0.2415; 0.3130)
S0.3	5	0.26248	0.01418	(0.22674; 0.29822)
S0.5	5	0.2477	0.0382	(0.2120; 0.2835)

Pooled StDev = 0.0376935

Tukey Pairwise Comparisons

Grouping Information Using the Tukey Method and 95% Confidence

Sample	N	Mean	Grouping
S0	5	0.2790	A
S0.1	5	0.2772	A
S0.3	5	0.26248	A
S0.5	5	0.2477	A

Means that do not share a letter are significantly different.

Interfacial Rheology of QSE Solutions

IR CONC

One-way ANOVA: E* versus Sample

Method

Null hypothesis All means are equal
 Alternative hypothesis Not all means are equal
 Significance level $\alpha = 0.05$

Equal variances were assumed for the analysis.

Factor Information

Factor	Levels	Values
Sample	7	Q0.1; Q0.2; Q0.3; Q0.4; Q0.5; Q0.75; Q1

Analysis of Variance

Source	DF	Adj SS	Adj MS	F-Value	P-Value
Sample	6	6142.3	1023.72	31.21	0.000
Error	27	885.7	32.80		
Total	33	7028.0			

Model Summary

S	R-sq	R-sq(adj)	R-sq(pred)
5.72738	87.40%	84.60%	78.75%

Means

Sample	N	Mean	StDev	95% CI
Q0.1	4	30.61	13.03	(24.73; 36.49)
Q0.2	5	15.84	2.29	(10.58; 21.09)
Q0.3	5	14.79	3.39	(9.53; 20.04)
Q0.4	5	11.687	1.236	(6.432; 16.943)
Q0.5	5	9.09	2.26	(3.83; 14.34)
Q0.75	5	-2.98	2.63	(-8.23; 2.28)
Q1	5	-16.04	7.98	(-21.29; -10.78)

Pooled StDev = 5.72738

Tukey Pairwise Comparisons

Grouping Information Using the Tukey Method and 95% Confidence

Sample	N	Mean	Grouping
Q0.1	4	30.61	A
Q0.2	5	15.84	B
Q0.3	5	14.79	B
Q0.4	5	11.687	B
Q0.5	5	9.09	B
Q0.75	5	-2.98	C
Q1	5	-16.04	D

Means that do not share a letter are significantly different.

IR CONC

One-way ANOVA: E** versus Sample

Method

Null hypothesis	All means are equal
Alternative hypothesis	Not all means are equal
Significance level	$\alpha = 0.05$

Equal variances were assumed for the analysis.

Factor Information

Factor	Levels	Values
Sample	7	Q0.1; Q0.2; Q0.3; Q0.4; Q0.5; Q0.75; Q1

Analysis of Variance

Source	DF	Adj SS	Adj MS	F-Value	P-Value
Sample	6	83.97	13.9957	24.90	0.000
Error	27	15.17	0.5620		
Total	33	99.15			

Model Summary

S	R-sq	R-sq(adj)	R-sq(pred)
0.749661	84.70%	81.29%	75.67%

Means

Sample	N	Mean	StDev	95% CI
--------	---	------	-------	--------

Q0.1	4	2.927	0.800	(2.158; 3.696)
Q0.2	5	1.742	0.323	(1.054; 2.430)
Q0.3	5	1.318	0.312	(0.630; 2.006)
Q0.4	5	0.7618	0.2031	(0.0739; 1.4497)
Q0.5	5	0.251	0.365	(-0.437; 0.939)
Q0.75	5	-0.870	0.988	(-1.558; -0.182)
Q1	5	-2.305	1.401	(-2.992; -1.617)

Pooled StDev = 0.749661

Tukey Pairwise Comparisons

Grouping Information Using the Tukey Method and 95% Confidence

Sample	N	Mean	Grouping
Q0.1	4	2.927	A
Q0.2	5	1.742	A B
Q0.3	5	1.318	B
Q0.4	5	0.7618	B
Q0.5	5	0.251	B C
Q0.75	5	-0.870	C D
Q1	5	-2.305	D

Means that do not share a letter are significantly different.

IR CONC

One-way ANOVA: tand versus Sample

Method

Null hypothesis	All means are equal
Alternative hypothesis	Not all means are equal
Significance level	$\alpha = 0.05$

Equal variances were assumed for the analysis.

Factor Information

Factor	Levels	Values
Sample	7	Q0.1; Q0.2; Q0.3; Q0.4; Q0.5; Q0.75; Q1

Analysis of Variance

Source	DF	Adj SS	Adj MS	F-Value	P-Value
Sample	6	4.261	0.7101	2.47	0.049
Error	27	7.765	0.2876		
Total	33	12.026			

Model Summary

S	R-sq	R-sq(adj)	R-sq(pred)
0.536274	35.43%	21.08%	0.00%

Means

Sample	N	Mean	StDev	95% CI
Q0.1	4	0.10615	0.01693	(-0.44402; 0.65632)
Q0.2	5	0.11183	0.01687	(-0.38026; 0.60392)
Q0.3	5	0.0938	0.0247	(-0.3983; 0.5859)
Q0.4	5	0.06648	0.02133	(-0.42561; 0.55857)
Q0.5	5	-0.0331	0.0921	(-0.5252; 0.4589)
Q0.75	5	1.071	1.389	(0.578; 1.563)
Q1	5	0.1601	0.0283	(-0.3320; 0.6522)

Pooled StDev = 0.536274

Tukey Pairwise Comparisons

Grouping Information Using the Tukey Method and 95% Confidence

Sample	N	Mean	Grouping
Q0.75	5	1.071	A
Q1	5	0.1601	A B
Q0.2	5	0.11183	A B
Q0.1	4	0.10615	A B
Q0.3	5	0.0938	A B
Q0.4	5	0.06648	A B
Q0.5	5	-0.0331	B

Means that do not share a letter are significantly different.

IR PH

One-way ANOVA: E* versus Sample

Method

Null hypothesis	All means are equal
Alternative hypothesis	Not all means are equal
Significance level	$\alpha = 0.05$

Equal variances were assumed for the analysis.

Factor Information

Factor	Levels	Values
Sample	3	P11; P3; P7

Analysis of Variance

Source	DF	Adj SS	Adj MS	F-Value	P-Value
Sample	2	242.93	121.463	23.49	0.000
Error	12	62.05	5.171		
Total	14	304.98			

Model Summary

S	R-sq	R-sq(adj)	R-sq(pred)
2.27401	79.65%	76.26%	68.21%

Means

Sample	N	Mean	StDev	95% CI
P11	5	19.897	1.103	(17.681; 22.113)
P3	5	10.042	1.666	(7.826; 12.258)
P7	5	14.79	3.39	(12.57; 17.00)

Pooled StDev = 2.27401

Tukey Pairwise Comparisons

Grouping Information Using the Tukey Method and 95% Confidence

Sample	N	Mean	Grouping
P11	5	19.897	A
P7	5	14.79	B
P3	5	10.042	C

Means that do not share a letter are significantly different.

IR PH

One-way ANOVA: E** versus Sample

Method

Null hypothesis	All means are equal
Alternative hypothesis	Not all means are equal
Significance level	$\alpha = 0.05$

Equal variances were assumed for the analysis.

Factor Information

Factor	Levels	Values
Sample	3	P11; P3; P7

Analysis of Variance

Source	DF	Adj SS	Adj MS	F-Value	P-Value
Sample	2	1.056	0.5282	4.42	0.036
Error	12	1.434	0.1195		
Total	14	2.491			

Model Summary

S	R-sq	R-sq(adj)	R-sq(pred)
0.345714	42.42%	32.82%	10.02%

Means

Sample	N	Mean	StDev	95% CI
P11	5	1.546	0.284	(1.209; 1.883)
P3	5	0.905	0.425	(0.568; 1.242)
P7	5	1.318	0.312	(0.981; 1.655)

Pooled StDev = 0.345714

Tukey Pairwise Comparisons

Grouping Information Using the Tukey Method and 95% Confidence

Sample	N	Mean	Grouping
P11	5	1.546	A
P7	5	1.318	A B
P3	5	0.905	B

Means that do not share a letter are significantly different.

IR PH

One-way ANOVA: tand versus Sample

Method

Null hypothesis	All means are equal
Alternative hypothesis	Not all means are equal
Significance level	$\alpha = 0.05$

Equal variances were assumed for the analysis.

Factor Information

Factor	Levels	Values
Sample	3	P11; P3; P7

Analysis of Variance

Source	DF	Adj SS	Adj MS	F-Value	P-Value
Sample	2	0.000440	0.000220	0.27	0.767
Error	12	0.009720	0.000810		
Total	14	0.010160			

Model Summary

S	R-sq	R-sq(adj)	R-sq(pred)
0.0284605	4.33%	0.00%	0.00%

Means

Sample	N	Mean	StDev	95% CI
P11	5	0.08056	0.01342	(0.05283; 0.10829)
P3	5	0.0878	0.0405	(0.0601; 0.1156)
P7	5	0.0938	0.0247	(0.0661; 0.1215)

Pooled StDev = 0.0284605

Tukey Pairwise Comparisons

Grouping Information Using the Tukey Method and 95% Confidence

Sample	N	Mean	Grouping
P7	5	0.0938	A
P3	5	0.0878	A
P11	5	0.08056	A

Means that do not share a letter are significantly different.

IR SALT

One-way ANOVA: E* versus Sample

Method

Null hypothesis	All means are equal
Alternative hypothesis	Not all means are equal
Significance level	$\alpha = 0.05$

Equal variances were assumed for the analysis.

Factor Information

Factor	Levels	Values
Sample	4	S0; S0.1; S0.3; S0.5

Analysis of Variance

Source	DF	Adj SS	Adj MS	F-Value	P-Value
Sample	3	116.3	38.777	5.81	0.008
Error	15	100.1	6.671		
Total	18	216.4			

Model Summary

S	R-sq	R-sq(adj)	R-sq(pred)
2.58286	53.76%	44.51%	27.15%

Means

Sample	N	Mean	StDev	95% CI
S0	5	14.79	3.39	(12.32; 17.25)
S0.1	5	14.80	3.04	(12.34; 17.26)
S0.3	5	10.398	1.665	(7.936; 12.860)
S0.5	4	9.274	1.417	(6.522; 12.027)

Pooled StDev = 2.58286

Tukey Pairwise Comparisons

Grouping Information Using the Tukey Method and 95% Confidence

Sample	N	Mean	Grouping
S0.1	5	14.80	A
S0	5	14.79	A

S0.3	5	10.398	A	B
S0.5	4	9.274	B	

Means that do not share a letter are significantly different.

IR SALT

One-way ANOVA: E** versus Sample

Method

Null hypothesis	All means are equal
Alternative hypothesis	Not all means are equal
Significance level	$\alpha = 0.05$

Equal variances were assumed for the analysis.

Factor Information

Factor	Levels	Values
Sample	4	S0; S0.1; S0.3; S0.5

Analysis of Variance

Source	DF	Adj SS	Adj MS	F-Value	P-Value
Sample	3	0.3845	0.12818	1.39	0.285
Error	15	1.3861	0.09240		
Total	18	1.7706			

Model Summary

S	R-sq	R-sq(adj)	R-sq(pred)
0.303981	21.72%	6.06%	0.00%

Means

Sample	N	Mean	StDev	95% CI
S0	5	1.318	0.312	(1.028; 1.608)
S0.1	5	1.505	0.271	(1.215; 1.795)
S0.3	5	1.2950	0.2193	(1.0052; 1.5848)
S0.5	4	1.090	0.412	(0.766; 1.414)

Pooled StDev = 0.303981

Tukey Pairwise Comparisons

Grouping Information Using the Tukey Method and 95% Confidence

Sample	N	Mean	Grouping
S0.1	5	1.505	A
S0	5	1.318	A
S0.3	5	1.2950	A
S0.5	4	1.090	A

Means that do not share a letter are significantly different.

IR SALT

One-way ANOVA: tand versus Sample

Method

Null hypothesis	All means are equal
Alternative hypothesis	Not all means are equal
Significance level	$\alpha = 0.05$

Equal variances were assumed for the analysis.

Factor Information

Factor	Levels	Values
Sample	4	S0; S0.1; S0.3; S0.5

Analysis of Variance

Source	DF	Adj SS	Adj MS	F-Value	P-Value
Sample	3	0.003644	0.001215	1.63	0.224
Error	15	0.011170	0.000745		
Total	18	0.014815			

Model Summary

S	R-sq	R-sq(adj)	R-sq(pred)
0.0272890	24.60%	9.52%	0.00%

Means

Sample	N	Mean	StDev	95% CI
S0	5	0.0938	0.0247	(0.0678; 0.1198)
S0.1	5	0.10468	0.01548	(0.07867; 0.13069)
S0.3	5	0.12872	0.01626	(0.10271; 0.15473)
S0.5	4	0.1210	0.0473	(0.0919; 0.1501)

Pooled StDev = 0.0272890

Tukey Pairwise Comparisons

Grouping Information Using the Tukey Method and 95% Confidence

Sample	N	Mean	Grouping
S0.3	5	0.12872	A
S0.5	4	0.1210	A
S0.1	5	0.10468	A
S0	5	0.0938	A

Means that do not share a letter are significantly different.

Estimation of Diffusion Coefficient

One-way ANOVA: D versus Sample

* NOTE * Cannot draw the interval plot for the Tukey procedure. Interval plots for comparisons are illegible with more than 45 intervals.

Method

Null hypothesis	All means are equal
Alternative hypothesis	Not all means are equal
Significance level	$\alpha = 0.05$

Equal variances were assumed for the analysis.

Factor Information

Factor	Levels	Values
Sample	11	Q0.01; Q0.025; Q0.05; Q0.1; Q0.2; Q0.3; Q0.4; Q0.5; Q0.6; Q0.75; Q1

Analysis of Variance

Source	DF	Adj SS	Adj MS	F-Value	P-Value
Sample	10	0.000000	0.000000	0.46	0.884
Error	12	0.000000	0.000000		
Total	22	0.000000			

Model Summary

S	R-sq	R-sq(adj)	R-sq(pred)
0.0000000	27.85%	0.00%	0.00%

Means

Sample	N	Mean	StDev	95% CI
Q0.01	2	0.000000	0.000000	(0.000000; 0.000000)
Q0.025	2	0.000000	0.000000	(0.000000; 0.000000)
Q0.05	2	0.000000	0.000000	(0.000000; 0.000000)
Q0.1	2	0.000000	0.000000	(0.000000; 0.000000)
Q0.2	2	0.000000	0.000000	(0.000000; 0.000000)
Q0.3	2	0.000000	0.000000	(0.000000; 0.000000)
Q0.4	2	0.000000	0.000000	(0.000000; 0.000000)
Q0.5	2	0.000000	0.000000	(0.000000; 0.000000)
Q0.6	2	0.000000	0.000000	(0.000000; 0.000000)
Q0.75	2	0.000000	0.000000	(0.000000; 0.000000)
Q1	3	0.000000	0.000000	(0.000000; 0.000000)

Pooled StDev = 1.336867E-10

Tukey Pairwise Comparisons

Grouping Information Using the Tukey Method and 95% Confidence

Sample	N	Mean	Grouping
Q0.4	2	0.000000	A
Q0.01	2	0.000000	A
Q0.05	2	0.000000	A
Q0.025	2	0.000000	A
Q1	3	0.000000	A
Q0.1	2	0.000000	A
Q0.5	2	0.000000	A
Q0.6	2	0.000000	A
Q0.75	2	0.000000	A
Q0.3	2	0.000000	A
Q0.2	2	0.000000	A

Means that do not share a letter are significantly different

PH

One-way ANOVA: D versus Sample

Method

Null hypothesis	All means are equal
Alternative hypothesis	Not all means are equal
Significance level	$\alpha = 0.05$

Equal variances were assumed for the analysis.

Factor Information

Factor	Levels	Values
Sample	4	P11; P111; P3; P7

Analysis of Variance

Source	DF	Adj SS	Adj MS	F-Value	P-Value
Sample	3	0.000000	0.000000	0.15	0.921
Error	2	0.000000	0.000000		
Total	5	0.000000			

Model Summary

S	R-sq	R-sq(adj)	R-sq(pred)
0.0000000	18.47%	0.00%	*

Means

Sample	N	Mean	StDev	95% CI
P11	1	0.000000	*	(0.000000; 0.000000)
P111	1	0.000000	*	(0.000000; 0.000000)
P3	2	0.000000	0.000000	(0.000000; 0.000000)
P7	2	0.000000	0.000000	(0.000000; 0.000000)

Pooled StDev = 1.128207E-10

Tukey Pairwise Comparisons

Grouping Information Using the Tukey Method and 95% Confidence

Sample	N	Mean	Grouping
P3	2	0.000000	A
P11	1	0.000000	A
P111	1	0.000000	A
P7	2	0.000000	A

Means that do not share a letter are significantly different.

SALT

One-way ANOVA: D versus Sample

Method

Null hypothesis	All means are equal
Alternative hypothesis	Not all means are equal
Significance level	$\alpha = 0.05$

Equal variances were assumed for the analysis.

Factor Information

Factor	Levels	Values
Sample	4	S0; S0.1; S0.3; S0.5

Analysis of Variance

Source	DF	Adj SS	Adj MS	F-Value	P-Value
Sample	3	0.000000	0.000000	4.22	0.099
Error	4	0.000000	0.000000		
Total	7	0.000000			

Model Summary

S	R-sq	R-sq(adj)	R-sq(pred)
0.0000000	75.99%	57.97%	3.94%

Means

Sample	N	Mean	StDev	95% CI
S0	2	0.000000	0.000000	(0.000000; 0.000000)
S0.1	2	0.000000	0.000000	(0.000000; 0.000000)
S0.3	2	0.000000	0.000000	(0.000000; 0.000000)
S0.5	2	0.000000	0.000000	(0.000000; 0.000000)

Pooled StDev = 4.881470E-11

Tukey Pairwise Comparisons

Grouping Information Using the Tukey Method and 95% Confidence

Sample	N	Mean	Grouping
S0.1	2	0.000000	A
S0.3	2	0.000000	A

S0	2	0.000000	A
S0.5	2	0.000000	A

Means that do not share a letter are significantly different.

One-way ANOVA: D0 versus Sample

* NOTE * Cannot draw the interval plot for the Tukey procedure. Interval plots for comparisons are illegible with more than 45 intervals.

Method

Null hypothesis	All means are equal
Alternative hypothesis	Not all means are equal
Significance level	$\alpha = 0.05$

Equal variances were assumed for the analysis.

Factor Information

Factor	Levels	Values
Sample	11	Q0.01; Q0.025; Q0.05; Q0.1; Q0.2; Q0.3; Q0.4; Q0.5; Q0.6; Q0.75; Q1

Analysis of Variance

Source	DF	Adj SS	Adj MS	F-Value	P-Value
Sample	10	0.000000	0.000000	30.25	0.000
Error	11	0.000000	0.000000		
Total	21	0.000000			

Model Summary

S	R-sq	R-sq(adj)	R-sq(pred)
0.0000023	96.49%	93.30%	85.96%

Means

Sample	N	Mean	StDev	95% CI
Q0.01	2	0.000018	0.000001	(0.000015; 0.000022)
Q0.025	2	0.000023	0.000004	(0.000020; 0.000027)
Q0.05	2	0.000021	0.000003	(0.000017; 0.000025)
Q0.1	2	0.000024	0.000005	(0.000021; 0.000028)
Q0.2	2	0.000009	0.000000	(0.000005; 0.000012)
Q0.3	2	0.000005	0.000001	(0.000001; 0.000008)
Q0.4	2	0.000004	0.000001	(0.000001; 0.000008)
Q0.5	2	0.000004	0.000000	(0.000001; 0.000008)
Q0.6	2	0.000004	0.000001	(0.000001; 0.000008)
Q0.75	2	0.000003	0.000000	(-0.000000; 0.000007)
Q1	2	0.000002	0.000000	(-0.000001; 0.000006)

Pooled StDev = 2.282998E-06

Tukey Pairwise Comparisons

Grouping Information Using the Tukey Method and 95% Confidence

Sample	N	Mean	Grouping
Q0.1	2	0.000024	A
Q0.025	2	0.000023	A
Q0.05	2	0.000021	A
Q0.01	2	0.000018	A
Q0.2	2	0.000009	B
Q0.3	2	0.000005	B
Q0.4	2	0.000004	B
Q0.6	2	0.000004	B

Q0.5	2	0.000004	B
Q0.75	2	0.000003	B
Q1	2	0.000002	B

Means that do not share a letter are significantly different.

One-way ANOVA: D8 versus Sample

* NOTE * Cannot draw the interval plot for the Tukey procedure. Interval plots for comparisons are illegible with more than 45 intervals.

Method

Null hypothesis	All means are equal
Alternative hypothesis	Not all means are equal
Significance level	$\alpha = 0.05$

Equal variances were assumed for the analysis.

Factor Information

Factor	Levels	Values
Sample	11	Q0.01; Q0.025; Q0.05; Q0.1; Q0.2; Q0.3; Q0.4; Q0.5; Q0.6; Q0.75; Q1

Analysis of Variance

Source	DF	Adj SS	Adj MS	F-Value	P-Value
Sample	10	0.000002	0.000000	489.35	0.000
Error	11	0.000000	0.000000		
Total	21	0.000002			

Model Summary

S	R-sq	R-sq(adj)	R-sq(pred)
0.0000213	99.78%	99.57%	99.10%

Means

Sample	N	Mean	StDev	95% CI
Q0.01	2	0.001108	0.000071	(0.001075; 0.001142)
Q0.025	2	0.000021	0.000002	(-0.000012; 0.000055)
Q0.05	2	0.000001	0.000000	(-0.000032; 0.000035)
Q0.1	2	0.000000	0.000000	(-0.000033; 0.000033)
Q0.2	2	0.000000	0.000000	(-0.000033; 0.000033)
Q0.3	2	0.000000	0.000000	(-0.000033; 0.000033)
Q0.4	2	0.000000	0.000000	(-0.000033; 0.000033)
Q0.5	2	0.000000	0.000000	(-0.000033; 0.000033)
Q0.6	2	0.000000	0.000000	(-0.000033; 0.000033)
Q0.75	2	0.000000	0.000000	(-0.000033; 0.000033)
Q1	2	0.000000	0.000000	(-0.000033; 0.000033)

Pooled StDev = 0.0000213255

Tukey Pairwise Comparisons

Grouping Information Using the Tukey Method and 95% Confidence

Sample	N	Mean	Grouping
Q0.01	2	0.001108	A
Q0.025	2	0.000021	B
Q0.05	2	0.000001	B
Q0.1	2	0.000000	B
Q0.2	2	0.000000	B
Q0.3	2	0.000000	B
Q0.4	2	0.000000	B
Q0.5	2	0.000000	B
Q0.6	2	0.000000	B

Q0.75	2	0.000000	B
Q1	2	0.000000	B

Means that do not share a letter are significantly different.

One-way ANOVA: D0 versus Sample

Method

Null hypothesis	All means are equal
Alternative hypothesis	Not all means are equal
Significance level	$\alpha = 0.05$

Equal variances were assumed for the analysis.

Factor Information

Factor	Levels	Values
Sample	3	P11; P3; P7

Analysis of Variance

Source	DF	Adj SS	Adj MS	F-Value	P-Value
Sample	2	0.000000	0.000000	26.55	0.012
Error	3	0.000000	0.000000		
Total	5	0.000000			

Model Summary

S	R-sq	R-sq(adj)	R-sq(pred)
0.0000016	94.65%	91.09%	78.61%

Means

Sample	N	Mean	StDev	95% CI
P11	2	0.000013	0.000003	(0.000009; 0.000016)
P3	2	0.000001	0.000000	(-0.000002; 0.000005)
P7	2	0.000006	0.000000	(0.000002; 0.000009)

Pooled StDev = 1.594613E-06

Tukey Pairwise Comparisons

Grouping Information Using the Tukey Method and 95% Confidence

Sample	N	Mean	Grouping
P11	2	0.000013	A
P7	2	0.000006	B
P3	2	0.000001	B

Means that do not share a letter are significantly different.

One-way ANOVA: D8 versus Sample

Method

Null hypothesis	All means are equal
Alternative hypothesis	Not all means are equal
Significance level	$\alpha = 0.05$

Equal variances were assumed for the analysis.

Factor Information

Factor	Levels Values
Sample	3 P11; P3; P7

Analysis of Variance

Source	DF	Adj SS	Adj MS	F-Value	P-Value
Sample	2	0.000000	0.000000	191.66	0.001
Error	3	0.000000	0.000000		
Total	5	0.000000			

Model Summary

S	R-sq	R-sq(adj)	R-sq(pred)
0.0000000	99.22%	98.71%	96.89%

Means

Sample	N	Mean	StDev	95% CI
P11	2	0.000000	0.000000	(-0.000000; 0.000000)
P3	2	0.000000	0.000000	(0.000000; 0.000000)
P7	2	0.000000	0.000000	(0.000000; 0.000000)

Pooled StDev = 1.164760E-09

Tukey Pairwise Comparisons

Grouping Information Using the Tukey Method and 95% Confidence

Sample	N	Mean	Grouping
P3	2	0.000000	A
P7	2	0.000000	B
P11	2	0.000000	B

Means that do not share a letter are significantly different.

One-way ANOVA: D0 versus Sample

Method

Null hypothesis	All means are equal
Alternative hypothesis	Not all means are equal
Significance level	$\alpha = 0.05$

Equal variances were assumed for the analysis.

Factor Information

Factor	Levels Values
Sample	4 S0; S0.1; S0.3; S0.5

Analysis of Variance

Source	DF	Adj SS	Adj MS	F-Value	P-Value
Sample	3	0.000000	0.000000	83.03	0.000
Error	4	0.000000	0.000000		
Total	7	0.000000			

Model Summary

S	R-sq	R-sq(adj)	R-sq(pred)
0.0000005	98.42%	97.23%	93.68%

Means

Sample	N	Mean	StDev	95% CI
S0	2	0.000005	0.000000	(0.000004; 0.000006)
S0.1	2	0.000001	0.000000	(0.000000; 0.000002)
S0.3	2	0.000003	0.000000	(0.000002; 0.000004)
S0.5	2	0.000009	0.000001	(0.000008; 0.000010)

Pooled StDev = 5.123576E-07

Tukey Pairwise Comparisons

Grouping Information Using the Tukey Method and 95% Confidence

Sample	N	Mean	Grouping
S0.5	2	0.000009	A
S0	2	0.000005	B
S0.3	2	0.000003	B C
S0.1	2	0.000001	C

Means that do not share a letter are significantly different.

One-way ANOVA: D8 versus Sample

Method

Null hypothesis	All means are equal
Alternative hypothesis	Not all means are equal
Significance level	$\alpha = 0.05$

Equal variances were assumed for the analysis.

Factor Information

Factor	Levels	Values
Sample	4	S0; S0.1; S0.3; S0.5

Analysis of Variance

Source	DF	Adj SS	Adj MS	F-Value	P-Value
Sample	3	0.000000	0.000000	39.63	0.002
Error	4	0.000000	0.000000		
Total	7	0.000000			

Model Summary

S	R-sq	R-sq(adj)	R-sq(pred)
0.0000000	96.75%	94.30%	86.98%

Means

Sample	N	Mean	StDev	95% CI
S0	2	0.000000	0.000000	(0.000000; 0.000000)
S0.1	2	0.000000	0.000000	(0.000000; 0.000000)
S0.3	2	0.000000	0.000000	(0.000000; 0.000000)
S0.5	2	0.000000	0.000000	(0.000000; 0.000000)

Pooled StDev = 1.128777E-09

Tukey Pairwise Comparisons

Grouping Information Using the Tukey Method and 95% Confidence

Sample	N	Mean	Grouping
S0.1	2	0.000000	A
S0.3	2	0.000000	B
S0	2	0.000000	B
S0.5	2	0.000000	B

Means that do not share a letter are significantly different.

CURRICULUM VITAE

PERSONAL INFORMATION

Surname, Name: Kirtil, Emrah
Nationality: Turkish (TC)
Date and Place of Birth: 13 May 1984, Bursa
Marital Status: Single
Phone: +90 312 210 56 37
Fax: +90 312 210 22 91
email: ekirtil@metu.edu.tr

EDUCATION

Degree	Institution	Year of Graduation
BS	METU Food Engineering	2011
High School	Bursa Anatolian High School, Bursa	2002

WORK EXPERIENCE

Year	Place	Enrollment
2012-Present	METU Dept. of Food Eng.	Research Assistant

FOREIGN LANGUAGES

Advanced English

PUBLICATIONS

1. Aydogdu, A., Radke, C. J., Bezci, S., & Kirtil, E. (2020). Characterization of curcumin incorporated guar gum/orange oil antimicrobial emulsion films. *International Journal of Biological Macromolecules*.
<https://doi.org/10.1016/j.ijbiomac.2019.12.255>
2. Aydogdu, A., Kirtil, E., Sumnu, G., Oztop, M. H., & Aydogdu, Y. (2018). Utilization of lentil flour as a biopolymer source for the development of edible films. *Journal of Applied Polymer Science*. <https://doi.org/10.1002/app.46356>

3. Bulut, M., Bayer, Ö., Kırtıl, E., & Bayındırlı, A. (2018). Effect of freezing rate and storage on the texture and quality parameters of strawberry and green bean frozen in home type freezer. *International Journal of Refrigeration*, 88. <https://doi.org/10.1016/j.ijrefrig.2018.02.030>
4. Kırtıl, E., Cikrikci, S., & Oztop, M. H. (2017). Recent Advances in time domain NMR & MRI Sensors and Their Food Applications. *Current Opinion in Food Science*. <https://doi.org/10.1016/j.cofs.2017.07.005>
5. Kırtıl, E., Dag, Damla, Guner, S., Unal, K. & Oztop, M. H. (2017), Dynamics of unloaded and green tea extract loaded lecithin based liposomal dispersions investigated by nuclear magnetic resonance T2 relaxation. *Food Research International*. <https://doi.org/10.1016/j.foodres.2017.06.064>
6. Kırtıl, E., Tonyali, B., Aydogdu, A., Yıldız Bulut, E., Cilek Tatar, B., & Oztop, M. H. (2017) Visualization of cakes differing in oil content with Magnetic Resonance Imaging. *International Journal of Food Properties*. <http://dx.doi.org/10.1080/10942912.2017.1326057>
7. Kırtıl, E., Aydogdu, A., Oztop, M.H. (2017). Investigation of physical properties and moisture sorption behaviour of different marshmallow formulations. *Acta Horticulturae* <http://doi.org/http://dx.doi.org/10.17660/ActaHortic.2017.1152.33>
8. Kırtıl, E., Kilercioglu, M., & Oztop, M. H. (2016). Modified Atmosphere Packaging of Foods. *Reference Module in Food Sciences* (pp. 1–6). <http://doi.org/http://dx.doi.org/10.1016/B978-0-08-100596-5.03218-2>
9. Kırtıl, E., & Oztop, M. H. (2016a). ¹H Nuclear Magnetic Resonance Relaxometry and Magnetic Resonance Imaging and Applications in Food Science and Processing. *Food Engineering Reviews*, 8(1), 1–22. <http://doi.org/10.1007/s12393-015-9118-y>
10. Kırtıl, E., & Oztop, M. H. (2016b). Characterization of emulsion stabilization properties of quince seed extract as a new source of hydrocolloid. *Food Research International*, 85, 84–94. <http://doi.org/10.1016/j.foodres.2016.04.019>

11. Kirtil, E., & Oztop, M. H. (2016c). Controlled and Modified Atmosphere Packaging. Reference Module in Food Science (pp. 1–2). Elsevier.
<http://doi.org/10.1016/B978-0-08-100596-5.03376-X>
 12. Kirtil, E., Oztop, M. H., Sirijariyawat, A., Ngamchuachit, P., Barrett, D. M., & McCarthy, M. J. (2014). Effect of pectin methyl esterase (PME) and CaCl₂ infusion on the cell integrity of fresh-cut and frozen-thawed mangoes: An NMR relaxometry study. *Food Research International*, 66, 409–416.
<http://doi.org/10.1016/j.foodres.2014.10.006>
 13. Kirtil, E., & Öztop, M. H. (2014). Enkapsülasyon Maddesi Olarak Lipozom ve Gıdalarda Kullanımı : Yapısı, Karakterizasyonu, Üretimi ve Stabilitesi. *Akademik Gıda*, 12(4), 41–57.
- Bodybuilding, Fitness, Writing, Hiking, Video Games